Proceedings of International Conference on Intelligent and Autonomous Systems

28 & 29 November 2015

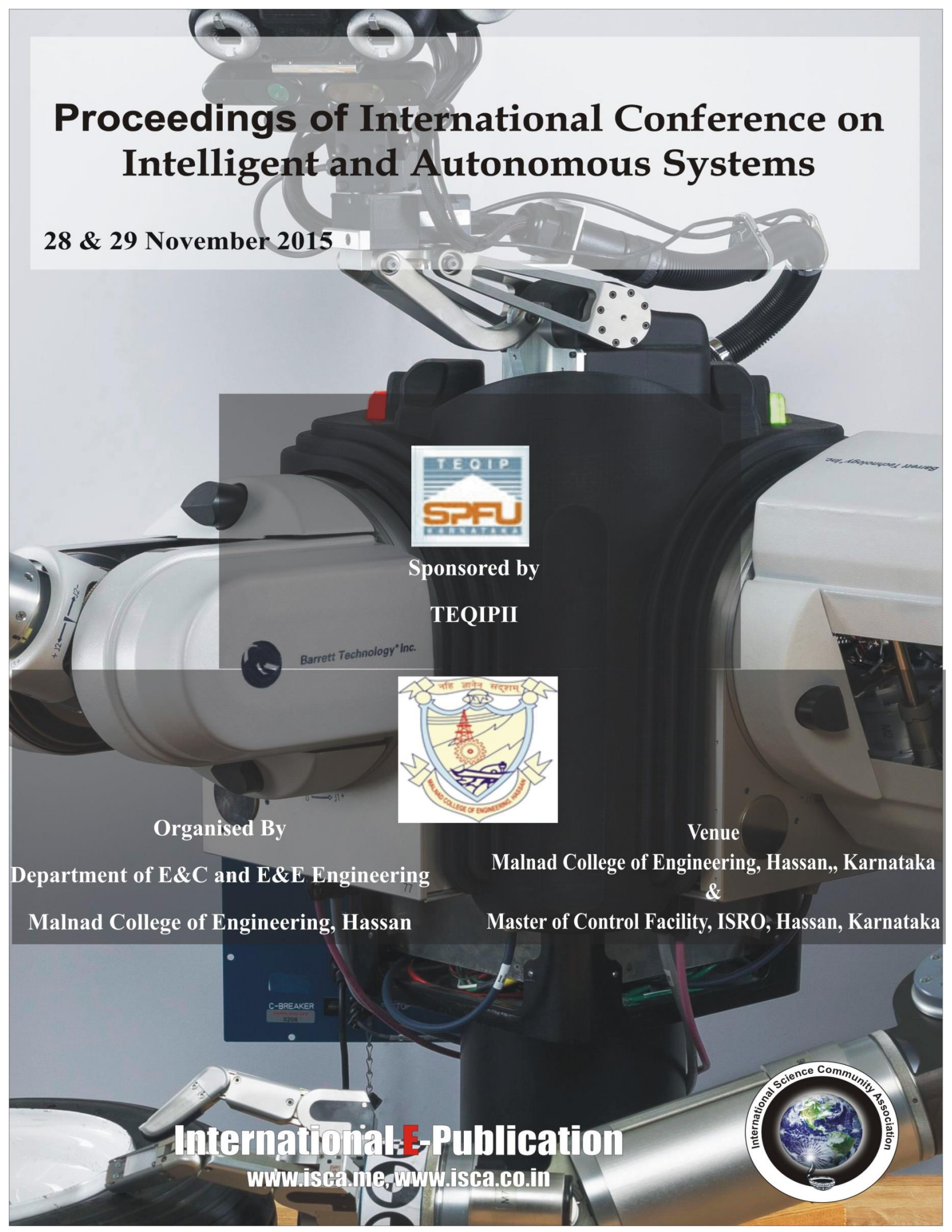

Sponsored by

TEQIPII

Organised By

Department of E&C and E&E Engineering

Malnad College of Engineering, Hassan

Venue

Malnad College of Engineering, Hassan,, Karnataka

&

Master of Control Facility, ISRO, Hassan, Karnataka

International E-Publication

www.isca.me, www.isca.co.in

Proceedings of

International Conference on

Intelligent and Autonomous Systems

28 & 29 November 2015

Organised By

Department of E&C and E&E Engineering

Malnad College of Engineering, Hassan

Editors

Dr.B.R.Sujatha and Dr.G.K.Purushothama

Dept. of E&C and E&E Engineering

Malnad College of Engineering,Hassan

2016

International E - Publication

www.isca.me , www.isca.co.in

International E - Publication

427, Palhar Nagar, RAPTC, VIP-Road, Indore-452005 (MP) INDIA
Phone: +91-731-2616100, Mobile: +91-80570-83382
E-mail: **contact@isca.co.in** , Website: **www.isca.me** , **www.isca.co.in**

ISBN: 978-93-84659-38-7

MALNAD COLLEGE OF ENGINEERING

(An Autonomous Institution affiliated to VTU, Belgaum)

Malnad College of Engineering with 53 years of legacy has and is imparting quality technical Education to thousands of students. An Autonomous Institution since 2007, the college is one among the leading technical Institutes in the country. The technical skill development & expansion of knowledge with state of the art facilities makes this Institute as one of the best among Autonomous Colleges. The College is determined to retain this level of superiority already in command & improve further in every sphere of academic activities including research orientation & overall development of the students.

To face new challenges, for active progress and to lead a successful life, education is mandatory. Ever growing need of competitive skills demands a suitable platform, which is being given by qualified scholars & technocrats. The faculty possess a much diversified vision of turning the dreams of students into a concrete reality. Our focus is mainly on imparting quality education which enables the student to also excel in other related skills. The academic autonomy has created a platform to involve industry leaders, academics par excellence, R&D heads and all stake holders to strengthen the curriculum and to produce quality engineers for today's need. Its autonomous programs have a balanced and updated curriculum based on employment/ students need and demands. Recognizing that all the students do not have the same interests and abilities, the programs are varied and seek to provide all the students with the best possible education. The institution has provided a great opportunity for its students to empower themselves with the wings of knowledge & power of innovation and imbibe an attitude akin to practice & positive thinking with caring concern for society and nature.

INTERNATIONAL CONFERENCE ON INTELLIGENT AND AUTONOMOUS SYSTEMS (ICIAS2015)

28th,29th November, 2015

Department of E&C Engineering and E&E Engineering
Malnad College of Engineering, Hassan

In collaboration with

(Sponsored by TEQIP-II)

Master Control Facility (ISRO), Hassan

MALNAD COLLEGE OF ENGINEERING, HASSAN
(Under the auspices of Malnad Technical Education Society®, Hassan)
An Autonomous Institution affiliated to
Visvesvaraya Technological University, Belagavi
(Recognized by AICTE and UGC NewDelhi)

You are Cordially invited to the
Inaugural function of

INTERNATIONAL CONFERENCE ON INTELLIGENT AND AUTONOMOUS SYSTEMS (ICIAS2015)
on
Saturday, 28th November, 2015

Dr. B. R. Sujatha
Program Chair

Dr. G. K. Purushothama
Finance Chair

Time:10.00 A.M.
Venue: Alumni Hall, MCE, Hassan

Chief Guest and Keynote Speaker

Prof. Dr.ir.Rob Fastenau
Dean of Faculty of Electrical Engineering, Mathematics & Computer Science
Delft University of Technology, Delft, the Netherlands

Guest

Dr. S. Venkateshwara Sharma
Deputy Director, ISAC (ISRO), Bangalore

President of the function

Sri. Ashok Haranahalli
Senior Advocate, High Court of Karnataka
Honourable Chairman, MTES®, Hassan

Gracious Presence

Sri. B.R. Gurudev, Ex. MLC
Honourable Vice Chairman, MCE, Hassan

Sri. R. T. Dyave Gowda
Honourable Secretary, MTES®, Hassan

Sri. R. Sheshagiri
Honourable Treasurer, MTES®, Hassan

Dr. K. S. Jayantha
Principal, MCE, Hassan

Dr. M. S. Raviprakasha
Vice Principal, MCE, Hassan

INTERNATIONAL CONFERENCE ON INTELLIGENT AND AUTONOMOUS SYSTEMS (ICIAS2015)

ORGANIZED BY

MALNAD COLLEGE OF ENGINEERING, HASSAN, KARNATAKA
AND
MASTER CONTROL FACILITY (ISRO), KARNATAKA, INDIA

28, 29 November 2015

COMMITTEES

CHIEF PATRON

Sri. Ashok Haranahalli, Chairman, MTES®, Hassan

PATRONS
Sri. R. T. Dyave Gowda, Secretary, MTES®, Hassan
Sri. R. Sheshagiri, Treasurer, MTES®, Hassan
Sri. B.R. Gurudev, Vice Chairman
Sri. S. Parameshwaran, Director, MCF, Hassan
Dr. S. Venkateshwara. Sharma, Dep. Dir, ISAC (ISRO), B'lore
Dr. Subramanya Udupa, ISAC (ISRO), Bangalore
Dr. K. S. Jayantha, Principal, MCE, Hassan
Dr. M. S. Raviprakasha, Vice Principal, MCE, Hassan

GENERAL CHAIR
Prof. Dr. K. C. Chidananda Gowda, BOG Chairman

TECHNICAL CHAIR
Dr. B. R. Sujatha, Professor,
Dept. of E&C Engineering, MCE, Hassan

FINANCE CHAIR
Dr. G. K. Purushothama, Professor,
Dept. of E&E Engineering, MCE, Hassan

ORGANIZING CHAIR
Dr. P. C. Srikanth, HOD, Dept. of E&C Engg. &
Dr. Vishwanath Hegde HOD, Dept. of E&E Engg.
MCE, Hassan

INTERNATIONAL PROGRAMME COMMITTEE
Dr. R. Venkatesh Prasad, Delft, the Netherlands
Dr. R. Raghavendra, GUC, Gjøvik, Norway
Dr. Nelson Joseph (Sweden)
Dr. M . Suresh, University of Wyoming, USA
Dr. Robert Kubichek, University of Wyoming, USA
Dr. Kalidas Shetty, NDSU, North Dakota, USA
Dr. Rajesh Kavessari, NDSU, North Dakota, USA
Dr. K. N. Bhanuprakash, Singapore

TECHNICAL PROGRAMME COMMITTEE
Dr. T. Srinivas, IISc, Bangalore
Dr. Muralidhar Kulkarni, NITK, Surathakal
Dr. Harigovindan, NIT, Puduchery
Dr. Bibhas Ghoshal, IIIT, Ahmedabad
Dr. P. S. Ramaiah, Andhra University
Dr. K. A. Radhakrishna Rao, PESCE, Mandya
Dr. R.Muralishankar , CMRIT, Bangalore
Dr. Narendranath Udupa, Philips Research, Bangalore
Dr. K. Manjunath, MCE, Hassan
Prof. Vijayvithal Bongale, MCE, Hassan
Dr. B. Ramesh, MCE, Hassan
Dr.Y.Arunkumar, MCE, Hassan
Dr. G. Shivakumar, MCE, Hassan
Dr. M. K. Ravishankar, MCE, Hassan
Dr. A. Geethakiran, MCE, Hassan

FINANCIAL ADVISOR
Dr. K. Gururajan

CONTACT PERSON
Mr. Raghavendraprasad Deshpande
9538647166

THEME

Unfolding Intelligent and autonomous systems for all fields of Engineering and Technology in an eco friendly manner.

KEYNOTE SPEAKER

Prof.Dr.ir.RobFastenau,
Dean of Faculty of Electrical Engineering, Mathematics & Computer Science,
Delft University of Technology,
Delft, The Netherlands

TOPICS OF INTEREST

Hardware Implementation for Signal Processing
Green communications and networking
Signal processing in Communication
Space/ Satellite Communication
Intelligent transport systems
Power system analysis
'Factories' in future
Wireless Networks
Structural analysis
Image processing
Smart buildings
Smart grids

For more details,
visit :
www.icias2015.org
contact:
mceicias2015@gmail.com

SUPPORTED BY
TEQIP II

TRACKS for Presentation in ICIAS2015

I Signal processing and System design

- Statistical Signal processing in Communication
- Image and video processing
- Medical Image acquisition & processing
- Pattern recognition, Cognition and analysis
- DSP Implementation and Embedded Systems
- Multidimensional/Multichannel/Mixed/ Optical Signal Processing
- Audio/Speech/Music Processing and Coding
- FPGA/CPLD ,VLSI design and implementation
- Antenna design
- Steganography

II Communications and Networking

- Digital communication
- Wired/Wireless Computer Networks
- Space and Satellite Communication
- Seismic, Radar, Sonar, Remote sensing
- Ad hoc/Sensor/ Body Area networks
- Storage networks
- Optical communication and Networks
- Software defined Radio
- Data Mining
- Cryptography

III Power Systems and Smart grid technologies

- Smart/Micro grid technologies
- Power Electronic Systems and Drives
- Power quality issues and Grounding
- Distribution System Automation
- Flexible AC Transmission Systems
- Renewable Energy-Hybrid Systems and Fuel cells
- Power market and power system economics
- EMI and over-voltage power system protection
- Bearing less drive technologies
- High Voltage Engineering and Insulation

IV Intelligent Systems/Applications

- Intelligent transport systems
- Smart buildings
- 'Factories' in future
- Intelligent manufacturing systems
- Internet of Things
- Robotics

International Conference on Intelligent and Autonomous Systems-ICIAS2015

Department of E&C and E&E Engineering

Malnad College of Engineering, Hassan,

in collaboration with

Master Control Facility (ISRO), Hassan

under TEQIP II

28th, 29th November, 2015

PROGRAM SCHEDULE

Date	TIME	EVENT
28 NOV 2015	9am to 9.45 am	Registration
	10am-11am	Inauguration
	11.00-11.30am	Tea Break
	11.30am-1.00noon	Key note address
	1.00-1.45noon	Lunch
	2.00pm-2.45 pm	Plenary sessions
	3.00pm-3.45pm	Presentations
	4pm-6pm	Visit to MCF, Hassan
	6.30-7.30pm	Entertainment programme
	7.30-8.30pm	Dinner
29 NOV 2015	9.30am- 10.30 am	Tutorial Talk-I
	10.45am-11.45am	Tutorial Talk-II
	11.45-12noon	Tea Break
	12noon-1.00pm	Presentations
	2.00-3.00pm	Valedictory session

MESSAGE

I am happy to know that the Departments of Electronics & Communication Engineering and Electrical & Electronics Engineering, Malnad College of Engineering, Hassan will be organizing an International Conference on ***Intelligent and Autonomous Systems-ICIAS2015*** during 28th, 29th November 2015.

I hope this conference will provide a unique opportunity to our faculty and students to interact and update their technical knowledge. I congratulate all the organizing committee members for the commendable work done by them.

I wish the conference a great success.

Shri.Ashok Haranahalli
Chairman
Malnad Technical Education Society®
Hassan

MESSAGE

I am indeed happy to know that the Departments of Electronics & Communication Engineering and Electrical & Electronics Engineering, Malnad College of Engineering, Hassan will be organizing an International Conference on ***Intelligent and Autonomous Systems-ICIAS2015*** during 28th, 29th November 2015.This conference will provide a unique opportunity to the faculty and students of Engineering colleges and from the industry to present their research ideas and interact with resource persons and further update their technical knowledge. I congratulate all the organizing committee members for the initiative taken to showcase our institution at the international level.
I wish the conference a great success.

Dr.K.S.Jayantha
Principal
Malnad College of Engineering
Hassan

MESSAGE

The Departments of Electronics &Communication Engineering and Electrical & Electronics Engineering, Malnad College of Engineering, Hassan is organizing an International Conference on ***Intelligent and Autonomous Systems-ICIAS2015*** during 28th, 29th November 2015.

This conference will provide a platform to researchers and engineers to present their work and also interact with resource persons to update their knowledge in the field of Autonomous systems. I appreciate the commendable work done by all the organizing committee members.

I wish the conference a great success.

Dr.M.S.Raviprakasha
Vice Principal
Malnad College of Engineering
Hassan

MESSAGE

We are happy in organizing an International Conference on *Intelligent and Autonomous Systems-ICIAS2015* during 28th, 29th November 2015 in collaboration with Master Control Facility(ISRO), Hassan and sponsored by TEQIP II.

The theme of the conference assumes great significance as all of these are of great relevance to the society. The topics are interdisciplinary and offer great scope for investigation and sustainable research in the field of Autonomous Systems.

We are happy that the keynote address will be rendered by renowned academician, researcher and scientist Prof.Dr. RobFastenau, Dean of Faculty of Electrical Engineering, Mathematics & Computer Science, Delft University of Technology, Delft, the Netherlands .

The plenary sessions on allied Topics is being conducted by Professors from renowned institutions including ISRO, IISc and NITs including Dr.R.Venkatesh Prasad,Professor, Electrical Engineering, Mathematics & Computer Science, Delft University of Technology, Delft, the Netherlands.These sessions will be highlighting the state of art in Autonomous systems and Internet of Things and thus will be highly useful to the participants and research scholars and to our faculty and students.

We thank our Chairman and all members of MTES®, Principal and Vice Principal of MCE, Hassan and TEQIP II authorities for all the help and support extended to us in organizing this conference.

We wish all the participants a useful stay in our institution.

Thank you

Dr.B.R.Sujatha and Dr.G.K.Purushothama
Chairpersons
ICIAS 2015
Dept. of E&C and E&E Engineering
Malnad College of Engineering
Hassan

Inauguration by the dignitaries

Start of a session…..

Table of Content

Private Network forming Routing Protocol for Adhoc Networks

Nagesh U.B
Department of Information Engineering
Vivekananda College of Engineering and Technology
Puttur, India
nageshub.ise@vcetputtur.ac.in

***Abstract*—The lack of infrastructure in mobile Ad Hoc networks has posed a lot of opportunities for the researches in relaying the data to destination. Mobility of nodes in such an environment offers many challenges due to link failures. Different routing protocols have considered specific aspect of such a network considerably the energy consumption, bandwidth, geographic location etc. for efficiently routing the packets. If security aspect is considered in such a protocol, they will be concentrating mainly on effect of different type attacks. In this paper a novel approach for securely routing the packets is proposed to support volatile nature of the network. Being membership history count the foundation, the routing decision is made according to the number of registrations made by a node with the source node and by establishing a private trusted path of its own to securely route the packets. The proposed protocol works in a safe manner to ensure data security and end to end connectivity. The results evaluated in the simulation reveal that, the proposed algorithm provides significant improvement in terms of delivery ratio and level of security.**

Keywords—MANET; Membership History; Network Stability; Security factor; Mobility

I. INTRODUCTION

Mobile Adhoc Networks (MANET) and its applications are widely used in today's IOT's and WSN's where in the mobility of nodes will drastically effect the infrastructure less network parameters like, end-to-end connectivity, delivery ratio, stability and energy consumption. The volatile nature of the node locations mainly lead to link failures which in turn may result in network degradation by affecting the performance of routing layer of TCP/IP stack in microkernel based lightweight operating systems like Contiki [1].

The inhabitant sensing nodes in the network are very sensitive to scarce resources. Managing these vital components has become bottleneck to the underlying operating system running on low powered (16 bit) controllers of the node. The node movement throughout the time in the network is more prone to security vulnerabilities, as data rich nodes are passes near an eavesdropping node. So finding a trusted path from source to data collection centers is the major challenge in such infrastructure less networks.

In this paper we propose an effective approach of path selection from source to aggregator where in route failure and link breakage can be considerably reduced. The algorithm follows a membership history based approach which can be another factor for identifying liveliness in the network like sequence number and distance to every other node. Furthermore this strategy is aimed to achieve more security in the route by employing hash distribution scheme which is entirely dependent on the membership history value of a node.

The reminder of this paper is organized as follows. Section II gives a brief introduction on past researches in the field of routing for Ad Hoc networks and WSN. Section III provides a picture of network model and simulation scenario we are using. Section IV presents the working flow of the proposed protocol. Section V presents the performance evaluation. Finally Section VI concludes this paper with summary.

II. RELATED WORKS

There are many researches on routing strategies for Ad Hoc network and one of its verities, the Wireless Sensor Networks. Here some of the major investigations which are suitable for both these categories are presented.

Data gathering and dropping it in local aggregators can be achieved in different ways such as by local storage using collaborative storage mechanisms (CBSM) [2], where data collected will be stored locally in a cluster based on the residual energy and importance of gathered data. But the freshness of data may override the storage capacity in nodes which leads to data loss.

However if the carrying of data to destination is the alternative solution, there are different strategies classified as reactive and proactive. The conventional proactive routing methods like DSDV and CGSR uses one of the parameter of the network to find out the path. In DSDV [3], the Bellman-Ford algorithm of finding shortest next hop node along with a destination sequence number is used to update a table entry and in turn to identify the most recent and best path in the network. Where as in CGSR [4], the available nodes are organized into clusters and by electing a cluster head according to LCC algorithm, the member nodes will communicate to the head by spreading codes on a CDMA system so as to carry the data packets from registered members of a cluster to the sink node.

In reactive routing protocols like TORA [5], it makes use of link reversal techniques to provide loop free paths to the

destination. Each node maintains one hop local topology information consisting of height of node H(n) from the destination and constructs a destination oriented directed acyclic graph (DAG). This approach provides more stability against link failures.

The AODV [6] on the other hand obtains multiple up-to-date paths to the destination on-demand by flooding *RouteRequest* packets along with a destination sequence number throughout the network.

In an another reactive approach MLRR [7], multiple routes can be found from source to destination by dividing the geographic node arrangement into different levels based on the distance from destination and by selecting an energy efficient node from each layer as member in the path.

III. Network Model and Assumptions

We consider a non-static wireless network containing homogeneous sensor nodes capable of performing all the possible application tasks powered with a16 bit microcontroller. The network is based on a flat homogeneous architecture (Fig.1) in which every node has the same physical capabilities like sensing, interacting with neighbor nodes and generating hash functions [8]. All nodes in the network are synchronous with a local network time. A new node admitting to the network will be assigned with current time stamp. We consider a node in the network as network aggregator which has the capabilities of both wireless and wired connectivity. This node is responsible for collecting routed data from all the nodes in the network. The aggregator is connected to a data center called as sink. The sink node could be a border router to connect to internet or to monitor the collected data in a terminal window.

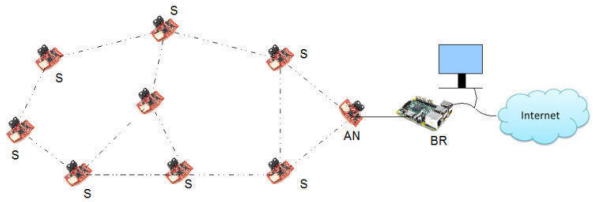

Fig. 1. Network model

IV. Private Network Forming Routing Protocol

The proposed Private Network forming routing protocol has two significances: (1) Member history based route construction and (2) a private network based secure packet relaying. We describe each of them in the followings sections.

A. *Member history determining network topology construction*

In our network architecture, we considered every node as a mobile node. So they are capable of registering with every other node in the network. Every node will maintain a table known as History Table which contains membership history details of every other node in the network which have come in contact with each other.

1) Member History Table: It is a two dimensional matrix with entries containing historical membership details of every node in the network which a node has come in contact with (N1, N2,…Nn) over the membership of it (H_{N1}, H_{N2}…H_{Nn}) with every other node in the network (Figure 2). That is a node was historically member of which all nodes and currently member of which node. In the table shown, nodes N_2, N_3 and N_4 are members of N_1 as 4, 3 and 5 times respectively which can also be seen in history of N_2.

A node will be given the membership of another node if it remains in its broadcast range for a predefined duration of time. This is checked by sending beacon packets periodically. The membership of a node in a session lasts until it remains in the coverage range of a particular node.

From the history table it can be proved that if a nodes history count over other nodes in the network is less compared to its membership under a specific node, the node is more mobile in the network or in other words it is less stable.

N1

	H_{N1}	H_{N2}	H_{N3}	H_{N4}
N_1	-1	4	3	4
N_2	4	-1	6	2
N_3	3	6	-1	3
N_4	5	3	5	-1

Fig. 2. Member history table

The stability of a node N having memberships of m nodes in the network over a period of time can therefore be given by:

$$SNn = \frac{\sum_{n=0}^{n=m} HNn}{T}$$

Therefore the network stability having density of mobile nodes as D is given by:

$$\frac{(\sum_{0}^{n} SNn)}{D}$$

The energy consumption also increases with mobility as it registers with more number of nodes which in turn is dependent on stability. We expect an average duration of membership and an average interval movement of every node in the network throughout the topology.

2) History count based path discovery: From the behavior of the network it can be understood that, a node having more membership of a particular node is less volatile and is more stable in the territory of a node. So we can consider it as private member of it and is more trusted node than any other.

If such a node has moved to any other location in the geographic area, we consider it as a private agent of it. This private node can ensure desired security for data which will be discussed in next section. Therefore the proposed protocol considers a node with highest membership value for the source as the preferred node in the path from source to destination.

Now the member of current node will select the next hop node which was historically member of the source node. If no such nodes which are members of source node are available under an intermediate node, then members of that node will be selected temporarily to select next hop and at the same time this is informed to the source node so that no such node will be selected in the future for a path from selected source node. This hop is temporary hop in the path the source has selected.

The temporary hops are fixed during data transmission if a new node which was member in history of the source node becomes the member of the intermediate node. Once the temporary path is cleared it is informed to the source node. The destination will reply with Route Reply packet to the source containing information about the path which has less number of hops. An example scenario of such a path discovery is shown in Figure 3.

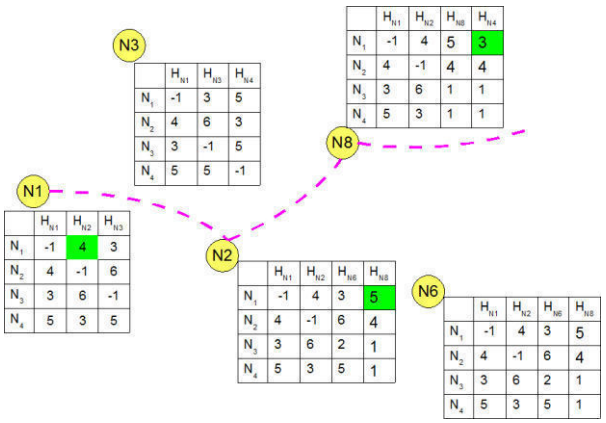

Fig. 3. PNRP path selection scenario

B. *Private Network Oriented Secure Packet Relaying*

According to our routing strategy a node will be given membership of another node if it remains in its broadcast range for predefined threshold duration of time, this is ensured by checking it availability periodically by sending beacon packets.

Every node in the network is capable of generating hash from the hash function it knows. When a node becomes the member of a particular node it will be treated as one of the secure agent of it and larger the membership count value, the more trusted it is. Under such a membership a hash function will be assigned to the trustworthy member node. This hash function will be always relying on the synchronous network time. That is any member of a particular node can derive hash value from the function it is currently holding at any interval of time. The hash function used here is the series function from which different series elements can be derived. The generated hash value is used as a secure key for encrypting the message such that a member node only can encrypt ant send it with anew hash key.

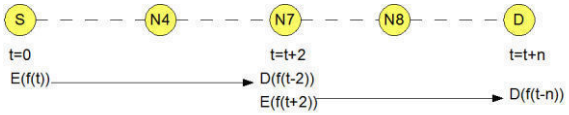

Fig. 4. Encryption in a route having *n* hops

If a message is sent from source node at time instant t then an intermediate node in the path will be securing the message by using hash values $f(x)_{t-1}$ and $f(x)_{t+1}$ hash values to decrypt and encrypt respectively (Figure 4). A route having *n* nodes will be divided into *e* (encryption count) number of parts as:

$$e = \frac{hop\ count}{avg.membership\ history\ count}$$

Therefore the *e* number of nodes will encrypt the message with new hash keys. So as the history count increases the encryption count factor also increases. This leads to increased number of encryptions as the network becomes more mobile. The hash function will be changed periodically by every node in the network and is done after completing one cycle of transmission so that fresh hash functions are distributed to member nodes.

V. PERFORMANCE EVALUATION

The performance of the proposed private network forming routing mechanism is judged through simulation in Matlab and C source codes. The protocol is tested for two important performance metrics: the delivery ratio of the network due to node mobility and the level of security by considering number of encryptions. Parameters those affect these metrics are node mobility, link failures and number of hops. The results are compared with shortest path routing algorithm. Simulation is carried out by considering a multi-hop network consisting of 50 nodes distributed randomly in a 500m x 500m square area. The sink is positioned within the region boundary at [500,250] location any node in the deployment can act as source. We consider a node at location [0, 250] as the source during simulation.

The important aspect considered in the simulation is that every node is a mobile node and is implemented by changing the node positions at regular intervals randomly. Radio transmission range is set to 50 meters. Threshold value of time for membership under any node is taken as 180 Seconds. The encryption scheme used in the simulation is simple XOR and the hash functions used for secret key generation are square and cube series functions at transmitter and receiver ends as:

$((x+t_0)^2$ and $(x+(t-t_n))^2$ or $(x+t_0)^3$ and $(x+(t-t_n))^3)$.

The following performance measures have been considered for comparing the proposed protocol with shortest next hop algorithm.

1) Delivery Ratio: This is the ratio of number of data packets delivered at the destination to the number of all data packets sent from the source.

2) Network Stability: The stability of the entire network is measured in terms of number of registrations by the nodes in the network with every other node. Higher the average number of registration, lower is the stability as they become more mobile. It is measured according to the equation discussed in previous section.

3). Security level: The security level is measured for a communication in a path by the number of encryptions employed in that path. This is given by the equation for e.

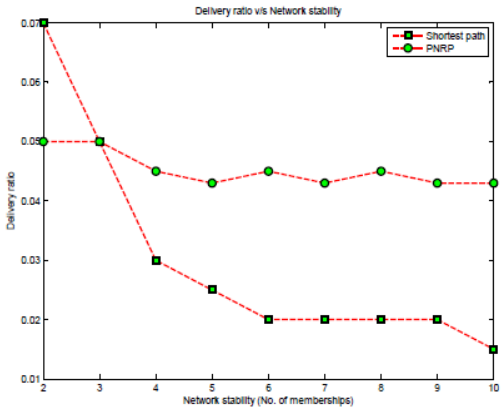

Fig. 5. Network stability vs. delivery ratio

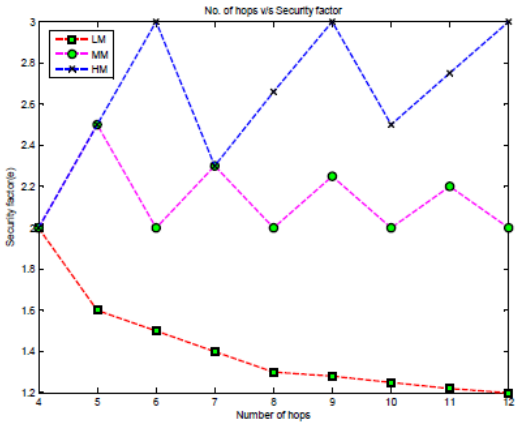

Fig. 6. Security level vs. number of hops

Scenario1: The proposed algorithm is tested by increasing the mobility factor and thereby increasing the number of history counts and its effect on number of packets delivered at the destination are observed.

Figure 5 shows the variation of delivery ratio for shortest path and the proposed PNRP algorithm. As we can see the delivery ratio remains almost steady in the PNRP compared to shortest path routing as we increase the mobility factor. This is because, as nodes become more mobile the link failure increases more and more in case of shortest path routing. But in the proposed scheme we select the stable next hop node which was member of the source node in the history.

Scenario 2: In an another case the proposed protocol is tested by considering the number of hops in a path after conducting many rounds of experiments and observing the number of encryption employed in a communication.

Figure 6 shows the variation in number of encryptions with low, medium and high rate of node mobility. As we can observe here, as the nodes become more mobile from low to high rate the number of encryptions also increases which is also dependent on number of hops in the path.

VI. CONCLUSIONS

Similar to any other routing strategies for mobile Ad Hoc networks the proposed PNRP also discovers the best path for relaying data from source to sink. The proposed algorithm achieves higher level of security as it incorporates encryptions which varies according to the path length. As the key is varied at certain intervals throughout the path and also the hash function is changed from time to time, there are less possibilities of compromise. Further the routing scheme follows totally private network forming approach as we route the packets to next hop nodes which were most recent members of source node in history as they also will be having recent hash functions.

REFERENCES

[1] Adam Dunkels, Bjorn Gronvall, Thiemo Voigt, Swedish Institute of Computer Science, “Contik-A Lightweight and Flexible Operating System for Tiny Networked Sensors”.

[2] Y. Yan, G. Chen, Sajal Das, “A Collaborattion based Storaage Management Scheme in Multimedia Sensor Networks,” IEEE/IFIP International Conference on Embedded and Ubiquitous Computing, 2008.

[3] C.E. Perkins and P. Bhagwat, “Highly Dynamic Destination-Sequenced Distance-Vector Routing (DSDV) for Mobile Computers,” Proceedings of ACM SIGCOMM 1994, pp. 234-244, August 1994.

[4] C. C Chiang, H. K. Wu. Liu, and M. Gerla, “Routing in Clustered Multi-Hop Mobile Wireless Networks with Fading Channel,” Proceedings of IEEE SICON 1997, pp. 197-211, April 1997.

[5] V. D. Park and M. S . Corson, “A Highly Adaptive Distributed Routing Algorithm for Mobile Wireless Networks,” Proceedings of IEEE INFOCOM 1997, pp. 1405-1413, April 1997.

[6] C. E. Perkins and E.M. Royer, “AdHoc On-Demand Distance Vector Routing,” Proceedings of IEEE Workshop on Mobile Computing Systems and Applications, 1999, pp. 90-100,February 1999.

[7] H. Wang, D. Peng, W. Wang, H. Sharif and H. Chen, “Interplay Between Routing and Distributed Source Coding in Wireless Sensor Network,” Proceedings of IEEE International Conference on Communications, 2007.

[8] Y. Hu, D. B. Johnson, and A. Perrig, “SEAD: Secure Efficient Distance Vector Routing for Mobile Wireless Ad Hoc Networks,” Proceedings of IEEE WMCSA 2002, pp. 3-13, June 2002.

Automatic Processing of Documents Filled in Kannada

Shruthi M
M.Tech, Signal Processing,
Siddaganga Institute of Technology, Tumakuru
Karnataka, India
mshruthi.ms@gmail.com

Dr. K. V Suresh
Professor, Dept. of ECE
Siddaganga Institute of Technology, Tumakuru
Karnataka, India
sureshkvsit@yahoo.com

***Abstract*—In this paper, we presented an automatic processing of forms filled in Kannada language. It includes 47 basic characters, 7 vowel modified consonants, 3 conjuncts and 10 numerals of Kannada language. The automatic process involves scanning of documents, which may result in skewed forms. The skewness of the form is detected using Hough line transform. The document (form) consists of printed characters and handwritten characters. A suitable pre-processing is carried out to extract only handwritten characters. Principal Component Analysis (PCA) is used to represent each character. This feature is then fed to back propagation neural network for classification. PCA has the recognition accuracy of 59.35%. Further, the performance of automatic process is improved by combining shape based features to PCA. This results in accuracy of 79.65%. This algorithm is implemented on Visual Studio using OpenCV library.**

Keywords—Back propagation; Form processing; Hue moments; Kannada; Principal Component Analysis

I. INTRODUCTION

In Indian context, many organisations such as government schools, hospitals, revenue offices and railway stations collect the information about people on paper based forms [1]. Most of these forms are in regional languages. The manual processing of these forms requires lot of work, time and also results in typographical errors, hence automatic processing of forms is preferred. In automatic form processing, data on the forms is captured and converted into machine readable format.

India is a multi-lingual and multi-script country having 18 official languages. Because of complex structure and similarity among shapes recognition of Indian scripts is very difficult. In this paper, recognition of Kannada script is considered.

The general automatic form processing (AFP) involves scanning of filled form using scanner or digital camera. The scanned form is then pre-processed to remove the uninformative variations in handwriting. The characters are then segmented and fed to suitable recognition engine. Several works are done on the recognition of Indian scripts.

The major pre-processing steps of AFP include noise removal, edge detection and morphological operations. Then the segmentation is performed to segment the text into individual characters. Thungamani M and RamakanthKumar P [2], discusses two important approaches such as classical approach where input image is divided into sub images and statistic approach where the image doesn't undergo any dissection. Mamatha H.R and SriKantamurthy K [3], proposed segmentation using projection profiles, where horizontal projection is used to segment text into different lines and vertical projection to segment individual characters.

Nethravathi et al [4] proposed an algorithm which reduces the symbol set of Kannada script. The vowel modifiers and consonant conjuncts which are not connected are considered as separate classes. Devanagari script has similar characteristics like Kannada. The recognition of this script consists of segmentation, decomposition and recognition [5]. But in this method only smaller subset of characters are considered.

An overview of character recognition methodologies with respect to offline character recognition systems such as pre-processing segmentation, representation, recognition and post processing methods are presented in [6].

The handwritten Kannada character (vowels and numerals) recognition using shape based features such as Fourier descriptor and chain codes are discussed in [7]. Support vector machine (SVM) is used as classifier and an accuracy of 95% is achieved. A brief survey on Devanagari script is presented in [8]. Performance of different feature techniques using different classifiers is tabulated. Gradient and PCA based features with neural network as classifier are found to have better recognition accuracy.

The handwritten numeral recognition of two popular Indian scripts such as Devanagari and bangla is presented in [9]. This uses multistage cascade recognition scheme using wavelet based multi-resolution representations and multi layer perceptron to achieve higher recognition accuracy. Unconstrained handwritten Kannada character recognition using very large dataset of 200 samples using ridgelet transform is discussed in [10]. To reduce the dimension of feature vector PCA is used. It is found that ridgelet offers promising result than PCA. A zone based methods for the recognition of Kannada vowels and consonants is presented in [11]. Character image is divided into 64 non-overlapped zones and crack codes are computed. SVM is used as classifier and an accuracy of 87.24% is achieved.

Literature survey records few papers on Kannada handwritten character recognition. Selecting a suitable feature extraction method is an important task to improve the

performance of system. In this paper, PCA and Hu based moments are used as features and neural network is used as classifier.

II. KANNADA SCRIPT

Handwritten character recognition of Kannada script is very challenging task because of its large dataset, shape similarity among characters and non-uniqueness in the representation of diacritics. Basic character set of Kannada is shown in Figure 1(a) and 1(b). Vowel modified consonants (kagunitha) are as in Figure 1(c). Additionally a consonant emphasis glyph called conjuncts [vattakshara] shown in Figure 1(d), exists for each 34 consonants.

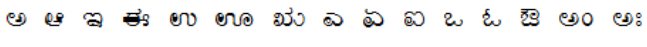

(a) Vowels

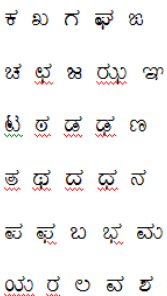

(b) Consonants

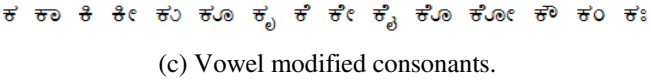

(c) Vowel modified consonants.

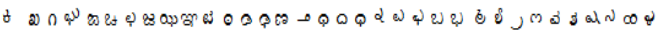

(d) Consonant conjuncts

Figure 1: Kannada character set.

This large number of dataset reduces the accuracy and increases the computational complexity of the system. This problem can be reduced by considering each of the non connected characters as separate symbols.

For automatic processing of forms template of birth certificate is created with different fields for base character, conjuncts and vowel modifiers. An example of filled form is shown in Figure 2.

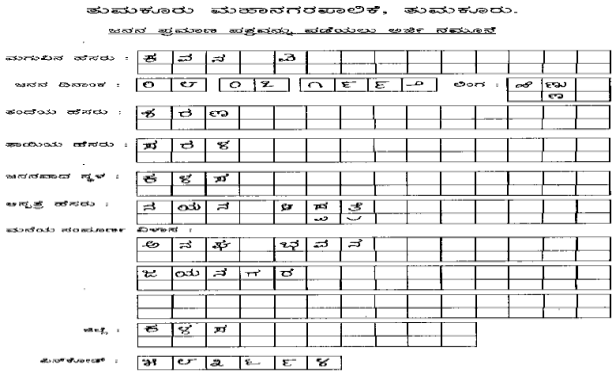

Figure 2: Template of Birth certificate.

III. METHODOLOGY

The block diagram of automatic form processing system is shown in Figure 3. It involves the scanning of filled form which then undergoes various pre-processing operations. From the pre-processed image individual characters are segmented using connected component analysis. To represent each character two feature extraction methods are used such as PCA and PCA combined with Hu moments. These extracted features are then fed to a back propagation neural network for classification.

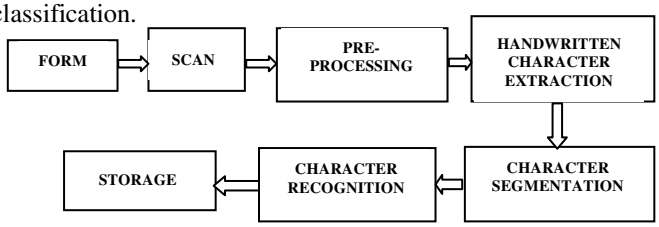

Figure 3: Block diagram of automatic form processing system

A. Pre-Processing

The scanned image undergoes various pre-processing operations to eliminate the imperfections and to remove the uninformative variations in handwriting. The major pre-processing steps include binarization, edge detection, skew detection and correction, and morphological operations as shown in Figure 4.

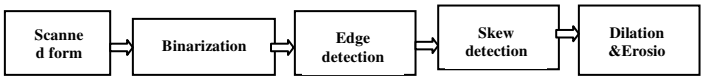

Figure 4: Pre-processing steps of AFP.

The forms filled in Kannada language are scanned using HP scanjet G3010 scanner. This scanned image is then converted to binary image. During the process of scanning the document may not be aligned properly. This inclination (skew) angle of the document is detected using Hough transform. The classical Hough transform was considered with the detection of lines in the image. The bounding boxes present in the form are used for skew detection. To make the line detection easier, edge detection using canny edge detector is performed before skew detection.

A straight line can be represented using polar parameters r and θ as:

$$r = x\cos\theta + y\sin\theta \qquad (1)$$

The parameter r represents the distance between straight line and origin and the θ represents the angle of vector from the origin to its closest point. Each point in the (x, y) domain is mapped onto the curves in the domain (r,θ) . Thus the equation (1) represents the family of straight lines passing through particular line (x, y) . If the curves of two different points intersect each other in polar space that indicates that both the points belong to the same line in image space. The angle at the point of intersection of all curves gives the angle of straight line as shown in Figure 5(b).

After finding the skew angle, the document is corrected using rotational affine transformation technique using cubic

interpolation technique. Figure 6(a) and 6(b) shows the skewed image and skew corrected image respectively.

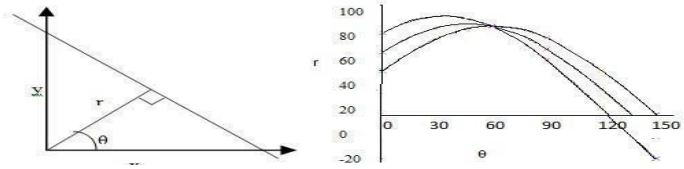

Figure 5: (a) Mapping of x and y to polar space. (b) Curves in polar space.

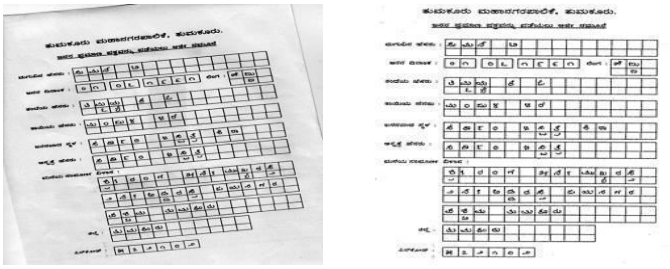

Figure 6: (a) Skewed image. (b) Skew corrected image.

The skew corrected image is then resized to 1024 x 1024. Since the form contains bounding boxes and printed characers along with the handwritten characters, morphological subtraction scheme is used to extract only the handwritten characters. This involves dilation, erosion and hole filling. Dilation adds pixels to the boundary of an object.This operation an an image *A* using structuring element *B* is shown in equation (2).

$$A \oplus B = \left\{ z \mid \left(\hat{B}\right)_z \cap A \neq \Phi \right\} \quad (2)$$

The data fields are then identified by filling holes. Then erosion is performed to etch the boundary expanded due to dilation. The erosion operation on an image *A* using structuring element *B* is given by

$$A \Theta B = \left\{ z \mid \left(B\right)_z \subseteq A \right\} \quad (3)$$

Then hole filling algorithm is applied by considering all 8 connected characters as foreground objects and boundary boxes as background objects. The resulting image contains only the handwritten characters.

B. Handwritten Character Segmentation

The characters are then segmented into individual characters using connected component analysis. Each connected component is then labelled. Equation (4) gives the expression for finding connected components.

$$X_k = (X_{k-1} \oplus B) \cap A \quad k = 1,2,3 \quad (4)$$

where $X_0 = p$, and b is a suitable structuring element.

By using the properties of region each character is cropped and stored.

C. Feature Extraction

In this work, two feature extraction techniques such as PCA and PCA+Hu moments for handwritten Kannada character recognition are discussed.

PCA transforms correlated variables into uncorrelated variables retaining maximum amount of variations. This helps to operate on data and make predictions. Each image is converted to single vector and stored as columns of matrix PXN . Mathematically principal components for PXN matrix $[X_1, X_2, ...X_N]$ are obtained by subtracting mean from each column. The resultant matrix is given by $B = [\hat{X}_1, \hat{X}_2, ...\hat{X}_N]$. Then the covariance matrix S is obtained by $S = \frac{1}{N-1} BB^T$. The eigen values and eigen vectors are calculated using $P^T SP = D$ where D is a diagonal matrix with the eigen values and P is a matrix of eigen vectors. Eigen vectors are arranged according to the descending values of the eigen values. The weight matrix W is determined as $W = PB^T$. This weight matrix is used for classification of characters. Principal Component Analysis (PCA) without dimensionality reduction is used.

Shape is one of the important features used for human perception, due to the fact that characters can be distinguished by their shapes. One of the ways to extract the shape details from the image is to extract their moments. Moments which are invariant to translation, scaling and rotation were introduced by HU in 1962. The seven invariant Hu moments are given by

$$hu[0] = \eta_{20} + \eta_{02}$$

$$hu[1] = \left(\eta_{20} - \eta_{02}\right)^2 + 4\eta_{11}^2$$

$$hu[2] = \left(\eta_{30} - 3\eta_{12}\right)^2 + \left(3\eta_{21} - \eta_{03}\right)^2$$

$$hu[3] = \left(\eta_{30} + \eta_{12}\right)^2 + \left(\eta_{21} + \eta_{03}\right)^2$$

$$hu[4] = \left(\eta_{30} - 3\eta_{12}\right)\left(\eta_{30} + \eta_{12}\right)\left[\left(\eta_{30} + \eta_{12}\right)^2 - 3\left(\eta_{21} + \eta_{03}\right)^2\right] + \left(3\eta_{21} - \eta_{03}\right)\left(\eta_{21} + \eta_{03}\right)\left[3\left(\eta_{30} + \eta_{12}\right)^2 - \left(\eta_{21} + \eta_{03}\right)^2\right]$$

$$hu[5] = \left(\eta_{20} - \eta_{02}\right)\left[\left(\eta_{30} + \eta_{12}\right)^2 - \left(\eta_{21} + \eta_{03}\right)^2\right] + 4\eta_{11}\left(\eta_{30} + \eta_{12}\right)\left(\eta_{21} + \eta_{03}\right)$$

$$hu[6] = \left(3\eta_{21} - \eta_{03}\right)\left(\eta_{21} + \eta_{03}\right)\left[3\left(\eta_{30} + \eta_{12}\right)^2 - \left(\eta_{21} + \eta_{03}\right)^2\right] - \left(\eta_{30} - 3\eta_{12}\right)\left(\eta_{21} + \eta_{03}\right)\left[3\left(\eta_{30} + \eta_{12}\right)^2 - \left(\eta_{21} + \eta_{03}\right)^2\right]$$

Where η_{pq} is the $(p+q)$ th order normalised central moment with:

$$m_{pq} = \iint_A x^p y^q f(x,y)\,dx\,dy$$

$$\eta_{pq} = \frac{m_{pq}}{m_{00}^{\gamma}} \quad \text{and} \quad \gamma = 1 + \frac{p+q}{2}$$

D. Handwritten Character Classification

The classification stage is the decision making part of a recognition system and it uses the features extracted in the previous stage. The classification capability of the network depends on the architecture and learning rule. The architecture considered in this paper is feed forward back propagation neural network. Each image is resized to 25 x 20, thus the input layer has 500 neurons. Here, only the recognition of 67 characters of Kannada is considered. Thus, the number of output neurons is 67. All the neurons in the architecture uses sigmoid as output function given by equation (4).

$$f(x) = \beta * (1 - e^{-\alpha x}) / (1 + e^{-\alpha x}) \qquad (4)$$

The standard sigmoid with β =1, α=1 is shown in Figure 7

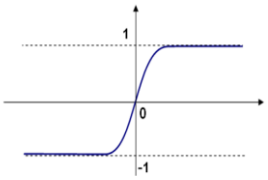

Figure 7: Symmetrical sigmoid function.

The network training parameters are shown in Table 1.

Table 1:Neural network training parameters.

Number of Input nodes	500
No. of Hidden layer	1
No. of Hidden nodes	135
Training epochs	50000
Goal achieved	10e-6
No. of Output nodes	67

IV. EXPERIMENTAL RESULTS

For automatic form processing template of the birth certificate created with all the relevant fields is considered. The form undergoes various pre processing operations such as dilation, data fields identification and erosion. The eroded image is then multiplied with binary image as shown in Figure 11. Hole filling is performed to extract only the handwritten characters, the resulting image is shown in Figure 12. Bounding box is fitted to each individual character using connected component analysis as shown in Figure 13. Features are extracted from each character and recognised using neural network. The recognised characters are then stored in relevant fields as shown in Figure 14. This algorithm is implemented on Microsoft Visual Studio 2010 using OpenCV library.

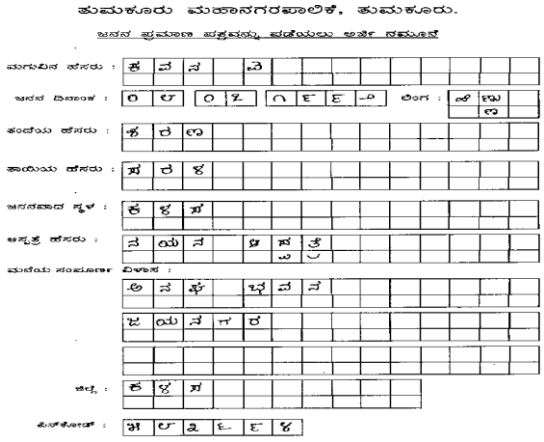

Figure 8: Original Image

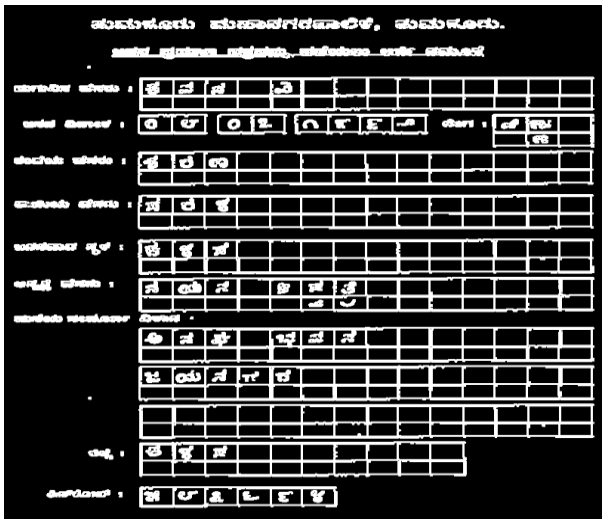

Figure 9: Dilated Image.

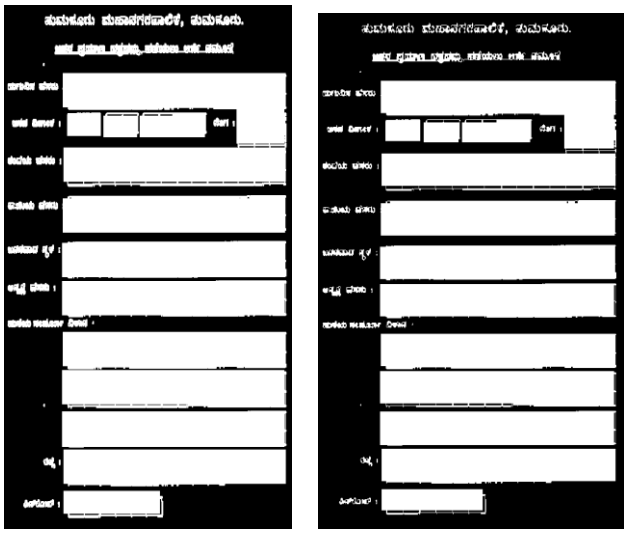

Figure 10: (a) Identified data entry fields.(b) Eroded image

The recognised characters are stored in database in relevant fields as shown in Figure

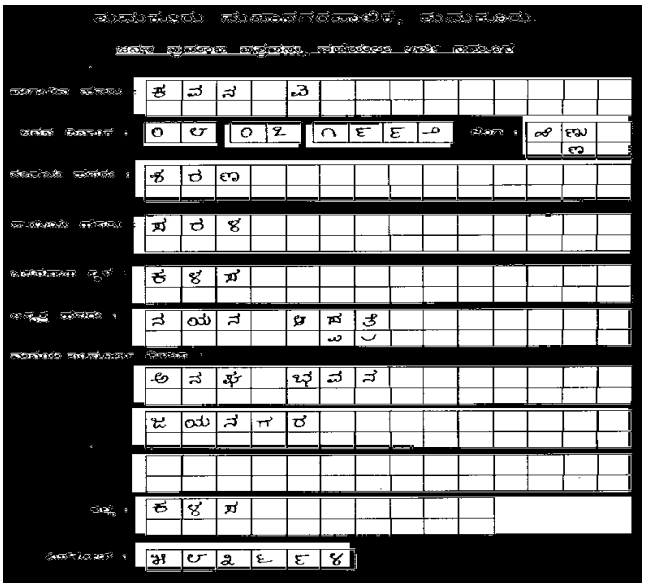

Figure 11: Eroded image multiplied with original image.

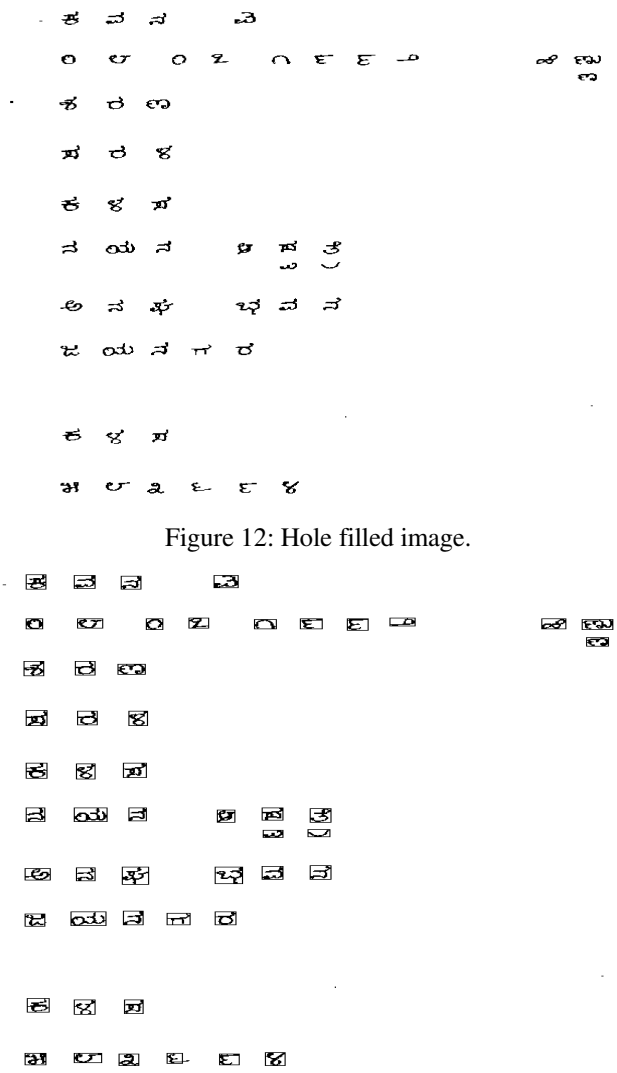

Figure 12: Hole filled image.

Figure 13: Segmentation using connected component analysis.

Figure 14: Recognised characters stored in relevant fields.

Performance of the feature extraction methods are compared for different number of classes.

Table 2: Recognition accuracy of PCA and PCA+Hu.

No. of classes	PCA(%)	PCA+Hu (%)
Numbers (10)	99.3	99.4
Vowels (13)	94	95.2
Numbers+Vowels(23)	71	82.97
Consonants(34)	68	71.82
Basic characters (67)	59.35	79.65

PCA represents the image information only in one direction where the variance is maximum. To improve the accuracy of PCA, shape based features such as Hu moments are combined. With the additional shape information, accuracy is increased to 79.65%.

V. CONCLUSION

In automatic processing of information sheets filled in Kannada, image is captured using scanner. The scanned image then undergoes various pre-processing operations. The skewness of the document is detected using Hough transform. The printed characters and the bounding boxes present in the form are removed using morphological subtraction. Two feature extraction methods such as PCA and Hu are used. The performance of PCA which has the accuracy of 59.35% is improved to 79.65% by combining Hu moments.

REFERENCES

[1] Afef Kacem, Asma Saidani, Abdel Belaid, "A system for an automatic reading of student information sheets", International Conference on Document Analysis and Recognition, pp 1265-1269, 2011.

[2] M. Thungamani and P. Ramakanth Kumar, "A Survey Methods and Strategies in Handwritten Kannada Character Segmentation", International Journal of Science Research, Vol 1, Issue 1, June 2012.

[3] H.R Mamatha and and K. Srikantamurthy, "Morphological operations and projection profile based segmentation of handwritten Kannada document", International Journal of Applied Information Systems (IJAIS), Vol 4, No.5, October 2012.

[4] Nethravathi B, Archana C.P, Shashikiran K, A.G Ramakrishnan and VIjay Kumar, "Creation of huge annotated database for Tamil and Kannada OHR", 12th IEEE International Conference on Frontiers in Handwriting Recognition, Nov 2010, Pages 415-420.

[5] R M. K. Sinha and H. N. Mahabala, "Machine Recognition of Devanagai Script", IEEE Transactions on Systems, Man and Cybernetics, Vol. Smc 9, No 8, August 1979.

[6] Nafiz Arica and Fatos T. Yarman-Vural, "An overview of character recognition focused on offline handwriting", IEEE Transactions on Systems, Man and Cybernetics-Part C: Application and Reviews, Vol 31, No. 2, May 2001.

[7] Rajput G.G and Horakeri R, "Shape descriptors based handwritten character recognition engine with application to Kannada characters", IEEE International Conference on Computer and Communication Technology, Sep 2011, Pages 135-141.

[8] R. Jayadevan, Satish R Kolhe, Pradeep M Patil and Umapada Pal, "Offline recognition of Devanagari script: A survey", IEEE Transactions on Systems, Man and Cybernetics –Part C: Applications and Reviews, Vol 41, No. 6, November 2011.

[9] Ujjwal Bhattacharya, and B.B. Chaudhuri, "Handwritten Numeral Databases of Indian Scripts and Multistage Recognition of Mixed Numerals", IEEE Transactions on Pattern Analysis and Machine Intelligence, Vol. 31, No. 3, March 2009.

[10] C. Naveena and V.N. Manjunath Aradhya, "An Impact of Ridgelet Transform in Handwritten Recognition: A Study on Very Large Dataset of Kannada Script", IEEE 2011 World Congress on Information and Communication Technologies, Pages: 618-621, December 2011.

[11] Ganpat Singh G Rajput and Rajeshwari Horakeri, "Zone based Handwritten Kannada Character Recognition Using Crack code and SVM", International Conference on Advances in Computing, Communications and Informatics (ICACCI), Publisher: IEEE, Aug 2013, Pages 1817-1821.

Chaos based Symmetric Encryption

Ms. Baby H.T.
Assistant Professor
Department of ECE
GEC,Hassan-573201
babygowda@gmail.com

Dr.Sujatha B.R.
Associate Professor
Department of ECE
MCE,Hassan-573202
brshsn61@gmail.com

***Abstract*—** In recent decades, cryptography is being used extensively for providing security on the Internet. Also cryptography has been of interest primarily to the military and diplomatic communities. In this paper, Chaos based Symmetric Encryption has been done based on a chaotic function to generate different multiple keys. It is seen that negligible difference in parameters of chaotic function generates completely different keys as well as cipher text. The main motive for developing the chaos based cryptosystem is to attain encryption that provides high security at higher speed but with lower complexity and cost over the conventional encryption algorithms.

IndexTerms—Cryptology, Cryptography, Encryption technique, Decryption Technique, Chaos Function, Logistic map, plain text, Cipher text.

I. INTRODUCTION

With the increased automation and use of internet in all works of life-military systems to business managed by common person, information security has become one of the major hindrances in the effective use of information technology in public domain. Information needs to be secured as they are valuable resources of any organization like other resources such as hardware, software, employee, financial resources etc. Several measures are also being taken to protect the resources and to prevent unlawful downloads of music, videos and to secure the system from different types of attacks. Also to avoid unauthorized access and illegal usage of information being transferred over the insecure communication channel, security systems need to be built and deployed. One way to achieve the goal of secure data transmission is to convert the data into unintelligible form prior to transmission. Most of the security systems rely on the use of cryptographic techniques to provide necessary security to the user's sensitive data against illegal usage. Modified version of traditional data encryption algorithms are needed to provide good quality and performance in a secure communication network environment. Cryptography also ensures the secrecy and authentication of information. It addresses a wide range of problems such as confidentiality, authenticity, integrity and non-repudiation. Several challenges in network security have encouraged researchers to develop chaos based data encryption techniques to provide a high degree of randomization and provide difficulties to hackers.

In a cryptographic application requiring ultimate security KEY is necessary for which a Random Number Generator is required. There are several physical phenomena presenting random like features, ranging from the Brownian motion to quantum effects. All these phenomena arise from the basic physical processes at the molecular or lower level, and are usually referred as "noise". Chaos is one of the possible behaviors associated with evolution of a nonlinear physical system and occurs for specific values of system parameters. Thus chaos based text encryption has suggested a new and efficient method for fast and secure data encryption [1].

The rest of the paper is organized as follows. In section II, chaos theory, cryptography, chaos based cryptography are described. In section III and IV, the implemented cryptosystem is described with an example. In section V, analysis of security of keys for the proposed approach is provided. In section VI, the paper is concluded.

II. CHAOS Theory

Cryptology is the science of encrypting data for security. It is mainly categorized into Cryptanalysis and Cryptography [2].

A. Cryptanalysis

Cryptanalysis is a procedure used to decipher the code into plain text by determining the key being used. It can also be termed as positive hacking to determine the robustness of the encryption technique used. It is divided into two types: *Passive attacks* and *Active attacks* [2].

B. Cryptography

Cryptographic system is the combination of encryption and decryption system. Based on the number of keys used to perform Encryption and Decryption they are mainly classified into two types.
1. Symmetric Encryption or Conventional Encryption
2. Asymmetric Encryption or Public Key Encryption

In Symmetric encryption, both encryption and decryption algorithms uses the same key to perform the operation. There are two requirements for secure use of Conventional encryption:

1. Strong encryption algorithm.
2. Sender and receiver must have obtained copies of the secret key in a secure fashion and must keep the key secure.

Asymmetric algorithms rely on one key for encryption and a different but related key for decryption. These algorithms have the following important characteristics:

1. It is computationally infeasible to determine the decryption key given only knowledge of the cryptographic algorithm and the encryption key.
2. Either of the two related keys can be used for encryption, with the other used for decryption.

In both the schemes the important component providing security is the 'KEY' and cryptographic algorithms such as DES, RSA, AES etc., are well known algorithms. Literature provides several schemes to generate KEYS which cannot be easily understood and generated by unintended recipients. Several researchers have given several methods of generating security keys and the common understanding is the KEY should be highly random.

C. Chaos Theory

Chaos theory is based on the observation that simple rules when iterated can give rise to apparently complex behavior. Systems which are basically non-linear and exhibiting apparently random behaviors for certain range of values of system parameters are referred to as Chaotic [3]. However, the solutions or trajectories of the system remain bounded within the phase space. This unstable state has a strong dependence on the values of the input parameters and initial operations of the system**.**

Chaos though appears to have noise characteristics has greater advantage over noise because a chaotic system in general has deterministic property. However an operational (meaning one that captures most essential features) definition of a chaotic system is: (i) the solution must be aperiodic (ii) the solution must be bounded (iii) the solution must be exponentially sensitive to initial conditions [4-5].

The rules that govern a chaotic system must satisfy certain properties: (i) The rule must be nonlinear (ii) In the case of maps; it must be non-invertible if it is one dimensional [6-10].

III. METHODOLOGY

A Chaos based Symmetric key encryption technique which uses one or more keys for encryption and decryption process is described in this paper. These keys are similar for both encryption and decryption process at any instant of time. Here we are using one-dimensional simple logistic map to generate the Chaos keys as given below:
For n=1 to j
X_{n+1}= {A*X_n (X_n-1)} *MOD* 256
Where A= any integer (1, 2, 3,…..)
X_n and X_n-1 = initial value of chaotic function which is (2, 3,…..)
j = Number of keys
Here, A and X_n are the initial parameters. A small change in these initial parameters causes large amount of nonlinear change in the Encrypted message.

A. KEY generation Scheme

1. To begin with, generate the Chaos KEYS by using the logistic map function at both ends (sender and receiver) by using equation (1).
   For n=1 to j
   X_{n+1}= {A*X_n (X_n-1)} MOD 256 (1)
2. Complexity of keys is increased by applying a gray code on X_{n+1} so that the keys are independent of each other.
3. Represent the keys in 8 bit binary form.

B. Encryption Scheme

The Chaos based Encryption equation will be of the form $C_i = E_{ki} (P_i)$ where P_i is the Plain text character, C_i Cipher text character and K_i represents the key value corresponding to the Plain text character and E_{ki} is the encryption function using k_i.
The Encryption procedure is as follows:
Step 1: Convert each Plain text character into equivalent ASCII value .
Step 2: Convert each ASCII Value of Plain text into 8 bit binary number.
Step 3: Perform XOR operation of 8 bit binary number obtained from step 1 with the corresponding CHAOS KEY.
Step 4: Find the 1`s complement of resultant value.

Step 5: Convert that value to corresponding character by using ASCII table, which is un-Readable cipher text.

C. Decryption Scheme

The Chaos based Decryption equation will be of the form $P_i = D_{ki}(C_i)$ which is the reverse process of Encryption algorithm.
The Decryption procedure is as follows:
Step 1: Convert each Cipher text character into equivalent ASCII value.
Step 2: Convert each ASCII character into 8 bit binary form.
Step 3: Find the 1`s complement of the resultant value.
Step 4: Perform XOR operation of 8 bit binary number obtained from the step 3 with the corresponding CHAOS KEY.
Step 5: Convert that value to corresponding character by using ASCII table, which is the Plain text.

IV. Simulation Example

A. KEY Generation

The One–dimensional Chaotic logistic map equation is assumed as $X_{n+1}= \{A*X_n (X_n-1)\}$ *MOD* 256
For initial parameters of A=2, X_0 =3 and j=4 we obtain X_{n+1} as follows:
X_{n+1} = *12, 8, 112, 32*

Adding further complexity to the keys, the gray code equivalent of the obtained random numbers X_{n+1} is obtained. Therefore, Keys are represented as K_1= 10, K_2 =12, K_3 =72, K_4 = 48.

Finally, these are used as the Chaos secret keys for both encryption and decryption.

B. Encryption Algorithm

Let Plain text P =APPLE
The encrypted Cipher text C obtained is ´**£ç***f*°

The obtained cipher text is in the un-readable form and also repeated characters in the plain text are coded into different characters.

C. Decryption Algorithm

Decryption algorithm converts the cipher text into plain text by using the same keys.
For Cipher text C= ´£ç*f*°

We obtain the Plain text P as APPLE

V. SIMULATION RESULTS

Matlab is used for KEY generation and encryption/decryption operations. The code is tested for different initial conditions which provide different chaos keys and different cipher texts for the same plain text even with slight changes in the initial conditions. The simulation results have been done for 3 different cases. In Case1 and Case2 we show that even with slightly changed initial values assumed for generating KEYS an entirely different cipher text is obtained. In Case3 we show how using a different initial value by a hacker results in incorrect decryption.

Case 1:
Let initial values A=2, X_n=3
Plain text P = Dept. of E&C, Government Engineering College Hassan-573201.
Generated keys for Encryption

16 12 72 95

Generated Cipher text is

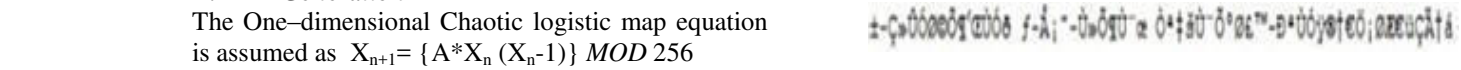

Case 2:
Let initial values A=4, X_n=7
Plain text P = Dept. of E&C, Government Engineering College, Hassan-573201.
Generated keys for Encryption

252 80 192 0

Generated Cipher text is

From the above results it is clear that,

i) Even a small change in the initial parameters of A and X_n causes a change in the KEY values which proves the Non-Linearity and randomness.

ii) For the same plain text a small change in the initial parameters produces a significant change in the cipher text.

Case 3: a) At the transmitter side:

Let initial values A=2, X_n=3

Plain text P = Dept. of E&C, Government Engineering College, Hassan-573201.

Generated keys for Encryption

10 12 72 48

Generated Cipher text is

±-Ç»ÛÓØ®Õ¶'ŒÙÓδ ƒ-Å¡˜-Ù»Õ¶Ù¨œ Ò°‡šÙ¨Õ°Ø£™-Ð°ÙÓý®†€Ö¡ØÆëüÇÃ†á

b) At the receiver side:

Assume that hacker has assumed the initial values as A=9, X_n=5

Generated keys for Decryption

238 226 142 0

Generated plain text from the received Cipher text is

‹¶DÊÎ©VÄ«àsÈÎ _'‹'^‰‹¨DÄ«¨W €£U-‡¨WÄ-®\'‹¡UÈÎŽQ— §^ÉÛñ ÖÞ÷

Plain text generated is not the original plain text. Therefore it is clear that if hacker tries to obtain the plain text from the ciphered text with assumed initial values it is impossible to obtain the original plain text even though the algorithms of KEY generation and Decryption is known to him.

VI. CONCLUSION

In this paper, a new chaos based text symmetric encryption using MATLAB has been implemented. This technique is able to protect the original text with a high level of security due to the randomly generated keys which are sensitive to initial conditions. The experimental results have demonstrated the excellent performance of the CHAOS based KEY generation technique.

REFERENCES

[1] Ankur A. Khare, "Secure and Fast Chaos based Encryption System", I.J. Computer Network and Information Security, 2014.

[2] William Stallings, "Cryptography and network Security principles and practice". 2006 Pearson Education.

[3] Brad Aimone, Stephen Larson "Chaotic Circuits and Encryption", Neurophysics Lab, pp. 1-12, 2006.

[4] A. Masmoudi, W. Puech and M.S. Bouhlel, "A new joint lossless compression and encryption scheme combining a binary arithmetic coding with a pseudo random bit generator", (IJCSIS) International Journal of Computer Science and Information Security, Vol. 8, No. 1, pp. 170-175, 2010.

[5] G. Alvarez, F. Montoya, M. Romera, G. Pastor, "Cryptanalysis of a Chaotic Encryption System", pp. 191-196, 2000.

[6] A. Palacios, H. Juarez, "Cryptography with cycling chaos", ELSEVIER, pp. 345-351, 2002.

[7] Muhammed Rezal, Kamel Ariffin, " Chaos Based Cryptography an Alternative to Algebraic Cryptography" Research Bulletin Institute for Mathematical Research, Volume 2, pp: 41-47, 2008.

[8] Chen Dongming, Zhu Zhiliang, Yang Guangming, "An improved Image Encryption Algorithm Based on Chaos", IEEE the 9th International Conference for Young Computer Scientists, pp: 2792-2796, 2008.

[9] Bogdan Cristea, Constantin Cehan, "Applications of Chaos Theory in cryptography", Military Equipment and Technologies Research International Conference, Bucharest, Romania, pp: 1-5, 2002.

[10] Dubrova E., Teslenko M. and Tenhunen H., "On Analysis and Synthesis of (n, k)-non- linear Feedback Shift Registers," Design, Automation and Test in Europe, pp: 1286-1291, 2008.

A Hybrid Approach For Image Denoising

B. N. Aravind
Research Scholar, SIT, Tumkur
Dept. of Electronics and Communication Engg.
Kalpataru Institute of Technology
Tiptur, Karnataka, India 572202
e-mail: aravin_bn@yahoo.com

K. V. Suresh
Dept. of Electronics and Communication Engg.
Siddaganga Institute of Technology
Tumkur, Karnataka, India 572103
e-mail: sureshkvsit@yahoo.com

***Abstract*— In today's world, image plays an important role in conveying information. Due to atmospheric conditions, camera sensors and/or lighting conditions the image usually gets degraded due to noise and blur. In this paper, degradation due to noise is considered and is assumed to be additive Gaussian. Here, a denoising method that uses both spatial and transform domain is proposed. Discrete wavelet transform performs denoising in transform domain followed by nonlocal means in spatial domain to get improved performance. The simulation results indicate that the proposed method shows an improvement over existing methods.**

Keywords – image denoising; wavelet transform; neighborhoods; nonlocal means.

I. INTRODUCTION

Image denoising is an ill-posed problem. Theoretically, it is difficult to recover an image since the knowledge about the origin, type and amount of noise is not fully known. During past two decades several methods have been proposed to improve the performance of denoising. These methods are broadly classified into two categories; Spatial and transform domain denoising.

A. Spatial domain denoising

The procedures where the denoising process is directly applied on intensity levels directly is considered as spatial domain method. Initial methods are developed using local mean and variance. Local Wiener filter [1] is one among them. The method assumes that, throughout the image, the gray level values will be similar. But this is not true for edges. Since the variance is high at edges, it fails to remove the noise in such regions [2]. Tomasi and Manduchi [3] introduced a non-linear filter known as bilateral filter. It is basically a non-iterative procedure and used photometric and geometric similarities among the neighborhood. This method demands for a bigger spatial window to make it non-iterative process, and choosing of larger window leads to smoothing of edges. It can also be used as iterative process and in such case, tuning of parameters is necessary to achieve good results [4]. Total variation (TV) [5] uses graphs and edge derivatives in order to find edges. TV is iterative procedure and it requires the fine tuning of fidelity and regularity terms to obtain better quality of edge reconstruction and noise suppression [6]. Nonlocal means (NLM) [6]–[8] considers that, an image consists of repeating structures and averaging over them will reduce the noise. This method is highly computational [9]. An image is modeled as Markov random field (MRF) and discontinuity adaptive (DA) method is used for denoising [10]. This method is iterative and needs to take care of parameters to obtain global minima.

B. Transform domain denoising

Literature indicates the existence of several transforms; Fourier transform, short time Fourier transform, wavelet transform, cosine transform, curvelets, contourlets etc. Among these, our interest of study is the wavelet based image denoising methods and hence our discussion is limited to that only. In wavelet based denoising, thresholding is the popular method. A pioneering work in this is done by introducing soft and hard thresholding [11]. Soft thresholding is a shrink or kill process and hard thresholding is keep or kill process. They are defined as;

$$T_{soft}(w) = \begin{cases} 0 & if\ |w| \le T \\ sign(w)(|w| - T) & if\ |w| > T \end{cases} \quad (1)$$

$$T_{hard}(w) = \begin{cases} 0 & if\ |w| \le T \\ w & if\ |w| > T \end{cases} \quad (2)$$

and $T = \hat{\sigma}_n\sqrt{2\log(n)}$; where $\hat{\sigma}_n$ is the estimation of the standard deviation of noise and n is the total number of the wavelet coefficients in detailed subband. The advantage of this algorithm is adaptivity and smoothness. But this algorithm tends to blur edges and retain artifacts. As a solution, Translation invariant (TI) denoising is introduced [12]. It takes the average over several shifted and denoised images and thereby reducing the artifacts. The methods is further taken by using multiwavelets to obtain better results [13]. Later it was identified that, in wavelets, neighboring coefficients has an effect on the current coefficient to be thresholded. A thresholding scheme is proposed by considering neighboring coefficients [14]. The results indicated an improvement over term-by-term method of

denoising. An improvement is obtained in the same method by using multiwavelets [15]. Neighshrinksure [16] uses steins unbiased risk estimate in order to achieve minimum error. A child-parent relationship is adopted between successive decompositions and bivariate shrinkage [17], [18] is introduced. In this method, if the parent coefficient is having the noise then it's obvious that, the child coefficients will also have noise.

Denoising is always a tradeoff between the removal of noise and quality of reconstructed image. Hence, some of the methods oversmooth the edges and some other retains artifacts. In this paper, we propose to use a two stage denoising scheme that involves neighshrinksure in wavelet domain as first stage and NLM in spatial domain second stage of denoising. It provides better noise suppression and artifact free results.

II. Implementation Details

The degradation model under consideration is the noise and hence the model is given by [19],

$$y = x + \eta \tag{3}$$

where, y, x are corrupted and original image respectively and η is Gaussian noise.

When the wavelet transform is applied to an image, most of the information is confined among few large valued coefficients. The transform is linear and hence the noise remains Gaussian even in wavelet domain [20].

Denoising is achieved both in transform and spatial domain in a sequential manner. Initial smoothing is achieved by using neighshrinksure [16]. Different threshold is calculated for different subbands using following procedure;

$$SURE(w_s, \lambda, L) = N_s + \sum_n ||g_n(w_n)||^2 + 2\sum_n \frac{\partial g_n}{\partial w_n} \tag{4}$$

The threshold N_s and neighbor window size L_s for the subband s is;

$$(\lambda^s, L^s) = arg \min_{\lambda, L} SURE(w_s, \lambda, L) \tag{5}$$

The neighshrinksure reduces the noise but artifacts are retained. The output of the first step is followed by the second step where NLM is applied to the result of first step in transform domain. NLM uses self-similarity concept and averaging to reduce noise and to remove artifacts. If P, Q1 and Q2 are the neighbors of each other, then NLM is given by,

$$NL[y](P) = \sum_{J \in I} w(p,q) y(q) \tag{6}$$

where, $w(p,q)$ is the weight meeting the condition $0 < w(p,q) \leq 1$ and $\sum_q w(p,q) = 1$; y is noisy representation. The final resultant image out of this will be noise suppressed and artifact free.

III. Results and Discussion

In this section, a comparison between existing methods and proposed method is presented. Peak signal to noise ratio (PSNR) is considered for quantitative evaluation and is given by,

$$PSNR = 10log_{10}\frac{255^2}{MSE} \tag{7}$$

where, MSE represents the mean square error. Quality is the similarity measure and is done by using mean structural similarity index (MSSIM) [27] given by;

$$MSSIM(x, \hat{x}) = \frac{1}{M}\sum_{j=1}^{M}(x_j, \hat{x}_j) \tag{8}$$

where, x_j and $\hat{x}_j$ is the original and reconstructed image respectively. M is the number of gray levels in the j^{th} local window.

Fig. 1 shows the test images considered for simulation (Lena, Barbara and Boat). The noisy versions are generated by adding Gaussian noise of different variance values. Soft thresholding [11], cycle-spinning [12], neighshrinksure [16], multispinning [22] are used for comparison with the proposed method. Fig. 2 shows the denoising of the Lena image degraded by the Gaussian noise of variance 20 (Fig. 2(a)). Fig. 2(b) shows the image denoised by soft thresholding. It can be observed that, the edges are over-smoothed and around the edges the artifacts are created. Cycle-spinning is also implemented using soft thresholding but over cyclically shifted images. The resultant averaged image will have reduced artifacts but the smoothness will prevail (Fig. 2(c)). Neighshrinksure is a neighborhood process and provides better results than that of term-by-term processes (Fig. 2(d)). It is good in reducing noise but as the noise increases, it creates artifacts. Multispinning uses neighborhood process for thresholding and is applied over randomly shifted images. It is reconstructed and averaged to get single image. It reduces artifacts but creates washing effect and is shown in Fig. 2(e). The result of proposed method is provided in Fig. 2(f). It can be observed that, in the reconstructed image the noise is suppressed and is free from artifacts. For better clarity of visualization, a part of the image is zoomed and shown in Fig. 3. The simulation is also done on Barbara and Boat image and obtained results are found to be better.

Table 1 and Table 2 shows the quantitative analysis (PSNR) and similarity index (MSSIM) respectively. It can be observed that, except at one case in all remaining, the proposed method provides better results.

IV. Conclusion

In this paper, two-level image denoising is proposed for suppressing additive Gaussian noise. The results obtained by proposed method is compared with various wavelet based techniques. It indicates that, our method provides an improvement over existing methods. For quantitative

analysis, PSNR and MSSIM are tabulated. The results depict the improvement in the quality.

(a) (b) (c)

Fig. 1. Images considered for simulation (a) Lena (b) Barbara (c) Boat

(a) (b) (c)

(d) (e) (f)

Fig. 2. Denoising of Lena image using various wavelet based methods. (a) Image with noise variance 20. (b) Soft thresholding (c) Cycle-spinning (d) Neighshrinksure (e) Multispinning (f) Proposed method.

(a) (b) (c)

(d) (e) (f)

Fig. 3. A part of Fig. 2(a) to (f) respectively, is zoomed to visualize the result better.

(a) (b) (c)

(d) (e) (f)

Fig. 4. Denoising of Barbara image using various wavelet based methods. (a) Noisy image with noise variance 20. Denoised by (b) Soft thresholding (c) Cycle-spinning (d) Neighshrinksure (e) Multispinning (f) Proposed method.

TABLE I. QUANTITATIVE ANALYSIS: PSNR (dB)

σ	Soft thresholding	Cycle-spinning	Neighshrinksure	Multispinning	Proposed method
Lena (512 × 512)					
10	32.3150	33.2535	34.2472	34.6043	**34.7994**
20	28.7052	29.7462	30.8608	31.1886	**32.0354**
30	26.5465	27.5761	28.9554	29.2425	**30.1999**
Barbara (512 × 512)					
10	29.9923	30.8175	32.6344	32.8938	**33.3497**
20	26.2656	27.0263	28.6142	28.9220	**29.7172**
30	24.2154	25.0307	26.4020	26.7864	**27.5072**
Boat (512 × 512)					
10	30.7081	31.5439	32.6133	**32.8561**	32.7113
20	27.3385	28.1711	29.0937	29.3193	**29.7392**
30	25.3045	26.2126	27.1258	27.3892	**27.9201**

TABLE II. STRUCTURAL SIMILARITY MEASURE: MSSIM

σ	Soft thresholding	Cycle-spinning	Neighshrinksure	Multispinning	Proposed method
Lena (512 × 512)					
10	0.9274	0.9452	0.9592	0.9615	**0.9622**
20	0.8675	0.8999	0.9171	0.9198	**0.9317**
30	0.8129	0.8560	0.8792	0.8797	**0.8999**
Barbara (512 × 512)					
10	0.9173	0.9396	0.9649	0.9659	**0.9693**
20	0.8334	0.8688	0.9179	0.9170	**0.9310**
30	0.7672	0.8077	0.8737	0.8680	**0.8888**
Boat (512 × 512)					
10	0.9072	0.9273	0.9556	0.9571	**0.9575**
20	0.8240	0.8550	0.8975	0.9009	**0.9069**
30	0.7602	0.7974	0.8462	0.8501	**0.8612**

REFERENCES

[1] J. Lee, "Digital image enhancement and noise filtering by use of local statistics," *IEEE transactions on pattern analysis and machine intelligence*, vol. 2, pp. 165–168, 1980.

[2] F. Jin, L. Fifguth, L. Winger, and E. Jernigan, "Adaptive wiener filtering of noisy images and image sequences," *IEEE proceedings of the international conference on image processing*, vol. 3, pp. 349–352, 2003.

[3] C. Tomasi and R. Manduchi, "Bilateral filtering for gray and color images," *IEEE proceedings of international conference on computer vision*, pp. 839–846, 1998.

[4] M. Elad, "On the origin of the bilateral filter and ways to improve it," *IEEE transaction on image processing*, vol. 11, pp. 1141–1151, 2002.

[5] F. C. Tony, S. Osher, and J. Shen., "The digital TV filter and nonlinear denoising," *IEEE transaction on image processing*, vol. 10, pp. 231–241, 2001.

[6] A. Buades, B. Coll, and J. M. Morel, "Image denoising methods, a new non-local principle," *International Journal of Computer Vision, Springer*, vol. 52, pp. 113–147, 2010.

[7] A. Buades, B. Coll, and J. M. Morel, "Image denoising by non-local averaging," *IEEE Proceedings of the International Conference on Acoustics, Speech and Signal Processing*, vol. 2, pp. 25–28, 2005.

[8] A. Buades, B. Coll, and J. M. Morel, "Non-local image and movie denoising," *International Journal of Computer Vision, Springer*, vol. 76, pp. 123–139, 2008.

[9] M. Mahmoudi and G. Sapiro, "Fast image and video denoising via nonlocal means of similar neighborhoods," *IEEE signal processing letters*, vol. 12, pp. 830–842, 2005.

[10] B. N. Aravind and K. V. Suresh, "A discontinuity adaptive prior for image denoising," *International Journal of computer applications*, vol. 110, pp. 13–19, 2015.

[11] D. L. Donoho, "Denoising by soft thresholding," *IEEE transaction on information theory*, vol. 41, pp. 613–627, 1995.

[12] R. R. Coifman and D. L. Donoho, "Translation invariant denoising," *Wavelet and statistics, Springer-Verlag*, vol. 103, pp. 125–150, 1995.

[13] T. D. Bui and G. Y. Chen, "Translation invariant denoising using multiwavelets," *IEEE transaction on signal processing*, vol. 46, pp. 3414–3420, 1998.

[14] T. Tony Cai and W. S. Bernard, "Incorporate information on neighboring wavelet coefficients," *Sankhya*, vol. B63, pp. 127–148, 2001.

[15] G. Y. Chen and T. D. Bui, "Multiwavelet denoising using neighboring coefficients," *IEEE signal processing letters*, vol. 10, pp. 211–214, 2003.

[16] Z. Dengwen and C. Wengang, “Image denoising with an optimal thresholding and neighboring window,” *Pattern recognition letters, Elsevier*, vol. 29, pp. 1694–1697, 2008.
[17] L. Sendur and W. S. Ivan, “Bivariate shrinkage functions for wavelet based denoising exploiting interescale dependency,” *IEEE transaction on signal processing*, vol. 50, pp. 2744–2756, 2002.
[18] L. Sendur and W. S. Ivan, “Bivariate shrinkage with local variance estimation,” *IEEE signal processing letters*, vol. 9, pp. 438–441, 2002.
[19] C. G. Rafael and E. W. Richard, *Digital image processing*, 3rd ed. Pearson Education, 2009.
[20] A. Pizurica, “Image denoising using wavelets and spatial context modeling,” *PhD Thesis*, Universiteit Gent, 2002.
[21] Z. Wang, A. C. Bovik, H. R. Sheikh, and E. P. Simoncelli, “Image quality assessment: From error visibility to structural similarity,” *IEEE transaction on image processing*, vol. 13, pp. 600–612, 2004.
[22] B. N. Aravind and K. V. Suresh, “Multispinning for image denoising,” *International Journal of intelligent systems, deGruyter*, vol. 21, pp. 271–291, 2012.

DC BUS VOLTAGE CLAMP METHOD TO PREVENT OVERVOLTAGE FAILURES

Rekha H. R.[1], Mohana Lakshmi J.[2], H. N. Suresh[3]

ABSTRACT - The influences of Pulse Width Modulation (PWM) switching and long cable length on motor insulations is a prominent field of research. The DC bus voltage clamp method investigates the effect of PWM switching and long cable length on the voltage insulation components inside an Adjustable Speed Drive (ASD). This method shows that high potential voltage insulation issue may exist on various components inside the ASD and cause earlier failures under very long cable or multiple drive conditions. A DC bus voltage clamp circuit is proposed to reduce these voltage stresses. First, it categorizes the high voltage components and analysis of the voltage stresses. It is found that the voltage stresses of the component can be simplified by analyzing the voltage differences between DC bus terminals and the ground potential. The effectiveness of this circuit is to be verified by simulation results.

Keywords - Adjustable Speed Drives (ASD), Pulse width Modulation (PWM), DC Voltage Clamp.

I. INTRODUCTION

Recently, the power electronics technology has enabled the Adjustable Speed Drives (ASD) to reach its higher switching frequency, reduce the acoustic noise and also control the voltage, current and torque. The fast dv/dt Pulse Width Modulation (PWM) switching of the inverter devices also induces frequency ground leakage current, high shaft insulation voltage, and high levels of bearing current. Chen and Lipo [1] pointed out the net common mode current flowing through three phase stator windings to the axial direction produces a time varying flux surrounding the motor shaft. This flux induces a shaft end-to-end voltage driving a circulating bearing current in turn. References [2]-[5] analyzed the PWM switching and cable length effect on bearing current, EMI emission, and motor insulation.

Now-a-days, the physical sizes of the ASD drive and its high voltage components have been reduced dramatically to remain competitive. Typical ways of reducing drive size is to replace the bus bars with Printed Circuit board (PCB), to integrate high voltage component with low voltage circuitry, to shrink the component sizes, and to reduce or remove unnecessary components. All above optimizations may increase voltage stresses of these components and cause unexpected voltage failures. This method investigates the effects of PWM switching and long cable lengths on voltage stresses for different components inside the ASD.

First, DC bus voltage clamp method categorizes the high voltage components and analysis of voltage stresses. It is found out that the voltage stresses of the component can be simplified by analyzing the voltage differences between DC bus terminals and the ground potential (GND). Then, a system model to describe this phenomenon is characterized and developed. It is found out that several potential high voltage stresses operating conditions (much higher than the DC bus voltage) may exist for some severe conditions. After that, a simple DC bus voltage clamp circuit is introduced to help reduce the voltage stresses. This circuit has the minimum number of components two diodes, one capacitor and one resistor. It clamps the voltage stresses of the ASD drive components to slightly higher than DC bus voltages. One advantage of this circuit is that it only operates when the GND is higher than dc+ or is lower than dc-. The wattage losses of the overall system and the voltage ratings of the discharging capacitors can be very low.

II. VOLTAGE STRESSES IN ADJUSTABLE SPEED DRIVE

A. High voltage components and their voltage Stresses in ASD

One characteristic of ASDs is to use low voltage control signals to control high voltage switching devices. Based on their functionality, there are two types of high voltage components. The first type of components are the main circuit components that transfer power from line to load side, including inverter. IGBT, rectifier diode/SCR, DC link choke, DC bus capacitor, snubber capacitor, and etc. They are all located in the differential mode circuit and their voltage stresses are generally no higher than the DC bus voltage. Selection of voltage ratings for these components is straight forward [6].

The second type of components provide protective separation between the control circuit and the main circuit, including opto-coupler, PCB, sensors, voltage/current transducer, Switch Mode Power Supply (SMPS) transformer, and etc. The High Voltage (HV) sides of these components are either no higher than the positive bus or no lower than the negative bus. The Low Voltage (LV) sides are the control voltage that is very close to GND voltage. Therefore, the insulation voltage of the protective separation component can be approximated as the voltage between GND and the DC bus terminals. Selection of the voltage ratings for these components may be influenced by the operating condition heavily and will be analyzed [7].

B. Differential mode voltage between DC bus terminals to the GND

The voltage stresses between the ground and the DC bus terminals can be calculated by adding the common mode and differential mode components. For the differential mode circuit, this voltage stresses can be approximated as half the DC bus voltage for a Y grounded system.
Where,

$$V_{pgpk\_DM} = \frac{V_{dc}}{2}; \quad (1)$$

$$V_{ngpk\_DM} = -\frac{V_{dc}}{2} \quad (2)$$

Where V_{pgpk_DM} is the maximum voltage between positive DC bus and the GND in differential mode circuit V_{ngpk_DM} is the minimum voltage between negative bus voltage and the GND in differential mode circuit.
For a corner grounded system, the maximum voltage stresses between DC bus terminals to the GND can be as high as DC bus voltage between positive bus and the GND and as low as negative DC bus voltage between negative buses to the GND as per eqns. (4) & (5):

$$V_{pgpk\_DM} = V_{dc}; \quad (4)$$

$$V_{ngpk\_DM} = -V_{dc} \quad (5)$$

C. Common mode voltage between DC bus terminal and the GND

The value of common mode voltage is determined by the cable length, common mode capacitance of the ASD drive, and PWM switching frequency. The main objective of this method is to investigate the voltage stresses of insulation components inside a drive. As a result, the common mode model of the cable and motor is simplified as a single L–C–R circuit .According to the conduction state of the input diode rectifier; there are three different simplified models of the common mode circuit for the ASD drive.

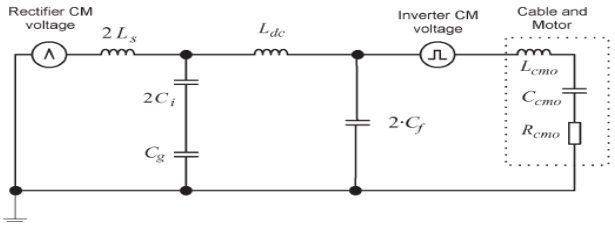

Fig. 1: ASD circuit with common mode circuit when choke differential current is non zero.

The Fig. 1 and 2 shows the equivalent circuit of common mode circuit when the rectifier has at least one switches of the upper (T1/T3/T5) diode/SCR and at least one switches of the lower diode/SCR (T2/T4/T6) conducting in the same time.

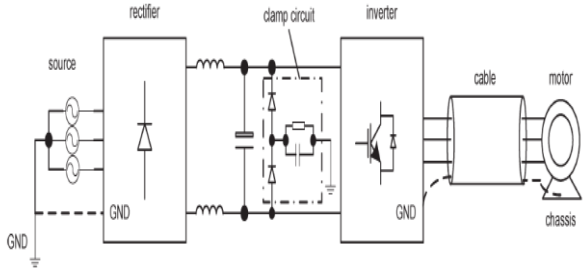

Fig. 2: Proposed clamp circuit is a solid Y ground system.

Under this condition, the common mode circuit and differential mode circuit are decoupled and it has been used as an equivalent circuit of the system for most of the reference papers. The common mode stresses generated by the PWM switching will be distributed to rectifier side, DC bus, and the inverter side components. A much less voltage stresses is generated inside the drive under this condition. Fig. 2 is typical equivalent circuit discussed by most researches. However, this is only true when the inverter is operated under high loaded condition where the rectifier circuit operates under continuous mode. There are two other operating conditions exist when the rectifier operated under discontinuous mode. Both states may generate higher voltage stresses to the drive components.

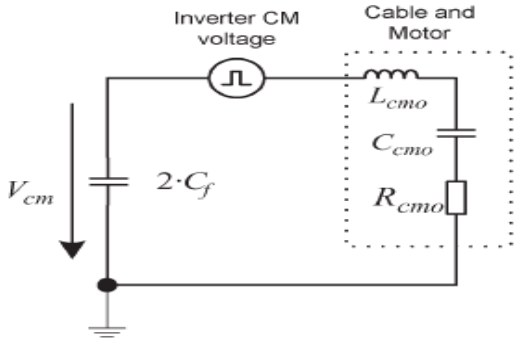

Fig. 3: Common mode circuit when rectifier side diode/SCR is all off.

Fig. 3 shows an equivalent circuit of the drive when there are no Diode/SCRs conducting. These operating states can be found widely when the rectifier has SCR switches. It exists when the system operates at light load or regenerating condition where both Diode/SCRs in the rectifier remains off state while the inverter is switching. Under this condition, the switching energy in the common mode circuit only distributed to the DC bus terminals and the inverter side components. The voltages tresses of the drive components are generally higher than that obtained in Fig. 1.

Fig. 4 shows the third equivalent circuits. Under this condition, only one side of the rectifier Diode/SCR is conducting. The common mode and differential mode circuit are combined together and cannot be separated.

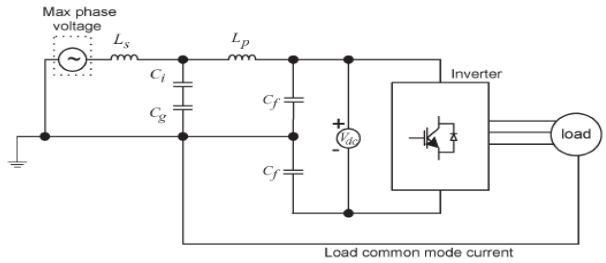

Fig. 4: ASD circuit when only one side chokes (upper) is conducting and the other side is anti-biased.

For the case of Fig. 4,where only upper side diode/SCR are conducting, the upper side voltage potential between GND and dc+ are clamped by the input circuit. At low speed or no load condition, the system may transit between these three conditions. As a result, the AC side common mode capacitor maybe in and out of different equivalent circuits and cause excessive voltages stresses between DC bus terminals to GND.

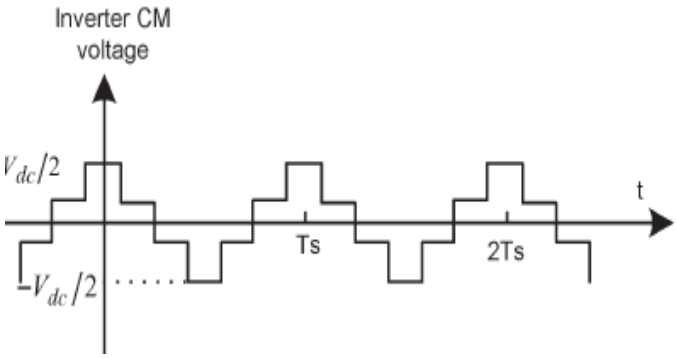

Fig. 5: Inverter common mode voltage at high speed.

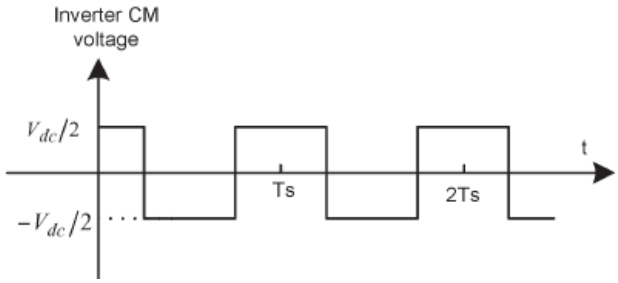

Fig. 6: Inverter common mode voltage at low speed.

The inverter common mode voltage is generated by the PWM switching of the inverter. Fig. 5 shows a typical common mode voltage generated by the PWM inverter at high speed. From this figure, the common mode voltage increase$\mathbf{V_{dc}/3}$. When the inverter operates at low speed, the highest common mode voltage steps generated as shown in Fig. 6. In this condition, the duty ratios of all three inverter legs are close to 50%. The common mode voltage may change from $\mathbf{V_{dc}/2}$ to $\mathbf{-V_{dc}/2}$ directly as shown in Fig. 6.

It should be noted that some articles have proposed common mode reduction PWM method (CMRPWM) for inverters. With this method, the zero vectors 000 and 111 are eliminated to reduce the common mode stresses. Under this condition, the common mode voltage only increases$\mathbf{V_{dc}/3}$ at each step. The voltage insulation between DC buses terminals to the GND will be reduced dramatically. However, this method does not create the best electrical performance to the system at low speed. It generates higher current stresses to DC bus capacitor, increase the harmonics and temperature of the motor winding and increase the audible noises at low speed. In this method, only the standard PWM control method will be discussed to represent the best electrical performance and the worst case for insulation components inside the drive.

D. Voltage stresses analysis and the capacitance ratio between ASD and the load at discontinuous mode.

For a RLC resonant circuit as shown in Fig. 6, a step change with an amplitude of $\mathbf{V_{dc}}$in the common mode voltage can induce as higher as two times of $\mathbf{V_{dc}}$ voltage spike in the capacitor $\mathbf{C_{mo}}$and 2 * $\mathbf{C_f}$ if the effect of the resistance can be neglected. Thus, the worst case common mode voltage stress in capacitor $\mathbf{C_f}$generated by a single common mode voltage step of $\mathbf{V_{dc}}$(zero speed) can be calculated as

$$\mathbf{V_{cmpk}} = \frac{2\mathbf{V_{dc}}.\mathbf{C_{cmo}}}{\mathbf{C_{cmo}}+2.\mathbf{C_f}} = (2 - \frac{4\mathbf{C_f}}{\mathbf{C_{cmo}}+2\mathbf{C_f}}) \quad (6)$$

where, C_f is the common mode capacitor in DC link, the $\mathbf{C_{cmo}}$is the equivalent common mode capacitor of the cable and motor. For majority of the applications, common mode filter capacitor $C_f$is much higher than C_{cmo}.The peak common mode voltage stresses of C_f are low and the voltage potential of GND is between dc+ and dc−. The voltage stresses of the protective insulation components are low.

For some special conditions where multiple cables or very long cables are associated, the total capacitance C_{cmo}may be higher than common mode capacitance $\mathbf{C_f}$. The peak voltage induced in the common mode capacitor will be increased to as high as twice the DC bus voltage. As a result, the voltage stresses of the protective separation component may be two times higher than the DC bus voltage as shown in Fig. 6.

E. Overall stresses adding DM and CM voltages.

The worst case voltage stresses of between the DC bus to the GND adding differential mode voltage for Y grounded system can be expressed as

$$\mathbf{V_{pg}} = \mathbf{V_{pgpk\_DM}} + \mathbf{V_{cmpk}} = (2.5 - \frac{4\mathbf{C_f}}{\mathbf{C_{cmo}}+2\mathbf{C_f}})\,\mathbf{V_{dc}} \quad (7)$$

$$\mathbf{V_{ng}} = \mathbf{V_{ngpk\_DM}} - \mathbf{V_{cmpk}} = -(2.5 - \frac{4\mathbf{C_f}}{\mathbf{C_{cmo}}+2\mathbf{C_f}})\,\mathbf{V_{dc}} \quad (8)$$

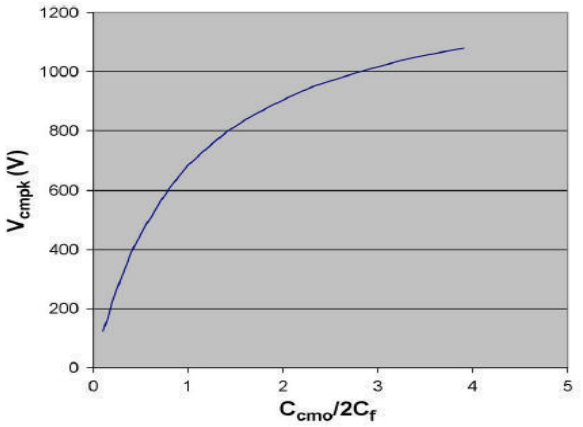

Fig. 7: Worst case peak common mode voltage between GND and the bus terminals.

The maximum voltage stresses existed between DC bus terminals when the common mode capacitance C_f is 0 and the inverter operated at low speed. It can reach as 2.5 times of the DC bus voltage at corner grounded system. However, this value is an ideal calculation by neglecting the damping of the output common mode circuit and the common mode capacitance of the power converter. Due to the conductor resistance and insulation resistance between cable and the ground, the peak voltage stress may never be able to reach this level.

III. Operation of Voltage Clamp Circuit

Clamping circuits are simple yet their operation can be hard to understand. A clamping circuit is used to "clamp" a signal to a fixed DC level. This is also known as "DC restoration." This term dates back to the first television receivers which needed to restore a transmitted signal to a reference value to set the black level.
The proposed voltage clamp circuit for an ASD is shown in Fig. 8:

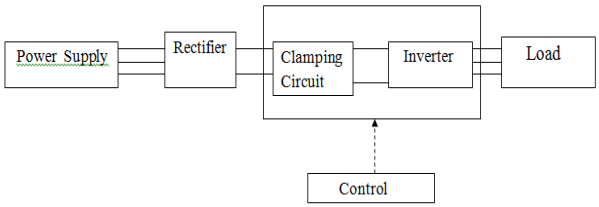

Fig. 8: Voltage clamp circuit for an ASD.

Components used in the voltage clamp circuit for ASD are as follows:
Power supply: Three phase AC power supply is used.
Rectifier: A rectifier is an electrical device that converts alternating current, which periodically reverses direction, to direct current.
Clamping circuit: A clamping circuit will bind the upper or lower extreme of a wave form to a fixed DC voltage level. These circuits are also known as DC voltage restorers. Clampers can be constructed in both positive and negative polarities. When unbiased, clamping circuits will fix the voltage lower limit (or upper limit, in the case of negative clampers) to 0 volts.
Inverter: A power inverter is an electronic device or circuitry that changes direct current to alternating current.
Load: Three phase induction motor, some types of single phase motor, synchronous motor.

The voltage clamp circuit has three modes of operation:

- Standby mode
- Clamping mode
- Discharging mode

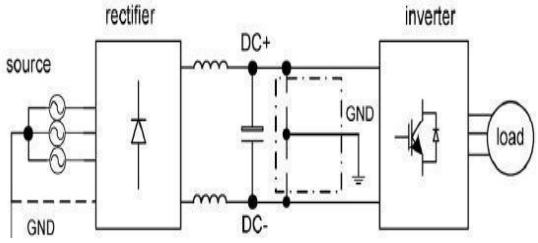

Fig. 9: Standby mode.

The circuit diagram for standby mode of operation is shown in Fig. 9. During normal condition, the voltage of the GND is always lower than the dc+ and higher than dc−, both diodes are anti-biased. The voltage difference between GND and bus terminal is less than $V_{dc} = V_{dc+} - V_{dc-}$.

If the GND is either higher than DC+ or lower than the DC−, one of the diodes starts to conduct. The common mode energy will be transferred to the RC snubber circuit, since the capacitance of this snubber circuit is selected to be much higher than the overall cable and motor common mode capacitance.

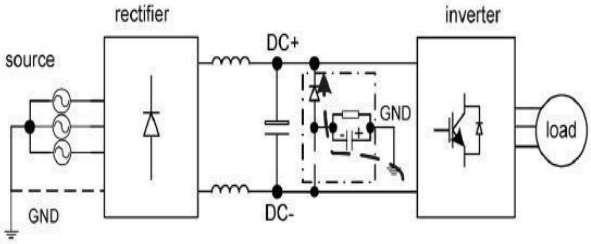

Fig. 10: Clamping mode when $V_{gnd} > V_{dc}+$.

The potential of the GND will be clamped to one of the two DC bus voltages (dc+ or dc−). Fig. 9 shows a circuit diagram at this mode when V_{gnd} is higher than V_{dc}. The voltage difference between GND and bus terminal is slightly higher than $V_{dc} = V_{dc+} - V_{dc-}$.

After the PWM switching transient is over, the GND potential is low than dc+ and higher than the dc−. Both diodes return to off condition. The energy of the snubber capacitor is now discharged by the snubber resistor.

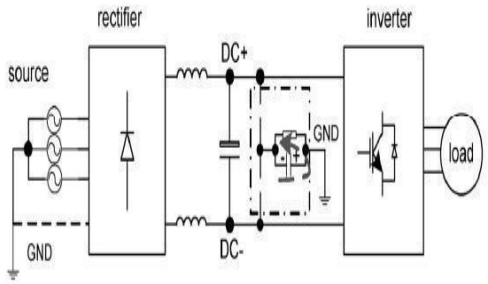

Fig. 11: Discharging mode.

The circuit diagram for discharging mode of operation is shown in Fig. 11. After all energies are discharged, the system goes back to standby mode. The voltage difference between GND and bus terminal is still less than $V_{dc} = V_{dc+} - V_{dc-}$.

To guarantee that the system goes back to standby mode during each switching cycle, the time constants of the RC snubber can be selected as much lower than the PWM frequency. Since the resistor is only used to discharge the power, the leakage inductance of the resistor is not critical as well. It should also be noted that the watt loss of the RC snubber resistor is proportional to the switching frequency of the inverter. The wattage of the resistor is much lower than the energy being charged/discharged by the inverter cable capacitance. While selecting the RC resistor, its wattage must be able to support the inverters to operate under the highest switching frequency.

IV. SIMULATION RESULTS AND ANALYSIS

The Simulation analysis to clamp the DC bus volatge has been carried out with and without clamp circuits using Matlab. The circuits are simulated for multiple drive systems also. The obtained results for the various conditions are discussed.

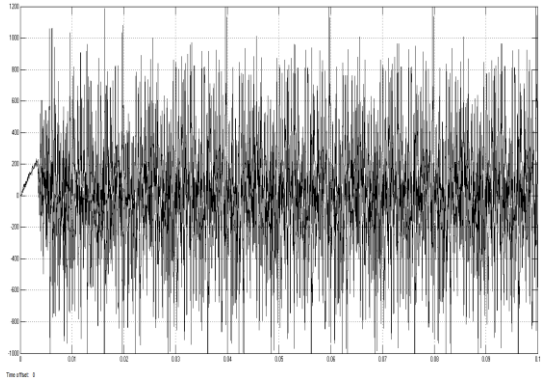

Fig. 12: Voltage stresses of the V_{pg} and V_{ng} without clamp circuit.

Fig. 12 shows the voltage between positive DC and ground terminal without voltage clamp circuit working under Y grounded system. It is seen that voltage stresses between DC bus terminals to the potential ground terminal increase up to 100V. Without voltage clamp circuit maximum voltage stresses is generated inside the Adjustable Speed Drives (ASD), and stress generated is about 2.4 times more than DC bus voltage.

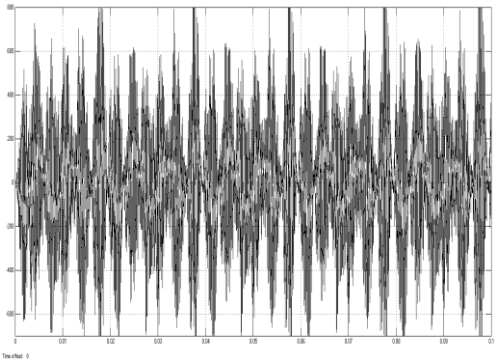

Fig. 13: Voltage stresses of the V_{pg} and V_{ng} with clamp circuit.

Fig. 13 shows the voltage between positive DC bus terminal and potential ground terminal with voltage clamp circuit working under Y grounded connection. From the above figure, we can notice that voltage stresses between DC bus terminal and potential ground terminal has reduced to 800V compare with Fig.12.

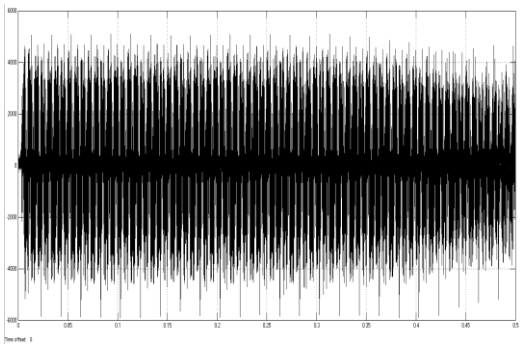

Fig. 14: Voltage stresses of the V_{pg} and V_{ng} without clamp circuit using multiple drive condition.

Fig.14 shows the voltage between positive DC and ground terminal without voltage clamp circuit working under Y grounded system.

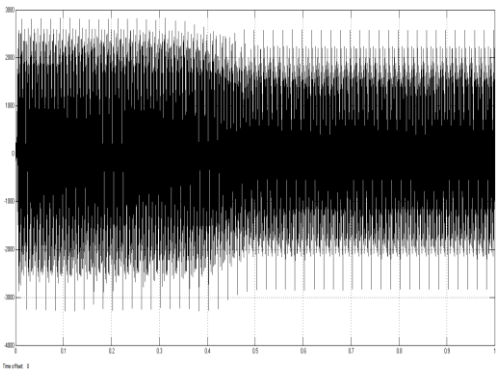

Fig. 15: Voltage stresses of the V_{pg} and V_{ng} with clamp circuit using multiple drive condition.

It is seen that voltage stresses between DC bus terminals to the potential ground terminal increase up to 4000V. Without voltage clamp circuit maximum voltage stresses is generated inside the Adjustable Speed Drives (ASD), and stress generated is about 2.4 times more than DC bus voltage.

Fig.15 shows the voltage between positive DC bus terminal and potential ground terminal with voltage clamp circuit working under Y grounded connection. From Fig. 15, one can notice that voltage stresses between DC bus terminal and potential ground terminal has reduced to less than 3000V compared with the one in Fig. 14.

VII. CONCLUSIONS

The work presented investigates the effect of PWM switching into long motor cables causing the voltage stresses on different components inside an ASD. It is shown that a potential voltage insulation problem may exist on certain ASD components and cause insulation failures under several extreme operating conditions. A DC bus voltage clamp circuit is proposed to mitigate the increased stresses. Simulation results are provided to verify its effectiveness. With the proposed clamp circuit, the voltage between the GND and DC bus terminals are clamped to slightly higher than the value of DC bus voltage.

REFERENCES

[1] S. Chen, T. A. Lipo and D. Fitzgerald, "Source of induction motor bearing currents caused by PWM inverters," *IEEE Transactions on Energy Conversions*, vol. 11, no. 1, pp. 25–32, March 1996.

[2] D. Busse, R. J. Kerkman, J. Erdman, D. Schlegel, and G. Skibinski, "Bearing currents and their relationship to PWM drives," *IEEE Transactions on Power Electronics*, vol. 2, no. 2, pp. 243–252, March/April 1997

[3] R. J. Kerkman, D. Leggate and G. Skibinski, "Interaction of drive modulation and cable parameters on AC motor transients," IEEE Transactions Power Electronics, vol. 33, no. 3, pp. 722–731, May/June 1997.

[4] G. Skibinski, D. Leggate, and R. J. Kerkman, "Cable characteristics and their influence on motor overvoltage," *IEEE Power Electronics Conference*, Atlanta, GA, Feb. 23–27, 1997, pp. 114–121.

[5] G. Skibinski, R. J. Kerkman, and D. Schlegel, "EMI emissions of modern PWM AC drives," *IEEE Transaction on Industrial Electronics*, vol. 5, no. 6, pp. 47–80, Nov./Dec. 1999.

[6] S. Ogasawara, H. Ayano, and H. Akagi, "An active circuit for cancellation of common-mode voltage generated by a PWM inverter", *IEEE Transactions on Power Electronics,* vol. 13, no. 5, pp. 835–841, Sep. 1998.

[7] A. Julian, G. Oriti, and T. Lipo, "Elimination of common-mode voltage in three phase sinusoidal power converters", *IEEE Transactions on Power Electronics*, vol. 14, no. 5, pp. 982–989, Sep. 1999.

[1]**Rekha H. R.** is a Post graduate student in Computer Applications in Industrial Drives in the Department of E & E Engineering at Malnad College of Engineering, Hassan, Karnataka. Her areas of interest include power Electronics and Electrical machines.

[2]**Mohana Lakshmi J.** is presently serving as Assistant professor at ATME College of Engineering, Mysore, Karnataka. She is a Gold medalist of VTU in her batch of M.Tech. program in *Computer Applications in Industrial Drives* in the year 2012. Her areas of interest include *Power electronics and drives control.* She is pursuing her Ph.D. program of VTU on part-time basis, under the supervision of Dr. H. N. Suresh.

[3]**Dr. H. N. Suresh** is presently serving as Professor at Malnad College of Engineering, Hassan, Karnataka, India. He obtained his **M.E**. degree in Electrical Engineering from **Indian Institute of Science (IISc**), **Bangalore**, India, in 1991. **Ph.D**. degree was awarded to him by **IISc, Bangalore** in the year 2000. His areas of interest include *High voltage insulation engineering* and *Power electronics applied to drives control.*

LOCALIZATION SCHEME FOR DEEP AND SHALLOW UNDERWATER WIRELESS SENSOR NETWORKS

Mr. Yashwanth N
Assistant Professor
Department of Electronics and Communication
Rajeev Institute of Technology
Hassan - 573201
Email: yashwanthrithsn@gmail.com

Dr. B R Sujatha
Associate Professor
Department of Electronics and Communication
Malnad College of Engineering
Hassan - 573202
Email: brshsn61@gmail.com

Abstract: *Underwater Wireless Sensor Networks (UWSNs) provide new opportunities to observe and predict the behavior of aquatic environments. In some applications such as target tracking or disaster prevention, sensed data is meaningless without location information. Reverse Localization Scheme (RLS) is an event-driven localization method triggered by detector sensors for launching localization process. However, when the monitoring area is deep RLS fails to meet the requirements. This paper proposes a multiple-hop reverse localization scheme (MHRLS) for UWSNs. MATLAB simulation results shows that MHRLS achieves much larger localization coverage than RLS while maintaining an allowable level of localization error and overhead in deep water environment. But in shallow water environment, MHRLS performance is comparable to that of RLS performance.*

Keywords: Underwater wireless sensor networks, reverse localization scheme, multiple-hop reverse localization scheme.

I. INTRODUCTION

From time immemorial, 'WATER' is an important popular resource of transportation for military and civilian personnel as two-thirds of the earth surface is covered by water. Scientific research has provided several underwater applications such as environmental monitoring, undersea explorations, disaster prevention, mine reconnaissance, etc. Traditional monitoring systems are expensive and complicated. These equipments/systems utilize individual and disconnected equipments to collect data from their surrounding environments. The emergence of UWSNs has provided new opportunities to explore the ocean for newer applications. The conventional, large, expensive, individual ocean monitoring equipments are being replaced by UWSNs having relatively small and less expensive underwater sensor nodes that are able to communicate with each other via acoustic signals. Many technologies for UWSNs have been researched, e.g., medium access control (MAC) and secure routing protocols, localization technologies and time synchronization schemes. Among these localization is one of the most required technologies since it plays a critical role in many applications.

Although various localization algorithms have been proposed for terrestrial WSNs, many are not suitable for UWSNs. Radio signals can propagate long distances through sea water only at extra low frequencies between 30 Hz and 300 Hz. But these low-frequency radio signals require long antennae and high transmission power. Relatively, acoustic signal attenuates less and travels greater distance in

water. Thus, acoustic signal is more suitable for UWSNs rather than electromagnetic signals.

Another aspect in UWSNs is that the movement of sensor nodes caused by water currents is inevitable. Therefore, localization schemes should consider the mobility of sensor nodes and dynamically obtain its 'position' to find routes between source and destination nodes. Several schemes have been proposed in the literature. Chandrasekhar *et al.* [3] have proposed an Area-based Localization Scheme (ALS). In this method anchor nodes periodically send out beacon signals at varying levels. A two-dimensional region is partitioned into non-overlapping subareas by the ranges of the different levels of anchor nodes. Each non-localized underwater sensor node keeps a list of anchors and corresponding lowest power level and forwards this information with the sensor data to the sink. Sink is able to estimate the node's location. This scheme provides an estimation of a sensor's location within a certain area, rather than the exact location (range-free localization technique).

A Dive and Rise Localization (DNRL) protocol is proposed by Erol *et al.* [4] for a mobile underwater wireless sensor network which utilizes mobile DNR beacons for localization. As GPS signals cannot propagate far through the water, the Dive 'N' Rise beacons carry GPS receivers and gain their coordinates when they rise to the surface and broadcast their positions periodically in deep water to help underwater node's localization when they dive. Ordinary sensor nodes use TOA range measurement technique to calculate their distance to the DNR beacons.

Multi-Stage Localization (MSL) is proposed by Lloret J *et al.* [5] to solve the coverage problem of DNRL by adding an iterative localization phase. In fact, it is the extended version of DNRL which dives to a predetermined depth. It is a multistage method which means the successfully localized nodes act as new anchor nodes and help others to estimate their locations, but the major drawback of this method is its high overhead due to iterative localization, so it is less energy efficient than DNRL. Moreover, the localized nodes provide their estimated locations with its estimation errors. Errors will be accumulated by the nodes which use the localized node's coordination as anchor node's position.

A Silent Positioning Scheme is proposed in UPS model by Cheng *et al.* in [6]. This method is distributed and works for stationary underwater acoustic sensor networks (UASNs). Silent positioning is a localization scheme for one-hop underwater networks [6]. Four anchors are employed which sequentially send out beacon signals. The underwater nodes do not send any localization messages, hence UPS is silent. The overhead and energy consumption of UPS is low. It is a range-based method which utilizes TDOA range measurement technique, so it does not require synchronization, but UPS is only able to localize the nodes where they reside inside the area enclosed by four anchor nodes.

Scalable Localization with Mobility Prediction (SLMP) is proposed in [7] by Zhou *et al.* It is a prediction-based localization method and it is assumed that every sensor node needs to determine its location periodically. Localization is performed in the same hierarchical architecture of LSL, with buoys, anchors and ordinary sensors.

The rest of the paper is organized as follows: Section 2 discusses the implemented localization schemes. Section 3 provides the simulation results followed by Section 4 having the conclusion.

II. LOCALIZATION SCHEMES

Localization schemes should consider the mobility of sensor nodes and dynamically obtain its 'position' to find routes between source nodes and destination nodes. RLS is one such scheme [2].

A. Reverse Localization Scheme

A reverse Localization scheme (RLS) for UWSNs is illustrated as in Fig. 1. Once a source node senses an unusual event such as movement of the sensor node because of drifting of water currents it inserts its depth information sensed by the pressure sensor and the sending time into the packet and tries to send the packet to anchor nodes directly. Once an anchor node receives the packet, it inserts its coordinate information and the receiving time into the packet and sends the packet to the sink. If the number of packets received by the sink is not less than 3, the sink is able to calculate the coordinate of the source node by trilateration. Instead of localizing all unknown nodes, RLS only localizes source nodes which greatly reduces the communication overhead and energy consumption.

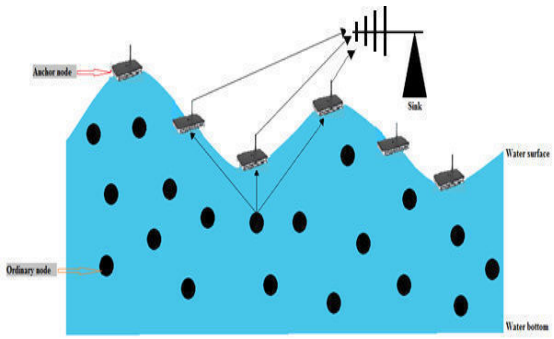

Fig.1. The schematic diagram of RLS.

B. Multiple-hop Reverse Localization Scheme

The drawback of RLS is the assumption that the ability of node's communication is so powerful that it can communicate with anchor nodes directly. As we know, this assumption is difficult to be satisfied when the monitoring area is deep. To overcome the drawback of RLS, in this paper, a multiple-hop reverse localization scheme (MHRLS) is implemented as shown in Fig. 2. Instead of assuming that an ordinary node communicates with anchor nodes directly, MHRLS assumes that an ordinary node communicates with anchor nodes in a multiple-hop fashion. The MHRLS performs two operations - One is routing, that is, how to send the packet from an ordinary node to the sink. The other is the localization, that is, to estimate the location of the source node recursively.

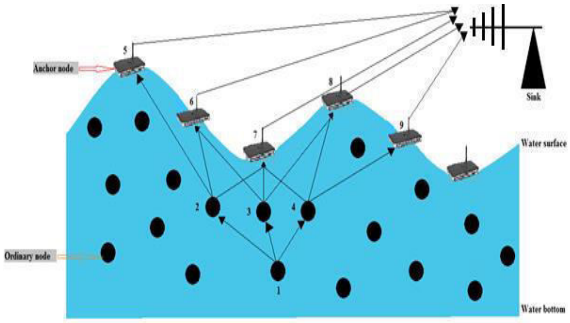

Fig. 2. The schematic diagram of MHRLS.

In *Multple-hop* localization, nodes are not directly adjacent to multiple anchor nodes and must use *non-adjacent* anchors and range estimates for localization, as illustrated in Fig. 3. Multiple-hop localization is neither a simple linear optimization nor is it computable with only local information. In single-hop localization, the accuracy observed in a single-cell deployment can be generalized to larger multi-cell deployments because each cell is roughly independent.

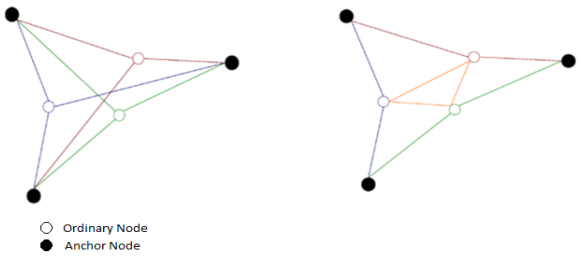

Fig. 3. Single hop and Multiple-hop Localization

In other words, a system shown to work in one room can reasonably be expected to work across an entire building if each room has enough anchors. The performance of a multiple-hop algorithm on a sensor network of 10 nodes, however, can be completely different from its performance on a network with 1000 nodes.

For the routing problem for MHRLS a new routing protocol based on *depth-based routing* (DBR) is investigated. In this routing protocol, upon sensing an unusual event, the source node broadcasts a HELLO packet having the depth information, node's ID, hop information (initial value is zero) and the sending time information into the packet. The procedure adopted by the neighbouring nodes to forward the packet received from source node is given in Fig.4. and the algorithm is as given below:

Algorithm 1: For Forwarding a Packet p

1: **IF** the current node is an anchor node

2: Insert the information of the receiving time T_r, node's ID, and the anchor node's coordinate into packet p

3: Send packet p to the sink

4: return

5: **ENDIF**

6: Get the previous depth D_p and the previous hop H_p from p

7: Get node's current depth D_c and compute the current hop H_c=H_p+1

8: **IF** (D_p -D_c) is less than the depth threshold D_{th} or H_c is larger than the hop threshold H_{th}

9: Drop p

10: return

11: **ENDIF**

12: Insert the information of the receiving time T_r, node's ID, node's depth, and H_c into p

13: Insert the sending time T_s into p and broadcast it

14: return

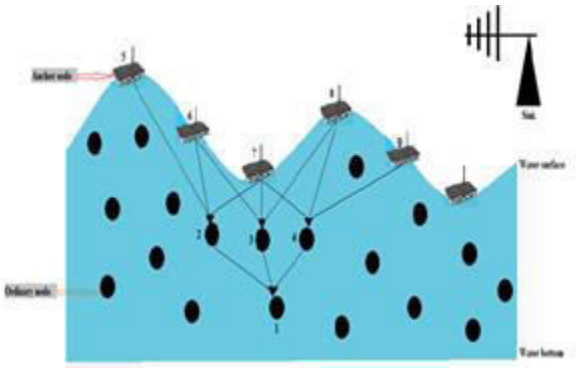

Fig. 4. The recursive localization process.

A typical UWSN shown in Fig. 4. performs localization process. We consider that node 1 is the source node to be localized. Nodes 2, 3, and 4 are qualified forwarders. Node 5, 6, 7, 8 and 9 are anchor nodes that send the packets they have received to the sink node. Let *dij* be the distance between node *i* and node *j*. After receiving a packet, for example, the packet from anchor node 5, the sink extracts the information of the sending time *Ts* and the receiving time *Tr* from the packet. Then *d*52 and *d*21 can be calculated by the sink based on *Ts* and *Tr* information via using *time of arrival* (TOA) technology. In the same way, other distances can also be obtained. After knowing the distances between different nodes, the sink can localize node 2 by utilizing *d*52, *d*62, and *d*72 via trilateration. In the same way, node 3 and node 4 can be localized. Then the sink utilizes node 2, node 3, and node 4 to localize the source node 1. However, if the localization error of node 2, node 3, or node 4 is large, they may be incapable of

participating in locating node 1. The localization error is calculated using equation 1[1].

$$\delta = \sum_i |(u - x_i)^2 + (v - y_i)^2 + (w - z_i)^2 - l_i^2| \quad (1)$$

where (u, v, w) is the estimated location of the unknown node, (x_i, y_i, z_i) is the reference node i's location, l_i is the measured distance between the unknown node and node i. In order to reduce the error propagation effect, each reference node has a confidence value c, which is associated with its location error. In our scheme c is defined as follows[1]

$$c = \begin{cases} 1 & for\ initial\ anchor\ node \\ 1 - \frac{\sigma}{\sum_i (u-x_i)^2 + (v-y_i)^2 + (w-z_i)^2} & others \end{cases} \quad (2)$$

A critical value C_{th} named confidence threshold is set. When $c >= C_{th}$, the node that has just been localized is qualified to participate in locating other unknown nodes. Otherwise, it is incapable of locating other unknown nodes. It is obvious that we can use C_{th} to trade off the localization error, the localization coverage, and the communication overhead.

The recursive localization scheme is utilized to localize the source node based on the information provided by the routing protocol. The procedure of the localization process is shown in Algorithm 2.

Algorithm 2: Recursive Localization

1: Extraction of the information of the sending time T_s and the receiving time T_r from the received packets.

2: Convert this time information into distance information between related nodes by using TOA

3: Calculate the number of each related unknown node's neighbours whose locations are known (m is the number)

4: **IF** m is not less than 3

5: Estimate node's location via trilateration

6: Calculate node's confidence value c

7: **IF** c is larger than C_{th}

8: This node updates into a new reference node and participates in locating other nodes

10: **ELSE**

11: This node cannot participate in locating other nodes

12: **ENDIF**

13: **ELSE**

14: Get back to step 3

15: **ENDIF**

III. RESULTS

The following simulation parameters have been considered

Area in deep water environment: 1000m ×1000m × 1000 m

Number of nodes: 400

Area in shallow water environment: 1000m×1000m×100m

Number of anchor nodes: 40

Distance measurements between nodes are assumed to follow normal distributions, with real distance as mean values and standard deviations to be one percent of real distances. 10% anchor nodes and 100 source nodes are considered in our simulations. Node's communication range is varied from 350m to 1500m. *Hop threshold* H_{th} is set to 3 or 4. D*epth threshold* D_{th} is set to 80% of node's communication range. *Confidence threshold* C_{th} is set to 0.9. Simulation runs are set to 100. The comparison of MHRLS is compared with that of RLS.

A. Deep Water Environment:

The performance of MHRLS in deep water environment is shown in Fig.5, Fig. 6, and Fig. 7. Fig. 5 shows that MHRLS achieves much larger localization coverage when node's communication range is smaller than 1000 m. This is reasonable since any node which can be localized by RLS can also be located by MHRLS. Fig. 6 and Fig. 7 show that the larger localization coverage is at cost of a slightly larger localization error and communication overhead. This is because, besides the anchor nodes, nodes that have just been localized may also participate in locating unknown nodes, which leads to larger localization error. Compared to RLS, ordinary nodes in MHRLS communicate with anchor nodes in the multiple-hop fashion resulting in increased overhead.

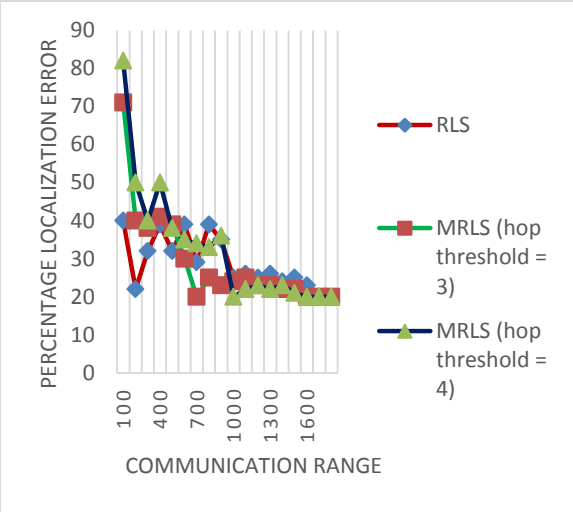

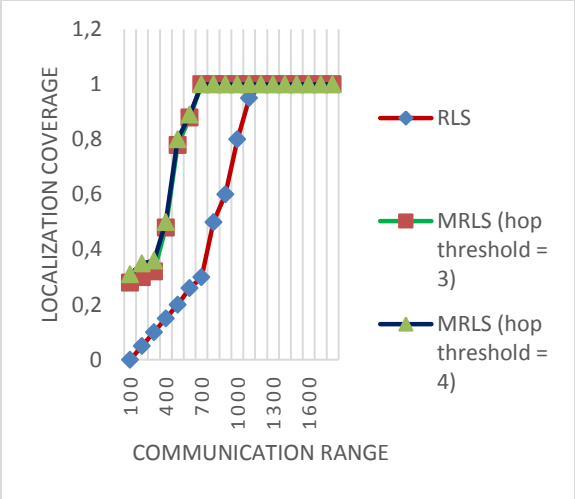

Fig. 5. Localization coverage in deep water environment

Fig. 6. Percentage Localization Error in deep water environment

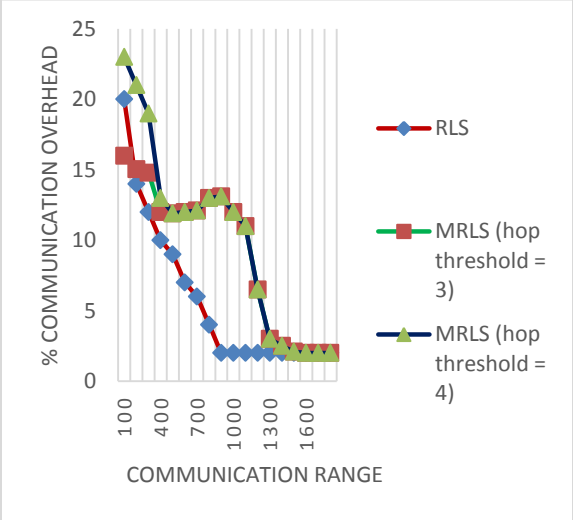

Fig. 7. Percentage communication overhead in deep water environment

B. Shallow Water Environment:

The performance of MHRLS in shallow water environment is shown in Fig. 8, Fig. 9, and Fig. 10. The MHRLS here degenerates into RLS when the monitoring environment is shallow enough. In other words, MHRLS can be used for deep and shallow environments.

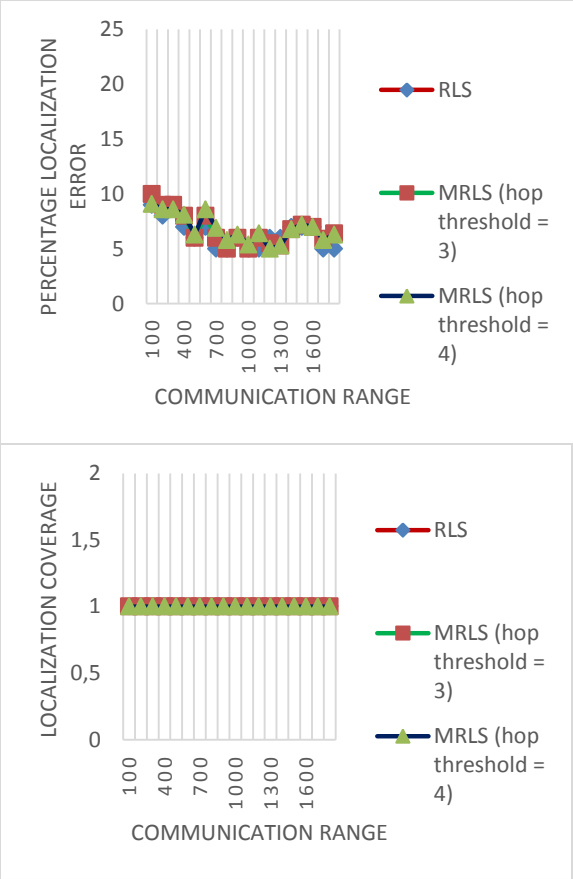

Fig. 8. Localization coverage in shallow water environment

Fig. 9. Percentage Localization Error in Shallow water environment

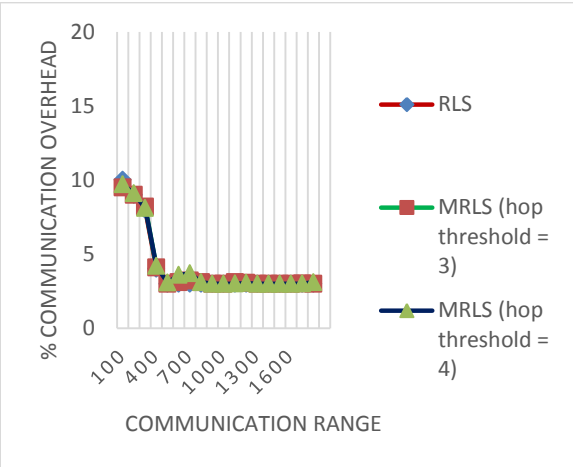

Fig. 10. Percentage communication overhead in shallow water environment

CONCLUSION

In this paper, performance comparison of RLS and MHRLS is done for deep and shallow water environments. MHRLS has dual advantage of providing routing and localization in deep water environment when compared to RLS consuming less overheads. Furthermore, with mobility of nodes due to water currents each algorithm cannot be evaluated on only one topology, but must be evaluated on a broad range of network topologies. For these two reasons, multiple-hop localization research is mainly focused on theoretical analysis and simulation with relatively few empirical systems and prototypes.

REFERENCES

[1] Zhang Senlin, Zhang Qiang, Liu Meiqin, Fan Zhen and Sheng Weihua, "A Multi-hop Reverse Localization Scheme for Underwater Wireless Sensor Networks", Proceedings of the 32nd Chinese control conference, July 26-28, 2013, China, pp. 7383-7388.

[2] Marjan Moradi, Javad Rezazadeh, Abdul Samad Ismail, "A Reverse Localization Scheme for Underwater Acoustic Sensor Networks", Sensors 2012, pp. 4352-4380.

[3] Chandrasekhar V, Seah W.K, "Area Localization Scheme for Underwater Sensor Networks", International Conference on OCEANS Asia Pacific IEEE, Singapore, 16 19 May 2006, pp. 1–8.

[4] Erol-kantarci M, Vieira L FM, Gerla M, "Localization with Dive—N'Rise (DNR) Beacons for Underwater Acoustic Sensor Networks", Second Workshop on Underwater Networks (WuWNet'07), Monreal, QC, Canada, 14 September 2007, pp. 97–100.

[5] Lloret J, Sendra S, Coll H, Garcia M, "Saving energy in wireless local area sensor networks", Comput. J. 2009, 53, pp. 1658–1673.

[6] Cheng X, Shu H, Liang Q, Du D.H.C, "Silent positioning in underwater acoustic sensor networks", IEEE Trans. Veh. Technol. 2008, 57, pp. 1756–1766.

[7] Zhou Z, Peng Z, Cui J H, Shi Z, Bagtzoglou A, "Scalable localization with mobility prediction for underwater sensor networks", IEEE. Trans. Mob. Comput. 2011, 10, pp. 335–348.

[8] I F Akyildiz, D Pompili, T Melodia, “Underwater acoustic sensor networks: Research challenges, Ad Hoc Networks”, 2003, 3(3), pp. 257-279.

[9] J Heidemann, W Ye, J Wills, A Syed, Y Li, “Research challenges and applications for underwater sensor networking”, IEEE Wireless Communications and Networking Conference, 2006, pp. 228-235.

[10] J E Faugstadmo, M Pettersen, J M Hovem, “Underwater wireless sensor network”, 4th International Conference on Sensor Technologies and Application, 2010, pp. 18-25.

[11] Y J Ren, N Yu, X L Guo, J W Wan, “Cube-scan-based three dimensional localization for large-scale Underwater Wireless Sensor Networks”, 2012 6th IEEE International Systems Conference, 2012, pp. 186-191.

[12] X Cheng, H Shu, Q Liang, “Silent positioning in underwater acoustic sensor networks”, IEEE Transactions on Vehicular Technology, 2008, 57(3), pp. 1756-1766.

[13] A Y Teymorian, W Cheng, L R Ma, X Z Cheng, X C Lu, Z. X. Lu, “3D underwater sensor network localization”, IEEE Transactions on Mobile Computing, 2009 8(12), pp. 1610-1621

[14] M Moradi, J Rezazadeh, A S Ismail, "A reverse localization scheme for underwater acoustic sensor networks”, Sensors, 2012, 12(4), pp. 4352-4380.

Techniques for Low-Power System Design - A Survey

P.V. Gopikrishna
Dept. of Electrical Engineering
Gogte Institute of Technology
Belgaum

Harsh Kamath
Gogte Institute of Technology
Belgaum

Dr.G.H.Kulkarni
Professor
Jain College of Engineering
Belgaum,

pvgopikrishna@git.edu

***Abstract*—Most of the systems implementations are initially made on FPGAs due to the ease of re-programmability, more recently dynamic re-programmability, speed and hardware cost constraints. As the focus shifts from bulky desktop computing to battery operated ASICs, the reduction in power consumption and size of chip layout are the biggest challenges. The need of low-power devices calls for trade-offs between various power reductions techniques. A low-power design requires reduction in power consumption at various stages of design without effecting the performance and quality of service. This paper studies such power optimization techniques and discusses various methods to address the low-power design issues.**

Keywords—Low-power; Dynamic power Management; Memories; Power consumption; Complimentary metal-oxide semiconductor (CMOS); Static power; Dynamic power; Field programmable gate array(FPGA).

I. INTRODUCTION

An improvement in circuit density corresponds to power dissipation and heat generation. The power optimization can be done at various levels like algorithmic, architectural, logical, and floor planning levels. The power consumption can also be optimized by modeling the FPGA for optimum internal power distribution. Analysis of circuits realized on FPGAs reveal that the increase in complexity of the circuits increase the parameters such as clock frequency, leakage current and load capacitance. The reduction in power consumption can be viewed from two perspectives, one is from the manufacturer's side that deals with the type of CMOS structure used and physics of the transistor. The other view is from the designer, which deals with the type of algorithm used for implementation and floor planning. The power consumption in CMOS circuits is broadly classified as static power dissipation and dynamic power dissipation. The power dissipation in CMOS circuits consist of the following individual components[1]

$$P_{Total} = P_{Switching} + P_{Short\text{-}Circuit} + P_{Static} + P_{Leakage} \quad (1)$$

The switching power and the short circuit power dissipation are categorized under dynamic power dissipations while the static power dissipation involves the leakage power. A designer can only optimize the dynamic power consumption and can do nothing about static power consumption. The power dissipated in charging the load capacitance is $P_{switching}$, Short circuit power is the power consumed during output transition of CMOS gates used as switches. P_{Static} is the power consumed by the device in the absence of the input signal. $P_{Leakage}$ is due to the leakage currents from reverse biased PN junction associated with the source and drain of MOS transistors. This leakage component increases with the device area and operating temperature of the device. $P_{switching}$ is the most prominent component among all these types of power dissipations, which is caused by charging and discharging of capacitance. This component of power dissipation is proportional to the load capacitance. The switching power is defined as[1]

$$P_{Switching} = C*V_{dd}*V_{swing}*\alpha*f \quad (2)$$

Where 'C' represents the capacitance, V_{dd} is the supply voltage, V_{swing} corresponds to change in voltage levels, α represents switching activity factor based on the probability of output transition and f is the operating frequency. The product α*C is referred to as effective switching capacitance and is represented by C_{eff}. In most of the circuits $V_{swing} = V_{dd}$, so that the equation is written as[1]

$$P_{switching} = C_{eff}*V^2_{dd}*f \quad (3)$$

The leakage power occurs due to V_{dd} and overlapped conductance of PMOS and NMOS transistors of the CMOS logic gate. The short circuit power can be written as[1]

$$P_{short\ circuit} = I_{mean}*V_{dd} \quad (4)$$

Where I_{mean} represents the average current drawn during input transition and V_{dd} is the supply voltage.

The designs of low-power systems involve minimization of these components [1]. The study reveals that the reduction in load capacitance and supply voltage has dramatic influence on overall power consumption. But there are certain limitations involved in reducing these parameters as the reduction may sacrifice the reliability and speed of the circuit. i.e., reducing V_{dd} leads to increase in circuit delays. If μ is the mobility, C_{ox} is the oxide capacitance, V_t is the threshold voltage, and W/L is the width to length ratio of the transistor, the delay is given by [1]

$$T_d = \frac{C_L * V_{dd}}{\mu * C_{ox} * (\frac{W}{L}) * (V_{dd} - V_t)^2} \quad (5)$$

In a dense circuit, the power dissipation causes heat generation. To keep the device at ambient temperature, various components such as fans and heat sinks have to introduced. These components increase the cost of implementation and also increase the area of the chip designed.

II. POWER REDUCTION TECHNIQUES

A. *Variable-voltage techniques*

Probably the most effective way to reduce power consumption is to lower the supply voltage. Previously systems were designed to work at fixed supply voltage but recent research show the possibility of systems to work with dynamically varying voltages. With the variable supply voltages, systems have achieved low-power consumption when compared to fixed voltage counterpart. Self-timed circuits are a special kind of dynamically varying voltage supplies that achieve low-power consumption by automatically putting the unused circuit parts into standby mode.

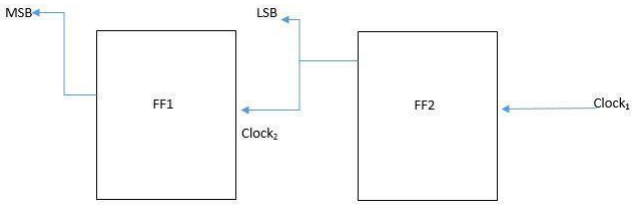

Fig.1. Simple counter circuit for demonstration

In the circuit of Fig.1. FF1 can be put into standby mode until the time equal to 1/frequency of $clock_1$ summed with the propagation delay. The delays are in the order of µs and even ns for more advanced circuits. Even more savings on power consumption can be made by setting up a supply voltage that adaptively adjusts to minimum supply voltage, while keeping all the performance requirements in mind.

The system architecture for adaptive supply voltage of synchronous systems is presented in Fig.2[2]. The proposed system consists of two FIFO buffers, state detection circuit, and a DC-DC converter for scaling voltage. Usually the efficiency of these DC-DC converters is above 90%.

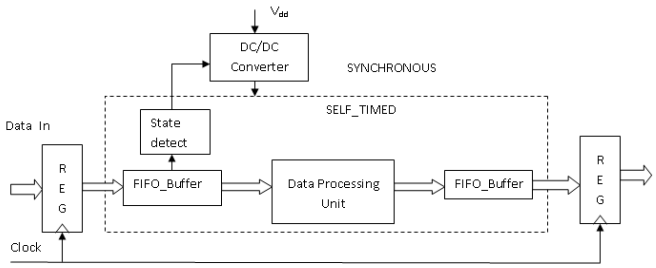

Fig.2. Self-timed circuit for adaptive supply voltage [2]

Since the circuit is a synchronous circuit, the input buffer is never full and the output buffer is never empty. The state detecting circuit tracks the buffers. As the buffer is running empty, the supply voltage is reduced. In contrast if the buffer is running full, there is a need for supply voltage to increase. The whole scenario reveals that the self-timed circuits have ability to scale voltage levels depending upon the buffer contents. The limitation of this technique is that the supply voltage must vary at a very slow rate. Otherwise it may interfere with the circuit operation.

Another technique is providing self-clocked systems [3]. The output of DC-DC converter is regulated to variable supply by using PID controllers. The self-clocked system provides the pulse and these pulses are used in pulse width modulation (PWM) for providing variable DC voltage.

B. *Dynamic power management*

The dynamic power usually concerns with the designer. The power consumption can be reduced by using appropriate architecture and algorithm. A genetic algorithm may be used for placing and routing purposes [4]. The genetic algorithm is used to minimize critical long paths and optimize the internal resources.

1. General Approaches

For reduction of power, the focus should be on those elements that can enter into low-power modes by temporarily losing functionality. One such element that may be used to reduce power is the memory. The power reduction in such elements can be done by using software techniques rather than hardware techniques. The idea here is to embed a code for deciding when the element must go to sleep mode, when to go to standby mode and also to decide when to turn off. Studies have shown that by increasing the cache memory size in place of conventional memory gives reduction in power consumption [5]. Therefore for the reduction in power consumption, a better option is to replace the SRAM which consumes more power with a cache memory.

2. Predictive Approaches

Some of the algorithms may be developed to predict the length of use of hardware sessions and shut down the component when idle to save power as shown in Fig.3[6]. The approach is based on the fact that the system can be possibly in one of the two states i) Waiting for I/O or ii) Performing computation. The predictive shut down systems work on the principle that, while preforming computations the event driven tasks such as I/O may be blocked[6].

If T_{block} is the blocking time and $T_{running}$ is the running time, the efficiency may be improved given that the system element is shut down for the duration T_{block} or whenever the element is in blocked state.

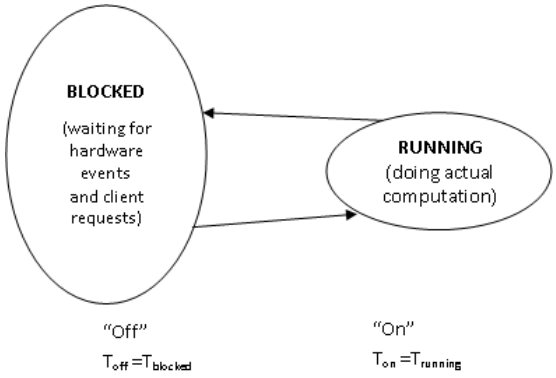

Fig.3. State transition diagram [6]

The system can be shut down by stopping the clock (f=0) or by reducing the supply voltage V_{dd} to zero. The instance at which the system can be shutdown depends on the design algorithm. The system may be shut down whenever it is idle for certain amount of time [7]. Care should be taken that the restarting of the shutdown element does not consume more power then what it would consume if it were ON for the whole time. More efficient techniques in predictive power management is to use a regression equation based on the components previous state and estimate the "off-time"

3. Stochastic Approaches

Power management policy is an algorithm that takes decision on the state of operation of system components. These policies shut down every system component as soon as it becomes idle and restore the element to its fully functional state whenever called for.

Stochastic models Fig.4[8] are just the probabilistic approaches to put the elements in off state whenever idle depending on its previous state.

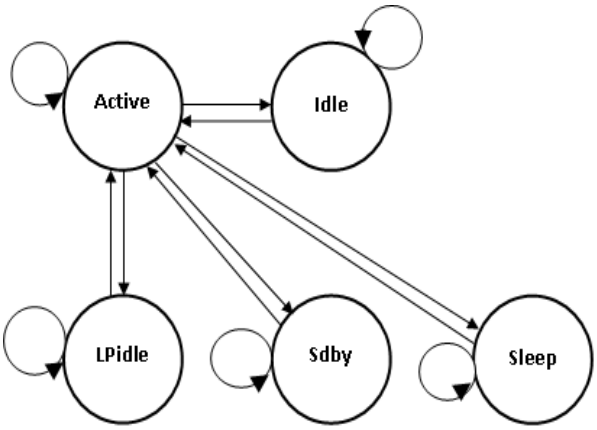

Fig.4. Stochastic state transition model [8]

A stochastic model involves the following components 1. Service requestor: It is modelled as Markov chain with a state transition matrix 2. Service provider: It serves to requests made by service requestor. This has only two states either 'on' or 'off' 3.Power manager: This component communicates with the service provider and attempts to issue commands for efficient power management based on a probabilistic model [8]. During the transition time, the transition depends on the previous state of the system.

C. Memory optimization techniques

Memory optimization techniques mainly focus on reducing the power consumed by memories. The techniques are extended to saving of power during data transfer between memories and processors.

Power consumption in memory-intensive operations can be reduced by minimizing the number of memory accesses. Various types of memory accessing techniques involve centralized serial access, centralized access and distributed memory access Fig.5[9]. The studies show that by using distributed memory access the power consumption becomes less [9], while most power consuming is centralized serial memory access.

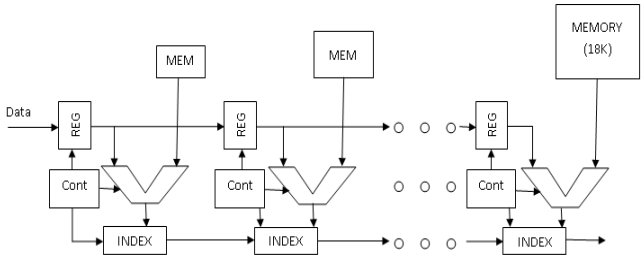

Fig.5. Distributed memory [9]

Also the data can be dynamically imported from a foreign system rather than storing it in memory. Such a foreign system is not considered as a part of the system being analyzed and hence power requirements for this system are not considered. Such techniques become more useful when the foreign system supplies common data to different processors.

D. Hardware-Software partitioning and approximate signal processing

Hardware-Software partitioning techniques attempt to find an optimum partitioning of assignment of task between hardware and software [10].

In some of the circuits where some amount of noise can be tolerated, we can use approximate signal processing techniques. The idea here in this approach is allowing some inaccuracies in the computation. This will lead to dramatic reduction in power consumption [11].

E. More recent techniques

A more recent Novel Placement technique spreads out power consumption across the whole device and also minimizes the power consumption [12]. This technique is based on finding optimum logic block placement according to the resource utilization table. Another recent development is on the Fly partial reconfiguration technology and is implemented on Xilinx FPGAs [13]. This feature enhances reconfigurability by

allowing designers to reconfigure a portion of FPGA while remaining design is still sustained. By this technique, considerable power saving is obtained. Currently Xilinx FPGAs like Virtex II, Virtex IV and Virtex V support this technology.

Conclusion

The paper reviewed techniques and tools for power efficient FPGA based system design. Power consumption is a very critical issue and should be handled with care for effective power utilization. Low power design involves dealing with the power dissipation problems at all the levels of design hierarchy.

III. REFERENCES

[1] Bill Moyer, "Low-power design for embedded processors", Proceedings of the IEEE, Vol.89, No.11, November 2001.
[2] L. Nielsen, C. Niessen, J. Sparso and K. van Berkel, "Low-power operation using self-timed circuits and adaptive scaling of supply voltage", IEEE transactions on VLSI circuits", Vol 2, No.4, pp. 425-435, December 1994.
[3] G. Wei and M. Horowitz "A low-power switching power switching power supply for self-clocked systems", International symposium on low-power electronics and design, pp. 313-317, August 1996.
[4] A. Garcia, L. Perez and R. Acuna, "Power consumption management on FPGAs", IEEE CONIELECOMP 2005.
[5] M. Lee and V.Tiwari, "A memory allocation technique for low-energy embedded DSP software", Symposium on low-power electronics, pp. 169-178, October 1996.
[6] M. Srivastave, A. Chandrakasan and R. Brodersen, "Predictive system shutdown and other architectural techniques for energy efficient programmable computation", IEEE transactions on VLSI systems, Vol.4, No.1, pp. 28-32, November 1997.
[7] Y. Lu and G. De Micheli, "Adaptive hard disk power management on personal computers", IEEE Great Lakes symposium on VLSI, February 1999.
[8] Q. Quiu and M. Pedram, "Dynamic power management based on continuous time markov decision processes", Design automation conference, pp.555-561, June 1999.
[9] D. Lidsak and J. Rabaey, "Low-power design of memory intensive functions", Symposium on low-power electronic, pp. 16-17, October 1994.
[10] T. Conte, K. Menezes and S. Sathaye, "A technique to determine power-efficient, high performance superscalar processors", Annual Hawaii international conference on system science, vol.1, pp.324-333, January 1995.
[11] R. Saied and C. Chakrabarti, "Scheduling for minimizing the number of memory accesses in low-power applications", VLSI signal processing, pp. 169-178, October 1996.
[12] Kostas Siozios, Dimitrios Soudris and Antonios Thanailakis, "Efficient Power Management Strategy of FPGAs Using a Novel Placement Technique".
[13] Sheetal U. Bhandari, Shaila Subbaraman and Shashank Pujari, "Power Reduction in Embedded System on FPGA using on the Fly Partial Reconfiguration", 2010 International Symposium on Electronic System Design.

Quantitative Detection of Fat Infiltration in MR Images

Rajath Elias Soans, Dr. James Shackleford
Department of Electrical and Computer Engineering, Drexel University, Philadelphia

Abstract— The objective of this study is to develop a tool for quantification of the fat infiltration in to thigh muscles which would facilitate identification of diagnostic biomarkers for diseases like Facioscalpulohhumeral Dystrophy (FSHD) characterized by fat infiltration into skeletal muscles and progressive weakness [1]. MRI images of thigh were analyzed using our tool to determine muscular fat fraction. Extraction of region of interest (ROI) was performed using Hough transform and an approximate center of the thigh was found. For each pixel, its intensity and distance from the ROI-center were used as features. An Irrelevance Score (IS) was assigned to each pixel using the two features such that all the muscle pixels within the thigh region and all the infiltrated fat pixels received a low score and all the pixels representing subcutaneous fat received high score. Pixels beyond the thigh region received IS=1. This feature was used in the first node of a decision tree with pixel intensity test in node 2. Any pixel with IS lesser than the decision boundary was qualified to be passed on to the second node for an intensity test. If the intensity of the pixel at the second node was found to be greater than intensity threshold, it was labeled as an infiltrated fat pixel and all the relatively dark pixels with IS<0.3 were classified as muscle pixels. Further, fat fraction was calculated as the ratio of area of infiltrated fat to area occupied by thigh muscles.

***Index Terms*—thigh fat segmentation, decision forest, Facioscalpulohumeral Dystropy**

INTRODUCTION

Development of objective and quantitative bio-markers greatly enhances the possibility to discover the potency of therapeutic interventions. Fat infiltration, quantified by fat fraction in muscle groups is a useful measure in establishment of diagnostic bio-markers [2]. These bio-markers provide information about the disease state and progression in the muscle groups of patients suffering from diseases like Facioscalpulohumeral Dystrophy (FSHD) [3][4]. In several muscular dystrophies including FSHD, MRI with T1 weighting can be adopted to show fatty infiltration and muscle volume changes. According to recent studies, correlation exists between muscle force and the level of fatty infiltration of muscular tissue, for in FSHD. Measuring fat infiltration within muscle group is challenging due to irregularity in infiltration pattern. Segmentation of tiny pockets of fat within muscle groups manually requires more time and effort and also involves subjectivity and human errors. Automating this procedure to extract fat fraction from muscle groups would be the objective behind this study.

METHOD

Our method was validated using T1 spin echo images obtained by performing MRI on patients' thighs. Each pixel x is should be associated to a class label

$$Y(x) \in \{fat, muscle, infiltrated\ fat, background\}$$

Each pixel is also associated with an intensity value, $I(x)$ and is at a certain distance, $D(x)$ from the approximate center of the thigh. These centers are estimated using Circular Hough Transform (CHT) which finds the best fitting circle around the thigh regions in the image. CHT also gives an approximation for the radius, r of the thigh.

The features mentioned above are used to obtain Irrelevance Score, $IS(x)$ as follows:

$$IN(x) = \frac{I(x)}{\max(I(x))};$$
$$DN(x) = \frac{D(x)}{\max(D(x))};$$

$if \quad D(x) > r' \; and \; I(x) == 0$ // background,

$r' = r + \Delta,$
$\Delta \cong 10\% \; of \; r \; to \; compensate \; estimation \; error$

$$then \quad IS(x) = 1$$
$$else \quad IS(x) = a * IN(x) + b * DN(x)$$

A decision tree [5] is constructed to perform classification and identify $Y(x)$ for every pixel, x in an image. The values of $a, b, B1$ and $B2$ were obtained by training the tree to maximize Information Gain (IG). The training was done using multiple subsets of data with known class label. Information gain was obtained by calculating the difference in entropy at each stage.

RESULTS

Image patches of size $3 * 3$ were extracted from MRI images to train the decision tree. Using our dataset, the following we found $a = 1,\ b = 5,\ B1 = 1.8\ and\ B2 = 101$.

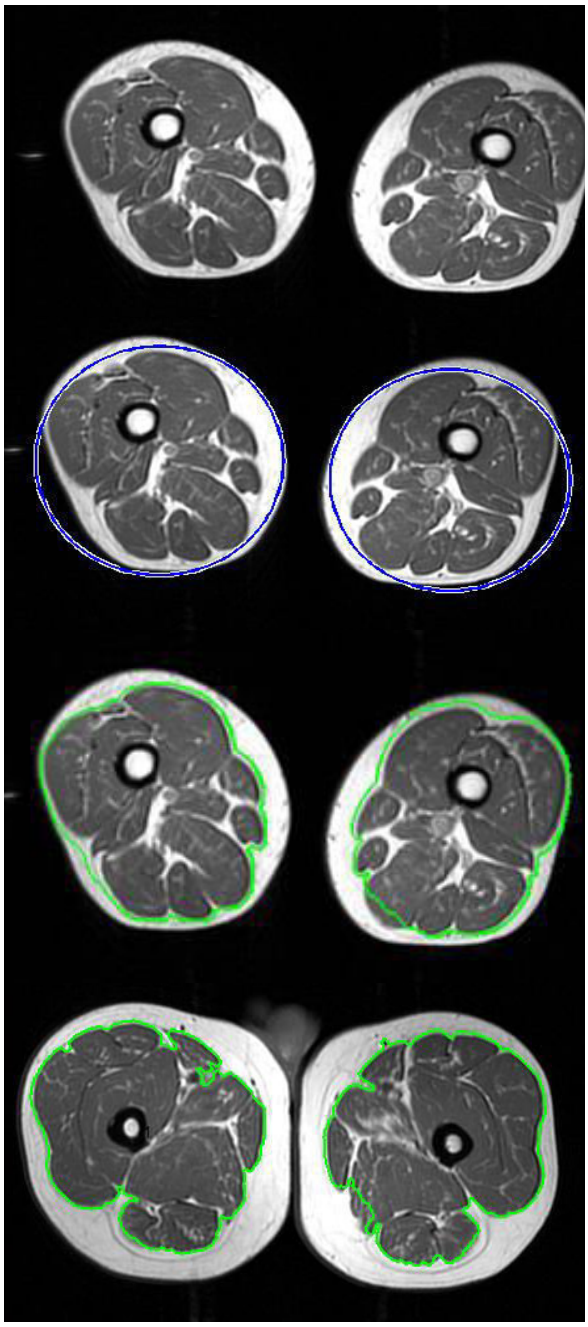

Thigh-fat segmentation result. Top to bottom shows the original image, circles obtained from CHT, and two examples of segmentation result

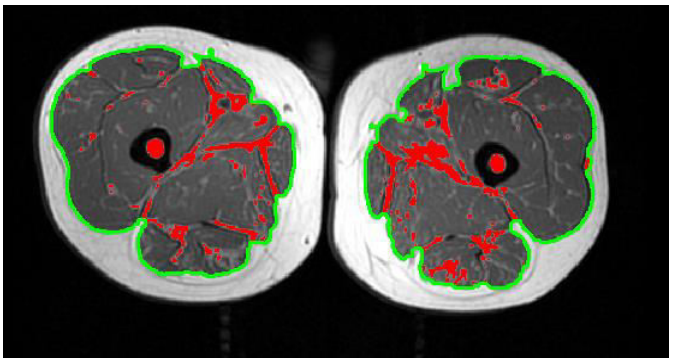

Segmentation of infiltrated fat. Infiltrated fat is shownin red color.

Fig 1 shows the results of segmentation algorithm at each stage. Fig 2 shows the infiltrated segmentation in color code.Results from our method, *(A)* were compared with manual segmentation, *(M)* and evaluation metrics like Dice co-efficient and Hausdorff distance were generated. Only the muscle mass along with infiltrated fat was considered for the segmentation evaluation as these the constitute region of interest (ROI). Results obtained with this study are listed below.

SEGMENTATION ALGORITHM VALIDATION TECHNIQUES

Metric	**Description**	**Result (40 slices)**
$Dice\ co - efficient$	$\frac{2(A \cap M)}{(A \cap M + A \cup G)} * 10$	94.2
$Hausdorff\ Distance$	$\max\{d_i^{am}\}, i = \{1 \dots n_a\}$ $where\ d\ is\ the\ minimum\ distance\ for\ i^{th}\ pixel\ in\ A\ to\ the\ set\ of\ pixels\ in\ M$	4.8 *mm*
$Fat\ Fractio$	$\frac{Total\ number\ of\ fat\ pixels}{Total\ number\ of\ pixels\ in\ ROI}$	0.23

REFERENCES

Janssen, Barbara H., et al. "Distinct disease phases in muscles of facioscapulohumeral dystrophy patients identified by MR detected fat infiltration." (2014): e85416.London, vol. A247, pp. 529–551, April 1955. *(references)*

Kan, Hermien E., et al. "Quantitative MR imaging of individual muscle involvement in facioscapulohumeral muscular dystrophy." *Neuromuscular disorders* 19.5 (2009): 357-362..

Mercuri, Eugenio, et al. "Muscle MRI in inherited neuromuscular disorders: past, present, and future." *Journal of Magnetic Resonance Imaging* 25.2 (2007): 433-440.K. Elissa, “Title of paper if known,” unpublished.

Olsen, David B., et al. "Leg muscle involvement in facioscapulohumeral muscular dystrophy assessed by MRI." *Journal of neurology* 253.11 (2006): 1437-1441.

Krzysztof Grabczewski, Norbert Jankowski, "Feature Selection with Decision Tree Criterion", *HIS*, 2005, Hybrid Intelligent Systems, International Conference on, Hybrid Intelligent Systems, International Conference on 2005, pp. 212-217, doi:10.1109/ICHIS.2005.43

Real Time Pest Detection and Control in Agricultural Plantation using Feature Extraction

Akshaya Kumar A[#1], Manisha B Surve[#2],Dr.Naveen Kumar S K[#3]

Abstract—Advancement in agricultural methods will boost the country's development. It is significant to use technology in the field of agriculture, since technology has been making an immense progress. There are a number of issues that affect the agricultural growth like environmental factors such as temperature, soil requirement, but of those, the issues caused due to pests and insects appear to be outlying. Thus the main objective of the present work is outlined to handle the pest issue at a top level. We propose herein an automatic pest drive away system using feature extraction techniques.

Image acquisition devices are used to acquire images of plantations at regular intervals. A digital camera is used, which act as an input device. The camera will capture the image of an insect sitting on plants. The image is then transferred to an image processing toolbox for processing. Processing of an image is based on MATLAB code. The object detection is done on the basis of color and shape. From image processor an interrupt signal will be sent to the microcontroller. There are two relays used which is connected to the microcontroller. The microcontroller will charge one relay, which will turn on the sprayer to drive away the insect. Another relay is used to turn off the sprayer.

Keywords— *pest,feature extraction-shape and color*,bicubic interpolation,filtering-.gaussian

INTRODUCTION

Agriculture is the mainstay of our civilization. Now a day's farmers are facing many problems for getting better yield. The main cause is due to rapid change in climate and unexpected level of insects. In order to get better yield there is need to reduce the level of pests. Research in agriculture is aimed towards increase of productivity and food quality at reduced expenditure and with increased profit, which has received importance in recent time [1]. A strong demand now exists in many countries for non-chemical control methods for pests or diseases. In fact, in production conditions, greenhouse staff periodically observes plants and search for pests. This manual method is highly time-consuming. With the recent advancement in image processing techniques, it is possible to develop an autonomous system for pest detection and also efficient control of pests is possible.

In this paper, we focus on Real-time pest detection. This implies to regular observation of plants. Images are acquired using cameras. Then the acquired image has to be processed to interpret the image contents by image processing methods.

- *Akshaya kumar A is currently pursuing post-graduation degree program in Electronics in Mangalore University, INDIA, PH-+919526328903. E-mail: akshayeliyana777@gmail.com*
- *Manisha B Surve is currently pursuing post-graduation degree program in Electronics in Mangalore University, INDIA, PH-+918762316886. E-mail: bmanishas@gmail.com*
- *Dr. Naveen Kumar S K is professor in department of Electronics, Mangalore university, INDIA, PH- +919448318252. E-mail: nave12@gmail.com*

Image Acquisition

Every image processing application always begins with image acquisition. The digital camera which acts as an input device will capture the image of a pest. The camera is interfaced with the system. Once the image is acquired the next step is to implement image processing technique in order to get the information about pest.

Image pre-processing

Image pre-processing creates an enhanced image that is more useful or pleasing to a human observer. The image preprocessing steps used in the system are:

1) Conversion of RGB image to gray image
2) Feature extraction
3) Resizing of the image
4) Filtering of the image.

Conversion of RGB to gray image

In RGB color model, each color appears in its primary spectral components of red, green, and blue. The color of a pixel is made up of three components; red, green, and blue (RGB), described by their corresponding intensities. RGB color image require large space to store. In image processing we have to process the three different channels. It consumes large time. So it is necessary to convert the RGB image into gray scale image. The information retained by gray

scale image is enough for the system so RGB image is converted to gray scale image for image processing [4].

Feature extraction

When the input image to an algorithm is too large to be processed and it is suspected to be redundant (e.g. the repetitiveness of images presented as pixels), then it can be transformed into a reduced set of features (also named a "features vector"). This process is called *feature extraction.* The extracted features are expected to contain the relevant information from the input image, so that the desired task can be performed by using this reduced representation instead of the complete initial image.

Sobel edge detection

A pixel is at an edge when intensity sharply changes to its neighbors. The edge itself is linear shapes along which that change is maximal. Looking at images as functions of intensity, we can rephrase this property to "a maximum of the first derivative". On the level of pixels we have a discrete input (x, y) ∈ Z and we can use the discrete differential operator to approximate the first derivative in either direction [2]. For x that is

$(\delta x(I))(x, y) = I(x, y) - I(x + 1, y)$

Resizing of the image

The extracted feature from the image is resized according to the requirement of the system. The different methods are available for image resizing. One of the methods used is bicubic interpolation. The bicubic interpolation generates more accurate results.

Bicubic interpolation

For two dimensional regular grid bicubic interpolation is used. The interpolated surface is smoother than corresponding surfaces. For Bicubic Interpolation (cubic convolution interpolation in two dimensions), the number of grid points needed to evaluate the interpolation function is 16, two grid points on either side of the point under consideration for both horizontal and perpendicular direction[3]. The bicubic convolution interpolation kernel is:

$$W(x)= \begin{cases} (a+2)|x|^2-(a+3)|x|^2+1 \text{ for } |x|<=1 \\ a|x|^3-5a|x|^2+8a|x|-4a \text{ for } 1<|x|<2 \\ 0, \text{ otherwise} \end{cases}$$

Where a is generally taken as -0.5 to -0.7

Filtering of the image

Filtering of the image depends on number of techniques. The best option depends on the image and how it will be used. Both analog and digital image processing may require filtering to yield a usable and attractive end result. There are different types of filters such as low pass filters, high pass filters, median filters etc. The low pass filters are smoothening filters whereas the high pass filters are sharpening filters. Smoothening filters are used for smoothening of the edges. Sharpening filters are used for enhancing the edges in the image. In this system the smoothening filters are used. The purpose of smoothing is to reduce noise and improve the visual quality of the image.

Gaussian filtering is used to blur images and remove noise and detail [4]. In one dimension, the Gaussian function is:

$$G(x) = \frac{1}{\sqrt{2\pi\sigma^2}} e^{-\frac{x^2}{2\sigma^2}}$$

Where σ is the standard deviation of the distribution. The distribution is assumed to have a mean of 0.

RESULT S AND DISCUSSION

The object of interest is a moving insects in the agriculture field, is focused with a fixed digital camera. The camera captures the video of the insects at the particular place in a regular interval. A set of properties of a captured video such as frames/second, number of frames, width, height, compression type, image size and file size which forms an example of a set of input video information. The video file frames has to be extracted for further processing. Several interpolated frames may be synthesized between each pair of original frames. An important advantage of using true motion estimation is that it results in better video quality.

Next stage is to convert the single moving frame F into the indexed image X and associated color map 'MAP' and stored in an array of image structure. If the frame contains true color data, then MAP is empty.

Morphological operation is applied to the external frames (images) to identify the new object (pest) entry into the agriculture field. As in this case, the static image being the agriculture field, the new object a pest is encountered from the frame numberX0 to frame number X29out of X30 frames. Take one of the frames from the video at regular

time interval. Then this image is then processed using MATLAB software. In this method, first image which is a reference image represents the reference pixel values of pest for comparison. Second image which is a input image, is taken by one of the frames of video. Using feature extraction process based on the color and shape of the object, we determine the entering of the object. Finally two images are compared and the differences in pixel values are determined. Frame difference which calculates the differences between two frames at every pixel position and store the absolute difference. It is used to visualize the moving objects in a sequence of frames. The third image, will be an output image. The reference and input images are compared by taking their difference where the output of this comparison *DR(x,y)* is determined by the following rule:

$$\boldsymbol{DR}(x,y) = \begin{cases} 0 & if\ R(x,y) = I(x,y) \\ I(x,y) & if\ R(x,y) \neq I(x,y) \end{cases}$$

Where *R(x, y)* and *I(x,y)* are the reference and input images, respectively at image coordinates *(x,y)[4,6]*.

Flow chart

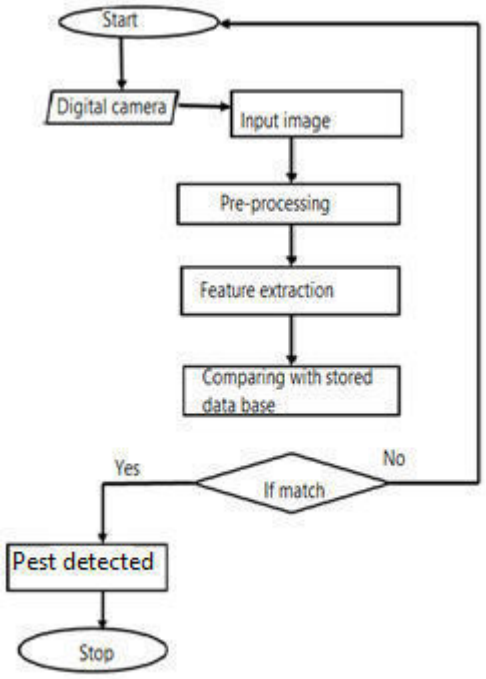

Flow chart of real time pest detection and control system

The obtained difference matrix is then threshold in order to determine the output image *O(x,y)*, which contains the object entered. To threshold the difference matrix, we first calculate its average pixel value using:

$$\boldsymbol{Davg} = \frac{\sum_{x=1}^{nx}\sum_{x=1}^{ny}\boldsymbol{DR1}(x,y)}{\boldsymbol{nxny}}$$

$$\boldsymbol{D}(avg) = \begin{cases} 0 & if\ R(x,y) = I(x,y) \\ I(x,y) & if\ R(x,y) \neq I(x,y) \end{cases}$$

If the Davg value is greater than zero then the reference image and input image are unmatched. The software determines the pest is not present in the agriculture field and if the Davg value is equal to the zero then the reference image and input image are matched. The software determines the pest is present in the agriculture field. Then a message will be displayed-" *object enter motor is ON"*.

Resultant image

Figure1. Reference image of real time pest detection and control system

Figure 2. Input image of real time pest detection and control system

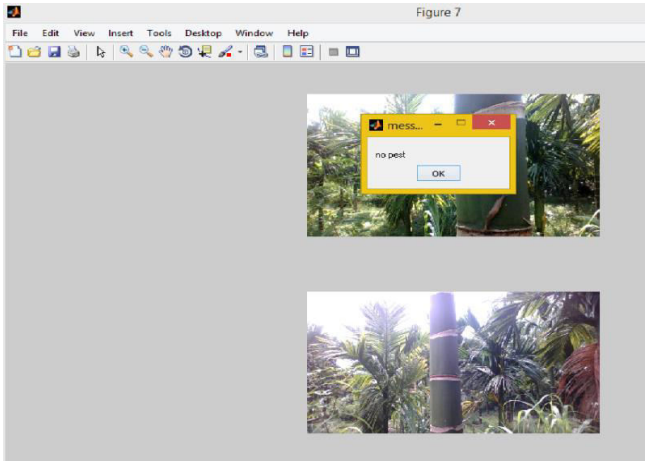

Figure 3. Output of real time pest detection and control system

Figure 4. Reference image of real time pest detection and control system

Figure 5. Input image of real time pest detection and control system

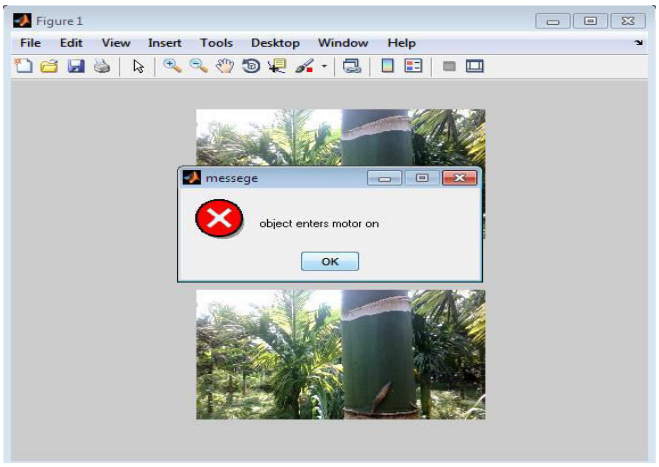

Figure 6.Output of real time pest detection and control system

PROPOSED HARDWARE METHOD

The system consists of the following modules:

1. Digital Camera
2. Sensor ULN2003
3. Microcontroller AT89C52
4. Sprayer

. The ULN2003A is an array of seven NPN Darlington transistors capable of 500mA, 50V output. A Darlington transistor (also known as Darlington pair) achieves very high current amplification by connecting two bipolar transistors in direct DC coupling so the current amplified by the first transistor is amplified further by the second one. AT89C52 is an 8-bit microcontroller and belongs to Atmel's 8051 family. AT89C52 has 8KB of Flash programmable and erasable read only memory (PEROM) and 256 bytes of RAM. AT89C52 has an endurance of 1000 Write/Erase cycles which means

that it can be erased and programmed to a maximum of 1000 times[5]. The figure shows the block diagram of real time pest detection and control system

Initially the system will be in sleep mode. A wireless sensor network (WSN) is used which is interfaced with microcontroller. When the sensor senses the presence of an insect it will send an interrupt signal to microcontroller. The microcontroller will turn on the camera. The camera will capture the image of an insect sitting on plant. The captured image is then sent for pre-processing. The processed image is compared with the stored database images. The database consists of images of insects which are harmful to the ecosystem. Based on the comparison with the parameters of the stored database, the system will generate the output by sending a Signal to microcontroller. The microcontroller AT89C52 in turn will charge the relay ULN2003. Once the relay is charged the sprayer will be turned on

BLOCK DIAGRAM

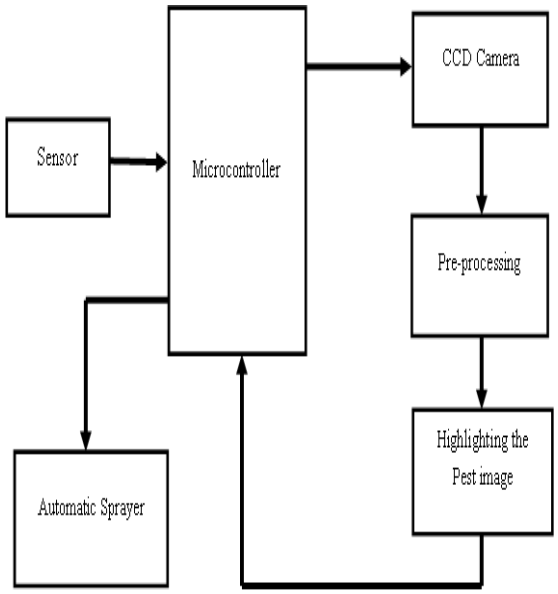

Block diagram of real time pest detection and control system

FUTURE WORK

In future works, the system can be modified by inclusion of Raspberry pi and high accuracy wireless cameras to make use of system to large extent. It will also reduce the overall cost of the system.

Various aspects of the developed system, such as hardware components (i.e. distributed wireless high-quality cameras can be used instead of a single web camera to monitor a large area), system requirements, and others can be further studied to improve the quality. Future efforts can concentrate on improving the reliability and robustness of both detection and security alerts tasks to achieve better performance.

CONCLUSION

In this paper Real Time Pest Detection and Control in Agricultural Plantation using feature selection has been developed. It is found to be viable and productive for agricultural production. The system can be employed in the places like farming, gardens, nursery, horticulture etc. It is rather simple to use and exhibits the same performance level as a classical physical access.

REFERENCES

1. S K Bodhe, Anup Vibhute,"Application of Image Processing in Agriculture": A Survey Int. Journal of Computer Applications (0975-8887) Vol. 52 –No.2, August 2012
2. André Aichert "Feature extraction techniques" January 9, 2008 CAMP MEDICAL SEMINAR WS0708
3. Shreyas Fadnavis "Image Interpolation Techniques in Digital Image Processing" Int. Journal of Engineering Research and Applications ISSN : 2248-9622, Vol. 4, Issue 10(Part -1), October 2014, pp.70-73
4. Gonzalez, R., R. Woods and S.Eddins, 2004. "Digital Image Processing using Matlab". Ist Edn,Printice Hall,ISBN:0130085197,pp:624
5. Kenneth J. Ayala'The 8051 microcontroller" 3rd edition 2004 - Computers - 412
6. Shafiqua T. Pathan, Sharyu S. Waghmare, Pranali P. Khadse, et.al., "A Survey Paper On A Novel Approach For Image Classification Based On SUSAN Low Level Image Processing Algorithm From Real Time Video", *International Journal of Scientific & technology Research*, Vol. 3, February 2014, pp. 201-205.
7. Anitha A, Gayatri J and Ashwini K, "Automatic Recognition Of Object Detection Using MATLAB", *International Journal of Advanced Research in Electronics and Communication Engineering (IJARECE)* Vol. 2, September 2013, pp. 749-756.
8. A.SAI SUNEEL, "Person r Object Tracking And Velocity Estimation in Real Time Videos", *Publications Of Problems & Application In Engineering Research*, Vol 04, 2013, pp. 292-299.
9. Furat N. Tawfeeq, "Real Time Motion Detection in Surveillance Camera Using MATLAB", *International Journal of Advanced Research in Computer Science and Software Engineering*, Vol. 3, September 2013, pp. 622-6

Fault Management Architecture for Multicast Routing in MANET

Channabasayya Mathad
Department of Electronics and Communication Engg
Kalpataru Institute of Technology
Tiptur, Karnataka, India.
mathad123@yahoo.com

Paramesha
Department of Electronics and Communication Engg
Govt. Engg College,
Hassan, Karnataka, India.

D Srinivasa Rao
Department of Electronics and Communication Engg
Jawaharlal Nehru Technological University
Hyderabad, Telangana, India.

Abstract - **MANET is a wireless network consisting of numerous nodes which enters and leaves the network in an unpredictable fashion. So, the path from a sender node to the receiver node in the network keeps changing regularly. In MANET, due to the absence of infrastructure, the movement of the nodes in the network cannot be easily tracked and hence node failure or disconnection is very difficult to be determined. This causes failure of the predetermined path which in turn leads to data loss. Thus in this work, we develop a Fault Management Architecture for Multicast Routing FMAMR technique in the MANET which helps in predicting the node movement pattern and hence aiding in node recovery so as to ensure network efficiency.**

Keywords – Check point interval, Fault tolerant, Group head, Fault management.

I. INTRODUCTION

The MANET is an independent network that is self-systemizing and this network consisting of mobile nodes can be formed quickly, where the nodes communicate with one another wirelessly. In MANET, the nodes move often and randomly, causing the network topology to vary in an unpredictable fashion [1, 2]. A wireless communication link is formed between two nodes, if the involved nodes are within one another's communication range. The irregular node movements lead to formation and breaking of the communication links randomly [3, 4]. Some of the applications of MANET are distance learning, gaming, multimedia conferencing, etc.[5]. But, repeated failure in the communication links occur due to some of the features of MANET such as node mobility, repeated disconnections, network division, restrained bandwidth, application requiring stabilized storage environment, etc. [6].

A. FAULT MANAGEMENT IN MANET

MANET is susceptible to numerous attacks, due to the absence of permanent infrastructure and restrained resources resulting in dynamic network topology. So, to recover the failed nodes, a fault tolerance system is required [5, 7, 8]. Most of the faults can be due to the hardware problems such as an imperfection in the interface, failed node, etc. It can also be due to the performance related issues like congestion in the router, faulty link which leads to increased loss rates in the packet. In the wireless network, classification of the various communication conditions is hard. Due to the mobile nature, the communication feature becomes more dynamic and varying with time, leading to variations in the topology. So, in this dynamic topology of MANET, fault management is a difficult task [9].

On fault detection, the conventional fault management system receives causes of the failure from the device level agents. Next, fault location and root cause for the failure is determined by correlating all the known symptoms during fault localization [9] [10].

We propose to develop fault management architecture for multicast routing to predict the movement using signal-to-noise ratio (SNR) values.

II RELETED WORK

The Zodiac Policy Subsystem (ZPS) design and implementation enabling administrators to securely specify, distribute and evaluate network control and system security policies to customize Zodiac behaviours. The Keynote language was employed by ZPS to specify all authorization policies with simple extension to support obligation policies [11].

In a Proposed Trusted Fault Tolerant (TFT) model with user recovery features in mobile Ad Hoc networking using Location Aided Routing (LAR) protocol. If after receiving packets the nodes moves away from the source to an unreachable location, the location fault occurs. However the node misbehaving increases [12].

In this proposed a primitive approach to fault management system in MANETs: network-invariant fault detection, localization and diagnosis with limited knowledge of the underlying network and traffic models. The statistical network/traffic measurements were observed in one network, and subsequently applied to other networks with satisfactory performance so as to derive fault management models [13].

In this proposed designed an ant colony based trust model for trust value evaluation of a mobile node in MANET. A trusted node possess low or negligible failure and security attack rate, high available battery power indicating high availability in the network and high

positive reference from other nodes. Hence trusted mobile node has secure checkpoint without additional overheads of cryptography. However node failure rate increases by decreasing the trust value [14].

In a biologically inspired control mechanism in which each autonomous vehicle find out its movements relying on the information within its local sensing area to create a MANET which was scalable and tolerant to node failures. However there was a possibility of connection failures [15].

III. THE PROPOSED FAULT MANAGEMENT ARCHITECTURE FOR MULTICAST ROUTING (FMAMR) IN MANET

A. OVERVIEW

In this paper, we propose to develop fault management architecture for multicast routing to predict the movement using signal-to-noise ratio (SNR) values [7]. The multicast group head (GH) stores all the information of all its group members by monitoring it for every pre-defined time interval. Then the SNR value of the nodes are determined and is send to all the neighbouring nodes. The GH after checking the present and past SNR values predicts the node movement pattern. It then estimates status of each node as crashed or normal, based on the predicted movement pattern and connectivity information. Then it sends the details of crashed nodes to other normal nodes. For fault recovery, each mobile node uses the stable storage available at its GH to take a checkpoint periodically [8]. Each GH maintains SENT list and DEPENDENCY list based on the messages sent and received by the node respectively. Then Roll back edges are computed using the DEPENDENCY list for performing rollback recovery of the crashed mobile node by employing log based check pointing [8].

To predict the node movement pattern efficiently, the network is considered to be tree structured. The GH predicts the movement pattern of all the nodes in its tree structured network using the SNR value. Along with the prediction of the nodes moved out of the network range, and crashed node movement, the GH also determines which nodes moved out of the network range, and crashed nodes.

This process is described in algorithm 1.

Algorithm 1

- In the network, after every T seconds, every node, x broadcasts a DISCOVER message to all of its one hop neighbours.

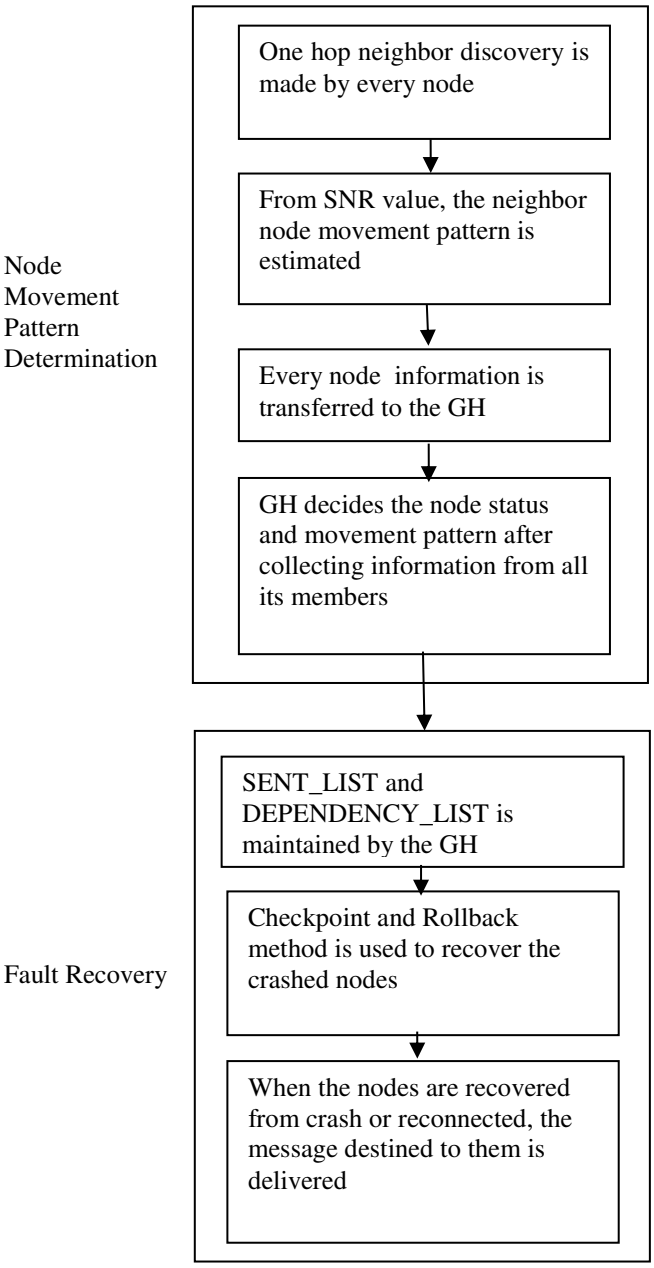

Fig.1 Determination of the Node Movement Pattern

When a one hop neighbour, y receives a DISCOVER message, it replies with a RESPONSE message.

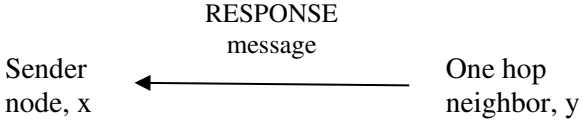

- When the sender node, x receives the RESPONSE message, it checks if the replied node, y is already a neighbour or a new neighbour.

- If the replied node is already a neighbour, then no change is done.
- If the replying node is not a neighbour, then it is added as a neighbour $N(x)_T$.
- After the predefined time interval T, the node sends its newly collected neighbour information to its parent node in the tree structure using a REPORT message.
- The parent node sends the received data from its child node along with its own neighbour information to its parent node.
- This process continues until all the information reaches the GH.
- When the GH receives information from its child nodes, it compares the most recently received information with the previously received information.
- If new node information is present in the recently received information, then the GH adds it as a member node.
- If node information is missing in the recently received information when compared with the previously received information, then the GH considers as the missing node has crashed and includes in the set of crashed nodes.
- This decision made by the GH is sent to all the member nodes in order to make all the member nodes of the tree structure aware of the recent node movements.
- The SNR value of the sender node and replying nodes are recorded every second.
- On the basis of SNR value recorded, the nodes movement are predicted according to the following rules.

$$\text{If } SNR^{i}_{x,y} > SNR^{i-1}_{x,y}, \forall\ 0 < i < n; \qquad (1)$$

Then node y is moving towards node x.

$$\text{If } SNR^{i}_{x,y} < SNR^{i-1}_{x,y}, \forall\ 0 < i < n; \qquad (2)$$

Then node y is moving away from node x.
Where n is the number of last few SNR values.

- The neighbour node is considered to be crashed or moved out of the range, if the following conditions are satisfied.

$$SNR^{i}_{x,y} \neq Nill \quad \forall\ 0 \leq i < m \text{ and}$$

$$SNR^{i}_{x,y} = Nill \quad \forall\ m \leq i < n \qquad (3)$$

Where m is an integer.
- The node is considered to have moved out of the communication range when the following condition is satisfied along with the equation (3).

$$0 < SNR^{m-1}_{x,y} < \sigma \qquad (4)$$

Where σ is a very small SNR value [7].

- Else, the nodes which satisfy the equation (3) are considered to be crashed.
- Every node maintains four groups: $Moving_{away}(x)_{Ta}$, $Moving_{towards}(x)_{Tt}$, and $Outofrange(x)_{To}$ and $crashedset(x)_{Tc}$. The $Moving_{away}(x)_{Ta}$ indicates the nodes that are predicted to be moving away from node x, $Moving_{towards}(x)_{Tt}$ are the nodes that are detected to be moving towards the node x and $Outofrange(x)_{To}$ group contains the nodes that have moved out of the communication range of x and $crashedset(x)_{Tc}$ is the set of neighboring nodes of x which has been crashed.
- Thus the GH considers all the information received from its member child nodes and takes decision about every node in every group after comparing the decision made by every individual node.
- This decision is then sent to all the member nodes. Thus, the movement pattern of every node in the network is predicted.

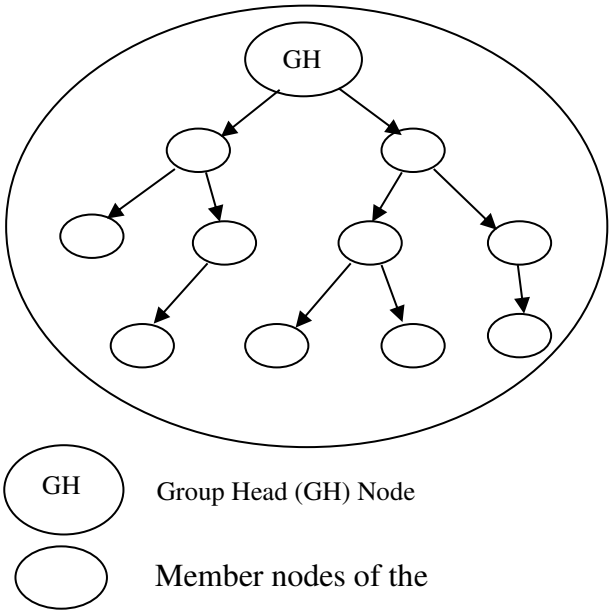

Fig.2: Network Structure.

B. FAULT RECOVERY

The crashed nodes in the network are recovered using the log based check pointing method. This method uses two lists: the SENT_LIST and the DEPENDENCY_LIST for recovering the crashed nodes using the check pointing periodically. The fault recovery technique is described in algorithm 2.

Algorithm 2

- When the GH receives the information from its member nodes, it stores its information. Then when the GH sends its decision to its members, it maintains a SENT_LIST.
- The SENT_LIST includes the information of the nodes with which it has communicated by receiving and sending the information in the form $SENT_n[i]$, where i indicate the member node number.
- The $SENT_n[i]$ consists of three fields: destination node ID, the message transmitted Highest Sequence Number (HSN) and the sender node's Check Point interval (CI) in which this message was sent.
- The GH maintains a DEPENDENCY_LIST to save the information about the message received by a node in a given CI.
- The DEPENDENCY_LIST contains two fields: the sender's ID and its corresponding CI.
- When a GH receives a message, it logs the message in its volatile memory. When all the related messages are received, it groups them together and writes them asynchronously into the stable storage place. Hence, minimizing the number of accesses to the stable storage.
- When a GH receives message and stores it in a storage space, there exists a dependency edge from the interval $C_{1,a}$ to $C_{2,b+1}$, when the message is transferred after $C_{1,a}$ and received before $C_{2,b+1}$.

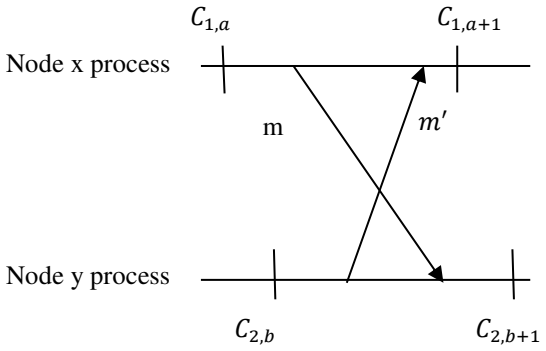

Fig.2: Inter-process communication

- A rollback edge from $C_{1,a+1}$ to $C_{2,b+1}$, but has yet not logged until $C_{1,a+1}$. This rollback method is used to recover the crashed nodes.

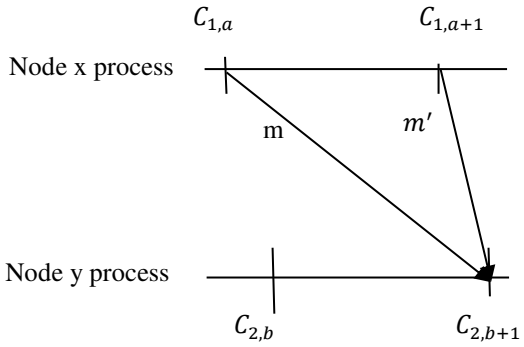

Fig.3: Checkpoint graph

- When a member node moves from one group or cluster to another. The GH transfers the DEPENDENCY_LIST and the SENT_LIST of the moving node to the new GH.
- If a node gets crashed due to any reason, its DEPENDENCY_LIST and the SENT_LIST information are maintained by the current GH until it is recovered using the rollback edge method and then it is then used as required.
- If a node gets disconnected, then the message to be delivered at this node is maintained at the GH until the node gets reconnected to the network.

Thus, the node in the network is handled from getting disconnected and eventually being lost or from crash.

IV SIMULATION

A. SIMULATION PARAMETERS

We use Network Simulator-2 NS-2 to simulate the proposed Fault Management Architecture for Multicast Routing. We use the IEEE 802.11 for MANETs as the MAC layer protocol. It has the functionality to notify the network layer about link breakage. In this simulation, the packet sending rate is varied as 10, 30, 50, 70 and 90 Kb. The area size is 1500 meter x 300 meter region for 50 seconds simulation time. The simulated traffic is Constant Bit Rate (CBR) and Exponential (Exp).

Simulation settings and parameters are summarized in table 1

No. of Nodes	50
Area	1500 m X 300 m
MAC	802.11
Simulation Time	50 Sec
Traffic Source	CBR
Rate	250 Kb
Propagation	Two Ray Ground
Antenna	Omni Antenna
Initial Energy	10.1 J
Transmission Power	0.665 W
Receiving Power	0.395 W
Mobile Speed	10, 20, 30, 40 and 50 m/s

B. PERFORMANCE METRICS

The newly proposed protocol is evaluated with the following parameters and compares the Opportunistic Rollback Recovery ORR [6] protocol with FMAMR.

C. Results and Analysis

Based on Speed

The node speed is varied in terms of 10, 20, 30.40 and 50 m/sec for the CBR traffic.

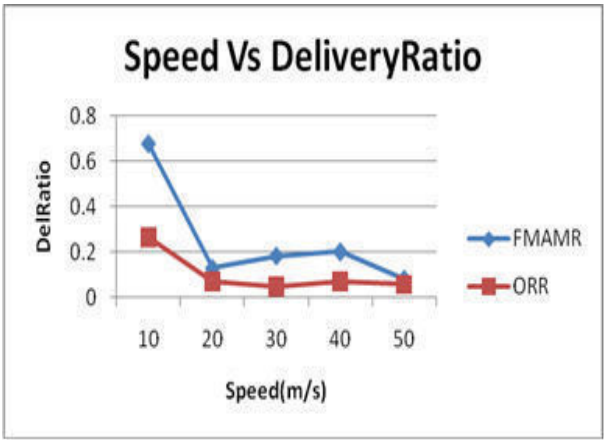

Fig 4: Speed Vs Delivery Ratio

The fig 4 represents the speed V/S delivery ratio, the ORR protocal performs outstanding performance over the FMAMR in terms of delivery ratio by 55%.

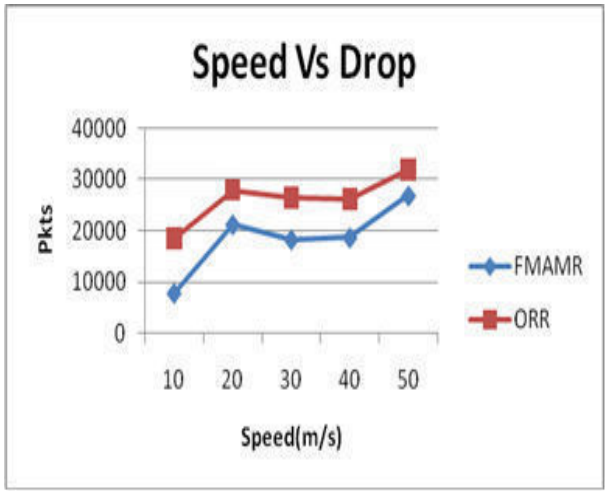

Fig 5: Speed Vs Packet Drop

In fig no 5 shows the speed V/S packets drop, the performance of ORR protocal is improved by 31% in terms of packet drop over a FMAMR protocol.

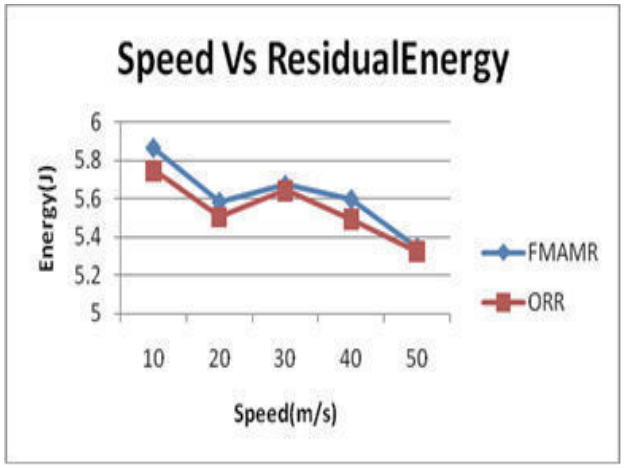

Fig 6: Speed Vs Residual Energy

Fig no 6 illustrate the residual energy V/S speed, there is improvement in performance of a FMAMR with ORR protocol by 2% in terms of residual energy.

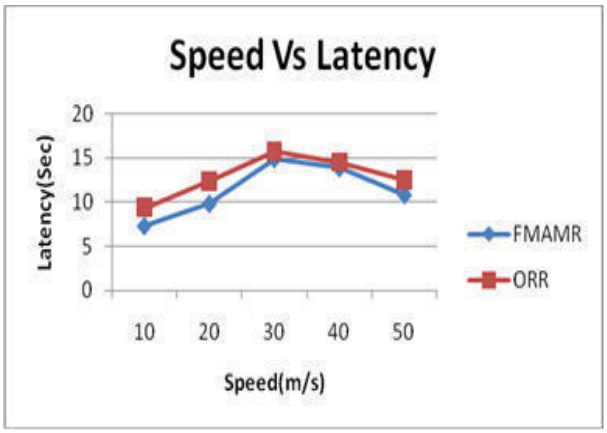

Fig 7: Speed Vs Latency

Fig 7 shows the graph of node speed V/S latency FMAMR have outstanding improvement over a ORR by 13% interms of latency.

V. CONCLUSION

In this paper, we have developed fault management architecture for the multicast routing in MANET. This work is achieved in two phases. Initially, the network is considered in a tree structure and then the node information consisting of the neighbouring node status is transmitted to the GH by every node in the group. Based on the overall information received about each node, the GH makes decision about the movement pattern of every node in its group. In the second phase, the nodes considered as missing or crashed by the GH is recovered by using the rollback technique. For the recovery of nodes, the GH uses the SENT_LIST and the DEPENDENCY_LIST. Thus, this proposed work efficiently performs fault management in a MANET.

REFERENCES

[1] Sheng Xu, Symeon Papavassiliou and Lev Zakrevski, "Fault-tolerant cluster-based routing approach in wireless mobile ad hoc networks", IEEE VTS 54th Vehicular Technology Conference, Vol.4, 2001.

[2] Casey K. Fung, Patrick C. K. Hung, William M. Kearns and Stephen A. Uczekaj, "Dynamic Regeneration of Workflow Specification with Access Control Requirements in MANET", IEEE International Conference on Web Services, 2006.

[3] Mohammad Moallemi, Mohammad Hossien Yaghmaee Moghaddam and Mahmoud Naghibzadeh, "A Fault-Tolerant Mutual Exclusion Resource Reservation Protocol for Clustered Mobile Ad hoc Networks", Eighth ACIS International Conference on Software Engineering, Artificial Intelligence, Networking, and Parallel/Distributed Computing, 2007.

[4] Sirisha Medidi and Jiong Wang, "A Fault Resilient Routing Protocol for Mobile Ad-hoc Networks", Third IEEE International Conference on Wireless and Mobile Computing, Networking and Communications (WiMob), 2007.

[5] D. Ben Khedher, R. Glitho and R. Dssouli, "A Novel Overlay-Based Failure Detection Architecture for MANET Applications", 15th IEEE International Conference on Networks, ICON 2007.

[6] Parmeet Kaur Jaggi and Awadhesh Kumar Singh, "Opportunistic Rollback Recovery in Mobile Ad hoc Networks", IEEE International Advance Computing Conference (IACC), 2014.

[7] Walee Al Mamun, Hanan Lutfiyya, David Kidston and Li Li, "Fault Detection in MANETs", IEEE Network Operations and Management Symposium (NOMS), 2012.

[8] Parmeet Kaur Jaggi and Awadhesh Kumar Singh, "Asynchronous Message Logging Based Rollback Recovery in MANETs", 2nd IEEE International Conference on Parallel, Distributed and Grid Computing, 2012.

[9] Angelo Sapello,Adarsh Sethi, Marian Nodine and Ritu Chadha, "Application of Time Series Analysis to Fault Management in MANETs", International Conference on Network and Service Management (CNSM), 2010.

[10] Xi Zhou, Yifan Ge, Xuxu Chen, Yinan Jing, Weiwei Sun, "A Distributed Cache Based Reliable Service Execution and Recovery Approach in MANETs", IEEE Asia -Pacific Services Computing Conference, 2011.

[11] Yuu-Heng Cheng, Mariana Raykova, Alex Poylisher, Scott Alexander, Martin Eiger and Steve M. Bellovin, "The Zodiac Policy Subsystem: a Policy-Based Management System for a High-Security MANET", IEEE International Symposium on Policy for Distributed Systems and Networks, 2009.

[12] Chandrasekaran S, Shanmugam Udhayakumar, Mohan Bharathy U and Jitendra Kumar Jain D, "Trusted Fault Tolerant Model of MANET with Data Recovery", Fourth International Conference on Intelligent Networks and Intelligent Systems, 2011.

[13] Akshay Vashist, Rauf Izmailov, Kyriakos Manousakis, Ritu Chadha, C. Jason Chiang, Constantin Serban and Syeed E. Ali, "Towards Network Invariant Fault Diagnosis in MANETs via Statistical Modeling: The Global Strength of Local Weak Decisions", IEEE Network Operations and Management Symposium (NOMS), 2012.

[14] Suparna Biswas, Priyanka Dey and Sarmistha Neogy , "Trusted Check pointing Based on Ant Colony Optimization in MANET" , Third International Conference on Emerging Applications of Information Technology (EAIT), 2012.

[15] Stephen Gundry, Jianmin Zou, Cem Safak Sahin, Janusz Kusyk and M. Umit Uyar, "Autonomous and Fault Tolerant Vehicular Self Deployment Mechanisms in MANETs", IEEE International Conference on Technologies for Homeland Security (HST), 2013

Implementation of Computer Vision Based Industrial Automation by Using Neuro-Fuzzy Algorithms

Manjunatha KC[1] H.S. Mohana[2] P.A Vijaya[3]
[1,]*M/s PSIPL-ERM Group of Companies, Challakere, Karnataka*
[2]*Malnad College of Engineering, Hassan, Karnataka*
[3]*B.N.M Institute of Technology, Bangalore, Karnataka*
manju.psipl@gmail.com, hsm@ mcehassan.ac.in, pavmkv@gmail.com

Abstract: *The development of computer vision based automated system for industrial safety and energy savings has presented in this paper. Noting is more important than the safety and health of the people who works in various manufacturing and process industries. Safety is the core value and must not be compromised in the view of other business issues and this applied to everyone involved in the industry. Firstly a computer vision based automated fire detection and suppression system for manufacturing industries is presented and secondly a Vision based non- magnetic object detection on moving conveyor in the steel industry is presented.*

A rule based generic collective model for fire pixel classification is proposed for a single camera with multiple fire suppression control valves. Neuro-Fuzzy algorithm is used to identify the exact location of fire pixels in the image frame. The fuzzy output is fed into supervisory control and data acquisition (SCADA) system to generate suitable analog values for the control valve operation according to fire characteristics. The method achieves up to 99% of accuracy in fire detection and automated suppression.

At single camera level, a vision based differential algorithm is applied to recognize an object. Image pixels based differential techniques; optical flow and motion based segmentations are used for traffic parameters extraction, the proposed approach extends those futures into industrial applications. The technique developed for non-magnetic object detection is having single static background. Establishing background and background subtraction from continuous video input frames forms the basis. Detection of non-magnetic materials which are moving with raw materials and taking immediate action at the same stage as material handling system will avoid the breakdowns or power wastage. The authors achieve accuracy up to 95% with the computational time of not more than 1.5 sec.

Keywords: *Onsite Emergency System (OES), SCADA, PLC, Fire rules, Neuro-Fuzzy algorithm, differential technique, dynamic selection, ego-motion.*

1. Introduction

Industrial automation initially deals with the automation of material handling, manufacturing and quality control. Field sensors, Programmable Logic Controllers (PLC), general process controllers and computers are included in the industrial process automation. Some of the well-known automated manufacturing and process sectors are chemical, cement, steel, power, petroleum, food processing and paper industries etc. there is an ascending interest in automating the manufacturing and verification process of application in industrial automation. Presently available sensor based automation tools are Distributed Control Systems (DCS), Programmable Logic controllers (PLC), Artificial Neural Networks (ANN), Human Machine Interface (HMI) and Supervisory Control and Data Acquisition (SCADA) etc. The research work begins with gathering the information and standard data base of industrial accidents and losses occurred in the recent decades. Study of Industrial Onsite Emergency Plan (IOEP) and reviewing of industrial critical zones have done subsequently. Iron processing and steel manufacturing industry has taken into consideration for our proposed experiments. Study of existing automation system for these industries plays very vital role in implementing computer vision based industrial automation. Automatic fire detection and suppression system within the industry is becoming increasingly very important as our need for highly reliable safety system grows. Similarly automatic loss prevention system within the industry is also plays very important role as the industrial production expenses grows. Agenda is to implement computer vision based automatic safety and loss prevention system for industries by the utilization of available automation systems is very economy system.

Firstly vision-based fire detection and automated suppression system offers several advantages. First, the cost is less, as this system is based on cameras and industries are mostly equipped with CCTVs for surveillance. SCADA and PLC may also be present if there is process

automation. Second, the response time is faster as it does not have to wait for any product of combustion. Fire suppression chemical control valve will be operational at the start of fire itself thus reducing the scope for spreading of fire. Finally, in case of false alarm, confirmation can be done from a control room without rushing to the location. As it is important to have a fast fire detection and suppression system, a computer vision based technique is proposed in this paper. This paper initially focuses on video and image processing for flame pixels detection. Once the fire is confirmed the focus is on the computation of location and intensity of the fire using neuro-fuzzy algorithms. Finally, the attention is on the fire suppression chemical control valve operation through SCADA, PLC and I/O configuration.

Second main application, extraction of non-magnetic object on raw material (Iron Ore, Coal, etc.) handling conveyor will be having lots of advantages like energy save and to avoid equipment damages through unnecessary jams in the path of material flow. In the meantime all raw material transfer points should be enabled with dry fog dust suppression system or pressurized water spray nozzles to avoid the dust. Otherwise dust may deposit on the camera face, it leads to an error. Machine vision based non-magnetic object recognition and removal on moving conveyors in steel industry has been one of the active research areas in computer vision and industrial smart control. It plays a very vital role in advanced industrial automation and process control systems. With an objective to recognize non-magnetic moving objects on moving conveyor through video monitoring system in steel processing industry, it is able to detect and to establish immediate alarm or system can stop the closed loop interlocked system for a moment to remove the non-magnetic material. This can be done in the Programmable Logic Controllers (PLC) and SCADA systems, by enabling suitable preprocessing with MATLAB platform.

2. Related Works

Several approaches have been suggested in literature to identify fire by using variety of image processing techniques. But very few systems have been attempted for automated fire suppression. Tao Chen, Hongyong Yuan, Guofeng Su, Weicheng Fan (2004) experimented an automatic fire searching and suppression system with remote controlled fire monitors for large space. A sensor based automated firefighting system with smoke and temperature detection has been attempted by Mohammad Jane Alam Khan Muhammed Rifat Imam, Jashim Uddin, M. A. Rashid Sarkar (2012). An autonomous fire extinguishing system that detects, targets, and extinguishes a fire within a working space by using heat sensors, a flow control system, servo motors, and a water extinguishing gun has been implemented by A. Rehman, N. Masood, S. Arif, U. Shahbaz (2012). Andrey N. Pavlov, Evgeniy S. Povemov (2009), conducted an experiment to test of automatic fire gas explosion suppression system. Changwoo Ha, Ung Hwang, Gwanggil Jeon, Joongwhee Cho, and Jechang Jeong (2012) proposed vision-based fire detection algorithm by using optical flow algorithm. Tian Qiu, Yong Yan and Gang Lu (2012) have attempted the determination of flame or fire edges. In Barron, Fleet, and Beachemin (1994) authors worked on comparison of different approaches of optical flow estimation. Comparison is done on the basis of accuracy and computational complexities. They have concluded differential technique is best suited for the competition of optical flow and hence the dynamic scene analysis. Entropy based features are used in Hsu, Tyan, Liang, Jeng, and Fan (2005), to check for the existence of vehicles and then tracking is achieved. Though this takes less computational time it suffers serious occlusion problem. Fusion of images and vector maps technique is used in Stilla and Michelses (2002) to discriminate vehicles from objects in the scene. This is suitable for military applications as overall system is complicated and expensive. A comparison of edge element association Edge Element Association (EEA) and marginalized contour approaches for 3D model based vehicle tracking in traffic scenes is implemented in Dehlcamp, Pece, Ottlik, and Nagel (2005). Tracking failures of two approaches, however, usually do not happen at the same time frames which can lead to insights into relative strengths and weakness of the two approaches. Since both the models are to be implemented on every frame computational time frame increases. Recursive optical flow estimation- Adaptive filtering approach is used in (Elad & Fener, 1998). This is modification over Horn and Schunck (Horn & Schunck, 1981) algorithms as it uses only parts of images. Hence sequence of images is used with adaptive filtering technique. The result achieved here is good at cost of linearly growing computational complexities because convergence to be achieved.

3. Algorithms

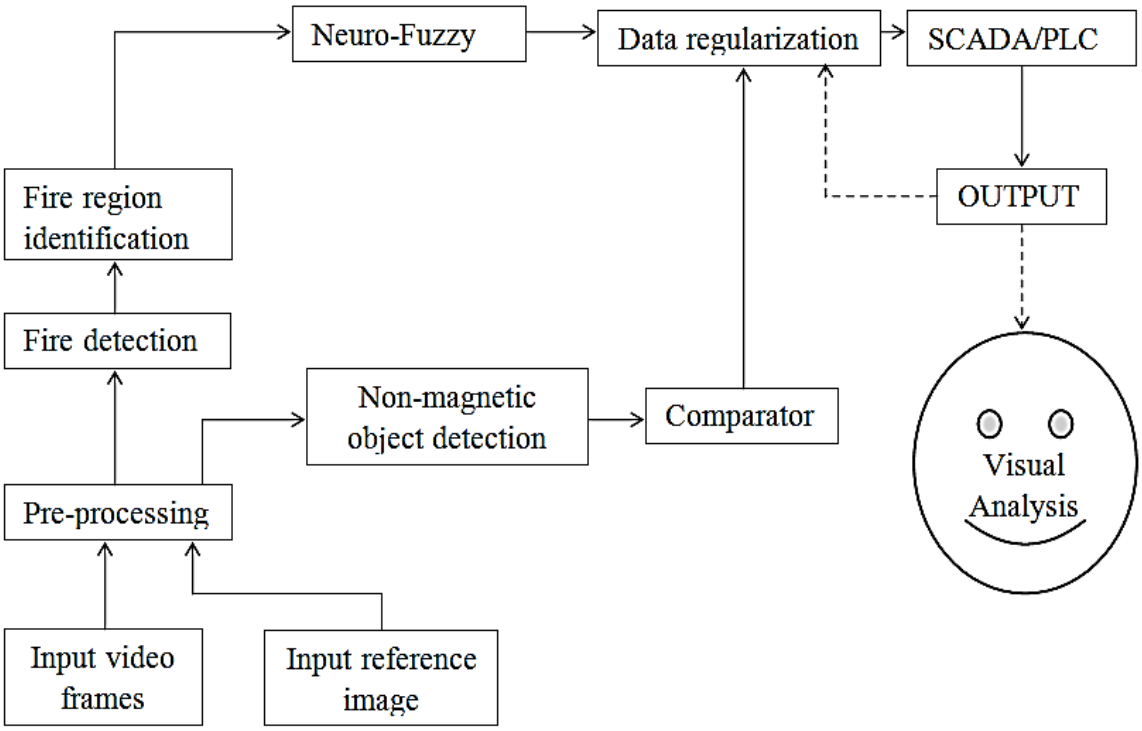

Fig1. System block diagram of computer vision based industrial automation.

- RGB to HSV Conversion
- Image Subtraction
- Binary Conversion.
- Impulse noise and Median filtering
- Edge Detection
- Boundary Detection and Fire Area Calculations.
- Neuro – Fuzzy algorithms
- Decision Rules for fire pixels
- Differential Methods
- Image Simple subtraction with dynamic selection.

4. Implementation

Following general considerations and assumptions are made in order to implement the Computer vision based industrial automation system.

- Analysis and study of literature survey pertaining to topic viz. computer vision, dynamic scene analysis, neuro-fuzzy methodologies and industrial automation.
- Review and survey of process industries for the identification of critical industrial zones or workplaces.
- Complete study of existing automation systems/technologies at process industries and their experimentations.
- Implementation of novel and simple methods/algorithms which supports computer vision, dynamic scene analysis and relative study of the same with conventional methodologies.
- MATLAB, SCADA/DCS and PLC platforms have been exploited for the implementation.
- Selection of applications to experiment the algorithms: application preferred to present and establish the novel approach in computer vision based industrial automation and industrial safety and loss prevention parameters. Safety and loss preventions are very important in present manufacturing and process industrial scenarios.

The block diagram of the implementation system is shown in fig.1. Consecutive video frames and reference image is acquired for the pre-processing. Frame rate of the video acquisition

has fixed to 25 frames per second and the frames are extracted by using frame grabber software at MATLAB platform. The reference image has been stored in BMP or JPG format with suitable pixel size. After preprocessing, the output image or data is exploited for the estimation of fire pixels at one stage and non-magnetic object detection in next stage. Subsequently, the neuro-fuzzy algorithms are used for the estimation of particular fire region and its suppression. Finally MATLAB output from neuro-fuzzy circuit has fed to SCADA/DCS and PLC system for the implementation of automated suppression system. On the other stage the non-magnetic object detection is done by utilizing MATLAB comparator and automation system (SCADA/PLC). Finally the visual analysis has been done after closed loop data regularization process.

5. Discussion on Results

Cases	Input image	Output image	Fire rules		N-F parameter		Automated action
Fire at Steel making furnace service door.		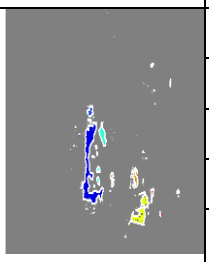	RGB	✓	RN	2	
			YCbCr	✓	ABV	252	
			CA	✓	FAV	4300	
					CVOP	60%	
Fire on electrical Cable trays.		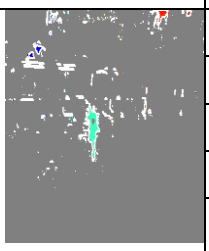	RGB	✓	RN	3	
			YCbCr	✓	ABV	195	
			CA	✓	FAV	2800	
					CVOP	50%	
Fire at steel furnace backflow discharge Point.		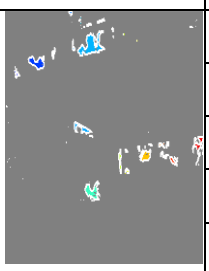	RGB	✓	RN	4	
			YCbCr	✓	ABV	200	
			CA	✓	FAV	1700	
					CVOP	50%	
Fire like lamp		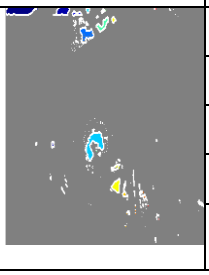	RGB	✓	NO FIRE		NO FIRE
			YCbCr	χ			
			CA	χ			

CA: Change in area, in pixel numbers, RN: Region number, ABV: Average brightness value of region in 0-255, FAV: Fire area value CVOP: Control valve opening percentage

Table (1): Results of automated fire suppression system.

For first case, Performance analysis has been carried out using five sets of videos. Varieties of fire image frames and fire-like image frames are included in table1. It has been observed that the proposed system has very high fire detection and automated fire suppression rate. Determination of change in fire area can differentiate most of fire-like regions with real fire regions.

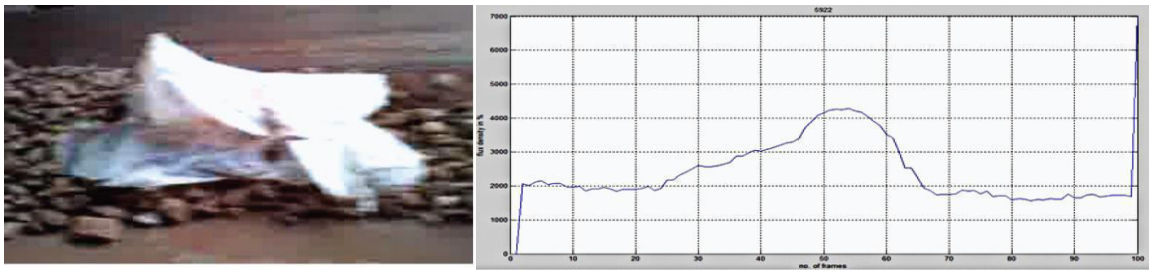

Figure2. A non-magnetic object on moving conveyor and its equivalent increase in white pixel count

Case	Object category	Actual No. of objects	No. of objects detected	Error positive	Error negative	Accuracy (%)
1.	Plastic bags etc.	12	12	0	0	100
2.	Ropes etc.	18	18	0	2	90
3.	Wooden pieces.	9	9	0	0	100
4.	Stone type	24	21	3	0	87.50
Average						**94.35%**

Table2: Results of Non-Magnetic object detection system

Four levels of threshold is implemented to mark the difference between two images and assigned with different colors in the output image. From the results obtained it is evident that the implemented algorithm is separating object from the back ground pixels, detection of non-magnetic object on moving conveyor in almost all the cases in table 2. Also, it works satisfactorily when there is a change in illumination & reflectance.

Conclusion:

The work carried out has produced very good and consistent results. Since fire can cause much damage and have devastating consequences, great efforts are put into the development of systems for its early detection and automated suppression.. The small deviations with different video streams taken under different light reflectance and illumination is minimum, this do not really hampers non-magnetic object detection. Further, efforts are going on to relate the above result with quantity of raw material movement on weighment systems.

References:

1. Tao Chen, Hongyong Yuan (2004). An automatic fire searching and suppression system for large spaces. *Elsevier Fire Safety Journal,*297-307, doi:10.1016/j.firesaf.2003. 11.007.
2. A. Rehman, N. Masood (2012). Autonomous Fire Extinguishing System. *IEEE Transactions*, 218-222.
3. Mohammad Jane Alam Khan, Muhammed Rifat Imam (2012). Automated Fire Fighting System with Smoke and Temperature Detection. *IEEE International Conference on Electrical and Computer Engineering*. 232-235.
4. *Andrey N. Pavlov,* Evgeniy S. Povemov (2009). Experimental Installation for Test of Automatic Fire Gas Explosion Suppression System. *10thB IEEE International Conference and Seminar EDM, 332-334.*
5. Changwoo Ha, Ung Hwang (2012). Vision-Based Fire Detection Algorithm Using Optical Flow. *IEEE Sixth International Conference on Complex, Intelligent, and Software Intensive Systems,* 526-530.
6. Tian Qiu, Yong Yan (2012). An Autoadaptive Edge-Detection Algorithm for Flame and Fire Image Processing. *IEEE Transactions On Instrumentation And Measurement,* 1486-1493.
7. Barron, J. L., Fleet, D. J., & Beachemin, S. S. (1994). Performance of optical flow techniques. *Interna-tional Journal of Computer Vision*, *12*(1), 43–77. doi:10.1007/BF01420984
8. Stilla, U., & Michelses, E. (2002). Estimating vehicle activities using thermal image sequences and maps. In *Proceedings of the Symposium on Geospatial Theory, Processing and Applications*.

Maximizing Aggregate Data Transferred in Vehicle-to-Infrastructure Networks for Drive-Thru Internet Applications

Harigovindan V P
Department of Electronics and Communication Engineering
National Institute of Technology Puducherry
India - 609605
Email: hari@nitpy.ac.in

***Abstract*—In this paper, we investigate performance anomaly problem that occurs when an IEEE 802.11 based road side unit is shared by more than one vehicle transmitting at distinct data rates. Essentially, the vehicle with the lowest data rate slows all other vehicles down to its rate, resulting in poor use of the wireless medium and reduced performance for all the vehicles. This anomaly in the performance is a result of unfair channel time allocation for vehicles when they use multiple data rates. In this paper, our aim is to simultaneously resolve this anomaly and maximize the aggregate data transferred by adjusting the transmission probability of each vehicle according to its data rate through changing the minimum contention window (CW_{min}) size. We consider a multi-rate V2I network, and derive closed form expressions for the optimal transmission probability and corresponding CW_{min} to meet the desired objectives. The analytical results are corroborated using extensive simulations.**

***Index Terms*—Performance anomaly, IEEE 802.11p, Multi-rate Vehicle-to-Infrastructure networks**

I. Introduction

Vehicular communication networks are highly mobile wireless networks envisioned to provide support for road safety, traffic management, and comfort applications by enabling vehicle-to-vehicle (V2V) and vehicle-to-infrastructure (V2I) communications [1]-[2]. The Dedicated Short Range Communications (DSRC) has been proposed as the emerging technology that supports vehicular communications. Recently IEEE 802.11p working group has come out with amendments required for the IEEE 802.11 specifications to support vehicular communication [1]. The higher layers of the protocol stack have been proposed by the IEEE working group 1609. The combination of IEEE 802.11p and the IEEE 1609 protocol suite is designated as wireless access in vehicular environment. The DSRC is based on IEEE 802.11 and is proceeding towards standardization under the standard IEEE 802.11p, whereas the entire communication stack is being standardized by the IEEE 1609 working group under the name Wireless Access in Vehicular Environments (WAVE) [2].

The IEEE 802.11p uses the Enhanced Distributed Channel Access (EDCA) Medium Access Control (MAC) sublayer protocol based on Distributed Coordination Function (DCF) [1]. DCF, which is based on Carrier Sense Multiple Access with Collision Avoidance (CSMA/CA), was originally developed for WLANs [3]. Under DCF, all stations compete for access by using CSMA/CA protocol; they sense the channel before transmitting, and if the medium is found idle for a minimum time equal to DIFS, the packet will be transmitted. More details of DCF can be found in [3]. The EDCA mechanism assigns four different priority classes for incoming packets at each node which are called Access Categories (AC). Each AC has its own channel access function when compared with 802.11 DCF in which all packets exploit the same access function to acquire the channel. Different access functions for different categories mean assigning different delay times, different minimum contention windows, and different number of back-off stages for each type of service [4].

The IEEE 802.11 protocol specifications allow multiple transmission rates at the physical layer (PHY), which use different modulation and coding schemes [6]. Higher data rates allow high quality links to transmit more data, but have a higher loss probability on low quality links. On the other hand, a low data rate is more resilient to low quality links, but fails to achieve a high throughput in a high quality link. Rate Adaptation is the problem of selecting the best transmission rate based on the real-time link quality, so as to obtain maximum throughput at all times. Design of efficient rate adaptive protocols is critical to optimum system performance. Several rate adaptation algorithms have been proposed in the literature for indoor wireless networks with limited mobility such as WLANs (eg., [8], [10]). Vehicular networks have vastly different characteristics from indoor wireless networks, as the link conditions in these networks change more rapidly due to the high mobility of the nodes. Recently, some works have considered the problem of designing rate adaptation protocols in the context of vehicular networks [11], [12].

Consider the V2I scenario, as shown in Fig.1 with vehicles connecting to intermittent and serial Road Side Units (RSUs) along the highway. Typically, as a vehicle enters the coverage of a RSU, it experiences poor signal quality (due to larger distance from the RSU), followed by a stronger signal quality as the vehicle nears the RSU, and a weakening signal after the vehicle passes the RSU. This typically translates into a low

transmission rate at the fringes of the RSU's coverage area and a high transmission rate near the center of the coverage area. However, a performance anomaly problem [7] occurs, when vehicles use multiple data transmission rates. Essentially, the vehicle with the lowest data rate (and likely with the poorest signal quality) slows all other vehicles down to its rate, resulting in poor use of the wireless medium and reduced performance for all vehicles. This problem is caused by the DCF protocol which provides equal channel access probability for all the vehicles. Accordingly the channel usage time of a vehicle gets drastically reduced as the vehicle moves towards the center region of the coverage area of the RSU, due to increased data rate. Furthermore, the performance anomaly problem degrades the aggregate network throughput as well.

In this paper, our aim is to maximize the aggregate data transferred while resolving the performance anomaly problem among vehicles of distinct data rates. We derive analytical expressions for the optimal CW_{min} required to meet the desired objectives. The analytical results are corroborated using extensive simulations. The rest of this paper is organized as follows: Section II presents related work. In Section III, we present an analytical model to compute the amount of data transferred in a single-lane V2I network with multiple data rates. In Section IV, we consider the problem of simultaneously solving the performance anomaly due to multiple data rates and maximizing the aggregate data transferred. The analytical and simulation results are presented in Section V. The paper is concluded in Section VI.

II. RELATED WORK

The performance of DCF has been extensively studied in the literature [9]-[12],[36]. Furthermore, an extensive body of research has been devoted to the performance evaluation of IEEE 802.11p standard [13]-[19]. Authors of [13],[14] propose a simple but accurate analytical model to evaluate the throughput performance of DCF in the high speed V2I communications. In [15] and [16], authors derive analytical models to characterize the average and the distribution of the number of bytes downloaded by a vehicle by the end of its sojourn through an AP's coverage range, in the presence of contention by other vehicles. In [17], authors propose a new vehicular channel access scheme to compromise the trade off between system throughput and fairness in V2I scenario. In [18], authors conduct a study on association control over the drive through Internet scenario. In [19], authors formulate a multi objective optimization problem to optimize both throughput and fairness in IEEE 802.11 based V2I networks. However, the analysis does not provide closed form solution for optimal transmission probability to meet the desired objectives. In our previous work [20], we have proposed a model to find the data transferred in V2I networks with homogeneous data rates among the vehicles and used this model to analyze the access unfairness among vehicles of distinct velocities by tuning their CW_{min} values. In [21], we have proposed TXOP tuning to resolve the access unfairness problem.

Differently from from all the papers mentioned above, the present work aims to maximize the aggregate data transferred in multi rate V2I network in which vehicles use distinct data rates depending upon their distance from RSU. assuming that the vehicle velocity to be uniformly distributed in the interval and that all the vehicles in the network move with the same mean velocity, we have analytical expression for the optimal transmission probability for the vehicles that maximize the aggregate data transferred while resolving the performance anomaly problem among them. We then conduct extensive studies on on the impact of vehicle density, vehicle speed(mean and standard deviation) and no. of vehicles on aggregate data transferred in the network.

Recently, the performance anomaly problem in a V2I network has been analyzed in [14] and [27]. In [27] the authors proposed MV-MAX (Multi-Vehicular Maximum), a new MAC protocol that opportunistically grants wireless access to vehicles with the maximum transmission rate. However MV-MAX suffers from certain fairness problem in the sense that channel access is given only to vehicles with good signal-to-noise ratio. Authors of [14] also considered performance anomaly problem in multi rate V2I networks. However closed form analytical expressions for optimum transmission probability and the corresponding CW_{min} were not obtained.

In this paper, we use the idea of CW_{min} based service differentiation to resolve the performance anomaly problem in V2I networks. The minimum CW is chosen so as to ensure that the amount of successfully transferred data of a vehicle at any time during its sojourn within the RSU's coverage is proportional to its data rate at that time. We then conduct extensive studies on the impact of parameters such as vehicle arrival rate, vehicle density, mean vehicle speed, traffic jam density, and number of vehicles on the amount of data successfully transferred by each vehicle during its sojourn time. It may be noted that authors of [19] have also considered the evaluation of throughput in multi rate V2I networks.

In Section IV, we consider maximizing the aggregate data transferred while resolving the performance anomaly problem in a single lane V2I network. Unlike [19], we derive closed form expression for optimal transmission probability of vehicle with data rate r_z $(z \in [1, N])$ to achieve the desired objective.

III. DATA TRANSFERRED IN MULTI-RATE SINGLE LANE V2I NETWORK

In this Section, we deduce an analytical expression for finding the amount of data transferred in multi-rate V2I networks where all vehicles move with the same mean velocity μ_v. Because of multiple data rate assumption, the coverage area of an RSU is divided into N zones. Consider vehicles that reside within zone z. We assume the vehicle speed to be a random variable with uniform distribution and derive closed form expression for various system parameters. Consider the V2I scenario in Fig.1, with vehicles connecting to intermittent and serial RSUs along the road. Assume that each node (vehicle) has always a frame ready for transmission (i.e., saturation assumption). Further, we assume perfect channel conditions

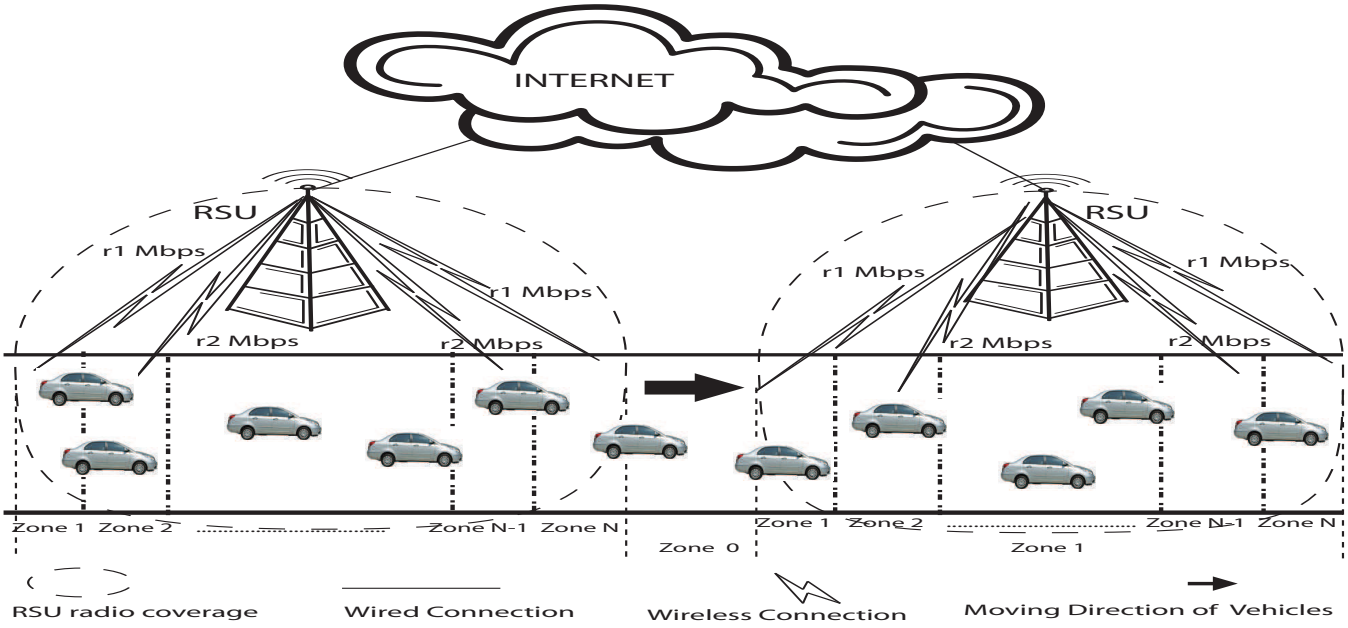

Fig. 1. Vehicle to Infrastructure Scenario

(i.e., no transmission errors), and ignore the effect of hidden and exposed terminals. Such assumptions are typically used for the performance analysis of MAC layer throughput of wireless networks [9],[20].

The area within the radio coverage of RSU is divided into multiple spatial zones denoted as $Z = \{1, 2, \ldots N\}$ such that within each spatial zone, vehicles have distinct payload transmission rate r_z, according to their distance from the RSU. It is assumed that vehicles within a zone z and those belonging to the mirror zone operate at the same data rate r_z. Let there be N zones, N can be either even or odd. Let d_z denote the length of spatial zone, $z \in Z$. The probability density function of V, the random variable representing the vehicle velocity is assumed to be uniform [28], [29] in the interval $[v_{min}, v_{max}]$, with μ_v representing the mean and σ_v representing the standard deviation. Accordingly $v_{max} = \mu_v + \sqrt{3}\sigma_v$ is the maximum speed and $v_{min} = \mu_v - \sqrt{3}\sigma_v$ is the minimum speed. The pdf of V is given by $f_V(v) = \frac{1}{2\sqrt{3}\sigma_v}$ for $\mu_v - \sqrt{3}\sigma_v \leq v \leq \mu_v + \sqrt{3}\sigma_v$; and 0 otherwise.

The residence time of a vehicle in zone z is defined as $T_z = \frac{d_z}{V}$; $z \in [0, N]$. The mean residence time of a vehicle in zone z is calculated as follows

$$\begin{aligned} E[T_z] &= d_z E\left[\frac{1}{V}\right] = d_z \int_{\mu_v - \sqrt{3}\sigma_v}^{\mu_v + \sqrt{3}\sigma_v} \frac{1}{V} \frac{1}{2\sqrt{3}\sigma_v} dV \\ &= \frac{d_z}{2\sqrt{3}\sigma_v} \; ln\left(\frac{\mu_v + \sqrt{3}\sigma_v}{\mu_v - \sqrt{3}\sigma_v}\right) \end{aligned} \quad (1)$$

The average successful payload information transferred by vehicles belonging to zone z $\left(G^{(z)}\right)$ is computed as follows:

$$G^{(z)} = \frac{\begin{pmatrix}\text{Average payload}\\ \text{information for zone } z\\ \text{transmitted in a slot time}\end{pmatrix}}{\text{Average length of a slot time}} \times \begin{pmatrix}\text{Mean residence}\\ \text{time of vehicles}\\ \text{zone } z\end{pmatrix}$$

$$G^{(z)} = \frac{p_{tr}^{(z)} p_s^{(z)} E[X]}{E[T_{slot}]} \times E[T_z] \quad (2)$$

where $E[X]$ is the average payload length (assumed to be equal for all vehicles), $p_{tr}^{(z)}$ is the probability that at least one vehicle in zone z transmits, $p_s^{(z)}$ is the probability of successful transmission by a vehicle in zone z, given that at least one vehicle in zone z transmits, $E[T_{slot}]$ is the average duration of a generic slot and $E[T_z]$ is the mean residence time for a vehicle in zone z within the coverage of RSU. The quantities are determined as follows: Let $\tau^{(z)}$ be the conditional probability that a vehicle transmits a frame in a randomly chosen time slot, given that the vehicle is in zone z and $n^{(z)}$ be the number of vehicles in zone z $(z = 1, 2 \ldots N)$. Then the probabilities $p_{tr}^{(z)}$ and $p_s^{(z)}$ are computed as follows:

$$p_{tr}^{(z)} = 1 - \left(1 - \tau^{(z)}\right)^{n^{(z)}} \quad (3a)$$

$$p_s^{(z)} = \frac{n^{(z)} \tau^{(z)} \left(1 - \tau^{(z)}\right)^{n^{(z)}-1} \prod_{r=1, r\neq z}^{N} \left(1 - \tau^{(r)}\right)^{n^{(r)}}}{p_{tr}^{(z)}} \quad (3b)$$

Let $p_c^{(z)}$ be the probability of collision given a vehicle in zone z transmits and is given by,

$$p_c^{(z)} = 1 - \left(1-\tau^{(z)}\right)^{n^{(z)}-1} \prod_{\substack{r=1 \\ r\neq z}}^{N} \left(1-\tau^{(r)}\right)^{n^{(r)}} \quad (4)$$

The conditional frame transmission probability that a vehicle in zone z transmits a frame in a randomly chosen time slot, given that the vehicle is in zone z, $\tau^{(z)}$ is given by [38],

$$\tau^{(z)} = \frac{2(1-(p_c^{(z)})^{L+1})(1-2p_c^{(z)})}{\begin{pmatrix}(1-2p_c^{(z)})\left(1-(p_c^{(z)})^{L+1}\right)+W_{min}^{(z)} \\ (1-(2p_c^{(z)})^{L^{'}+1})(1-p_c^{(z)})+W_{min}^{(z)}2^{L^{'}} \\ (p_c^{(z)})^{L^{'}+1}(1-2p_c^{(z)})(1-(p_c^{(z)})^{L-L^{'}})\end{pmatrix}} \quad (5)$$

Let σ be the duration of an empty slot time and $E[T_c^{(z)}]$ and $E[T_s^{(z)}]$ respectively the mean time the channel is sensed busy due to collision and successful transmission by a node in zone z. For N= 2 (two data rates), the mean duration of slot time $E[T_{slot}]$ is computed as follows:

$$\begin{aligned} E[T_{slot}] = {} & (1-p_{tr})\,\sigma + \sum_{z=1}^{2} p_{tr}^{(z)} p_s^{(z)} E[T_s^{(z)}] + \\ & \sum_{z=1}^{2}\prod_{r=1 r\neq z}^{2}\left(1-p_{tr}^{(r)}\right) p_{tr}^{(z)}\left(1-p_s^{(z)}\right) E[T_c^{(z)}] \\ & + p_{tr}^{(1)} p_{tr}^{(2)} max(E[T_c^{(1)}], E[T_c^{(2)}] \end{aligned} \quad (6)$$

In (6), first term is the mean duration of an idle slot, second term is the mean duration of a successful slot when the successful transmission is by either $rate-1$ vehicle or $rate-2$ vehicle, third term is the mean duration of collision slot when the collision is among $rate-1$ (zone 1)nodes or $rate-2$ (zone 2) nodes only; and the last term represents the mean duration when collision is among both $rate-1$ and $rate-2$ nodes. Similarly $E[T_{slot}]$ can be found out for any N (number of zones) values, but skipped here because of cumbersome expressions.

The data transferred by vehicles in zone z for zone z, $G^{(z)}$, is then calculated using equations (2) - (6). However for this the number of vehicles in zone z must be known.

A. Network size in zone z, n_z

Based on Greenschilds macroscopic traffic model, the number of vehicles in zone z can be determined as follows:

$$n^{(z)} = \frac{nd_z}{\sum_{n\in z} d_n} = k_{jam}\left(1-\frac{\mu_v}{v_{free}}\right) d_z \quad (7)$$

To compute the data transferred, first of all $\tau^{(z)}$ and $p_c^{(z)}$ are determined using (4) and (5). It may be noted that (4) and (5) form a set of nonlinear equations which can be solved numerically [9]. Once $\tau^{(z)}$ and $p_c^{(z)}$ are known, $G^{(z)}$ can be determined.

IV. Resolving Performance Anomaly through CW_{min} based differentiation

Consider a vehicle with mean speed μ_v. In zones α and β ($\alpha \neq \beta$), these vehicles transmit at data rate r_α and r_β respectively. To resolve the performance anomaly problem caused by distinct data rates within zones α and β, we suggest that the data throughput of a vehicle within a zone must be made proportional to their data rate in the corresponding zone. Accordingly we get the following relative relation for the transmission probabilities of vehicles when they reside in zones α and β:

$$\tau^{(\alpha)} \cong \tau^{(\beta)}\frac{r_\alpha}{r_\beta};\ \ \alpha,\beta \in (1,N), \alpha\neq\beta, \alpha = 1,2,...,N \quad (8)$$

The CW_{min} values, which will simultaneously maximize the aggregate data transferred and resolve performance anomaly, are to be determined as a solution to the following problem.

$$maximize\,(G) \quad s.t\ \ \frac{\tau^{(\alpha)}}{\tau^{(\beta)}} \cong \frac{r_\alpha}{r_\beta} \quad (9)$$

Now $G = \sum_{z=1}^{N} G^{(z)}$ where $G^{(z)}$ is given by (2), substituting (3a) and (3b) in (2), we get the following equation for G. which is given by as:

$$G = \sum_{z=1}^{N} G^{(z)} = \frac{\begin{pmatrix}\sum_{z=1}^{N} n^{(z)}\tau^{(z)}\left(1-\tau^{(z)}\right)^{n^{(z)}-1} \\ \prod_{r=1,r\neq z}^{N}\left(1-\tau^{(r)}\right)^{n^{(r)}} E[X]\,E[T_z]\end{pmatrix}}{E[T_{slot}]} \quad (10)$$

From the constraint imposed in (8), we can write $\tau^{(z)}$ as a function of $\tau(1)$ as follows:

$$\tau^{(z)} = \frac{r_z}{r_1}\tau^{(1)} = \xi_z\tau^{(1)} \quad (11)$$

where we define ξ_z as $\frac{r_z}{r_1}$. Substituting (11) in (10) and assuming $\tau^{(1)} \ll 1$, we can approximate G by the following expression:

$$G = \frac{\alpha_o\tau^{(1)} - \beta_o{\tau^{(1)}}^2}{\gamma_o\tau^{(1)} + \delta_o} \quad (12)$$

where $\alpha_o = \sum_{z=1}^{N} n^{(z)}\xi_z$;
$\beta_o = \sum_{z=1}^{N}\left(n^{(z)}\left(n^{(z)}-1\right)\xi_z^2 + \sum_{\substack{r=1\\r\neq z}}^{N} n^{(r)}n^{(z)}\xi_r\xi_z\right)$;
$\delta_o = \sigma$
$\gamma_o = \sum_{z=1}^{N} n^{(z)}\xi_z\left(E[T_s^{(z)}]-\sigma\right)$ The optimal transmission probability of a vehicle in zone 1, ($\tau^{(1)}$) that maximizes G can be obtained by differentiating (10) with respect $\tau^{(1)}$ and equating to zero, i.e., $\left.\frac{dG}{d\tau^{(1)}}\right|_{\tau^{(1)}=\tau^{*(1)}} = 0$. Accordingly, $\tau^{*(1)}$ and $\tau^{*(z)}$ are given by

$$\begin{aligned} \tau^{*(1)} &= \frac{\sqrt{(\beta_o\delta_o)^2 + \alpha_o\beta_o\gamma_o\delta_o} - \beta_o\delta_o}{\beta_o\gamma_o} \\ \tau^{*(z)} &= \xi_z\tau^{*(1)} \end{aligned} \quad (13)$$

Let $p_c^{*(z)}$ be the collision probability of vehicle in zone z corresponding to optimal transmission probability $\tau^{*(z)}$; $z \in [1, N]$ computed above. Once the optimal transmission probability is known, the optimal CW_{min} for a vehicle in zone z can be obtained from (5) as:

$$W_{min}^{(z)} = \frac{\left(\frac{2}{\tau^{*(z)}} - 1\right)\left(1 - (p_c^{*(z)})^{L+1}\right)(1 - 2p_c^{*(z)})}{\begin{pmatrix} (1 - (2p_c^{*(z)})^{L'+1})(1 - p_c^{*(z)}) \\ +2^{L'}(p_c^{*(z)})^{L'+1} \\ (1 - 2p_c^{*(z)})(1 - (p_c^{*(z)})^{L-L'}) \end{pmatrix}} \quad (14)$$

where $z = 1, .., N$ and $p_c^{*(z)}$ is computed using (4) for a given $\tau^{*(z)}$.

V. Analytical and Simulation Results

In this Section, we present the analytical as well as the simulation results. The analytical results corresponds to the mathematical models presented in the previous Sections and are obtained using MATLAB. To validate the analytical results, we also present simulation results. We simulate a drive-thru Internet scenario as shown in the Fig.1 based on IEEE 802.11p using NS-2.34 [34]. Our simulation has two components: a mobility simulator and a wireless network simulator, which are connected by trace files that specify the vehicle mobility during simulation. Our mobility simulations are performed on the basis of macroscopic freeway model developed by Greenshields. We have used the VanetMobiSim-1.1[35] to simulate our vehicle traffic scenario. For the simulation of wireless network and the protocol stack, we use NS-2.34. The output from VanetMobiSim simulation is a traffic generator trace file that corresponds to position coordinates of each vehicular node at every time steps. This traffic generated trace file of the mobility model serves as the input to NS-2. To evaluate the performance of the network, the trace file generated from NS-2 can be analyzed by using an AWK script, to find the amount of successfully transmitted packets. We simulate the road segment as composed of as many lanes as the number of classes of vehicles; e.g., for the case of two classes, a two lane road segment is simulated. Vehicle of class i arrive according to a Poisson process with rate λ_i veh/sec. Lane i is used by vehicles belonging to class i of mean velocity μ_{v_i}. The probability distribution for class i velocity V_i is assumed to be uniform in $(v_{min,i}, v_{max,i})$ with μ_{v_i} representing the mean vehicle speed and σ_{v_i} , the standard deviation. Traffic jam density k_{jam} = 80 veh/km/lane and the free flow speed is selected as v_{free} = 160 km/hr [14],[20],[32]. The vehicle density is kept constant throughout a particular simulation run, by making the vehicles that exit the highway re-enter from the other end.

While the MAC layer is simulated based on EDCA, we choose physical layer based on IEEE 802.11b. The 802.11b system parameters used for obtaining the results are given in Table I [9]. We divide the communication range of an RSU into multiple zones according to specifications given in Table II [15],[16]. The data rate of a vehicle depends on the zone to which it belongs and are listed in Table II. We have selected system parameters according to IEEE 802.11b instead of IEEE 802.11p, since we could only find the details of zone length duration and the corresponding data rate details for IEEE 802.11b. However, the results and the observations are applicable for other forms of IEEE 802.11 based physical layer specifications as well. We record the trace files of vehicle mobility from the VanetMobiSim-1.1 and use them for the network simulation using NS-2. Each node in the network simulation represents one vehicle of the mobility simulations, moving according to the represented vehicle's movement history in the trace file. In our simulations, the topology is such that all vehicles are sending CBR traffic to the RSU. All the vehicles employ the basic access mechanism (RTS/CTS not used). In the mobility simulations, since vehicles that exit the highway are made to re-enter from the other end, upon each such renewal arrival we clear the transmission history of vehicles with the back-off stage set to zero.

TABLE I
System Parameters

Parameter	Value
Packet payload	8184 bits @ 1, 2, 5.5, 11 Mb/s
MAC header	272 bits @ 1, 2, 5.5, 11 Mb/s
PHY header	128 bits @ $1Mb/s$
ACK	112 bits +PHY header @ $1Mb/s$
Channel Bit Rate	1, 2, 5.5, 11 Mb/s
Propagation Delay	$2\mu s$
Slot Time	$50\mu s$
SIFS	$28\mu s$
DIFS	$128\mu s$
Simulation time	$100sec$
Simulation area	$4500\,m \times 600\,m$

TABLE II
7 Zone Parameters

Zone z	1	2	3	4	5	6	7
$d_z(m)$	25	30	40	60	40	30	25
$r_z(Mbps)$	1	2	5.5	11	5.5	2	1

TABLE III
Number of nodes and mean residence time of vehicles for $k_{jam} = 80\ veh/km/lane$, $\mu_{v_f} = 160km/hr$, $\mu_v = 20km/hr$,$\sigma_v = 5km/hr$ for single lane multi rate network

Zone z	1	2	3	4	5	6	7
$E[T_z]\,(sec)$	6.8431	8.2117	10.9490	16.4235	10.9490	8.2117	6.8431
n_z	2	3	3	5	3	3	2

TABLE IV
CW_{min} Settings for $k_{jam} = 80\ veh/km/lane$, $\mu_{v_f} = 160km/hr$, $\mu_v = 20km/hr$,$\sigma_v = 5km/hr$ for single lane multi rate network

$CW_{min}Setting$	Zone z						
	1	2	3	4	5	6	7
Optimal	479	240	88	44	88	240	479

We assume that the highway can be divided into different number of zones, where each zone corresponds to a data rate.

TABLE V

DATA TRANSFERRED($pernode\ and\ total$) FOR DEFAULT, SUBOPTIMAL AND OPTIMAL CW BEFORE MAXIMIZATION AND AFTER MAXIMIZATION OF AGGREGATE DATA TRANSFERRED, (k_{jam} = 80 VEH/KM/LANE, μ_v = 20 km/hr, σ_v = 5 km/hr, $r_1 = r_7$ = 1 $Mbps$,$r_2 = r_6$ = 2 $Mbps$, $r_3 = r_5$ = 5.5 $Mbps$, r_4 = 11 $Mbps$

CW_{min} Setting	Data transferred(Mb)											
	g_1, g_7		g_2, g_6		g_3, g_5		g_4		Total (G)		Ratio $\left(\frac{g_4}{g_1}\right)$	
	A	S	A	S	A	S	A	S	A	S	A	S
Default	.191	.197	.230	.265	.306	.329	.460	.475	6.288	6.44	2.4	2.5
Optimal	.1071	.1298	.258	.294	.962	.983	2.797	2.918	22.54	23.19	28.0	28.3

A: Analysis S: Simulation

It is assumed that there is a rate adaptation protocol that helps to choose the best transmission rate among the rates permitted by the standard. Initially we consider a single lane network in which all vehicles move with the same mean velocity. Later we extend the results to the multi-lane case. We select maximum back off stage $L^{'}$ to be equal to 5. For a given mean velocity and jamming density, the numbers of vehicles in each zone is calculated using (7). Table III gives the number of vehicles and the mean residence time in each zone for a mean velocity μ_v = 20 km/hr and σ_v = 5 km/hr. These results are used to study the throughput performance of V2I networks as described below.

In the remaining part of this section, we use the following terminologies to represent various cases. We refer 'basic configuration' for the case in which default CW_{min} values are used for the study. In Section IV, we considered the maximization problem and obtained optimal CW_{min} for vehicles belonging to different zones (rates). We refer this case as the 'optimal configuration'. Table IV gives the CW_{min} values used by vehicle in each zone z under optimal for k_{jam} = 80 veh/km/lane, σ_v = 5 km/hr and μ_v = 20 km/hr for a single lane multi rate network. The results are shown in Table V for the four data rates case (that corresponds to seven zones) for default and optimal values of CW_{min}. It is also observed that tuning CW_{min} according to data rate results in considerable improvement in aggregate data transferred. With k_{jam} = 80 veh./km/lane, σ_v = 5 km/hr and μ_v = 20 km/hr, for the optimal CW_{min} configuration, the aggregate data transferred improves by 257% as compared to the default CW_{min} settings.

We select : $L = 7, L^{'} = 5, E[X] = 8184$ bits. For default setting, we select the CW_{min} of the vehicles (in each zone) to be equal to 16. $W_{S,min}$ = 16, $W_{F,min}$ = 16.The MAC parameters such as $TXOP$ (transmission opportunity), $AIFS$ (Arbitration Inter Frame Space) are kept the same for all the nodes in the network. We use (13) and(14) to find optimal CW_{min} for vehicles belonging to distinct zones operating with different data rates. With these CW_{min} values, we find the amount of data successfully transferred by each vehicle and the aggregate data transferred in the network.

Fig. 2 shows the aggregate data transferred (in Mb) versus vehicles' mean velocity. Results are shown for default and optimal values of CW_{min}. As the mean velocity of vehicles increases, the aggregate data transferred reduces owing to the reduced residence time of vehicles in the coverage area of RSU. It is clear from the figure that tuning CW_{min} according to (13) and (14) results in significant improvements in aggregate data transferred as compared to that obtained when default CW_{min} values are used. Fig. 3 shows the data transferred (in Mb) per vehicle in each zone for the case of 7 zones and four distinct data rates given Table II. Results are

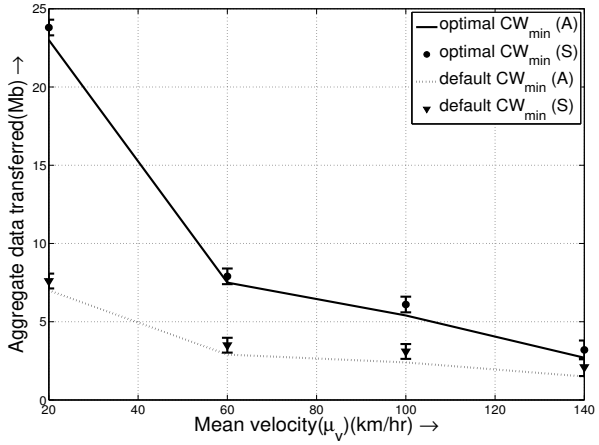

Fig. 2. Aggregate data transferred (Mb) for default and optimal values of CW_{min} for k_{jam}= 80 veh/km/lane, σ_v= 5 km/hr.)

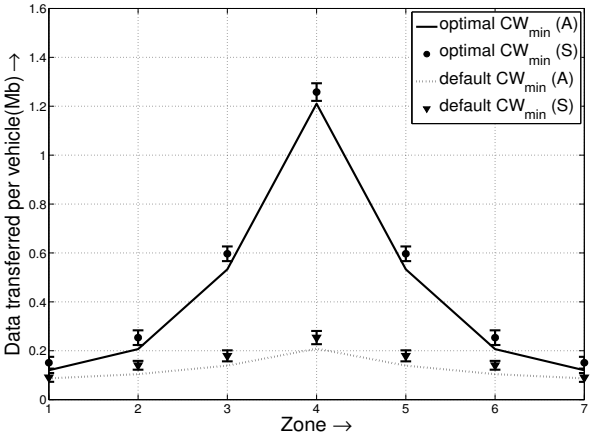

Fig. 3. Data transferred (Mb) per vehicle for default and optimal value of CW_{min} (single lane case) for k_{jam}= 80 veh/km/lane, μ_v= 50 km/hr, σ_v= 5 km/hr

shown for default and optimal values of CW_{min}. We consider k_{jam} = 80 veh/km/lane, σ_v = 5 km/hr and μ_v = 50 km/hr. Further, with these CW_{min} settings, zones which are located near the center of the coverage area (which use higher data rates) experience larger amount of data transfer as compared to those zones which are situated at the fringes of RSUs coverage area (where lower data rate is used). Fig. 4 shows the

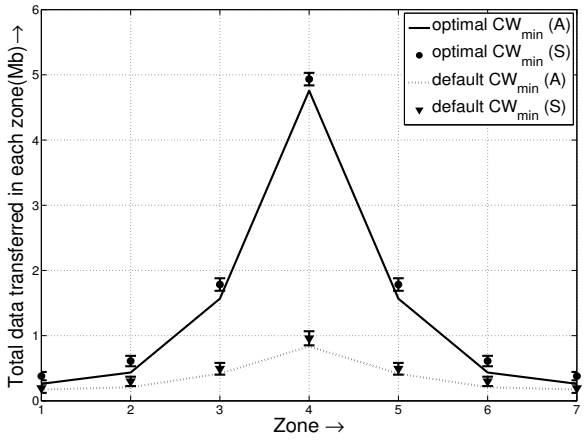

Fig. 4. Total data transferred (Mb) in each zone for default and optimal value of CW_{min} for k_{jam}= 80 veh/km/lane, μ_v= 50 km/hr, σ_v= 5 km/hr

aggregate data transferred (in Mb) per zone for the 7 zones. We consider k_{jam} = 80 veh/km/lane, σ_v = 5 km/hr and μ_v = 50 km/hr. It can be observed that tuning CW_{min} according to (13) and(14) improves the aggregate data transferred. Fig.

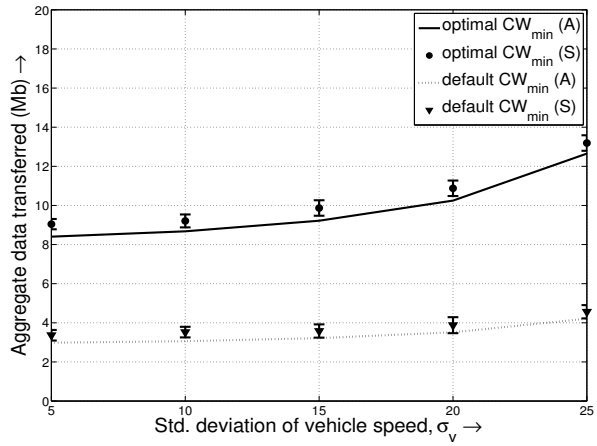

Fig. 5. Aggregate data transferred (Mb) for default and optimal values of CW_{min} for k_{jam}= 80 veh/km/lane, μ_v= 50 km/hr for different values of σ_v

5 shows the impact of vehicle speed standard deviation on aggregate data transferred for the single-lane case. Keeping the mean velocity as a constant, as the standard deviation of vehicle speed increases the mean residence time also increases slightly (from (1)). Accordingly the aggregate data transferred increases slightly with the vehicle speed standard deviation.

VI. CONCLUSION

In this paper, we analyzed data communication performance of vehicles in multi rate vehicle-to-infrastructure (V2I) network used for drive-thru Internet applications. We addressed the performance anomaly problem that occur when a road side unit (AP) is shared by vehicles with distinct data rates. We derived analytical expression for tuning CW_{min} to resolve the above problems and simultaneously, maximize the data transferred. Optimal transmission probabilities were derived for vehicles belonging to distinct zones that correspond to distinct data rates. We observed that tuning CW_{min} according to data rate can resolve the performance anomaly problem and significantly improve the data transferred. Furthermore, the analytical model have been used to evaluate the impact of vehicle speed variability on the data communication performance.

REFERENCES

[1] "IEEE P802.11p draft amendment to standard for information technology telecommunications and information exchange between systems LAN/MAN specific requirements Part 11: WLAN medium access control (MAC) and physical layer (PHY) specifications: Wireless access in vehicular environments (WAVE)," July 2010.

[2] H. Hartenstein and K. P. Laberteaux, "A Tutorial Survey on Vehicular Ad Hoc Networks," IEEE Commun. Mag., pp. 164-171, 2008.

[3] "IEEE Standard for Information technology Telecommunications and information exchange between systems Local and metropolitan area networks Specific requirements Part 11: Wireless LAN MAC and PHY Specifications, 2007".

[4] "IEEE 802.11e/D4.0, Draft Supplement to Part 11: Wireless LAN MAC and PHY specifications: MAC Enhancements for Quality of Service (QoS)," November 2005.

[5] V. Bychkovsky, B. Hull, A. Miu, H. Balakrishnan, and S. Madden, "A measurement study of vehicular internet access using in situ Wi-Fi networks," in ACM Proc. of MOBICOM, 2006.

[6] J. Ott and D. Kutscher, "Drive-thru internet: IEEE 802.11b for 'automobile' users,"in IEEE Proc. of INFOCOM, 2004.

[7] M. Heusse, F. Rousseau, G. Berger-Sabbatel, and A. Duda, "Performance Anomaly of 802.11b." In IEEE INFOCOM, 2003.

[8] A. Kamerman and L. Monteban, "WaveLAN II: A high-performance wireless LAN for the unlicensed band," Bell Labs Technical Journal, 1997.

[9] G. Bianchi, "Performance Analysis of the IEEE 802.11 Distributed Coordination Function," IEEE JSAC, 18 (3) (2000) 535-547.

[10] G. Holland, N. Vaidya, and V. Bahl, "A rate-adaptive MAC protocol for multihop wireless networks," in Proceedings of Mobicom, 2001.

[11] D.J. Deng, C.H. Ke, H.H. Chen, and Y.M. Huang, "Contention window optimization for IEEE 802.11 DCF access control," IEEE Trans. Wireless Commun. 7 (12) (2008), pp. 5129-5135.

[12] J. Camp and E. Knightly, "Modulation rate adaptation in urban and vehicular environments:Cross-layer implementation and experimental evaluation," in Proceedings of ACM MobiCom, September 2008.

[13] Tom H. Luan, Xinhua Ling, and Xuemin (Sherman) Shen, "MAC Performance Analysis for Vehicle-to-Infrastructure Communication,"in proc. Wireless Communications and Networking Conference (WCNC), April 2010.

[14] Tom H. Luan, Xinhua Ling, and Xuemin (Sherman) Shen, "MAC in Motion: Impact of Mobility on the MAC of Drive-Thru Internet," to appear in IEEE Transaction on Mobile Computing.

[15] W. L. Tan, W. C. Lau, and O. Yue, "Modeling Resource Sharing for a Road-side Access Point Supporting Drive-thru Internet," in Proc.of ACM VANET, 2009.

[16] W. L. Tan, , W. C. Lau, O. Yue, and T. H. Hui, "Analytical Models and Performance Evaluation of Drive-thru Internet Systems," IEEE JSAC , vol.29, no.1, pp.207-222, January 2011.

[17] Sheu, S. T., Cheng, Y. C., & Wu, J. S. (2010, May). A channel access scheme to compromise throughput and fairness in IEEE 802.11 p multi-rate/multi-channel wireless vehicular networks. In Vehicular Technology Conference (VTC 2010-Spring), 2010 IEEE 71st (pp. 1-5). IEEE.

[18] Xie. L., Q. Li, Mao. W, Wu. J, and Chen. D, "Achieving Efficiency and Fairness for Association Control in Vehicular Networks," proc. of IEEE ICNP 2009: pp.324-333.
[19] Alasmary. W, and Basir. O, "Achieving Efficiency and Fairness in 802.11-based vehicle-to-infrastructure Communications," in proc. of IEEE VTC- Spring, Budapest, May 2011.
[20] V. P. Harigovindan, A. V.Babu and Lillykutty Jacob,"Ensuring fair access in IEEE 802.11p-based vehicle-to-infrastructure networks", EURASIP Journal on Wireless Communications and Networking 2012, 2012:168.
[21] Harigovindan, V. P., A. V. Babu, and Lillykutty Jacob. "Tuning transmission opportunity (TXOP) limits for providing bit-based fairness in IEEE 802.11 p V2I networks." In Proceedings of the International Conference on Advances in Computing, Communications and Informatics, pp. 248-254. ACM, 2012.
[22] Pravin Shankar, Tamer Nadeem, Justinian Rosca and Liviu Iftode, "CARS: Context-Aware Rate Selection for Vehicular Networks," in proc. of IEEE ICNP 2008, pp 17-22, Florida, USA.
[23] A.V. Babu and Lillykutty Jacob, "Fairness Analysis of IEEE 802.11 Multi-rate Wireless LAN, IEEE Transactions on Vehicular Technology," Vol. 56, PP. 3073-3088, Sept. 2007.
[24] G. Tan and J. Guttag, "Time-based Fairness Improves Performance in Multi-rate Wireless LANs." In USENIX Annual Technical Conference, 2004.
[25] S.-H. Yoo, J.-H. Choi, J.-H. Hwang, and C. Yoo, "Eliminating the Performance Anomaly of 802.11b. Lecture Notes in Computer Science," 3421:1055-1062, 2005.
[26] D.-Y. Yang, T.-J. Lee, K. Jang, J.-B. Chang, and S. Choi, "Performance enhancement of multi-rate IEEE 802.11 WLANs with geographically scattered stations," IEEE Trans. Mobile Comput., vol. 5, no. 7, pp. 906-919, Jul. 2006.
[27] D. Hadaller, S. Keshav, and T. Brecht, "MV-max: Improving wireless infrastructure access for multi-vehicular communication," in ACM SIGCOMM Workshop on Challenged Networks (CHANTS-06), 2006.
[28] Xiaomin Ma, Xianbo Chen, Hazem H. Refai, "Performance and Reliability of DSRC Vehicular Safety Communication: A Formal Analysis," EURASIP J. Wireless Communication and Networking, 2009.
[29] Hao Wu, Richard M. Fujimoto, George F. Riley, Michael Hunter, "Spatial Propagation of Information in Vehicular Networks," IEEE Transactions On Vehicular Technology, Vol.58, No.1, January 2009.
[30] Todd Murray, Tammy Murray, Michael Cojocari, and Huirong Fu, "Measuring the Performance of IEEE 802.11p Using ns-2 Simulator for Vehicular Networks," in: Proc. IEEE. EIT, 2008, pp. 98 - 503
[31] Sven Wiethlter, Christian Hoene, "An IEEE 802.11e EDCF and CFB Simulation Model for ns-2, http://www.tkn.tuberlin.de/research/802.11e ns2/," Technical Report TKN-03-019, Telecommunication Networks Group, Technische Universitt Berlin, Nov. 2003.
[32] R. P. Roess, E. S. Prassas, W. R. Mcshane, "Traffic Engineering," Pearson Prentice Hall, third edition, 2004.
[33] G. Anastasi, E. Borgia, M. Conti, and E. Gregori, "Wi-fi in ad hoc mode: a measurement study," in Proc. of IEEE PerCom, 2004.
[34] The NS2 Simulator, http://www.isi.edu/nsnam/ns.
[35] Harri, J., and Marco Fiore. "VanetMobiSim Vehicular Ad hoc Network mobility extension to the CanuMobiSim framework." Institut Eurcom Department of Mobile Commu 6904 (2006).
[36] F. Cali, M. Conti, and E. Gregori, "Dynamic Tuning of the IEEE 802.11Protocol to Achieve a Theoretical Throughput Limit," IEEE/ACM Trans. Networking, 8 (6) (2000), pp. 785-799.
[37] Y. Xiao, "Performance Analysis of Priority Schemes for IEEE 802.11 and IEEE 802.11 e wireless LANs," IEEE Trans. Wireless Commun. 4 (4) (2005), pp. 506-1515.
[38] P. Chatzimisios, A. C. Boucouvalas, and V. Vitsas, "IEEE 802.11 packet delay - A finite retry limit analysis," in Proc. IEEE Globecom, 2003, pp. 950954.

A Novel approach to Brain Tumor Detection using k-means clustering and Object Labeling Algorithm

Chethan Kumar S. N.
PG Scholar
Dept.of ECE
Malnad College of Engineering
Hassan-573202
chetusn2011@gmail.com

Keerthi D.S.
Assistant Professor
Dept.of ECE
Malnad College of Engineering
Hassan-573202
dsk@mcehassan.ac.in

Vinod Gonsalves
Software Consultant
Hassan-573201
vinodgons@gmail.com

Abstract

In this paper, we propose an efficient brain tumor detection method, which can detect tumor and locate it in the brain MRI images. Throughout the few years, various image processing techniques have been employed to detect malignant tumor in brain MRI image. The popular one being fuzzy c-means method, morphological operation, template matching approach, k-means clustering, cohesion based self-merging, bayes classifier etc. With decent accuracy .But when the tumor is close to the bone this method has been inefficient. We proposed to extract the tumor image using k-means algorithm followed by object labeling algorithm along with prepossessing steps such as noise removal, median filtering and morphological operations. The accuracy of our method is compared with existing method such as fuzzy c-method and k-means clustering.

1 Introduction

Image segmentation holds an important position in the area of medical image processing [1]. Segmentation can be used to detect tumor from MRI image. Throughout the few years, different segmentation methods have been used for tumor detection but it is time consuming process and also gives inaccurate result. So, computer aided system can be designed for accurate brain tumor detection from MRI images. Brain tumor can be broadly classified as primary brain tumor(the tumor originates in the brain) and secondary brain tumor (spread to brain from somewhere else in the body through metastasis) [2]. Primary brain tumors do not spread to other body parts and can be malignant or benign and secondary brain tumors are always malignant. Malignant tumor is more dangerous and life threatening than benign tumor. The detection of malignant tumor is more difficult than benign tumor. For the accurate detection of the malignant tumor that needs a 3-D representation of brain and 3-D analyzer tool. Different brain tumor detection algorithms have been developed in the past few years. M. Masroor Ahmed and Dzulkifti Bin Mohammad [1] proposed brain tumor detection method using K-means algorithm. It is observed that tumor is detected along with non-tumor region. Also, Greg Hamerly and Charles Elkan have presented an al-gorithm using K-means clustering [3]. This algorithm can be used for better result in image segmentation. J.

Selvakumar et al. [2] has been developed brain tumor detection with K-means clustering algorithm and finally they have used FCM for better result. An adaptive K-means algorithm is considered in [4] to detect micro calcifications in digital mammograms for breast cancer detection. FCM technique is used in [5] to extract WM, GM and CSF from MRI image. M. Shasidhar, V. Sudheer Raja, B. Vijay Kumar [6] has modified FCM for fast convergence of the algorithm. In [7] a technique called Cohesion Based Self Merging (CSM) is used to re ne the detected tumor area.

In addition, algorithm using threshold technique based segmentation has also been investigated in tumor detection problem in [8]. Kiran Thapaliya and GooRak K won [9] has detected tumor from MRI image using techniques based on morphological operations. In template matching approach had cited to detect the tumor. A. Elamy, M.Hu [10] has predicted the growth of the tumor using similarity measure approach by combining Bayes Classifier. In this paper, we develop a brain tumor detection technique for T2-weighted MRI images, T2-weighted MR images brain tumor appears as hyper-intense with respect to normal brain tissue

The existing brain tumor detection methods are based on different unsupervised learning algorithms (K-means, Fuzzy C-means (FCM) etc.). K-means is partitioned clustering approach and in FCM, membership value of each pixel is calculated so that a particular pixel can belong to a cluster center. Threshold is a particular intensity value which satisfies a predefined intensity value, it is used to separate object or Region of Interest (ROI) from the image background, chosen in the range of 0 to 255. But it is observed that clustering methods followed by threshold cannot detect tumor properly from MRI image, because the image consist of several non-brain tumor tissue. For this reason we formulate the proposed method using K-means algorithm followed by Object labeling algorithm also, some preprocessing steps (median filtering and morphological operation) is used for tumor detection purpose. In this paper, an efficient brain tumor detection method, which can detect tumor and locate it in the brain MRI images is proposed. This method extracts the tumor by using K-means algorithm followed by some pre-processing steps like median filtering and Morphological operation and finally Object labeling algorithm is applied to detect the This approach produces better results when compared to the existing techniques.

The existing Brain Tumor detection methods in MRI scanned images perform poorly when the tumor is close to the bone. We, therefore, propose a novel method to overcome the problem and compare them against the existing methods.

The paper is organized as follows: The existing technique in section II .The new algorithm is proposed in Section III. Experimental results are presented in Section IV and Section V concluded the paper.

2 Existing Techniques

A) k-means Clustering and Perona-Malik Anisotropic Diffusion Model

Segmentation of images holds an important position in the area of image processing. A well-known segmentation problem within MRI is the task of labeling voxels according to their tissue type which include White Matter (WM), Grey Matter (GM), Cerebrospinal Fluid (CSF) and sometimes pathological tis-sues like tumor etc. It is an efficient method for automatic brain tumor segmentation for the extraction of tumor tissues from MR images. It combines Perona and Malik anisotropic diffusion model for image enhancement and k-means clustering technique for grouping tissues belonging to a

specific group. It is observed that tumor is detected along with non-tumor region.

Result

- It produces reliable results by using the above al-gorithm.
- The proposed system is efficient and less error sensitive due to unsupervised approach.
- Results show that unsupervised segmentation methods are better than supervised segmentation methods.
- It uses k-means algorithm which is simple and efficient.

Limitation

- It is observed that tumor is detected along with non-tumor region.

B) k-means clustering and FCM algorithm

Normally the anatomy of the Brain can be viewed by the MRI scan or CT scan. In this method the MRI scanned image is taken for the entire process .It is based on the Magnetic field and radio waves .There are different types of algorithm were developed for brain tumor detection. But they may have some draw-back in detection and extraction. This method uses computer aided method for segmentation (detection) of brain tumor based on the combination of two algorithms .so it gives the accurate result for tumor

Segmentation. This method focuses on detection of mass tumor and its shape detection. K-Means is the one of the unsupervised learning algorithm for clusters

. Clustering the image is grouping the pixels according to some characteristics. The k-means algorithm i initially it has to de ne the number of clusters k. Then k-cluster center are chosen randomly. The distance between the each pixel to each cluster centres are calculated. The distance may be of simple Euclidean function. Single pixel is compared to all cluster centers using the distance formula. The pixel is moved to particular cluster which has shortest distance among all. Then the centroid is re-estimated.

Fuzzy C-Mean (FCM) is an unsupervised clustering algorithm that has been applied to wide range of problems involving feature analysis, clustering and classier design. FCM has a wide domain of applications such as agricultural engineering, astronomy, chemistry, geology, image analysis, medical diagnosis, shape analysis, and target recognition. The fuzzy logic is a way of processing the data by giving the partial membership value to each pixel in the image. The member-ship value of the fuzzy set ranges from 0 to 1. Fuzzy clustering is basically a multi valued logic that allows intermediate values i.e., member of one fuzzy set can also be member of other fuzzy sets in the same image. The clusters are formed according to the distance be-tween data points and cluster centres are formed for each cluster. The Algorithm Fuzzy C-Means (FCM) is a method of clustering which allows one piece of data to belong to two or more clusters. This method is frequently used in pattern recognition.

Result

- This method allows the segmentation of tumor tissue with accuracy and reproducibility comparable to manual segmentation.
- It also reduces the time for analysis.
- It uses FCM algorithm for accurate tumor shape extraction.

Limitation

- It is observed that clustering methods followed by threshold cannot detect tumor properly from

MRI image, because the image consist of several non-brain tumor tissue.

C) Fuzzy c-means technique with histogram based centroid initialization for brain tissue segmentation

In this approach produced the optimal results within 14-18 iterations in 2.5-11 sec/slices while the existing FCM took 3.5- 15 sec/slice. The results indicate that the knowledge about the data sets to be clustered can be used e effectively to initialize the centroids for FCM algorithm. In the existing FCM, the centroids are initialized randomly. This leads to in-crease in time to reach the optimal solution. In order to accelerate the Segmentation process an application specific knowledge is used to initialize the centers of required clusters. To segment brain portion, we use the knowledge about the MRI intensity characteristics of brain regions to initialize the centroids. The performance of existing FCM and the proposed approach with centroid initialization is evaluated by applying the methods on several data sets. The comparison is done in terms of processing time and the values obtained as final centroids.

Result

- The results reveal that the proposed method with 14 iterations is sufficient to segment the normal brain volumes.

Limitation

- Initialization of centroids is complicated and there is still scope for improvement in mechanisms to initialize centroids efficiently.

D) Cohesion based Self Merging algorithm

It presents segmentation of brain MRI for the purpose of determining the exact location of brain tumor using CSM (Cohesion based Self Merging) based partitional K means clustering algorithm. CSM has at-attracted much attention as it gives efficient result as a self-merging algorithm compared to other merging processes. The CSM is an interesting Hybrid clustering algorithm proposed in the literature. Although the algorithm has a good performance, it suffers from in-stability of its results. CSM partitions the input data set into several small sub clusters in the first phase, and then continuously merges the sub clusters based on cohesion in a hierarchical manner in the Second phase. Cohesion-based clustering is very robust and possesses the excellent Tolerance to outliers in various workloads. More importantly, CSM able to cluster the data set of arbitrary shape very efficiently, and provide better clustering result than those by prior methods.

Result

- It is simpler and computationally less complex.
- Computation time and the effect of noise is less.
- The probability of obtaining the exact location of tumor is more.

Limitation

- The tumor that originates near the skull is some-times not detected in its early.

3 PROPOSED METHOD

The basic purpose of this paper is to show only the tumor region. In this paper, different types of T2- weighted images are used for tumor detection. The complete procedure for the proposed algorithm is given below.

A) Pre-processing

This is the first step of the proposed method. In this step, some noises and skull remove from the images using median filter and morphological operations.

1.) Noise Removal: Median filter acts as noise removal nonlinear tool. In this filtering technique each image pixel is replaced by the neighbor-hood median pixel. Median filter is robust and widely used in image processing because it pre-serves edges while removing noise. Another ad-vantage is that it does not create any new intensity image pixel because median is an existing pixel value in the neighborhood window (3 x 3).

2.) Morphological Opening: Morphological opening is another important preprocessing (skull removing) step. Two gray scale morphological operations, Erosion and Dilation is used for this purpose. Here, 3 x 3 square Structuring Element (SE) is considered for tumor detection.

B) Segmentation

After preprocessing step, MRI Image is segmented by K-means clustering algorithm. It is fairly simple when compared with frequently used fuzzy clustering methods [1]. K cluster centers are randomly chosen from image data. Then distance is computed for each pixel with the K cluster centers. The pixel belongs to that cluster center which gives minimum distance. Then the K cluster centers are recomputed and this process is repeated until the centers converge.

C) Construct Binary Image

Then, binary image is constructed by Threshold approach. Threshold intensity is defined as the pixel intensity value which satisfies a predefined value. After applying K-means, threshold intensity is applied over segmented image. In gray scale image 255 is considered as foreground or object pixel and 0 is considered as background pixel.

D) Object Labeling Algorithm

In this paper, binarized image is labeled using Object Labeling algorithm. The purpose of this algorithm is to label different objects within the image [11].

E) Detect Tumor

In the final step, detect the tumor region from labeled MRI image. The tumor occupies maximum area in the labeled image, so there is exactly one label in the labeled image whose frequency value will be the maximum. The steps of this approach are given be-low:

Step I : Let there are n labels l0,l1,l2,.l(n-1) in the labeled image. Count frequency (occurrence) of each label from the labeled image. Let the frequencies are f0,f1,f2,.f(n-1) for labels l0,l1,l2,.l(n-1) respectively.

Step 2: Find max f0,f1,f2,.f(n-1) Let this frequency is fmax.
Step 3: Search for the label l_k 0 <= k <= (n 1)from the set l0,l1,l2,.l(n-1) which have the frequency value fmax.

Step 4: Perform 8-adjacency with respect to l_k in the labeled image.

Step 5: Construct binary image from the labeled image.

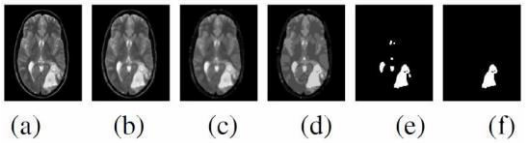

(a) (b) (c) (d) (e) (f)

Figure 1: Tumor detection using proposed method: (a)Original image(b)applying median filter (c)applying morphological opening (d)applying K-means method (e) applying threshold (f) detected tumor.

4 EXPERIMENTAL RESULTS

A) Loading of MINC files

The input image is extracted from the data set and it is stored in MINC le which is used to read it. The figure shown below shows the input image which is stored and read by MINC les.

B) Pre-processing

Median Filtering : The noise present in input image is usually Gaussian noise and salt and pepper noise ,is removed by Median filtering .

Morphological Opening :Morphology is a broad set of image processing operations hat process image

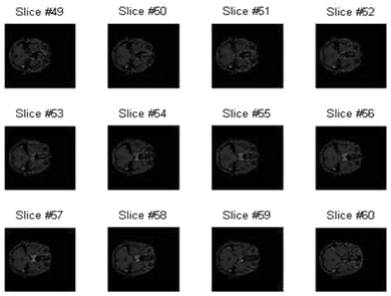

Figure 2: Input MRI image read and stored by MINC

based on shapes .the most basic Morphological Operations are dilation and erosion . Dilation: The value of the output pixel is the maximum value of all the pixels in the input pixel's neighborhood.

Erosion: The value of the output pixel is the minimum value of all the pixel in the input pixel's neighborhood

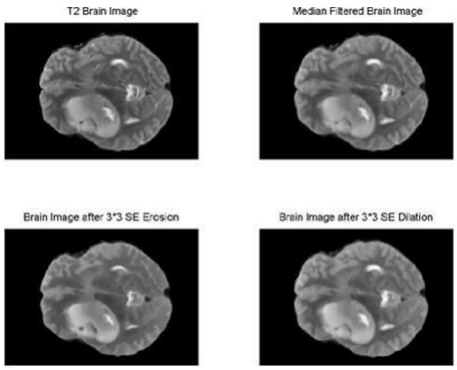

Figure 3: Pre-processing output

C) Segmentation

The goal of segmentation is to simplify and/or change the representation on an image into something that is more meaningful and easier to analyze. Image segmentation is typically used to locate object and boundaries (lines, curve ,etc.)in images, Using K-means clustering, four images are formed, each image showing each cluster at a time.

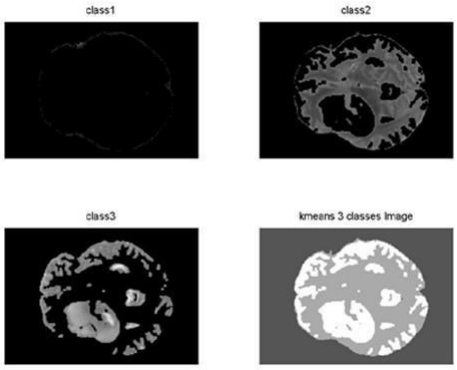

Figure 4: Segmentation results

D) Object Labeling Algorithm

The image obtained from segmentation is converted into a binary image by means of thresholding .These binary images are labeled based on their region .The region with the highest pixel intensity is the detected tumor.

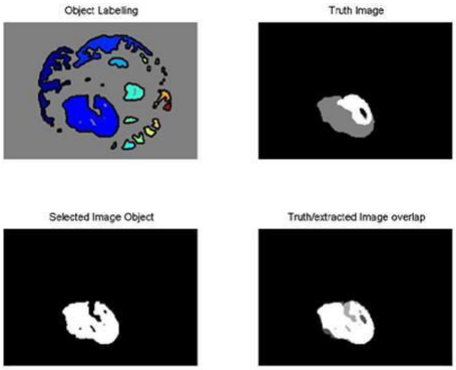

Figure 5: Object Labeling Output and Detection of Tumor

D) Comparison of Graph

The proposed method is applied on different types of tumor affected T2 weighted MRI images(10 images). The shape and size of the tumor is different and varying from image to image. The results (tumor detection) of the different MRI images using K-means followed by threshold method, FCM -k-means and proposed method with ground truth. Overall error is calculated from false alarm and miss alarm. Finally, accuracy of the proposed system is measured with the help of overall error. It is observed from the result that percentage of accuracy of the proposed method is better than the other method. False alarm is defined as if ground truth image consist unchanged pixel in the binary tumor image but proposed binary tumor image consist changed pixel. Similarly, Miss Alarm is defined as if ground truth image consist changed pixel in the binary tumor image But proposed binary tumor image consist unchanged pixel and

$$\text{Overall Error} = \text{FalseAlarm} + \text{MissAlarm} \quad \ldots (4.1)$$

$$\text{Accuracy} = 1 - \frac{\text{Overall Error}}{\text{Image Dimension}} * 100 \quad \ldots (4.2)$$

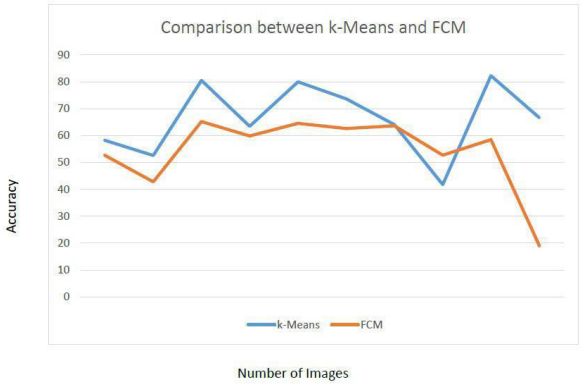

Figure 6: Performance Evaluation of K-means and FCM.

5 Conclusion

Through this paper, the tumor is extracted using k-Means clustering followed by Object Labeling Al-gorithm along with preprocessing steps like Median Filtering and Morphological opening. The results obtained thus prove this approach to be more efficient compared to the existing techniques with accuracy up to 83 percentages. Based on extensive tests, the pro-posed approach demonstrates the following main ad-vantages over the previous works. First it can detect tumor which originates near the skull. Secondly, the entire process is highly automatic

We believe that this initial work can be extended to provide additional insights into the following issues:

1) The present classification of classes is based only on pixel intensity. In future, the Classifications of classes can be based on connectivity of pixels.

2) Output for more number of classes can be experimented with.

References

[1] M. M. Ahmed and D. B. Mohammad, \Segmentation of brain mr images for tumor extraction by combining k-means clustering and perona-malik anisotropic diffusion model," IJIP, pp. 27-34, 2008.

[2] J. Selvakumar, A. Lakshmi, and T. Arivoli, \Brain tumor segmentation and its area calculation in brain mr images using k-mean clustering and fuzzy c-mean algorithm," Proceedings in IEEE-International Conference On Advances In Engineering, Science And Management,, pp. 186-190,2012.

[3] G. Hamerly and C. Elkan, \Learning the k in k-means,"in Proceedings 17th Annual Conference on Neural Information Processing Systems (NIPS), pp. 281-288,2003.

[4] B. C. Patel and G. R. Sinha, "An adaptive k-means clustering algorithm for breast image segmentation," International journal of Computer Applications, vol. 7, no. 4, pp. 35-38, 2010.

[5] T. Kalaiselvi and K. Somasundaram, "Fuzzy c-means technique with histogram based centroid
initialization for brain tissue segmentation in mri of head scans," in Proceedings in IEEE-international Symposium on Humanities, Science and Engineering Research, 2011, pp. 149-154.

[6] M. Shasidhar, Y. S. Raja, and B. Y. Kumar, "Mri brain image segmentation using modified fuzzy c-means clustering algorithm," in Proceedings in IEEE-International Conference on Communication Systems and Network Technologies, 2011, pp. 473-478.

[7] S. Koley and A. Majumder, "Brain MRI segmentation for tumor detection using cohesion based self-merging algorithm," in Proceedings IEEE-3rd International Conference on Communication Soft-ware and Networks, 2011, pp. 781-785.

[8] M. U. Akram and A. Us man, "Computer aided system for brain tumor detection and segmentation," in Proceedings IEEE-International Conference on Computer Networks and Information Technology, vol. 1,2011, pp. 299-302.

[9] K. Thapaliya and G. Kwon, "Extraction of brain tumor based on morphological operations," in Proceedings IEEE-8th international Conference on Computing Technology and Information Management, 2012, pp. 515- 520.

[10] A. Elamy and M. Hu, "Mining brain tumors and tracking their growth rates," in Proceedings IEEE-Canadian Conference On Electrical and Computer Engineering, Seaside, CA, USA, 2007, pp. 872-875.

[11] B. Chanda and D. D. Majumder, Digital Image Processing and Analysis, 2nd ed. PHI Learning Pvt. Ltd, 2011.

Comparison of wireless communication routing protocols

[1] J. S. Awati,
PhD scholar, VTU, Belgaum, Karnataka, and Asst. Prof.,Rajarambapu institute of technology, Sakharale, Maharashtra.
Jsa.awati@gmail.com

[2]Dr. M. R. Patil,[2]Dr. S. A. Patil
Principal, Jain AGM Institute of Technology, Jamkhandi, Karnataka.
Head, ETC Department, D.K.T.E's Engineering and textile institute, Ichalkaranji, Maharashtra.
meenakshirpatil@gmail.com,
shrinivasapatil@gmail.com

*Abstract:***Wireless sensor networks are used for different applications. In wireless sensor networks the different routing protocols are implemented for various applications. This paper deals the difference between some routing protocols. The routing protocols considered are Bellman-Ford, AODV, DSR, DYMO, Fisheye, IARP, IERP and LANMAR. The simulation is performed on Exata developer version 5.1.This paper helps to understand the different routing protocols.**

*Keywords:***Routing, protocol, nodes, parameters**.

I. INTRODUCTION

Wireless communication is done through air. The packets are transmitted and received through air media. The transmission of packets and reception of packets without loss of packets is very critical task. For packet transmission and reception the protocol plays very important role. Protocol means set of rules followed in wireless communication. Router is a very important device in wireless communication. In wireless networks router forwards the data packets. A router is connected between two wireless networks. Routers are connected where two or number of wireless networks are connected. In wireless networks routers are located at gateways. Routers performs the critical task for traffic directing. Router performs the traffic directing functions on the wireless sensor networks.Routing protocol controls the most suitable paths for packet forwarding to the correct destination. Routing protocol deals with the router sharing information with other nodes and how handles and controls the data transmission for packets to correct destination through air. A routing protocol uses software tools and routing algorithms to determine the optimal wireless sensor networks and data transmission and wireless communication between the different wireless nodes. The requirement of the network changes with application specific.

II. OBJECTIVES

- Describe different routing protocols
- Differentiate different various routing protocols.

III. DIFFERENT ROUTING PROTOCOLS

There are number of routing protocols. Number of researchers are working on various routing protocols. Lot of researchers are developing their own routing protocols. The following are the some of the routing protocols used in wireless communication.

A. DSR (Dynamic Source Routing):

Different packets may have different routes even if the source and destination are same. Hence this routing protocol is called as dynamic source routing. This source does not require the symmetric links. In this routing protocol all nodes are willing to forward the packets towards other nodes in the wireless networks. In this routing protocol all the nodes are overhearing and due to this no energy

saving and speed is moderate. Intermediate routes consumption the source route implanted in the packets header for determining the destination of packets to be forwarded. In this routing protocol the packet header size grows with the length of the route. In this routing protocol every node needs to turn on its receiver continuously.

B. Bellman-Ford Routing Protocol:

This routing protocol is based on mathematical equations. This is based on algorithm and distance vector routing protocol. This routing protocol uses two steps first one is to initialize the shortest paths and second step is to calculate the shortest paths.It maintains the distance vector for maintaining the cost of the all the nodes. If new distance vector or cost of neighbor is changed this routing protocol recalculate the distance vector and broadcast new distance vector to all neighboring nodes.

C. AODV (On-demand Distance Vector Routing Protocol):

In this routing protocol each node maintains a routing table. This routing table contains the information related reaching destination nodes. This routing table performs two phases. First phase is route discovery and second phase is route maintenance. AODV routing protocol deals with route table management.

D. Fisheye State Routing (FSR) Protocol:

Fish do have 360^0 vision. Fish eye have higher concentration of optic nerves close to the focal point and elsewhere is less in the fish eye. As a result the fish eye captures with high detail in the points near to the focal point. This concentration is utilized in the fisheye routing protocol. This approach translates into an accurate information in the immediate neighbor of node and less detail as the distance increases. In fisheye routing protocol maintain the topology table based on the up-to-date information received from neighboring nodes and periodically exchange it with their local neighbors.

E. LANMAR (Landmark Adhoc Routing Protocol):

In this routing protocol nodes exchange their routing table each other. A landmark of each subnet is propagated to the whole network. The sources can find joined teams in their landmark table. LANMAR works well with affinity team model. This routing protocol is easy to manage.

F. DYMO Routing Protocol (Dynamic MANET On-demand Routing Protocol):

DYMO is a successor of the AODV routing protocol. This is the simplified AODV routing protocol. DYMO consists of two protocol operations. First operation is route discovery and second operation is route maintenance. When a node needs to send a packet to a destination which is currently not in its routing table, this protocol discover the on-demand route. Route maintenance is the process of responding to changes in topology that happens after a route has initially been created.

G. Zone Routing Protocol (ZRP):

ZRP have two routing protocols. IARP (IntraA-zone Routing Protocol) and IERP (IntEr-Zone Routing Protocol) are two protocols of ZRP. IARP maintains routing information for node which are present within the routing zone of the wireless node. IERP is a family of reactive protocols which offers enhanced route discovery and route maintenance services based on local connectivity monitored by IARP.

IV. WIRELESS NETWORK IMPLEMENTATION

1 to 9 nodes are selected as host. Two networks are implemented, one wireless subnet is 1 through 4 and other wireless subnet is 5 through 9.Traffic used is CBR. Source ID is node 4 and destination ID is node 6. Items to send are 100. Item size is 512 bytes. Interval 1 second, start time is 1 second and end time is 25 seconds.Coordinate system selected is Cartesian, altitude range above sea level is 1500km and weather mobility interval selected is 10 seconds. Number channels selected are 1. Each node is selected as host.

The network Layer parameter selected are Ipv4 network protocol, 60 seconds IP fragment hold time, IP fragmentation unit is 2048 bytes, ICMP enabled and Redirect is enabled with 1 second retry time. Override non-static routes are allowed. Router advertisement lifespan is 1800 seconds with minimum router advertisement interval is 450 seconds and maximum router advertisement interval is 600 seconds. Maximum number of solicitation is 3. IP input queue size is 150000 bytes, IP output queue size is strict priority and Number of IP output queue are 3. The

Wireless subnet properties are Network layer properties are Network Protocol IPv4, IP fragment hold time 60 seconds and IPfragment unit is 2048 bytes. Omni directional antenna model is selected and antenna height is 1.5 meters.

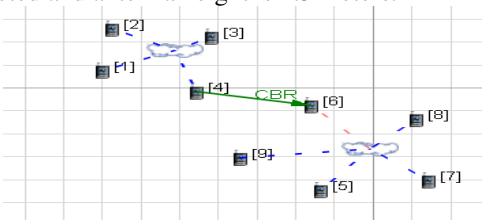

Fig. 1. Wireless Network Implemented

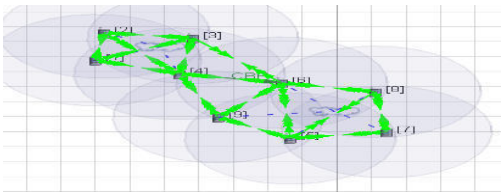

Fig. 2. Wireless Network simulation

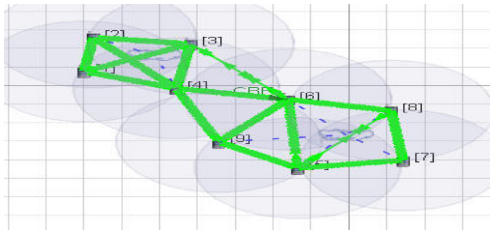

Fig. 3. Wireless Network simulation

Fig. 1 show the wireless network implemented. Fig. 2. and fig. 3. show the simulation performance. Network is implemented in Exata emulator version 5.1.

V. RESULTS

The network is tested of different routing protocols. Some of the parameters are considered for differentiating the routing protocols.

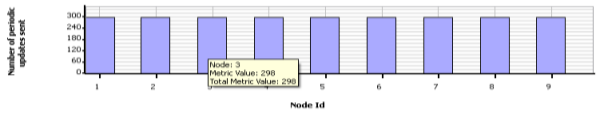

Fig. 4 Number of periodic updates sent, comparison type: node

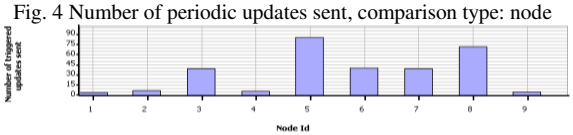

Fig. 5. Number of triggered updates sent, comparison type node

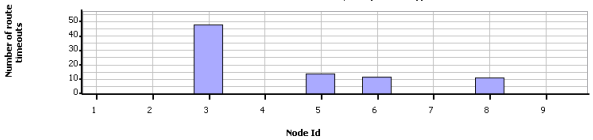

Fig. 6. Number of route timeouts, Comparison: Node

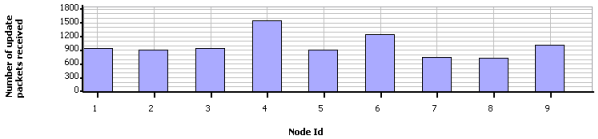

Fig. 7. Number of update Packets received, comparison: node

Fig. 4, fig.5, fig.6 and fig.7 are the comparison of nine nodes for Bellman-ford routing protocol is taken. Similar all types of comparison can be possible for different protocols.

VI. DIFFERENCE BETWEEN ROUTING PROTOCOLS

Total unicast messages sent metric value is 24 and total unicast data sent is 12288 and unicast offered load is 4274.09 for all the routing protocols kept same.

Table 1. Difference between Routing Protocols:

Parameters	Bellman ford	AODV	DSR	DYMO
Unicast session start / Fragment received	1.00306 seconds	1.01972 seconds	1.12974 seconds	1.01404 seconds
Unicast session finish / last fragment received	24.0033 seconds	24.0036 seconds	24.0036 seconds	24.0036 seconds
Total fragments received	24	24	24	24
Total unicast messages received	24	24	24	24
Total data received	12288	12288	12288	12288
Average end to end delay	0.00334552 seconds	0.00403043 seconds	0.00861481 seconds	0.00379396 seconds
Throughput received	4274.05 seconds	4277.09 seconds	4297.66 seconds	4276.04 seconds
Average jitter	0.00024 seconds	0.000918169 seconds	0.00570186 seconds	0.000671414 seconds

Table 2. Difference between Routing Protocols:

Parameters	Fisheye	IARP	IERP	LANMAR
Unicast session start / Fragment received	3.00318 seconds	1.00306 seconds	1.00882 seconds	1.00306 seconds
Unicast session finish / last fragment received	24.0033 seconds	24.0031 seconds	24.0071 seconds	24.0033 seconds
Total fragments received	22	24	24	24
Total unicast messages received	22	24	24	24
Total data received	11264	12288	12288	12288
Average end to end delay	0.00335893 seconds	0.00341513 seconds	0.0070265 seconds	0.00333885 seconds
Throughput received	4291.03 seconds	4274.08 seconds	4274.41 seconds	4274.03 seconds
Average jitter	0.000244762 seconds	0.000212232 seconds	0.000409697 seconds	0.000205217 seconds

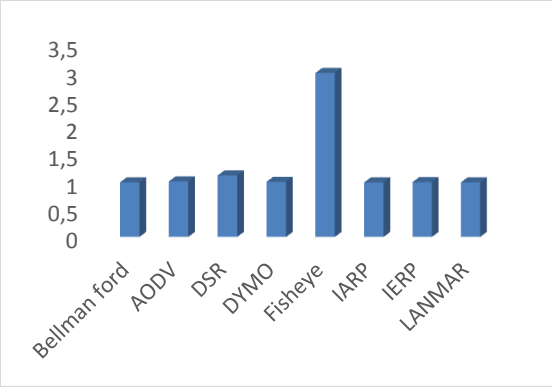

Fig.8. Comparison based on parameters selected are unicast session start or fragments received

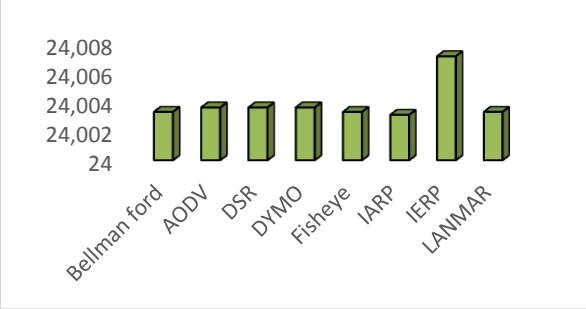

Fig.9.Comparison based on parameters selected are Unicast session finish / last fragment received

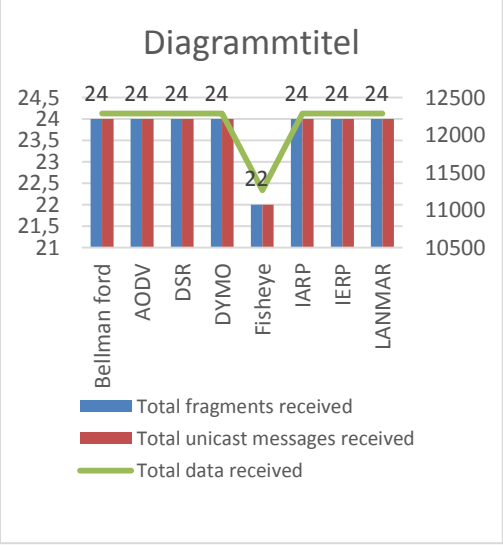

Fig.10. comparison based on parameters selected are total fragments received, total unicast messages received and total data received

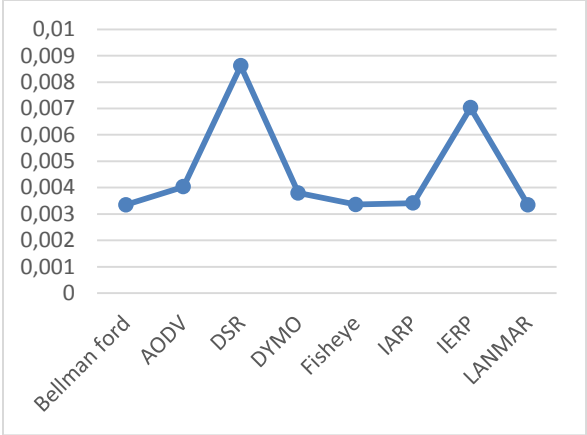

Fig.11.Comparison based on parameter selected is average end to end delay

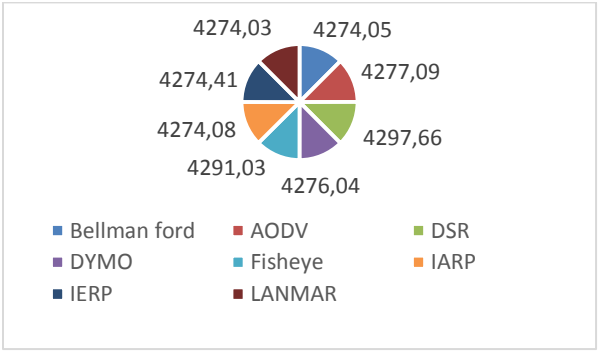

Fig.12. Comparison based on parameter selected is throughput received

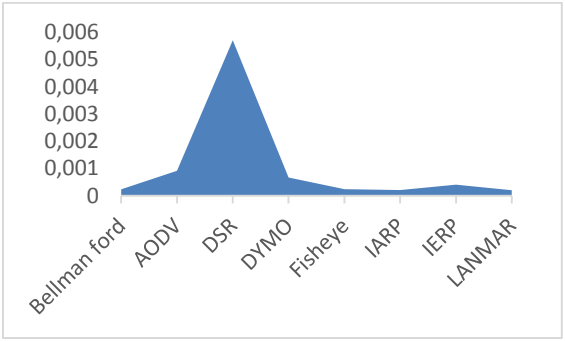

Fig.13.Comparison based on parameter selected is average jitter

VII. CONCLUSION

In wireless sensor networks the different routing protocols are implemented for different applications. This paper showed the difference between Bellman-Ford, AODV, DSR, DYMO, Fisheye, IARP, IERP and LANMAR routing protocols. The simulation results showed the difference between different parameters. This paper helps to understand the different routing protocols based on different parameters.

SMART VIBRATING BAND FOR VISUALLY IMPAIRED

Kainath Saniya Junaidi
Telecommunication department
GSSSIETW
Mysore, Karnataka
kainathjunaidi@gmail.com

Gopika Gopinath
Telecommunication department
GSSSIETW
Mysore, Karnataka
gopikagopinath1910@gmail.com

Hasuvatthi Chaitra Mallesh
Telecommunication department
GSSSIETW
Mysore, Karnataka
chaitramallesh33@gmail.com

Anusha Mayuri
Telecommunication department
GSSSIETW
Mysore, Karnataka
anusha.amruthesh@gmail.com

Mrs.Latha M
Assistant Professor,
Telecommunication department
GSSSIETW
Mysore, Karnataka
latha@gsss.edu.in

Abstract*—There are a millions blind persons around the world, and Many of these persons use the white cane which is the most successful and widely used travel aid for the blind. White cane is purely mechanical device used to detect obstacles on the ground, uneven surfaces, holes, steps, and other hazards. Guide dogs are very capable guides for the blind, but they require extensive training. Furthermore, many visually impaired people are elderly and find it difficult to care appropriately for another living being. There are also navigating tools for visually impaired such as sonar walking stick, sensor devices with voice and vibration alert characteristics. A band with vibrating properties is one device that constantly monitors the surroundings of the blind person and alerts him of the obstacles ahead.*

***Index Terms*— Sensor, Microcontroller chip, CMOS batteries.**

I. INTRODUCTION

A typical walking stick is used by moving the stick from one side to side and detecting objects through feel .Guide dogs are trained to lead their owners around obstacles .The sonar walking sticks can detect the obstacles without any constant movement of the stick. Throughout an average day a typical person will encounter many obstacles. Some typical obstacles encountered might include: hanging signs, tree branches, light poles, fire hydrants, people, curbs, furniture and stairs.

The main problem with white cane is that users must be trained in its use for more than 100 hours; in addition, the white cane requires the user to actively scan the small area ahead of them. The white cane is also not suited for detecting potentially dangerous obstacles at head level. Guide dogs require extensive training, and they are only useful for about five years. Although the dogs can be trained to navigate various obstacles, they are partially (red–green) colorblind and are not capable of interpreting street signals. The human half of the guide dog team does the directing, based upon skills acquired through previous mobility training. The handler might be likened to an aircraft's navigator, who must know how to get from one place to another, and the dog is the pilot, who gets them there safely. Furthermore, many visually impaired people are elderly and find it difficult to care appropriately for another living being.

II. OBJECTIVE

In order to overcome the imperfections of existing electronic and mechanical travel aids, a solution is proposed to constantly monitor a blind and alert him of T obstacles even when he is not conscious about it.

The idea of this study is to design sensor band with vibrating alert feature that can detect obstacles within the designed range (150 cm) (the average person can cover 10 ft in about four steps, this allows for sufficient time for the user to avoid obstacles) also, the purpose of this project was to create a prototype of a device that can help blind people to travel with increased independence, safety and confidence.

III. PRINCIPLE OF OPERATION

The purpose of this project was to create a prototype of a device which will sense d surroundings and intimated the person with a vibration that can help blind people to travel with increased independence, safety and confidence.

The ability to aid the visually impaired is a field that has the potential to advance itself with the improvement of technology. The smart vibrating band designed in this, offers a cheaper solution, to assist those who need it with the use of the Arduino Mini Pro.

The figure 1 shows the flow of the operation. The design consists of a microcontroller chip(arduino mini pro) that is interfaced with the sensor. The sensor is programmed in such a way that it , if there is an obstacle in the circumference of 10feet then the sensor senses and intimates the microcontroller chip. The code is written in such a way that if the obstacle appears from front then the vibrator vibrates once, if it appears from back then it vibrates twice hence in a similar manner according to the direction the vibrator intimates the visually impaired accordingly with the programmed number of vibrations, which is shown in the flowchart.

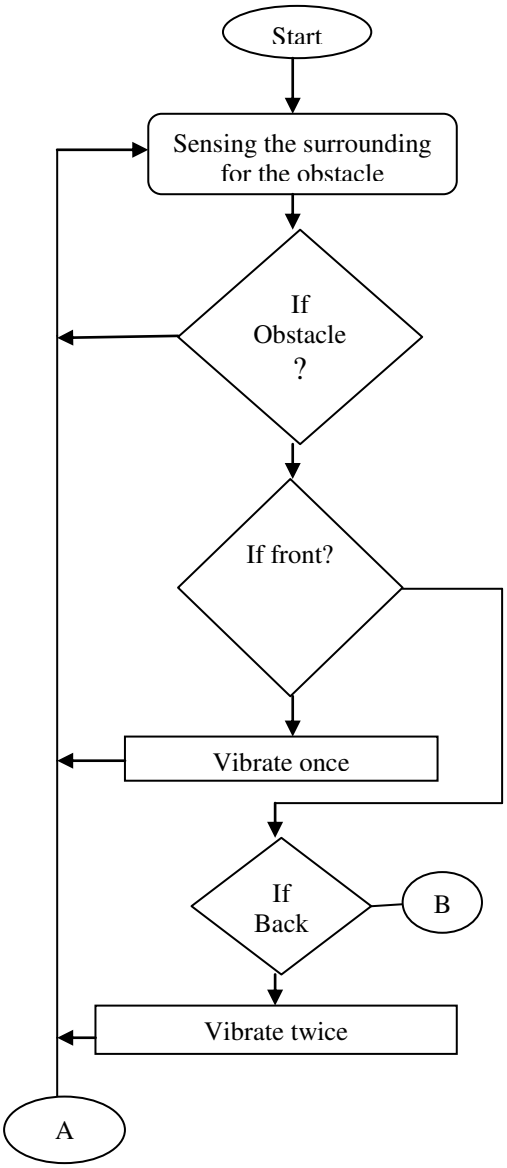

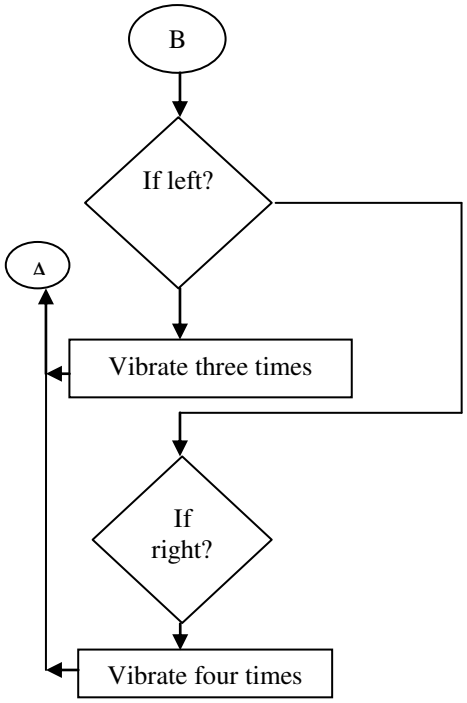

Figure 1.Flow of the operation

IV. REQUIREMENTS

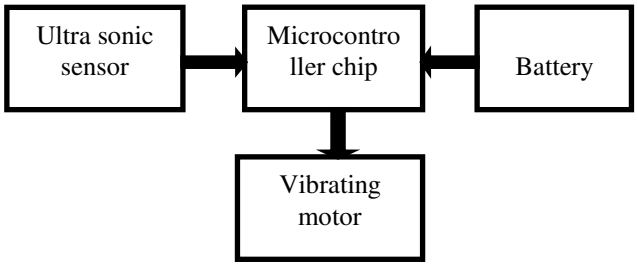

Figure 2. Basic block diagram

Figure 1 shows the block diagram of our design in which the ultrasonic sensor provides an input to microcontroller when there is an obstacle and there is a vibration produced in the motor as the microcontroller output.

A. ULTRASONIC SENSOR

Ultra sonic sensor suit the best for this project as it can detect any object that lies on the ground, situated a distance of certain meters from the user. The sensor will then detect the presence of any object that lies within that meters by detecting the reflected sound beam. The time intervals at which the transmitter will transmit ultrasound depend on the walking speed of the user. Also it is low cost, and efficient. Here we use HC-SR04 series ultrasonic sensor.

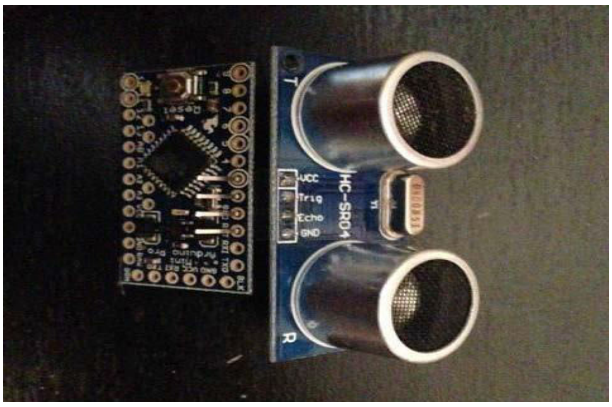

Figure 2. Ultrasonic sensor with Arduino mini pro

B.MICRO CONTROLLER CHIP

Both the sensors and the vibration interface would be controlled through microcontroller. One of the biggest microcontroller names in the market is the Arduino family, with over 20 different board models. To meet the design spec of being lightweight and portable, the Arduino Mini Pro was chosen. This model is small and lightweight, while still operating at a frequency of 16 MHz to provide timely feedback to the user. CMOS batteries of 5v are used in the system; all the components require 5v supply for the working of the system. They are portable, light, and less expensive.

C. VIBRATING MOTORS

To determine how the device would alert the user the proximity of objects first, audio signals were considered. However, an audio signal would be difficult to hear in a loud area and cause confusion to the user. A good alternative to audio signals would be a vibrating interface. The vibration interface would indicate to the user the proximity of an object with different vibration intensities and speeds. In addition to being a much more discrete way to notify the user, it is also much more cost effective.

D.SOFTWARE

Arduino IDE is the software that is used to develop the source code of the microcontroller. It is chosen because it is widely used and the language is easy to understand. It is compatible for various kinds of microchip development system tools. FTDI DRIVER is used for connecting Arduino software to the system.

V. CONCLUSION

With the proposed architecture, if constructed with at most accuracy, the blind people will able to move from one place to another without others help. The band sends and receives ultra sonic waves. The reflections of these waves help the user navigate around obstacles in their pathway. A vibrator pad on the band will vibrate with different frequencies and intensity depending on where the object is located relative to the user. Also the design is reliable and cost effective.

Acknowledgement

The work described in this paper is supported by President, Hon. Secretary and CEO Geetha Shishu Shikshana Sangha (R),Mysuru. Authors would like to thank Principal, AAO GSSS Institute of Engineering and Technology for women, Mysuru for their guidance and constant support.

REFERENCES

1. Mohd Helmy Abd Wahab, Amirul A. Talib, Herdawatie A.Kadir, Ayob Johari, A.Noraziah, Roslina M. Sidek, Ariffin A proposed "Smart cane: assistive cane for visually impaired people", IJCSI, Vol.8 Issue 4, in July 2011.
2. G. Gayatri, M. Vishnupriya, R. Nandhini, Ms. M Banupriya proposed "smart walking stick for visually impaired", IJCSI,Vol.3 Issue 3, in March 2014.
3. M, Bousbia Salah A.larbi and M.Bedda suggested an approach for the measurement of impaired people‖ in proc 10th IEEE International Conference on Electronic Circuits and Systems
4. Lise A. Johnson and Charles M. Higgins in "A Navigation Aid for the Blind Using Tactile-Visual Sensory Substitution" proposed the objective of this study is to improve the quality of life for the visually impaired by restoring their ability to self-navigate.
5. Yuan, D.; Manduchi, R focused dynamic environment exploration using a virtual white cane‖, in Computer Vision and Pattern Recognition, 2005.
6. Tahat, A.A., described a wireless ranging system for the blind long-cane utilizing a smart-phone‖, in Telecommunications, 2009. ConTEL 2009.
7. Bolgiano, D. Meeks; ―A Laser Cane for the Blind‖, in Quantum Electronics, IEEE Journal.
8. Mahendran.N, "Multiple Sensor Feeding Supported Building Automation System Using Arduino Platform with Exposure of 802.15.4 Functionalities." *International Journal of Engineering Trends and Technology*, 4.2 (2013): 77-81.
9. R. Y. Kanemori and J. E. Ehrenberg "A microcomputer-based echo integration system for fish population assessment", *Proc. Oceans 1978 MTS-IEEE Joint Conf.*, pp.204 -207 1978 [10] Sip, Kim-Yeung , in "Edge detecting apparatus and automatic device with same" , Patent No. 8018793 suggested an edge detecting apparatus for using in an automatic device and configured for detecting edges of a surface on which the automatic device moves is provided.

Study of Radio Frequency Identification Systems

Amulya S
Dept. of Telecommunication
GSSSIETW, Mysuru
amulyahemanth46@gmail.com

Chandana H L
Dept. of Telecommunication
GSSSIETW, Mysuru
chandanachani@gmail.com

Dr. Parameshachari B D
Associate Professor and HOD
Dept. of Telecommunication
GSSSIETW, Mysuru
pbdgsss@gmail.com

Abstract: **In recent years, evaluation of RFID systems, study of electromagnetic wave propagation and scattering of UHF wave and microwave transmitted from tag antenna to reader antenna in In-door and out-door is indispensable. In this paper, we describe the characteristics of Electro- Magnetic wave scattering, diffraction and interference by obstacles in propagation channel. Antennas and Propagation aspects in current active and passive UHF RFID systems. We consider a "reader-tag-reader" link and concentrate on each part of it: reader antennas, polarized antennas, propagation channel, propagation coupling, RFID tags and its characteristics, factors of performance, signal attenuation and detuning of antenna vast application of RFID in different fields. In recent years, Radio Frequency Identification (RFID) systems have been gaining growing interest both from scientific and industrial communities. The capability to mark objects and people with passive transponders (Tag), in fact, allows the easy development of cost- effective and low-power-consumption wireless sensor networks (WSN) with undoubted benefits on applications ranging from logistics to healthcare, robotics, security, automotive, and many others.**

Index terms—RFID tags, Propagation aspects, Reader antenna.

I. INTRODUCTION

Radio Frequency Identification (RFID) is an automatic wireless data collection technology with long history roots. In a passive RFID system, the reader transmits a modulated RF signal to the tag consisting of an antenna and an IC chip powered only by RF energy. The chip responds to the reader by varying its input impedance and thus modulating the backscattered signal. First functional passive RFID systems with a range of several meters appeared in early 1970's. Since then, RFID has significantly advanced and experienced a tremendous growth.

Multiple articles and several books dedicated to RF and other aspects of passive UHF RFID systems have been published in the recent years. Performance of any wireless system depends on several antenna characteristics and propagation channel properties which include:

- Antennas
- Operating frequency band
- Sensitivity to nearby objects with different properties.
- Propagation channel
- Path loss

Depending on wireless communication system, some of these characteristics may be more important than others. All antenna characteristics and channel properties described above are also important for RFID systems. However, passive UHF RFID systems based on modulated backscatter differ from traditional wireless systems which involve active transceivers on either side of the link.

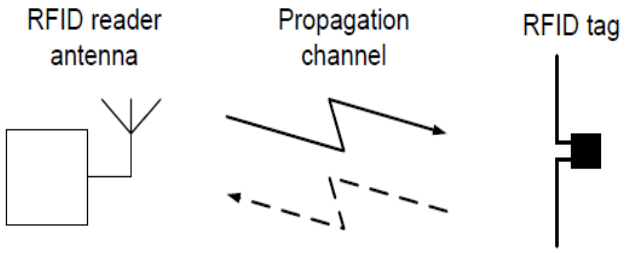

Figure: "Reader-tag-reader" link in passive UHF RFID system.

Tags (transponders) are powered only by RF energy, and RFID readers (transceivers) must transmit and receive simultaneously in order to be able to communicate with tags. This puts a different emphasis on some of the antennas and propagation aspects in "reader-tag-reader" link (shown in Figure 1) which we discuss in this paper, such as Tx/Rx isolation of RFID reader antenna system. We limit our discussion to far field region only. Near field UHF RFID is a separate subject which has been previously discussed in literature and which currently receives a lot of attention as a possible alternative to HF RFID for item level tagging and NFC applications.

II. RFID READER ANTENNAS

A. *General Considerations*

Particular RFID applications often define tag form factors and require specific tag performance (such as range, directionality, sensitivity to material). This, as well as operating frequency band, often restricts tag antenna choice and puts limits on maximum attainable tag antenna gain. However the best possible impedance match between the antenna and the RFID chip is always important for the best tag performance. Since RFID chip impedance depends on both frequency and absorbed power, matching for maximum tag range is usually done at the chip threshold power level.

Many important aspects of RFID tag antenna design have been covered in existing literature. These aspects include optimization of tag antenna gain, polarization, directionality, impedance matching, etc. A large number of various RFID tags, both flexible and rigid, are commercially available from different companies. Detailed comparative performance evaluations of various tags can be found in. Below, we

concentrate on three main tag performance characteristics and methods of measuring them, specifically:

- Tag sensitivity;
- Tag range;

B. Tag Sensitivity

Tag sensitivity is the minimum signal strength (field or power) at the tag location needed to power up (read) the tag.

C. Tag Range

Tag range is typically defined as the maximum distance at which tag can be read. It is an easily understandable, directly measurable, and thus commonly used tag performance characteristic.

III. OPERATION THEORY OF RFID TAGS

The, passive RFID tags does not have its own power supply (i.e. battery less) ,so it depends on the received signal to power up the tag circuitry and resends the data to the reader. In this section, the operation of RFID tags is discussed and analyzed as well as the powers at the tag terminals and reader antenna are calculated.

A) **Link budget**: To calculate the power available to the reader Pr, the polarization losses will assume to be neglected and line-of-sight (LOS) communication is presented. As shown in Fig. 1, Pr is equal to GrP'r and can be expressed as shown in equation (1) by considering the tag antenna gain Gt and the tag-reader path loss

$$P_r = G_r P'_r = G_r P'_t \left(\frac{\lambda}{4\pi d}\right)^2 \quad (1)$$

$$= G_r G_t P_b \left(\frac{\lambda}{4\pi d}\right)^2 \quad (2)$$

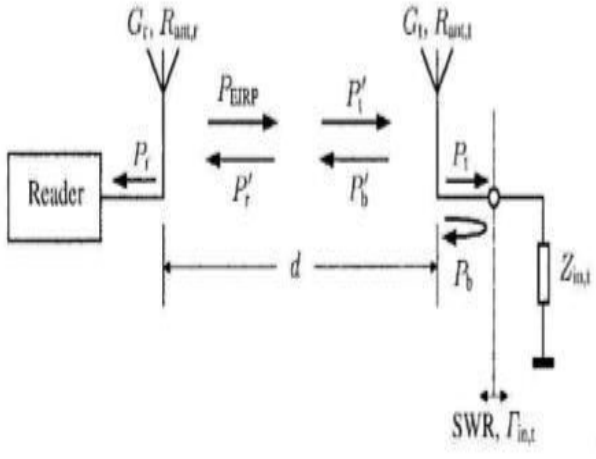

Figure: Link budget calculation

P'b can be calculated using SWR between the tag antenna and the tag input impedance:

$$P_b = P_t \left(\frac{SWR-1}{SWR+1}\right)^2 \quad \ldots (3)$$

Or can be expressed using the reflection coefficient at the interface as shown below:

$$P_b = P_t \left|\Gamma_{in}\right|^2 \quad \ldots (4)$$

The transmitted power is attenuated by reader-tag distance, and the available power at the tag is:

$$P_t G_t = P_{EIRP} \left(\frac{\lambda}{4\pi d}\right)^2 \quad \ldots (5)$$

Substituting equations in equation (1) will result in the link power budget equation between reader and tag.

$$P_r = G_r G_t^2 \left(\frac{\lambda}{4\pi d}\right)^4 \left(\frac{SWR-1}{SWR+1}\right)^2 P_{EIRP} \quad \ldots (6)$$

Or can be expressed in term of, so equation will become:

$$P_r = G_r G_t^2 \left(\frac{\lambda}{4\pi d}\right)^4 \left|\Gamma_{in}\right|^2 P_{EIRP} \quad \ldots (7)$$

The received power by the reader is proportional to the (1/d)4 of the distance and the matching between the tag antenna and tag RFID IC as well as (Pr) is depending on the gain of the reader and tag antennas. In other words, the Read Range of RFID system is proportional to the fourth root of the reader transmission power PEIRP.

B) Complex conjugate concept: For the ac circuit shown in Figure which consists of fixed voltage with peak value Vs and an internal impedance Zs=Rs+jXs and an external load ZL=RL+jXL, the load will deliver (1/2 Vs) when ZL=Zs*

.

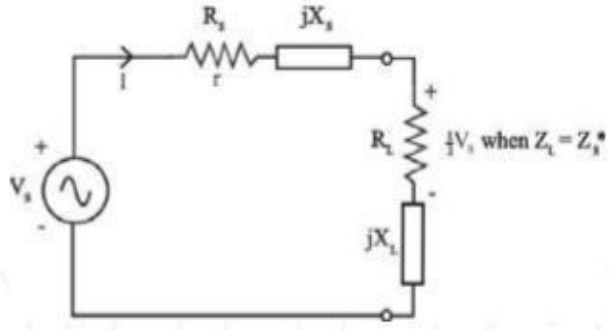

Figure: Context for maximum power transfer theorem

The maximum power transfer theorem states that: for a linear network with fixed source impedance, the maximum power is delivered from the source to the load when the load impedance is the complex conjugate of the source impedance, that is:

$$Z_L = Z_s^*$$

Which means that RL=Rs and jXL=-jXs, and the circuit is said to be conjugately matched. The available source power is

given by:

$$available\ source\ power = \frac{|V_s|^2}{8R_s} \quad \ldots (8)$$

As mentioned before, the RFID tag consists of an antenna and RFID integrated circuit (RFID IC) which can be illustrated by its equivalent circuits as shown below:

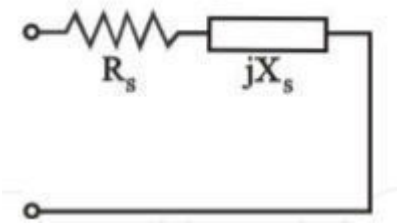

IV. PROPOSED TAG ANTENNA

Micro strip antennas are the most common form of planar antennas. The basic structure is illustrated in Fig. 1(b): a dielectric substrate is sandwiched between a square/rectangular radiating patch and a ground-plane (see Fig. 1(b)). The antenna operating frequency is determined by L, whereas w fixes its radiation resistance. In order to have a broadside radiation with a good efficiency, the simplest design approach consists in setting L equal to λ/2. Nevertheless, this resulting antenna is too large if used in some application fields, as for in the UHF-RFID. In order to overcome this shortcoming, a large number of methods have been proposed; among these, a possible technique consists in short circuiting one of its radiating edges. This way, the physical length L which guarantees the desired broadside radiation is reduced of 50%, becoming λ/4. The consequences of this approach are a lower gain and a broader beam-width. Another possible method to achieve a size reduction of the patch antenna, which has been more recently investigated, is based on the space filling property of fractal geometries. This resulting structure shows a reduced size and a smaller bandwidth when compared to a standard rectangular patch.

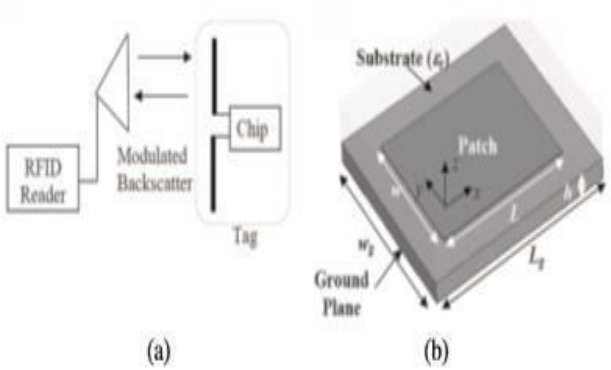

Figure1: (a) RFID system operation. (b) Design parameters of a conventional rectangular patch antenna.

Taking advantage from the two above mentioned design approaches, the radiating structure here proposed consists of a short circuited fractal antenna, whose layout is shown in Fig. 2(d). Specifically, starting from a rectangular patch, two posts have been applied at one end of its feeding edge. Then a further size reduction has been obtained by using a second-order iteration Koch curve in designing the antenna non-radiating edges. In Fig. 2, the layouts of the proposed short-circuited fractal antenna (Fig. 2(d)), of the conventional rectangular patch (Fig. 2(a)), of the fractal antenna (Fig. 2(b)), and of the short-circuited one (Fig. 2(c)) have been compared. The shown layouts are referred to a working frequency of about 866MHz (EU standard for UHF- RFID applications) and to a standard and cost-effective FR4 substrate. In Fig. 3, for instance, the return loss of the four structures obtained through the planar full-wave simulator Ansoft Designer is reported. In particular, the advantage in terms of size-reduction of the short- circuited fractal antenna is clear. In fact, it has been calculated that its size reduction with respect to a rectangular patch antenna is 89.8%; whilst an 85.5% and a 45.8% size reduction is reached when the same structure is compared to the fractal and the short-circuited patch antennas respectively. Finally, it is evident that, with respect to a conventional patch, the short-circuited fractal antenna exhibits a smaller bandwidth; however, such a bandwidth is larger enough to satisfy the UHF-RFID requirement.

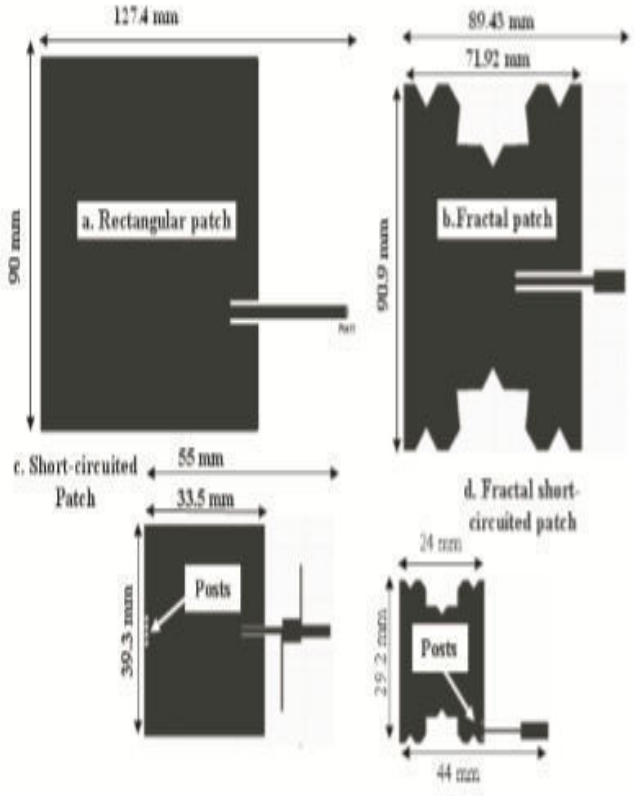

Figure2: Layout comparison among: a rectangular (a), a fractal (b), a short circuited (c) and the proposed short-circuited fractal patch (d).

V. PROPOSED READER ANTENNA

In this paper, the design of the micro strip patch antenna array including all the components such as Wilkinson power dividers, phase shifters, and antenna elements will be specified. Moreover, phased array simulations and measurements will be presented. The field measurements which are taken using a commercial RFID system will be provided to show that the coverage of the RFID system is actually extended.

VI. RANGE EXTENSION OF THE RFID SYSTEM USING A PHASED ARRAY ANTENNA SYSTEM

The read range of a passive tag is limited by its ability to provide sufficient voltage and power at the antenna to power the tag's integrated circuit. To extend the range of an UHF passive RFID system, in a basic sense, received power should be increased.

In our approach, one of the antennas of the bi-static reader will be replaced by the phased antenna array, with a more directive beam with higher gain. Increased antenna gain will increase the radial range; however, due to the narrower beam width the angular coverage will be decreased. In our technique, the phased array can be steered to two different directions so that the angular coverage is not affected; instead, it will be extended.

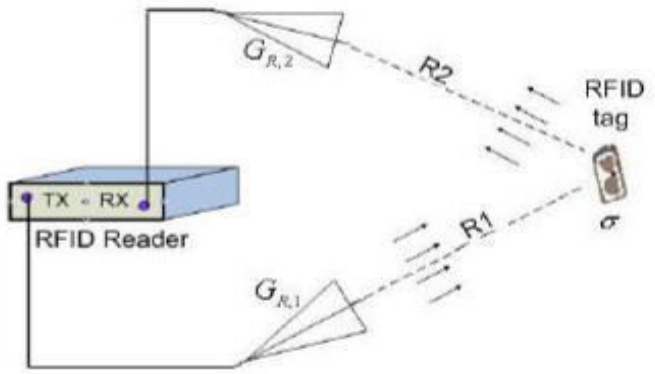

Figure: Bi-static RFID System

One might argue that ERP will be increased by using high gain antenna; however, if the average power is calculated, it will be the same as fixed beam less directive antenna because the beam will be steered back and forth between these two states and, decrease the average power. In normal operation, the beam will be shifting between the two states for a predetermined amount of time.

VII. IMPLEMENTATION AND RESULTS

A schematic view of the proposed antenna array is plotted in Figure 4. The phased array consists of four (2x2) patch antenna elements, Wilkinson power dividers, phase shifters enabled by SPDT switches. By using transmission line based phase shifters, the main beam of the array can be steered to two main directions, shown in Figure 3 as State1 and 2. The main purpose of steering the main beam of the array is to extend the coverage while increasing the gain of the antenna. A typical radiation pattern of a microstrip patch antenna is shown in Figure 3 as radiating into the half space, also shown in the Figure, a more directive beam of a phased antenna array with two different pointing directions

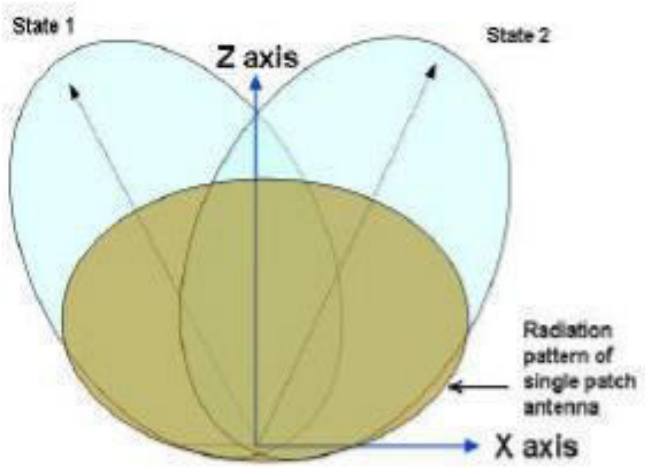

Figure: Extending Coverage Area

VIII. FACTORS EFFECTING THE PERFORMANCE

- It's not necessary to understand the intricacies of the communication methods used, but end users do need to understand the basic characteristics of the different systems and what affects their performance. Because low- and high-frequency systems use inductive coupling, the size of the reader field is smaller and can be more easily controlled. Ultra-high frequency systems that use propagation coupling are harder to control, because energy is sent over long distances. The waves can bounce off surfaces and reach tags you never expected them to reach; you might even read tags you don't want to read. Low- and high-frequency systems also work better than UHF systems around metal and water. The radio waves don't bounce off metal and cause false reads. And they are better able to penetrate water; UHF radio waves are absorbed by water.
- Detuning the antenna: With propagation coupling, the antenna is tuned to receive waves

of a particular frequency. When an antenna is placed on an object or product packaging that is not "RF friendly," the antenna can be detuned, making it difficult for the tag to receive enough energy to reflect back a signal. There are several ways to deal with this issue. Products with a lot of water and metal are particularly challenging to tag, and some antennas can be specially designed to be in tune when close to water or to couple with the metal to improve the ability to read the tag. Another way is to create an air gap between the tag and the object. In the case of metal, an air gap can increase performance if done correctly, because waves will reflect off the metal and provide more power to the tag.

- **Signal attenuation:** Attenuation in RFID usually refers to the reduction in energy emitted by the reader or in the energy reflected back by the tag. If less energy is able to reach the tag, then the tag must be closer to the reader to be read. The energy emitted by the reader naturally decreases with distance; the rate of decrease is proportional to the inverse square of the distance. Passive UHF RFID tags (those with no batteries) reflect back a signal at very low power levels. A tag's reflected signal decreases as the inverse fourth power of the distance between tag and reader. In other words, the signal emitted by the reader attenuates natural with distance, and the signal reflected by a passive tag attenuates at a much faster rate.
- **Electromagnetic interference:** EMI is **essentially** noise that makes it harder to get a clear signal back from the UHF tag. It can be caused by a wide variety of machines. Motors emit EMI and may need to be shielded to prevent interference with RFID systems. Conveyors with nylon belts cause interference, as do most robots on manufacturing line.

IX. APPLICAATION OF RFID

- RFID Asset tracking in education, law enforcement, corporate environments, manufacturing, healthcare.
- Protecting tools in Manufacturing plants, construction yards and shelves of hospitals.

X. CONCLUSION

RFID is a very dynamic discipline. In this paper, we presented a brief discussion of major antennas and propagation aspects which on our opinion are important in current passive UHF RFID systems. A compact Tag-antenna for UHF-RFID applications has been presented. The proposed radiating structure is a patch antenna which takes advantage from the joint use of short circuiting posts and fractal geometries. This way, a size reduction of 89.8% has been obtained with respect to a conventional rectangular patch. Some interesting recent technology developments related to antennas and propagation in UHF RFID systems include:

- Near-field UHF RFID;
- Semi-passive (BAP) RFID systems ;
- Ultra-wide band RFID systems ;
- Tags for operating on metal ;
- Tags with multiple antennas ;
- Tags with low static scattering ;
- Tags with sensor capabilities ;
- New RFID ICs with better RF sensitivity;
- Full system modeling and simulation ;
- Techniques to determine tag location ;
- Multistatic reader antenna configurations;
- Novel portal and conveyor belt solutions.

We believe that these and other forthcoming developments open a plethora of new research issues and challenges in antennas and propagation for RFID systems of the future.

Acknowledgement

The work described in this paper is supported by President, Hon. Secretary and CEO Geetha Shishu Shikshana Sangha (R),Mysuru. Authors would like to thank Principal, AAO GSSS Institute of Engineering and Technology for women, Mysuru for their guidance and constant support.

REFERENCES

1. E. COCA, V. POPA, "EXPERIMENTAL RESULTS AND EMC CONSIDERATIONS ON RFID LOCATION SYSTEMS", *RFID EURASIA CONF.,* 2007, PP. 1-5.
2. D. ARNAUD-CORMOS ET AL., "ELECTROMAGNETIC ENVIRONMENT OF RFID SYSTEMS", *EUROPEAN MICROWAVE CONF.,* OCT. 2007, PP. 1652 – 1655
3. Y. Kim et al., "Effects of reader interference on RFID interrogation range", *European Microwave Conf.* Oct. 2007, pp. 728 – 731
4. U. Muhlmann and H. Witschnig, ''Hard to read tags: an application specific experimental study impassive UHF RFID system" *Elektrotechnik & Informationstechnik,* vol. 124, no. 11, 2007, pp. 391–396.
5. J. K. Schindler et al., " The control of electromagnetic scattering by impedance loading", *Proceedings of the IEEE*, vol. 53, no. 8, Aug. 1965, pp. 993 - 1004
6. M. Kim et al., "Automated robot docking using direction sensing RFID", *IEEE International Conference on Robotics and Automation*, April 2007, pp. 4588 – 4593
7. Y. Zhang, M. Amin, and S. Kaushik, "Localization and tracking of passive RFID tags based on direction estimation", *International Journal of Antennas and Propagation,* Article ID 17426, 2007
8. "Multistatic antenna configuration for radio frequency identification (RFID) systems", US Patent 7265675
9. METRO Group Future Store Initiative, "Angle of position object location system and method", US Patent

Cooperative Localization in Cognitive Radio Networks

HARISH.M IEEE member
University of Wyoming, Wyoming, USA
harishmuralidhar@gmail.com

Abstract— **In cognitive networks, localization is an important and challenging research area. In the absence of cooperation between primary and secondary nodes, determining the positions of primary nodes is extremely difficult and challenging to researchers. This is further complicated as the wireless communication parameters such as path loss exponent, transmit power etc., are not available. In this paper, a localization technique that does not require these parameters is implemented and its performance is investigated combining the database technique and the centroid localization techniques. A two-step localization strategy is adopted. To begin with, a mean-square error method is used to find a close match between the actual received power and the database power and subsequently the primary node estimates. Centroid localization (CL) and weighted centroid localization (WCL) techniques are then adopted to obtain an estimate of the position of the primary nodes. The root-mean squared error (RMSE) of the CL and WCL techniques are computed and analysed. Without using the database, the pure centroid localization techniques are applied and its performance is evaluated.**

Keywords:Localization,Cognitive networks, centroid, weighted centroid,root mean square.

I INTRODUCTION

With the rapid growth in the demand for wireless services affording mobility and ubiquitous connectivity, radio frequency spectrum has become a scarce commodity and needs to be conserved. Lot of research is being done in designing spectrum efficient communication networks including the cognitive networks.

Over the past decade, the concept of cognitive radio (CR) [1][2] has received much attention to efficiently use the available radio spectrum. Mitola [1] introduced the CR concept and subsequently several supporting concepts have since been proposed in literature [2][3].

Generally,in cognitive radio networks, there are two types of users-the licenced users named as primary nodes and the unlicenced secondary nodes. As a result of the strict requirement imposed on the secondary nodes, spectrum sensing, spectrum management (access) and localization have emerged as important research topics aimed at finding efficient methods of utilizing the radio spectrum without interfering with the primary nodes [4]. This spectrum awareness has been viewed through statistical detection and temporal usage in [4][5][6]. In this paper the PN spectral user is detected from geo-location point of view by blindly localizing the radio user in space. This has to be done intelligently incorporating several factors such as energy efficiency and network adaptation. In the absence of cooperation between primary and secondary nodes, determining the positions of primary nodes is extremely difficult and challenging to researchers. This is further complicated as the wireless communication parameters such as path loss exponent, transmit power etc., are not available. Also, a localization technique that does not require these parameters is implemented and its performance is investigated combining the database technique and the centroid localization techniques.The Weighted centroid localization (WCL) technique is a tool that satisfies the the mentioned requirements for blindly localizing radios in a CR environment and has received much attention in literature [7][8][9]. By estimating the several parameters of the etc., localization algorithm's performance can be further improved[10].Bearing in mind that in CR networks the PNs and SNs generally do not cooperate, recent research advances [11][12][13][14] have focused on blind localization of PNs in a CR network. A survey in [15] presents a good classification of the localization propagation models such as transmit power, PLE algorithms used in wireless sensor networks. The techniques presented in [15] are directly applicable for CR networks as well.

In this work, localization technique that combines the database generation method and the centroid and weighted centroid methods is implemented. This method consists of two stages, (1) database generation and

(2) estimation of PN position by comparing the measured received signal strength (RSS) with the database by matching. In the first-stage, mean-square error (MSE) method is used to find a close match between the actual received power and the database power and subsequently the PN location estimates are obtained.WCL is then adopted as a fusion strategy (second-stage) to give an estimate of the PN position. The performance of the WCL is then evaluated using the root-mean squared error (RMSE) and the results compared with the traditional centroid localization(CL) technique. The results obtained are compared with the direct CL techniques that does not involve the use of database. It is assumed that the SNs are each equipped with a radiometer to obtain RSS measurement for detection purpose and to obtain the location of the PN.

The remainder of this paper is organised as follows. Section II provides a detailed description of the system model. Section III provides details regarding the

cooperative path loss exponent estimation and the generation of the database. In section IV the MSE-based power matching and fusion techniques used for the localization of the primary node is presented in detail. Simulation results in Section V illustrate the performance of the database localization technique. SectionVI concludes the paper.

II. SYSTEM MODEL

A CR network with N number of SNs randomly distributed in a square area having a single PN randomly located at a point (x_p, y_p) within the same area as the N number of SNs is considered . The system model incorporates two area scenarios of practical interest- a 50 m by 50 m area, and a 3 km by 3 km area. These area scenarios model the Femto cell network, and macro cell network, respectively. The location coordinate (x_k, y_k), $k \in \{1, 2, ...,N\}$, of the k-th SN is assumed to be known to every other SN node while the location (x_p, y_p) of the PN is unknown. The log-normal shadowing model [13] is adopted as the general model for all the transmissions in the considered system. The SN to SN transmission is modelled using the log-normal model [13] given in equations 1 and 2.

$$P_r(d_{ik}) \sim N(\overline{P_r(d_{ik})}, \boldsymbol{\sigma}_{dB}) \quad (1)$$

$$\overline{P_r(d_{ik})} = P_t^s - P_L(d_o) - 10\,\alpha \log\left(\frac{d_{ik}}{d_o}\right) \quad (2)$$

where $P_r(d_{ik})$ is the mean received power in dBm at the k-th SN located at a distance d_{ik} from the transmitting SN i, P_t^s is the transmit power in dBm, $P_L(d_o)$ is the path loss at reference distance d_0 of 1 m, α is the path loss exponent, and σ dB is the standard deviation of the shadowing component. For ease of evaluation, unity antenna gains for all the systems is assumed. The presence of noise results in shadowing effect on localization estimation computation .The noisy received power in (1) and (2) is considered as in (3).

$$\varphi(d_{ik}) = 10\log_{10}\left(\left(\sqrt{10^{p_r(d_{ik})/10}} + n\right)^2\right) \quad (3)$$

where n denotes the zero mean additive white Gaussian noise(AWGN) with noise power σ_n^2.
Similarly, the PN to SN transmission is modelled as in the SN to SN transmission case
but with d_{0k} and P_t^p substituted for d_{ik} and P_t^s in

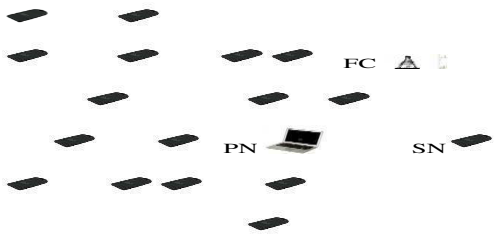

Figure 1: A network of SNs and PN with the FC

equations (1)–(3),respectively. Fig.1 shows the randomly placed SNs and PN network along with the FC node.

III. COOPERATIVE PLE ESTIMATION

In a wireless scenario, with the environment being hostile and random, the path loss exponent (PLE)is unknown and also a dynamically varying parameter. Its estimate is required to improve the localization performance. The PLE estimation is a well-known problem in literature [10]. In this paper, an estimation of PLE α is obtained based on the idea given in [10]. Using equations (2) and (3), α is determined for the link between the transmitting SN i and receiving SN j as follows.

$$\hat{\alpha}_{ij} = \frac{P_t^s - P_L(d_o) - \varphi(d_{ij})}{10\log(d_{ij}/d_o)} \quad (4)$$

where $P_L(d_o) = 20\log_{10}(4\pi d_0 f/c)$ is the free-space path loss [13], f = 600 MHz is the carrier frequency and c $=3\times10^8$ m/s is the speed of light. Transmitting power of all the SNs is assumed to be equal.The estimated α_{ij} are sent to the fusion centre (FC) in Fig. 1 which then takes the average to estimate α. An estimate α for the entire SN network is then obtained by averaging all the N(N − 1) estimated α_{ij} as follows.

$$\hat{\alpha} = \frac{1}{N(N-1)} \sum_{i=1}^{N} \sum_{j=1}^{N} \hat{\alpha}_{ij} \qquad j \neq i \quad (5)$$

The estimated α is transmitted to all the SNs. Fig. 2 and Fig. 3 depict the relationship between the RMSE of the estimated PLE and the number of SNs for a true value of α = 3 and for different areas of dimensions 50 m by 50 m and 3 km by 3 km, respectively.

IV. LOCALIZATION TECHNIQUES

A two-stage localization strategy is adopted. The first stage consists of a database creation which stores the mean received power levels and the second stage consists of matching of the received PN signal power to that in the database and hence making an estimate on the PN position. The MSE-based matching technique is used to match the actual received power with the mean received powers in the database and consequently obtaining the PN estimates. In the second stage once every SN estimates its own PN position by matching the received signal power from the PN to the database then the estimates are reported to the FC. The FC then fuses all the received PN location estimates from all the N SN nodes and uses the CL and WCL estimation methods to obtain a final estimate for the pair (x_p, y_p). The subsequent sections will illustrate the two-stage localization process.

A. Database Creation and Power Matching Technique

The estimated PLE obtained in Section III is then used in the creation of the database which consists of mean received power values between PN positions and SN locations. The considered area consists of G number of grid positions with a spacing of Δ. Based on

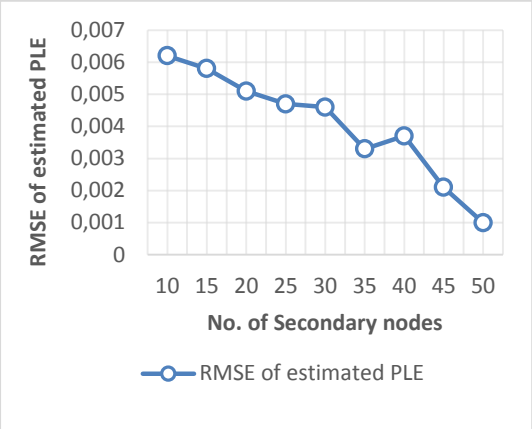

Figure 2: RMSE of the estimated PLE for shadowing standard deviation σ = 6 dB in a 50 m by 50 m square area and α = 3.

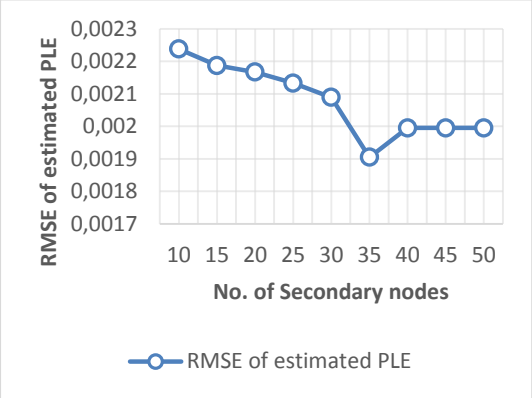

Figure 3: RMSE of the estimated PLE for shadowing standard deviation σ = 6 dB in a 3 km by 3 km square area and α = 3.

every grid position in the region to every SN for various transmit power levels of the estimated α is generated. In this database generation scheme, each SN will have a copy of its own database, generated independently of other SNs databases. A database with a set of received signal strengths is formulated as below. The distance between the i-th grid position and the k-th SN is defined as l_{ik}, with i = 1, 2, ...,G. The database is then created with a set of computed values for the mean received power levels Pr(i, j, k) assuming a range of transmit power levels P_{tj} with j = 1, 2, ...,L. The mean received power is obtained as follows.

$$P_r(i, j, k) = P_{tj} - P_L(d_o) - 10\,\hat{\alpha}\log\left(\frac{l_{ik}}{d_o}\right) \quad (6)$$

where Pr(i, j, k) is the mean received power in dBm at the k-th SN located at a distance l_{ik} from the i-th PN grid position, P_{tj} is the j-th transmit power in dBm, $P_L(d_o)$ is the pathloss at reference distance d_0 of 1 m, α isthe estimated PLE obtained in Section III. Once the actual power $\psi_k(d_{0k})$ at the k-th SN, where d_{0k} is the distance between the transmitting PN 0 and the k-th SN, is received during the online phase, a database entry that closely matches the actual received power is obtained using the MSE-based matching technique given by(7).

$$\hat{P}_r(i, j, k) = \psi_k(d_{ok}) - P_r(i, j, k))^2 \quad (7)$$

As there is a database for each and every SN, there would be multiple estimates of the PN location i.e., given M number of SNs, the matching technique will output M estimates of the PN location. Moreover, the database entries (i, j) for the k-th SN may not always have a unique value for the received power Pr(i, j, k) considering the log-distance path loss model which gives us estimation errors because of matching being done.

B. Centroid Localization Techniques

The estimation strategy employed in Section IV-A will result in multiple estimates of the PN location. Hence, the need for a fusion strategy to give a single PN location estimate.Two techniques employed- The first technique is the CL which simply averages the coordinates of the multiple estimates obtained in Section IV-A. The CL technique estimates the location of the PN as follows

$$(\hat{x}_p, \hat{y}_p) = \left(\frac{\sum_{K=1}^{N} x_p^k}{N}, \frac{\sum_{K=1}^{N} y_p^k}{N}\right) \quad (8)$$

where N is the number of PN location estimates, (x_p^k, y_p^k) is the coordinate of the estimated PN location resulting from the use of the k-th SN database. The second approach is the power-based WCL which directly uses the received powers as the weighting coefficients. For each estimated location, the corresponding estimated received power $\psi_k(d_{ok})$, k = 1,2, ...,N is obtained and used as the weighting coefficient w_k. The WCL technique estimates the location of the PN as follows

$$(\hat{x}_p, \hat{y}_p) = \left(\frac{\sum_{K=1}^{N} w_k X x_p^k}{\sum_{K=1}^{N} w_k}, \frac{\sum_{K=1}^{N} w_k X y_p^k}{\sum_{K=1}^{N} w_k}\right) \quad (9)$$

where w_k represents the weighting coefficient for the (x_p^k, y_p^k) coordinate of the estimated PN location resulting from the use of the k-th SN database.

V. SIMULATION

The performance of database based CL and WCL techniques are analysed through simulations. In particular, the RMSE of the PN location estimate is derived for a varying number of SNs in a given square area. The simulation results are obtained under various area dimensions. Specifically a 50m by 50 m area and a 3 km by 3 km area is considered.The SNs are randomly placed within a grid while the PN is fixed. Also shadowing standard deviations of σ = 6 dB, noise power $\sigma_n^2 = -110$ dBm with true path loss exponent α = 3 is assumed for simulation experiments. For each set of a number of SNs and a fixed PN, a number of simulations are done,where in each iteration the SNs are randomly placed and the PN location estimate using the CL and WCL, respectively, is obtained. Fig. 4 and Fig. 5 shows the CL and WCL performances of database based scheme for the different areas of dimensions 50 m by 50 m and 3 km by 3km, respectively, and for σ = 6 dB. For all the considered area scenarios, the RMSE of the estimated PN location decreases with increasing

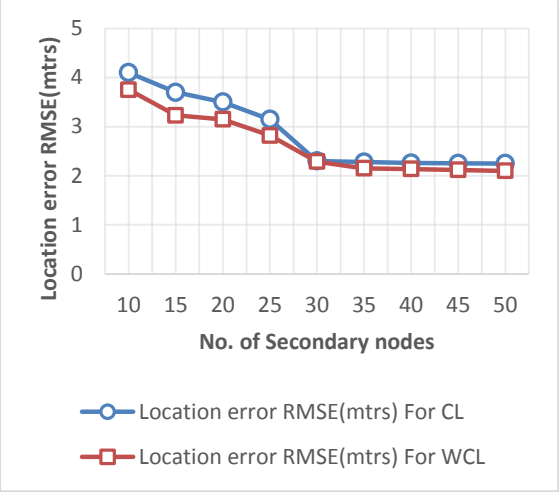

Figure 4: Database-CL and WCL localization performance for a 50 m by 50 m square area. The PN location is fixed

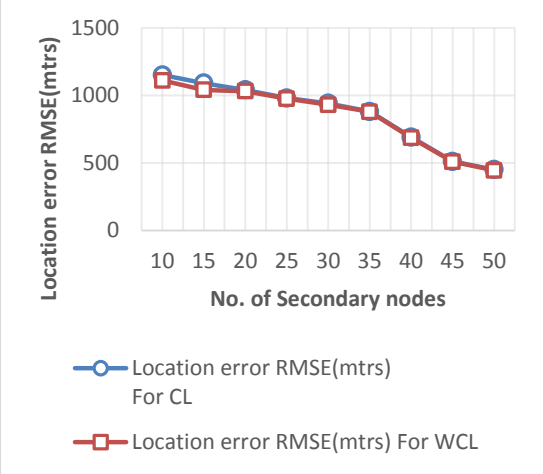

Figure 5: Database -CL and WCL localization performance for a 3km by 3 km square area. The PN location is fixed.

number of SNs. Further the localization is performed using pure CL and WCL estimation techniques and simulation results are compared. In particular, CL and WCL techniques without utilizing the database technique simulated and results obtained is compared with the performance with the database-centroid based scheme.As depicted Fig. 6 for 50m by 50 m area and σ = 6 dB, this scheme using the database performs better than the pure CL and WCL estimation techniques. Thus this localization technique has a significant improvement in the location error as compared to the pure CL and WCLestimation techniques. The RMSE of the estimated PN location decreases with increasing number of SNs and with increased area size. Fig.7 illustrates the location error for a 3 km by 3km area and σ = 6 dB, respectively.

In both area scenarios, there is a significant improvement in the location error in the database-CL and WCL schemes as compared

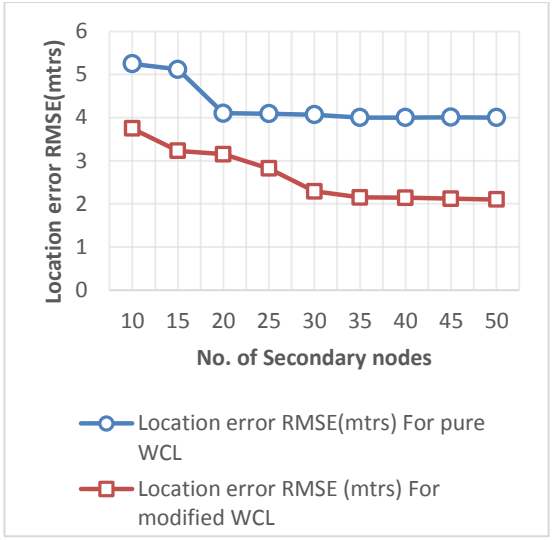

Figure 6: RMSE of both schemes for an area of 50m by 50 m and σ = 6 dB with the PN location fixed

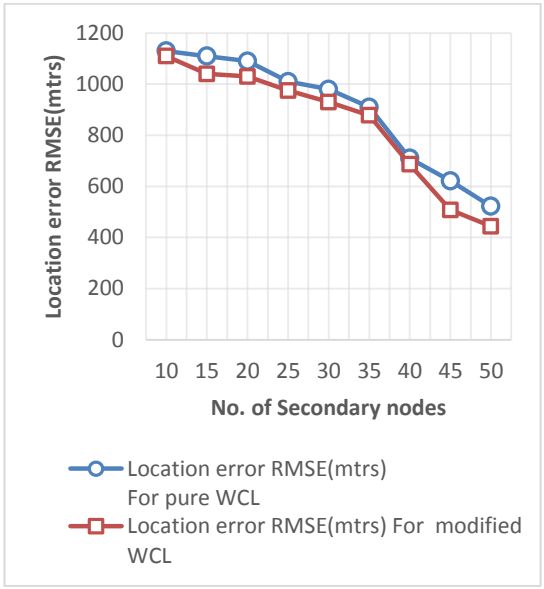

Figure 7: RMSE of both schemes for an area of 3km by 3km and σ = 6 dB with the PN location fixed

to the pure CL and WCL estimation techniques. One interesting aspect of this scheme is that it can achieve much lower location error for large location areas as shown in Figure 7.

VI. CONCLUSION

In this paper a study of the PN localization problem when combining the database and centroid techniques is done. In particular ,the PN localization is performed in two stages- in the first stage the database technique is employed to obtain multiple PN location estimates. The centroid techniques are then employed in the second stage to come up with a final PN location estimate. The location error in terms of the RMSE is evaluated in order to analyse the performance of the database-CL and WCL schemes under varying area scenarios. A comparative study of the

two schemes is done. It is seen from the simulation results that database scheme has a significant improvement in the localization error. However, database creation requires processing memory and power. But databases once created can be used unless there is a change in the topology of the network. Therefore, dynamic updation of databases is required.

ACKNOWLEDGMENT

The author would like to thank all the authors/contributors whose ideas have helped in the implementation of the algorithms in this paper.

REFERENCES

[1] J. Mitola III and G. Q. Maguire Jr, "Cognitive radio: making software radios more personal," *IEEE Personal Communications*, vol. 6, no. 4,pp. 13–18, 1999.

[2] S. Haykin, "Cognitive radio: brain-empowered wireless communications," *IEEE Journal on Selected Areas in Communications*, vol. 23,no. 2, pp. 201–220, 2005.

[3] ABSOLUTE: *EU-FP7 ICT IP Project*. [Online] Available: http://www.absolute-project.eu.

[4] K. Sithamparanathan and A. Giorgetti, *Cognitive radio techniques:spectrum sensing, interference mitigation, and localization*. Artech House, 2012.

[5] K. Sithamparanathan, G. Baldini, R. Piesiewicz, G. Giambene, Y. Jiang,B. S. Yeo, and R. Shorey, "Preliminary experimental results on the spectrum sensing performances for UWB-cognitive radios for detecting ieee 802.11 n Wi-Fi systems," *IEEE ISWCS*, p. 111, 2009.

[6] S. Kandeepan, A. Giorgetti, and M. Chiani, "Timedivisional cooperative periodic spectrum sensing for cognitive radio networks" in *IEEE International Conference on Communications (ICC)*, pp. 1–6, 2010.

[7] A. Mariani, S. Kandeepan, A. Giorgetti, and M. Chiani, "Cooperative weighted centroid localization for cognitive radio networks," in *IEEE International Symposium on Comms. and Information Technologies* , pp. 459–464, 2012.

[8] J. Wang, P. Urriza, Y. Han, and D. Cabric, "Weighted centroid localization algorithm: theoretical analysis and distributed implementation," *IEEE Transactions on Wireless Communications*, vol. 10, no. 10,pp. 3403–3413, 2011.

[9] M. Kazemi, M. Ardebilipour, N. Noori, "Improved weighted RSS positioning algorithm for cognitive radio," in *IEEE 10th InternationalConference on Signal Processing (ICSP)*, pp. 1502–1506, 2010.

[10] G. Mao, B. Anderson, and B. Fidan, "Path loss exponent estimation for wireless sensor network localization," *Computer Networks*, vol. 51,no. 10, pp. 2467–2483, 2007.

[11] O. Duval, A. Punchihewa, F. Gagnon, C. Despins, and V. Bhargava,"Blind multi-sources detection and localization for cognitive radio," in *IEEE GLOBECOM Global Telecomms. Conference*, pp. 1–5, 2008.

[12] S. S. Ivrigh, S. M.-S. Sadough, and S. A. Ghorashi, "A blind source separation-based positioning algorithm for cognitive radio systems," *Research Journal of Applied Sciences*, vol. 4, 2012.

[13] T.S.Rappaport ,Wireless communications; principles and practice.*Prentice-Hall PTR New Jersey*, 1996.

[14] Kagiso Magowe, K. Sithamparanathan " Co-operative Blind localization of primary users in an cognitive radio environment" *IEEE International Conference on Signal processing and Communication systems*,15-17 Dec 2014, pages 1-8.

[15] G. Han, H. Xu, T. Q. Duong, J. Jiang, and T. Hara, "Localization algorithms of wireless sensor networks; a survey" *Telecommunication Systems*, pp. 1–18, 2011.

A Novel Software Model for Enhancement of System Performance and Security through an Optimal Placement of PMU & FACTS

Kiran R, Dr. B.R. Lakshmikantha, & Dr. R.V. Parimala

Assistant Professor, Dayananda Sagar Academy of Technology & Management, Bangalore, Karnataka, India. Kiran.bengaluru@gmail.com
Principal, Dayananda Sagar Academy of Tech & Mgmt, Bangalore, Karnataka, India. brlakshmikntha@gmail.com
Prof & HOD., Dayananda Sagar Academy of Technology & Mgmt, Bangalore, Karnataka, India, parimalaritti@gmail.com

***Abstract*—Secure operation of power systems requires monitoring of the system operating conditions. Phasor measurement units (PMU) are the device which uses synchronized signals from the GPS satellites and provide the phasors information of voltage and currents at a given substation. The optimal locations for the PMUs must be determined, in order to avoid redundant use of PMUs. The objective of this paper is to make system fully observable by using minimum number of PMUs & the implementation of stability software at 22OkV grid for on-line estimation of the power system transfer capability based on voltage and thermal limitations and for security monitoring.**

This software utilizes State Estimator (SE) and synchrophasor PMU data sets for determining the power system operational margin under normal and contingency conditions. This software improves security of transmission system by continuously monitoring operational margin expressed in MW or in bus voltage angles, and alarms the operator if the margin violates a pre-defined threshold.

***Index Terms*-- State Estimator (SE), Flexible ac Transmission Systems (FACTS), optimal location, Phasor measurement units (PMU).**

INTRODUCTION

Phasor Measurement Unit (PMU) is a device that is capable of measuring incoming and outgoing voltages and currents. In addition to measuring voltage and current, the phase angle can also be calculated directly. The PMU device is capable of providing phasor measurements in a continuous format. Through the use of Global Positioning Satellite (GPS), all of the PMUs in a power system can be synchronized in time. The synchronization of the PMUs is an advantage over traditional analog meters. The synchronized phasor data from GPS satellites can improve bad data detection and assure better accuracy for iterative state estimation algorithms.

State estimators provide optimal estimates & information of voltage phasors at bus based on the available measurements and knowledge about the power system network topology. These measurements are produced by the remote terminal units (RTU) at the substations and include magnitudes of bus voltages, branch currents, real/reactive power flows and power injections. Phasor measurement unit have become available at selected substations in the power system. The most important issue faced by the power system engineers is how to select the best optimal locations to install new PMUs. The direct phasor measurement for system monitoring applications is not a new idea [1]. This work is later extended to investigate the optimal location of PMUs where each PMU will provide current and voltage phasors at its associated bus and at all the incident branches. Therefore with relatively small number of PMUs much less than the number of buses in the system, it is possible to fully monitor the system. This problem is solved by using heuristic algorithms. This paper is concerned about the optimal placement of PMUs in the power system, so that they can provide the maximum benefits for the power system.

Increasing variability of the power system operating conditions and influence of uncertain factors on the operation require improving on-line power system security assessment and monitoring of a power system. Conventional off-line calculation of the power system transfer capabilities become inefficient and needs to be conducted on real time in order to provide the “power system operators the situational awareness necessary to identify and plan for contingencies and to operate their systems reliably” [2]. That also benefits real-time market by reducing overly conservative transmission limits calculated off-line. With the installation of Phasor Measurement Units (PMUs) in the system enhances the reliability and improves the economic efficiency of bulk power system. Use of synchrophasor data allows continuous monitoring and computation of operating margins of the power system at much higher resolution rates. The software developed in this paper is the on-line voltage stability analysis tool that introduced the concept of using PMU measurements to calculate power system operational margins, [5]. This software performs on-line calculation of power system transfer capability based on steady-state, voltage and thermal conditions, and monitors power system security by using synchrophasor measurements.

OBSERVABILITY ANALYSIS USING PMUS

Observability based on topology uses the graph theoretical methods to find the optimal locations for the phasor measurement unit placement and to make the system topologically observable. A brief introduction to PMU based topological observability is given as follows.

PMU based Topological Observability:
For making the power system topologically observable using PMUs, following rules are to used,
1. If current phasor and voltage phasor at one end of a branch are known, voltage phasor at the other end of the branch can be calculated using Ohm's law.
2. Branch current can be calculated, if voltage phasors at both the ends of a branch are known.
3. If there is zero injection bus without a PMU, whose outgoing currents are known except for one, then the unknown outgoing current can be calculated using Kirchhoff's Current Law (KCL).
Based on the above rules, two types of measurements can be obtained from PMUs. *Direct measurements* are defined as the PMU bus voltage phasor and outgoing currents from PMU bus and *pseudo measurements* are defined as measurements obtained by utilizing the above rules. Using these rules, many graph theoretical methods are developed, like spanning tree based method, integer linear programming based method, depth first search method have been suggested to place PMUs in the power system for ensuring the full topological observability. In this paper, these above said methods have been modified to determine optimal PMU locations & proposed method is explained in section V.

SOFTWARE MODEL

A. *NOVEL APPROACH FOR VOLTAGE STABILITY ANALYSIS*

This software defines the range of power system parameters under which the system may securely operate. The software developed is a voltage stability analysis and security monitoring tool.
SE solution or PMU data are used to calculate this software boundary. Each point on the boundary corresponds to at least one of the following pre-loped or post-contingency violations: (a) voltage stability, (b) voltage violation, (c) interface MW flow violation. Each operating point inside of the boundary is secure and each operating point outside is considered as insecure. Operational margin is the "health" indicator of the system [3,4].
Coordinates for quantifying the boundary are MW flow on interfaces or PMU angle difference between bus voltages. Use of angles for monitoring could be more informative than the use of MW as instantly reflecting the change in the system security state after tripping of a transmission element [6,7]. Monitoring MW flow allows updating the security status with frequency of SE solutions but the use of PMU angles enables to do so with the PMU sampling rate.

B. *Optimal Corrective Actions*

Software developed has Optimal Mitigation Measures module which develops corrective actions to mitigate any pre or post-contingency detected voltage violations or instability. The following remedial actions are available: (a) FACTS settings, (b) Transformer Tap Change, (c) AVR voltage settings, (d)Phase Shifter settings, (e) Capacitor and Reactor Switching, (f) MW Dispatch, (g) Line Switching in and out, (h) Optimal Capacitor and Reactor Placement and Sizing. (i) Load Curtailment.

C. *Alarming*

Alarms are computed in terms of phase angle difference margin in degrees and MW operational margin for monitored interface and are based on SE data or PMU data.
There are two levels of user-defined alarming thresholds **Alert** and **Alarm** specified in MW & degrees.
This software is tested on a 3-bus 220kV HSR layout network as an example.

SOFTWARE ARCHITECTURE

Phasor Data Concentrator (PDC) streams PMU data to software. Scenario setting is a set of files for specifying all parameters necessary for power transfer analysis. The structure and content of files are designed to provide modeling flexibility and to minimize maintenance efforts.

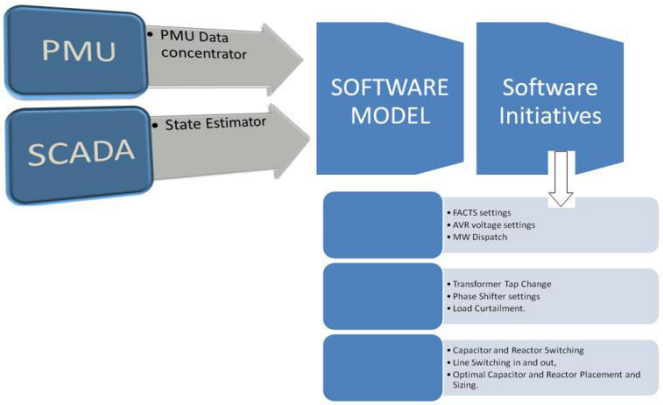

Figure 1: Software Architecture
Software developed comprises "PMU data streamer" and "SE solutions streamer" & 'stability analysis' modules. These components allow simulating real-time environment by streaming PMU data and SE solutions to software. Any process in Real-time mode case can be studied with desired modification of power flow and/or scenario settings.

PROPOSED PMU PLACEMENT METHOD

To illustrate observability based on topology and optimal placement of Phasor Measurement Units to ensure the full observability, a shortest path finding algorithm has been used in this paper to determine optimal Phasor Measurement Unit location.

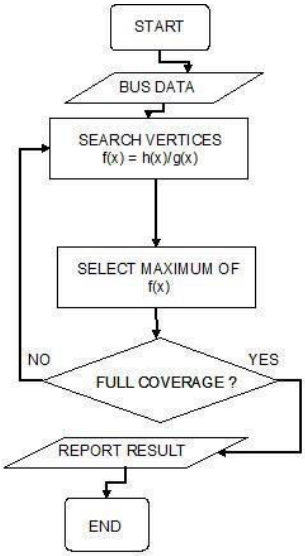

Figure 2: Procedure for optimal placement of PMUs to ensure the full observability

A brief description of the shortest path finding algorithm is given below. The blacksmith algorithm observes the bus data. Blacksmith algorithm then searches through every vertex and determines an associated cost in following that path. Once all costs have been determined, the maximum value of the ratio of h(x) and g(x) is selected and that path is explored. If full coverage of the system hasn't been achieved, the vertices will be searched again including the path that has been previously explored and their associated costs will be computed. The maximum value of the ratios will be selected and that path will be explored. This process continues until a solution is found. The flowchart of the proposed shortest path finding method is shown in Fig. 2.
The final optimal solution so obtained ensures the complete observability.

STATCOM AND UPFC

The Static Synchronous Compensator (STATCOM) is shunt connected reactive compensation equipment, which is capable of generating and /or absorbing reactive power whose output can be varied so as to maintain control of specific parameters of the electric power system. The STATCOM provides operating characteristics similar to a rotating synchronous compensator without the mechanical inertia .The STATCOM employ solid state power switching devices and provide rapid controllability of the three phase voltages, both in magnitude and phase angle.
The STATCOM basically consists of a step-down transformer with a leakage reactance, a three phase GTO/IGBT voltage source inverter (VSI), and a DC capacitor. The AC voltage difference across the leakage reactance produces reactive power exchange between the STATCOM and the power system, such that the AC voltage at the bus bar can be regulated to improve the voltage profile of the power system, which is the primary duty of the STATCOM.
However a secondary damping function can be added into the STATCOM for enhancing power system oscillation stability. The basic objective of a VSI is to produce a sinusoidal AC voltage with minimal harmonic distortion from a DC voltage.
The principle of STATCOM operation is as follows: The voltage is compared with the AC bus voltage system. When the AC bus voltage magnitude is above that of the VSI magnitude; the AC system sees the STATCOM as inductance connected to its terminals. Otherwise if the VSI voltage magnitude is above that of the AC bus voltage magnitude, the AC system sees the STATCOM as capacitance to its terminals. If the voltage magnitudes are equal, the reactive power exchange is zero. If the STATCOM has a DC source or energy storage device on its DC side, it can supply real power to the power system. This can be achieved by adjusting the phase angle of the STATCOM terminals and the phase angle of the AC power system. When phase angle of the AC power system leads the
VSI phase angle, the STATCOM absorbs the real power from the AC system, if the phase angle of the AC power system lags the VSI phase angle, the STATCOM supplies real power to AC system. The real and reactive powers in STATCOM are given by the following equations 1 and 2.

$$P_{12} = (V_1 V_2 / X_{12}) \sin(\delta_1 - \delta_2) \text{ -------- (1)}$$

$$Q_{12} = (V_2 / X)(V_1 - V_2) \text{ -------- (2)}$$

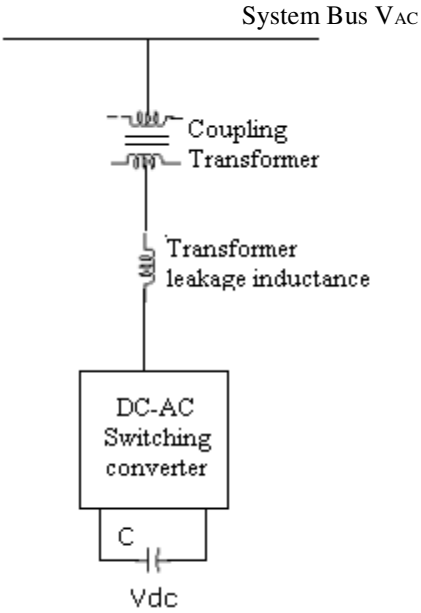

Fig.3. Single - line diagram of a STATCOM.

The Voltage Source Converter or Inverter (VSC or VSI) is the building block of a STATCOM and other FACTS devices. A very simple inverter produces a square voltage waveform as it switches the direct voltage source on and off. The basic objective of a VSI is to produce a sinusoidal AC voltage with minimal harmonic distortion from a DC voltage.
In the last decade commercial availability of Gate Turn off thyristor (GTO) devices with high power handling capability, and the advancement of other types of power semiconductor devices such as IGBT's have led to the development of controllable reactive power sources utilizing electronic switching converter technology [8]. These technologies additionally offer considerable advantage over the existing ones in terms of space reduction and performance. The GTO thyristor enable the design of solid-state shunt reactive compensation equipment based upon switching converter technology.
This concept was used to create a flexible shunt reactive compensation device named Static Synchronous Compensator (STATCOM) due to similar operating characteristics to that of a synchronous compensator but without the mechanical inertia. Single-line diagram of STATCOM is shown in Fig 3.
The advent of Flexible AC Transmission systems (FACTS) is giving rise to a new family of power electronics equipment emerging for controlling and optimizing the performance of power system, e.g. STATCOM, SSSC and UPFC. The use of voltage source inverter (VSI) has been widely accepted as the next generation of the reactive power controllers of the power system to replace the conventional VAR compensator, Such as the thyristor-switched capacitors (TSC) and thyristor controlled reactors (TCR).

New type of STATCOM based on VSI with phase shifted SPWM is given by Liang[9], Modeling and simulation of DSTATCOM is dealt by Giroux[10]. Dynamically voltage restoration with injection is given by [11]. Compensation of voltage sag by [12]. Power Electronic solution to power quality is given by [13].Analysis of thyristor based STATCOM is given by Song[14].overview of STATCOM technologies is given by Liu[15]..

PRINCIPLE OF UPFC

The basic components of the UPFC are two voltage source inverters (VSIs) sharing a common dc storage capacitor, and connected to the power system through coupling transformers. One VSI is connected to in shunt to the transmission system via a shunt transformer, while the other one is connected in series through a series transformer.

A basic UPFC functional scheme is shown in fig.4.

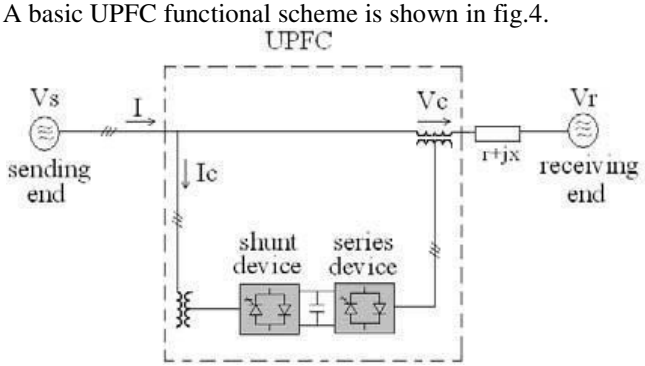

Fig.4 Basic functional scheme of UPFC

The series inverter is controlled to inject a symmetrical three phase voltage system (Vse), of controllable magnitude and phase angle in series with the line to control active and reactive power flows on the transmission line. So, this inverter will exchange active and reactive power with the line. The reactive power is electronically provided by the series inverter, and the active power is transmitted to the dc terminals. The shunt inverter is operated in such a way as to demand this dc terminal power (positive or negative) from the line keeping the voltage across the storage capacitor Vdc constant. So, the net real power absorbed from the line by the UPFC is equal only to the losses of the inverters and their transformers. The remaining capacity of the shunt inverter can be used to exchange reactive power with the line so to provide a voltage regulation at the connection point.

The two VSI's can work independently of each other by separating the dc side. So in that case, the shunt inverter is operating as a STATCOM that generates or absorbs reactive power to regulate the voltage magnitude at the connection point. Instead, the series inverter is operating as SSSC that generates or absorbs reactive power to regulate the current flow, and hence the power flows on the transmission line.

The UPFC has many possible operating modes. In particular, the shunt inverter is operating in such a way to inject a controllable current, ish into the transmission line. The shunt inverter can be controlled in two different modes:

VAR Control Mode: The reference input is an inductive or capacitive VAR request. The shunt inverter control translates the var reference into a corresponding shunt current request and adjusts gating of the inverter to establish the desired current. For this mode of control a feedback signal representing the dc bus voltage, Vdc, is also required.

Automatic Voltage Control Mode: The shunt inverter reactive current is automatically regulated to maintain the transmission line voltage at the point of connection to a reference value. For this mode of control, voltage feedback signals are obtained from the sending end bus feeding the shunt coupling transformer.

The series inverter controls the magnitude and angle of the voltage injected in series with the line to influence the power flow on the line. The actual value of the injected voltage can be obtained in several ways.

Direct Voltage Injection Mode: The reference inputs are directly the magnitude and phase angle of the series voltage.

Phase Angle Shifter Emulation mode: The reference input is phase displacement between the sending end voltage and the receiving end voltage.

Line Impedance Emulation mode: The reference input is an impedance value to insert in series with the line impedance.

Automatic Power Flow Control Mode: The reference inputs are values of P and Q to maintain on the transmission line despite system changes.

CASE STUDY & SIMULATION RESULTS

ObservabilityAnalysis

The proposed method for optimal PMU placement has been tested on the IEEE 14-bus system.

Optimal pmu placement for IEEE 14-bus system

Case	*Optimal Locations*	*No. of locations*
IEEE 14 bus system	*1 6 8 9*	*4*

Voltage StabilityAnalysis

Specification of Test System

The effectiveness of the software developed is carried out on 3-bus 220kV HSR layout network.

Optimal setting of FACTS were computed using *MATLAB* software. Simulation studies using MATLAB programming code, on a 3-bus network are presented to illustrate the methodology and to demonstrate the benefits of the proposed method.

To validate the performance of the software model developed for voltage stability analysis, a 3-bus 220kV HSR layout network is used.

In this paper, contingency like overloading is considered.

(i) Over loading

At steady state, the profile of bus voltages, active power & reactive power is as shown in Table I. When the overload occurs, the software recognizes the overloading effects from the PMU data or state estimator & initiates the control measures.

The following remedial actions are available: (a) FACTS settings, (b) Transformer Tap Change, (c) AVR voltage settings, (d)Phase Shifter settings, (e) Capacitor and Reactor Switching, (f) MW Dispatch, (g) Line Switching in and out, (h) Optimal Capacitor and Reactor Placement and Sizing. (i) Load Curtailment. & an action depends upon the priorities.

In this paper, software initiated FACTS settings changes, so the system regained its original steady state conditions as shown in fig

The voltage magnitudes at steady state & overloaded condition is shown in Table I.

TABLE I

HSR LAYOUT BUS VOLTAGE MAGNITUDE IN KV	
STEADY STATE	OVERLOADED
228.57	180.637
229.5	180.216
228.64	179.861
227.72	177.27
228.4	176.423
228.14	172.137
228.25	169.766
228.25	170.166
228.25	169.946
228.49	168.188
228.06	169.316
227.89	168.978
227.94	168.189
227.98	168.288
227.96	168.508
228.14	166.358
228.03	167.729

At t = 0.25sec, the breaker is closed in series with the load which overloads the system. Fig.5. depicts the decrease in voltage at load bus-1. The fall in voltage at load bus-1 is due to the increased voltage drop.

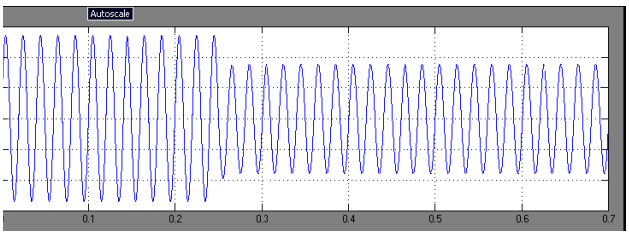

Fig.5 Voltage at HSR Bus

The voltage is injected in the system by STATCOM which reverts the system to its original state as shown in fig.6. & thus mitigating the sag. System reaches a stable point as the voltage reaches its nominal value.

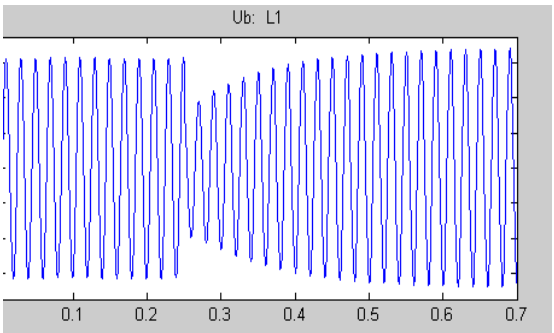

Fig.6 Voltage at HSR Bus with STATCOM

Control action is initiated to UPFC. The voltage is injected in the system by UPFC which also reverts the system to its original state as shown in fig.7. & thus mitigating the sag.

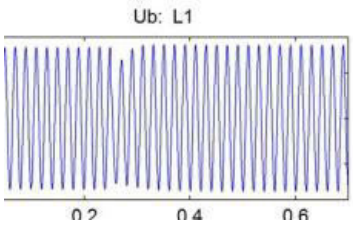

Fig.7 Voltage at HSR Bus with UPFC

The reactive and real power flow cannot be controlled in the system, when UPFC is not connected to the transmission line. Fig. 8a shows the reactive power & active power flow through the transmission line without UPFC. Fig. 8b shows the reactive power flow & active power flow through transmission line which is controlled by UPFC. With the presence of UPFC, transmission capability of the existing transmission line is highly improved. The transmission capability of the system is raised as shown in the simulation results.

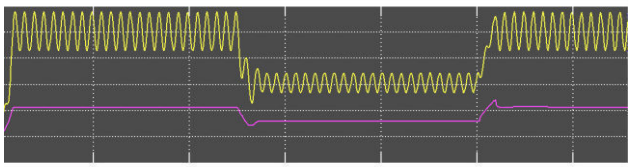

Fig. 8a shows the active power through the line without UPFC.

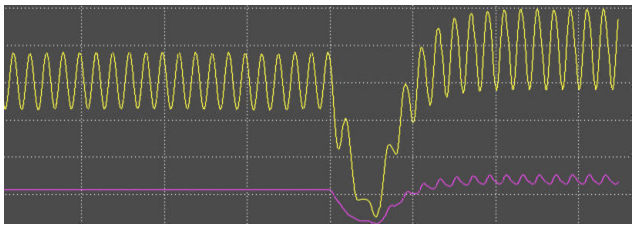

Fig. 8b shows the active power flow

VIII. CONCLUSIONS

This paper suggests a simple programming method for optimal placement of Phasor Measurement Unit in power system to provide complete topological observability of the power system. This paper uses a novel software model for power system stability & control. The proposed controllability & observability analysis has been tested on the HSR-3 bus system and IEEE 14-bus system respectively. The proposed method is quite effective and simple to adopt.

This paper uses UPFC & STATCOM to improve the voltage stability & power system stability in a multi bus system. The load voltage reaches its nominal value with in 0.25sec. The simulation results with and without STATCOM & UPFC are presented. The simulation results indicate the usefulness of UPFC & STATCOM to mitigate the voltage sag & to enhance the power system stability. With the presence of UPFC in the power system, transmission capability of the existing transmission corridor is highly improved. The raise in the transmission capability of the transmission corridor can be noticed from the simulation results.

IX . REFERENCES

[1] R F.NUQUI AND A. G. PHADKE, "PHASOR MEASUREMENT UNIT PLACEMENT TECHNIQUES FOR COMPLETE AND INCOMPLETE OBSERVABILITY," *IEEE TRANS ON POWER DELIVERY,* VOL. 20, NO. 4, OCT. 2005, PP. 2381- 2388.

[2] FERC AND NERC REPORT, ARIZONA-SOUTHERN CALIFORNIA OUTAGES ON SEPTEMBER 8, 2011: CAUSES AND RECOMMENDATIONS, APRIL 2012.

[3] S. LOCKWOOD ET AL., "UTILITY EXPERIENCE COMPUTING PHYSICAL AND OPERATIONAL MARGINS", 2004 IEEE PSCE, PSCE2004-000616.PDF.

[4] M.Y. VAIMAN, M.M. VAIMAN, N. ABI-SAMRA. "ON-LINE COMPUTATION OF PHYSICAL AND OPERATIONAL MARGINS IN BULK POWER SYSTEMS", CIGRE SESSION 2000, PARIS, 2000.

[5] M. Y. VAIMAN, M. M. VAIMAN, S. MASLENNIKOV, E. LITVINOV, X. LUO, "CALCULATION AND VISUALIZATION OF POWER SYSTEM STABILITY MARGIN BASED ON PMU MEASUREMENTS", SMARTGRIDCOMM 2010, PP: 31-36, 10.1109/SMARTGRID.2010.5622011.

[6] J. TATE, AND T. OVERBYE, "LINE OUTAGE DETECTION USING PHASOR ANGLE MEASUREMENTS", *IEEE TRANS. POWER SYST.,* VOL.32 , NO 4, PP.1644 -1652 , NOV. 2008

[7] I. DOBSON, "VOLTAGES ACROSS AN AREA OF A NETWORK", *IEEE TRANS. POWERSYST.*, VOL.27 , NO 2, PP.993 - 1002 , MAY 2012

[8] STATIC SYNCHRONOUS COMPENSATOR, CIGRE, WORKING GROUP 14.19,1998.

[9] Y.LIANG AND C.O.NWANKPA ,"A NEW TYPE OF STATCOM BASED ON CASCADING VOLTAGE- SOURCE INVERTER WITH PHASE SHIFTED UNIPOLAR SPWM".

[10] P.GIROUX, G.SYBILLE, AND H. LE-HUY," MODELING AND SIMULATION OF A DISTRIBUTION STATCOM USING SIMULINK'S POWER SYSTEM BLOCKSET", IN PROC. ANNU. CONF. IEEE INDUSTRIAL ELECTRONIC SOCIETY, PP, 990-994.

[11] S.S.CHOI, B.H.LI,&D.D.VILATHGAMUWA, "DYNAMIC VOLTAGE RESTORATION WITH MINIMUM ENERGY INJECTIONS", IEEE TRANS., POWER SYSTEM, VOL.15, PP51-57, FEB-2000.

[12] M.H.HAQUE "COMPENSATION OF DISTRIBUTION SYSTEM VOLTAGE SAG BY DVR AND DSTATCOM", POWER TECH PROCEEDINGS 2001,IEEE PORTO VOLUME: 1, SEPT.2001.

[13] AMBRA SANNINO,JAN SVESSON AND TOMAS LARSSON. "POWER- ELECTRONIC SOLUTIONS TO POWER QUALITY PROBLEMS" ELECTRIC POWER SYSTEMS RESEARCH VOLUME 66, ISSUE 1, JULY 2003, PAGES71-82.

[14] JIANYE CUEN,SHAN SONG, ZANJI WANG, "ANALYSIS AND IMPLEMENT OF THYRISTOR BASED STATCOM", 2006.INTERNATIONAL CONFERENCE ON POWER SYSTEM TECHNOLOGY.

[15] QINGGUANG YU,PEI LI,WENHUA, LIU, XIAORONG XIE,OVERVIEW OF STATCOM TECHNOLOGIES",2004 IEEE INTERNATIONAL CONFERENCE ON ELECTRIC UTILITY DEREGULATION,RESTRUCTURING AND POWER TECHNOLOGIES,APRIL 2004.

X. BIOGRAPHIES

Kiran R obtained his B.E and M.Tech from Visveswaraya Technological University in 2010 and 2012 respectively He is pursuing Ph.D degree under Visveswaraya Technological University, Belgaum, Karnataka State, India.

Presently he is working as an Assistant Professor in Department of Electrical & Electronics Engineering at Dayananda Sagar Academy of Technology & Management. His areas of interest are in PMU, FACTS controllers & optimization of Power System.

Dr.B.R.LakshmiKantha is serving as Principal in Dayananda Sagar Academy of Technology & Management, Bangalore. He obtained his B.E., M.E in Electrical & Electronics Engineering & Power System from Bangalore University. He obtained his Ph.D under Viswesvaraya Technological University. His research areas are FACTS Controllers, Renewable Energy Sources, and Stability of power systems.

Dr. R.V. Parimala is serving as Professor & HOD in Department of Electrical & Electronics Engineering, Dayananda Sagar Academy of Technology & Management, Bangalore. She obtained her B.E., M.Tech in Electrical & Electronics Engineering & Power System from Mysore University in 1985 & 1996 respectively. She obtained her Ph.D under Viswesvaraya Technological University. Her research areas are Distribution automation, network reconfiguration, Colored Petri net application in the area of power system.

DESIGN AND ANALYSIS OF MPA USING H-SHAPED DRA WITH DUMBBELL DGS FOR WIDE BAND APPLICATIONS

[1]Mr. Murthi Mahadeva Naik G
Associate Professor
Dept. of ECE
Malnad College of Engineering
Hassan, Karnataka, India-573202
murthyishu1@gmail.com

[2]Dr. Naveen Kumar S K
Professor, Dept. of Electronics
Mangalore University
Mangalore
nave12@gmail.com

[3]Sangeetha B L
Assistant Professor
Dept. of ECE
Vivekananda College of Engineering & Technology
Puttur, Karnataka, India-574203
rakshasangeetha@gmail.com

***Abstract*:** The objective of this work is to design and analyze an H-shaped DRA with DGS to study study the response of the microstrip patch antenna (MPA). The MPA accomplished Dumbbell DGS is included in the ground plane under the patch to improve antenna performances. A FEM based electromagnetic solver, Ansoft HFSS is used for simulation. The proposed antenna is outlined to operate over frequency range from 3.6 GHz to 17.5 GHz. Various measurable factors are acquired which comprises Gain, Radiation pattern, Directivity and S-parameter. It is inferred by means of simulation results and the design is favorable enough to cover normal range. The design is carried out at the solution frequency band: Ku Band, centering at 18 GHz. A dumbbell slot is integrated in ground plane which is excited using a 50ohm Microstrip line.

Keywords: Wide band; defected ground structure (DGS); Circular slot; Radiation Pattern, DRA.

I.INTRODUCTION

The process of accumulating change of advanced wireless communication frameworks has grown up drastically the imposition for antennas, ability to be implanted in compact, or not, gadgets which serve a wireless land mobile or physical satellite system. Throughout the most recent 50 years antenna innovation has been an indispensable partner of the communication revolution and the field of antennas is active, incredible and overwhelming. In the overall society these days exchange of data assumes momentous part and are quickly changing from "wired to remote". In recent decades, there is dreadful growth and progression in wireless innovation and communication. Wireless innovation equips less lavish selective and the method for communication is malleable and pliable. With the more prominent extension for application territories of the antenna innovation, microwave designers are compelled to grow the being used recurrence band upto V and E bands from the first emerging HF and VHF bands. The configuration and inclination of the radio wire is decisive and must meet the framework prerequisites. A worthy design of the antenna can abate system prerequisites and enhance all out framework execution. As eyes and eyeglasses serve to a human the same purpose antenna serves to the communication system. Wider extensive data transmission items are needed for the improvement in wireless communication technology. For new designed cell phones, low profile antennas are chiefly suitable. Mix among parts has become significant issue as the advancement of wireless communication technology grows swiftly.

Antennas empower wireless communication between two or more stations by managing signals towards the stations. The IEEE Standard Definition of terms for antennas (IEEE std 145-1983) characterizes the antennas or aerial as "a means for radiating and receiving radio waves". Antenna is standout amongst the most genuine segments for wireless communication system. In the radio wave frequency for accepting and transmitting signals from and into the air as medium, Antenna is one of the vital components. Antenna is a transducer which transmits or receives electromagnetic waves. The capacity of an antenna is to change over a RF (Radio Frequency) signal from a transmitter to spreading electromagnetic wave or then again, change over a proliferating wave to an RF signal in a receiver.

A. Microstrip Antenna

In 1970's microstrip antenna turned out to be exceptionally prominent for space borne applications. Present days they are utilized for business and government applications, for example, mobile radio and wireless communication. Microstrip patch antenna is widely put into impact in numerous applications, to great extent in wireless applications. In the course of the most recent two decades, Microstrip patch antennas have been the point of strenuous, on account to their assorted points of interest and better prospects [6]. There exists different advantages of microstrip antennas over

conventional microwave antenna and accordingly are utilized as a part of mixture of functional applications.

Microstrip antennas are planar resonant caries. They spill from their edges and emanate beams. Microstrip antenna shown in Figure1, which comprised of a metallic patch on substrate at one side and other side ground plane..

Patch is usually made of directing material such as gold or copper and can have the capacity to take any shape. Feed lines and transmitting patch for the most part photo etched on the dielectric substrate.

So as to diminish unpredictability investigation and the demonstration of performing forecast, the patch is normally square, rectangular, roundabout, triangular, and circular or a couple of unique common shapes. The length L of the rectangular patch can vary $0.3333\lambda_o < L < 0.5\lambda_o$, where λ_o is the free-space wavelength. The patch is decided to be very thin such that $t << \lambda_o$ (where "t' is the patch thickness). The height "h" of the dielectric substrate can vary $0.003\ \lambda_o \leq h \leq 0.05\ \lambda_o$. The dielectric constant of the substrate (ε_r) is normally in the extent $2.2 \leq \varepsilon_r \leq 12$.

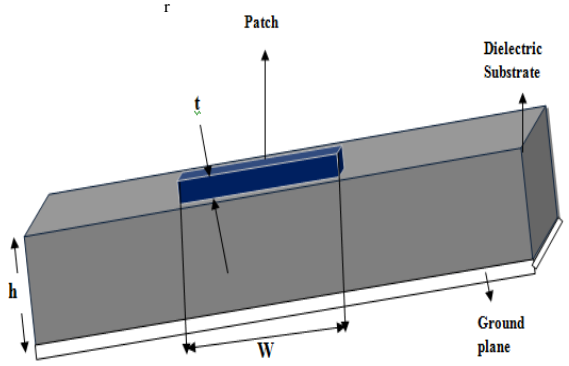

Figure 1: Microstrip Patch Antenna

B. Defected Ground Structure

As there is quick improvement in wireless communications genuine effort has been devoted to decrease the size of microstrip antenna. A few techniques have been proposed later such as Defected Microstrip Structure (DMS), dielectric substrate of high permittivity, Defected Ground Structure (DGS) at ground plane or union of them. Lately, there has been a progressive interest in the utilization of DGS in microstrip innovation. In the improvement of scaled down antennas, DGS has been widely utilized. To make better the qualities of numerous microwave devices DGS have been created. Regardless of the DGS has benefit in the area of the microwave filter pattern, microstrip antenna pattern for mixture of applications, for example, cross polarization minimization and mutual coupling minimization and so on..,

C. DRA

At microwave frequencies a radio antenna generally use Dielectric Resonator placed upon a metal surface and a ground plane comprises a ceramic material of variety of shapes. From the transmitter circuit radio waves are brought into the resonator material and form the standing waves, by switching the standing wave back and forth in between resonator walls the radio power is permitted to emanate into free space as the walls of the resonator are partially transparent to radio waves. DRAs offer straightforward coupling planes to almost all transmission lines utilized at microwave and mili meter-wave frequencies.

II. DESIGN CONSIDERATIONS

This section comprises of the method of design configuration of antenna using DGS structures. The implementation of the antenna begins by understanding evolution of the microstrip antenna and designing a particular frequency of interest. The designed antenna is simulated using HFSS. This confines the properties study of the antenna for instance radiation pattern, working frequency, and antenna gain. The divulged writing overviews are put into operation from reference books and IEEE publish paper. The simulation has been done by utilizing High Frequency Structure and Simulator (HFSS).

A. Frequency of operation

In the microwave range of frequencies, wide band is a part of the EM spectrum. Wide Band with IEEE acknowledged frequency range is utilized by the Satellite Communication Systems. Subsequently, in this frequency range, the antenna patterned must be able to operate. The working frequency chosen for the outline is 16GHz.

B. Dielectric Constant of Substrate

The dielectric material chosen is RT/duriod 5800 which has a dielectric constant of 2.2 and FR4 which has dielectric constant 4.4. Substrate with high dielectric constant has been picked as it brings down the traits of the antenna.

C. Height of dielectric substrate

Surface waves are fortified inside the substrate as thickness of substrate increments. Surface waves emerge in not desired radiation, diminishes antenna efficiency and adds counterfeit coupling between different circuits or antenna elements. Subsequently, the height of the substrate is taken to be 0.762mm.

D. **The Dumbbell DGS characteristic**

In outlining the dumbbell DGS, the measurement of the DGS comprises of the dumbbell head (a), slot length atween the dumbbell (d) and slot

width (s). The dumbbell structure is depicted in Figure 2. The proposed dumbbell DGS structure was accomplished by changing the dimension and setting the position of the DGS on the ground plane. The placing of the DGS on the ground plane is put between the two microstrip fed, but underneath the lower layer. In this case, utilizing dumbbell shaped DGS of three elements, which are separated by (r). The quantity of unit element DGS was incremented to notice the manipulation to the reference antenna which was outlined without DGS. The dumbbell DGS from one unit until three were described here with the same size and distance.

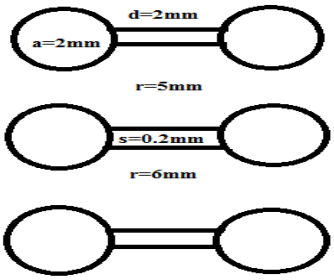

Figure 2: Dumbbell shaped DGS

The physical dimensions of the H-shaped microstrip patch antenna are shown in Figure 3. It can be divided into three parts: a middle conductor strip with length W2 and width L2, and two identical conductor strips with length W1 and width L1 on both sides.

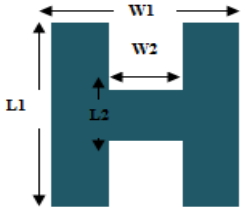

Figure 3: Configuration of the H-shape

The diagram of designed MPA is shown in Figure 4. A 50 ohm microstrip line of width 'W' and length 'L' is utilized for feeding the structure and situated on the another side of the substrate. It demonstrates the top perspective of the proposed antenna, whereas Figure 5 indicates the bottom perspective of the proposed antenna outline. The dumbbell DGS is located on the opposite side of the feed line indicated in the bottom layer substrate. The dielectric material utilized has the thickness of 0.762mm with dielectric permittivity (ε_r) of 2.2 and tangential loss (tan ±) of 0.0009. The lower layer substrate comprises of a microstrip line feeding system, and three dumbbell slots are embedded on the ground plane. The predefined things are chosen to procure the maximum bandwidth: Microstrip feed technique, Low permittivity of the patch substrate, 13.2mm dielectric height of FR4 segments, Thin feed substrate, DGS slot.

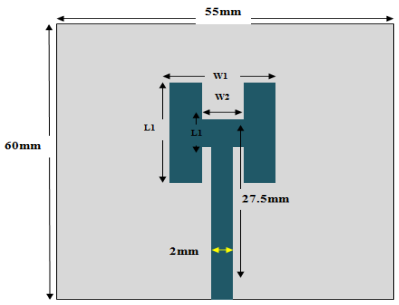

Figure 4: Proposed antenna (top view)

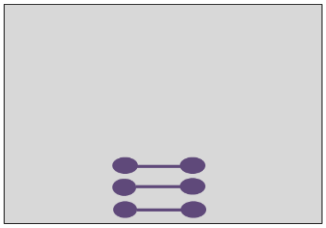

Figure 5: Proposed antenna (bottom view)

TABLE 1: DIMENSIONS OF THE DESIGN

Parameters Name	Parameter Dimensions
Length of Substrate	60 mm
Width of Substrate	55 mm
Height of Substrate	0.762 mm
Length of Ground plane	60 mm
Width of Ground plane	55 mm
Length of Feed line	27.5 mm
Width of Feed line	2 mm

III. DESIGN OF PROPOSED ANTENNA

The Proposed antenna design is as follows,

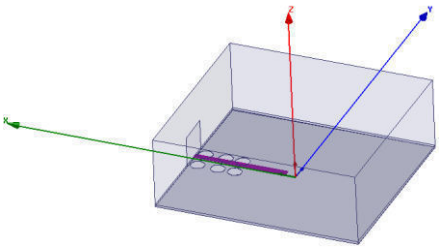

Figure 6: Bottom view of design in HFSS

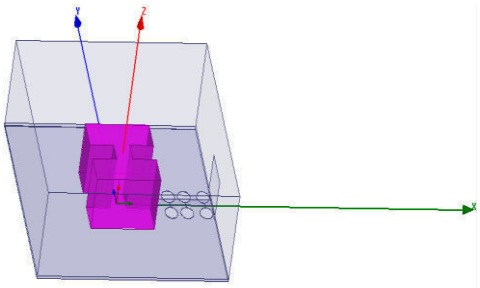

Figure 7: Top view of design in HFSS

IV. SIMULATED RESULTS

The return loss, 3D polar plot, peak gain are acquired using HFSS v15.0. The results are as follows,

(A) Return Loss-RT/Duriod

The simulated S11 vs Freq characteristic plot of an antenna is shown in Figure.8. An impedance bandwidth is accomplished experimentally in the range of 3.6 GHz to 17.5 GHz. The return loss level is under 10dB. The resonances occur at 5.7 GHz, 8.4 GHz, 9.6 GHz, 11.2 GHz, 12.4 GHz and 12.9 GHz. The S11 levels at these resonances are -31.47 dB, -31.82 dB, -28.53 dB, -21.02 dB, -27.43 dB and -27.19 dB in a relative manner. The value of return loss is in the worthy range of <-10dB.

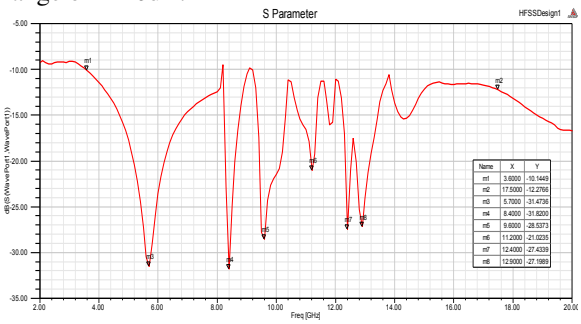

Figure 8: Return Loss for RT/Duriod substrate

(B) Return Loss-FR4

The simulated S11 vs Freq characteristic plot of an antenna is shown in Figure.9. An impedance bandwidth is accomplished experimentally in the range of 2.0 GHz to 12.1 GHz. The return loss level is under 10dB. The resonances occur at 2.7 GHz, 5.3GHz, 7.4 GHz, 8.9GHz and 10.2 GHz. The S11 levels at these resonances are – 40.85 dB, -25.04 dB, -24.80 dB, -21.64 dB and -19.20 dB in a relative manner. The value of return loss is in the worthy range of <-10dB.

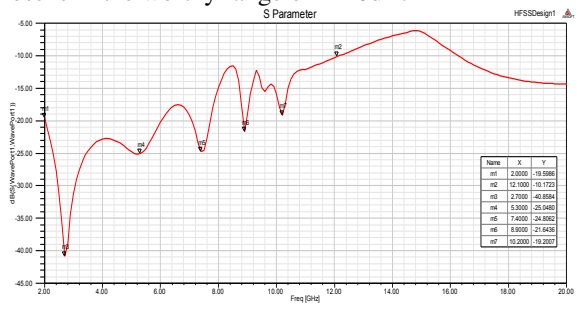

Figure 9: Return Loss for FR4 substrate

(C) VSWR-RT/Duriod

The simulated VSWR vs Frequency is shown in Figure.10. VSWR less than 2 is regarded as the impedance bandwidth. The VSWR< 2 is acquired at the resonant frequency.

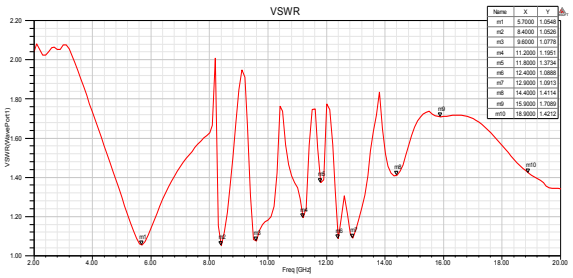

Figure 10: VSWR vs Freq for RT/Duriod

(D) VSWR-FR4

The simulated VSWR vs Frequency is shown in Figure.11. VSWR less than 2 is regarded as the impedance bandwidth. The VSWR< 2 is acquired at the resonant frequency.

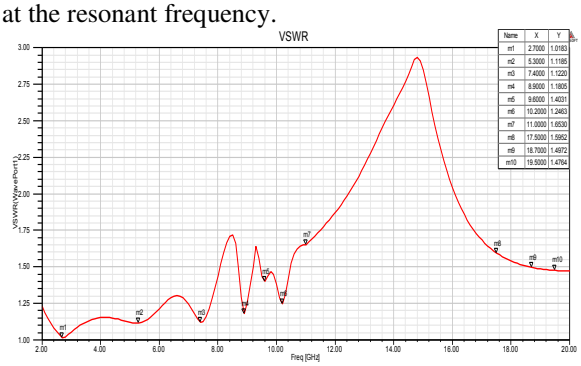

Figure 11: VSWR vs Freq for FR4

(E) Smith Chart-RT/Duriod

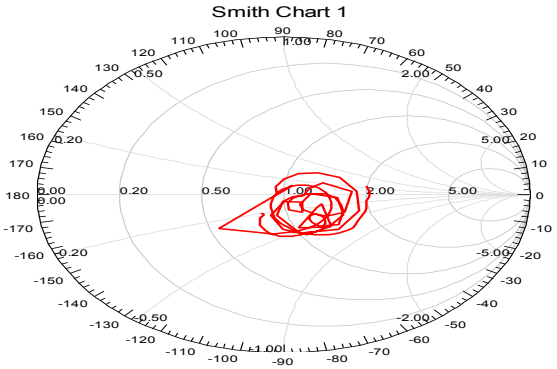

Figure 12: Smith Plot for RT/Duriod

(F) Smith Chart-FR4

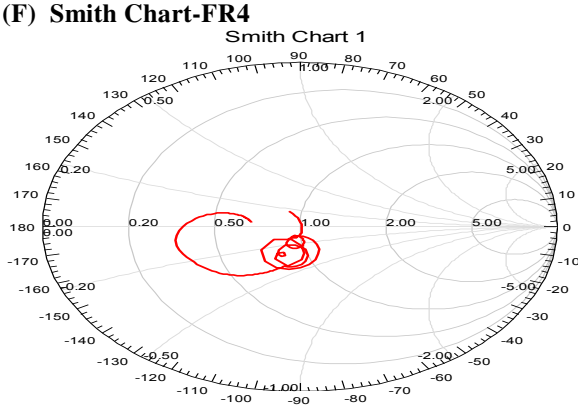

Figure 13: Smith Plot for FR4

(G) Radiation Pattern:

The radiation patterns are plotted at resonance frequencies 5.1 GHz, 7 GHz and 9.7 GHz. As a function of space coordinates, the antenna radiation pattern or antenna pattern is described as a mathematical function or graphical representation of the radiation attributes of the antenna. Radiation properties enclose field strength, power flux density, and directivity phase or polarization and radiation intensity. In effect, the three dimensional pattern is measured and logged in a cascade of two dimensional patterns. Nevertheless for most practical applications, some plots of the pattern as a function of θ for few specific values of φ, plus some plots as a function of φ for few specific values of θ, provide most of the utilitarian and necessary information.

The radiation of the antenna is explicated in terms of the field strength E (in V/m), and the graphical representation is called field strength pattern or field radiation pattern. Likewise if the radiation of the antenna is conveyed in relation to the power per unit solid angle, then the graphical representation is called power radiation pattern or power pattern.

It was observed that the radiation pattern provides positive gain characteristics at the frequency 5.2 GHz as shown in the Figure 14. The beneath Table 2 defines the choice of the frequency for obtaining a gain of 16.6809 dBi.

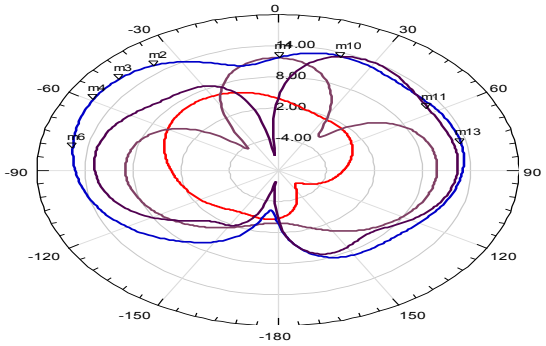

Figure 14: Radiation at frequency 5.2 GHz

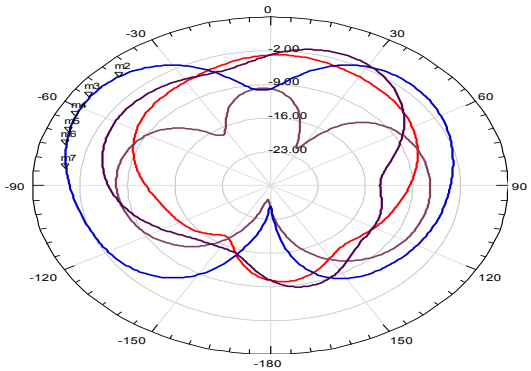

Figure 15: Radiation at frequency 6.1 GHz

It was observed that the radiation pattern provides positive gain characteristics at the frequency 6.1 GHz as shown in the Figure 15. The beneath Table 2 defines the choice of the frequency for obtaining a gain of 2.2592 dBi. In table the highlighted row provides the maximum gain.

TABLE 2: VARIATIONS IN GAIN FOR BOTH SUBSTRATES AT DIFFERENT ANGLES

RT/Duriod				FR4			
Name	**Theta**	**Angle**	**Magnitude**	**Name**	**Theta**	**Angle**	**Magnitude**
m1	1	1	11.8027	m1	-44	-44	1.6720
m2	37	37	15.3168	**m2**	**55**	**55**	**2.2592**
m3	-48	-48	16.4282	m3	-63	-63	2.0470
m4	**-59**	**-59**	**16.6809**	m4	-69	-69	1.6406
m5	-80	-80	15.8759	m5	-74	-74	1.1916
m6	20	20	13.3046	m6	-83	-83	0.2504
m7	57	57	12.1933	-	-	-	-
m8	77	77	13.3888	-	-	-	-

(H) Peak Gain

It is observed that the peak gain ranges from 4.84 to 17.09 dBi.

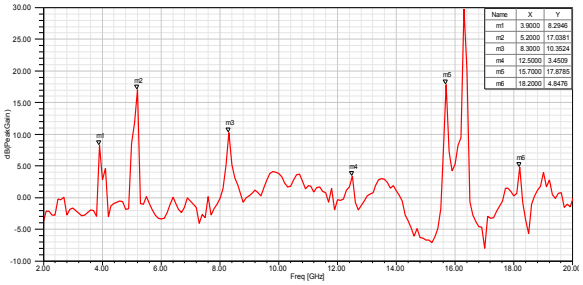

Figure 16: Peak Gain in dBi for RT/Duriod

It is observed that the peak gain ranges from 1.48 to 3.17 dBi.

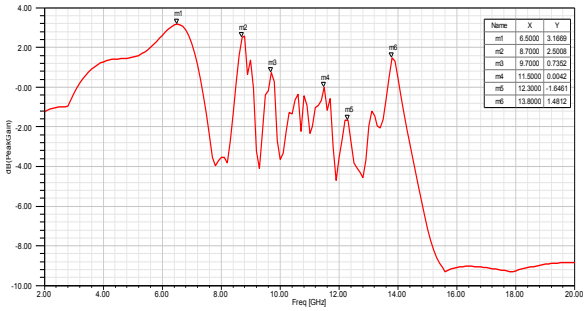

Figure 17: Peak Gain in dBi for FR4

V. PHYSICAL PARAMETRIC STUDY OF ANTENNA

In parametric analysis distinct values are provide to a specified parameter, for example, feed dimensions, DGS slot dimensions, patch length, patch width, etc.., are studied, by altering one attribute at a particular time and keeping all other different parameters constant so as to obtain optimized antenna for the desired wide applications

and results are noted. The values which are satisfactory are considered.

1.) Effect of altering Feed Width

The feed width is varied from 0.4 to 3 mm which signifies that the return loss increases at the beginning upto 2.2mm and later starts decreasing as the width is increased. The figure beneath indicates the impact of the feed line upon the S parameter. Talking about the resonant frequency and bandwidth it also starts increasing upto specified point. In Table.3, the highlighted row specifies that it is the best width so as to obtain the satisfactory result.

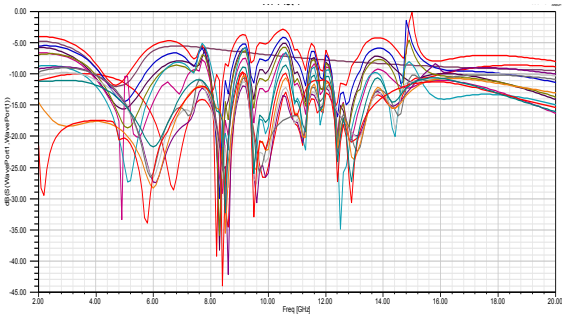

Figure 18: Variations in Return loss with feed width for RT/Duriod

TABLE 3: FEED LINE VARIATIONS FOR RT/DURIOD

Feed Width (mm)	Resonating Frequency (GHz)	Bandwidth (MHz)
0.4	4.4-5.0	600
0.6	4.2-5.3	1100
0.8	4.3-5.6	1300
1.0	4.0-6.0	2000
1.2	4.1-6.1	2000
1.4	3.9-7.2	3900
1.6	3.6-6.2	2600
1.8	2.1-8.9	6800
2.0	**2.1-19.7**	**17600**
2.2	2.1-19.6	17500
2.4	4.2-19.2	15000
2.6	3.7-19.7	16000
2.8	4.2-15.3	11100
3.0	4.5-15.6	11100

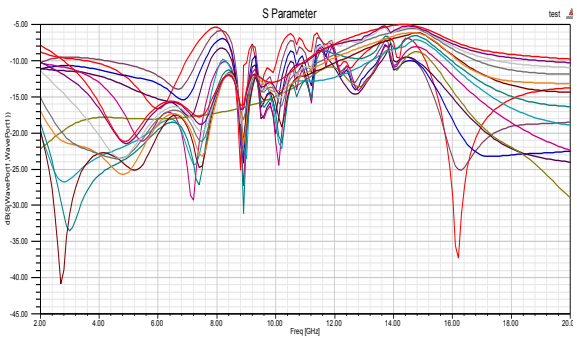

Figure 19: Variations in Return loss with feed width in FR4

TABLE 4: FEED LINE VARIATIONS FOR FR4

Feed Width (mm)	Resonating Frequency (GHz)	Bandwidth (MHz)
0.4	3.7-5	1300
0.6	4.2-7.3	3100
0.8	2.1-7.5	5400
1.0	2.1-7.7	5600
1.2	2.1-11.4	9300
1.4	2.1-11.3	9200
1.6	2.1-11.4	9300
1.8	2.1-11.3	9200
2.0	**2.1-12.1**	**10000**
2.2	2.1-11.6	9500
2.4	2.1-11.4	9300
2.6	2.1-11.2	9100
2.8	2.1-11.0	8900
3.0	2.9-10.9	8000

2.) 3D Field Distribution

The Φ component of electric field as a function of Φ is measured in x-y plane ($\theta=90^0$) for horizontal antenna. The field component can be exhibited as Eϕ ($\theta=90^0$, Φ) and it is called E plane pattern. The Φ component of electric field as a function of Φ is measured in x-z plane ($\theta=0^0$). The field component can be exhibited as Eϕ (θ, $\Phi=90^0$) and it is called H-plane pattern.

The relationship atween the co-polarization (desired) and cross-polarization (undesired) components provide the 3D field distribution plots. Furthermore it provides an enigmatic picture as to the nature of polarization of the fields propagating by means of the patch antenna.

VI. ACKNOWLEGMENT

The authors explicit their thanks to the management of Malnad College of Engineering and the Department of Electronics and Communication Engineering for their incessant support during this period of work.

VII. CONCLUSION

Upon the finish of the project the accompanying evaluation of the work is introduced for wide band applications by contrasting the designs with distinctive substrate utilizing microstrip feeding is given.

General working of the proposed antenna is understood. The significant parameters that alter design and applications were studied and their implication was understood. The design of antenna is done using the software HFSS. Accordingly, the

methodology of designing the antenna using HFSS software was concentrated on. The simulation is done and satisfactory results of the configuration are obtained. At the operating frequency, the S11 plot for antennas has a extent of not exactly -10dB which suggests that the matching impedance is accomplished.

An impedance transmission capacity resonating from 3.6 GHz to 17.5 GHz has been achieved. A gain of 16.68 dBi is achieved in impedance bandwidth. The antenna yields favorable radiation pattern in the impedance bandwidth range for RT/Duriod. However, for the FR4 substrate impedance transmission capacity resonating from 2.1 GHz to 12.1 GHz has been achieved. A gain of 2.55 dBi is achieved in impedance bandwidth.

The diverse antenna attributes such as return loss, impedance, VSWR, directivity, gain, bandwidth, operating frequency, field distribution and mesh generation are reviewed for designing the antenna. A brief study on the impact of physical parameters on the antenna parameters is done.

Spatially to begin with, the work starts with the outlining of the antenna operating at 18 GHz for wide band applications. The designed antenna provides better results. It is deduced that physical attributes such as feed line width, DGS positions, etc.., impacts the antenna results. Modifying the attributes of the antenna for a particular resonant frequency operation of the MSA provides optimized results is taken note.

In table 5 the final results of the project is provided which implies the values of all the simulated characteristics.

TABLE 5: FINAL RESULTS OF BOTH THE SUBSTRATES

Substrate Name	Frequency (GHz)	Return loss (dB)	Resonating Frequency (GHz)	VSWR	Gain (dBi)	Peak Gain (dBi)	Bandwidth (MHz)
RT/Duriod	5.2	-20.3838	3.6-17.5	1.2116	16.6809	17.0381	17700
FR4	6.1	-19.5211	2.1-12.1	1.2363	2.2592	3.1669	10000

As it can be observed from the simulated results RT/Duriod is better in all the parameters compared to FR4 substrate.

REFERENCES

[1] Mukesh Kumar Khandelwal and Santanu Dwari, "Design And Analysis of Microstrip DGS Patch Antenna with Enhanced Bandwidth for Ku Band Applications" IEEE Transactions on Antennas and Propagation, 2013.

[2] Xian-Ling Liang and Tayeb A. Denidni, "H-Shaped Dielectric Resonator Antenna for Wideband Applications" IEEE Antennas and Wireless Propagation letters, vol. 7, 2008.

[3] D.Guha, M.biswas and Y.M.M.Antar, "Microstrip patch antenna with defected ground structure for cross polarization suppression", IEEE antenna and wireless propagation lett, Vol.4, pp.455-458, 2005.

[4] M.Salehi, A.Motevasselian, A.Tavakoli, T. Heidari, "Mutual coupling reduction of microstrip antenna using defected ground structure", IEEE Singapore International Conference on Communication System, pp. 1-5, 2006.

[5] H Liu, X Sun and J. Mao, "harmonic suppression with photonic bandgap and defected ground structure for a microstrip patch," IEEE microwave and wireless component letters, pp.1-2, 2005.

[6] Howell, J. Q., "Microstrip antennas," Dig. Int. Symp. Antennas Propagat. Soc., 177–180, Williamsburg, VA, Dec. 1972.

[7] L. H. Weng, Y. C. Guo, X. W. Shi, and X. Q. Chen, An Overview on defected ground structure. Progress in Electromagnetic Research B, Vol. 7, 173–189, 2008.

[8] M. Kulkarni, Microwave and Radar Engineering, 2nd edition, Umesh publication.

[9] SAMUEL Y.LIAO, Microwave devices and circuits, Third edition, Prentice hall, Englewood Cliffs, New Jersey 07632

[10] Constantine A. Balanis, Antenna Theory Analysis and Design, Ed. 3. John Wiley, 2007.

COMPARISON OF DCT AND DWT CODING TECHNIQUES FOR MEDICAL IMAGES

Sanjana Gogate, Nischitha C N, Rohini Nagapadma

***Abstract*- Digital images in their raw form require an enormous amount of storage capacity. Considering the important role played by digital imaging, it is necessary to develop a system that produces high degree of compression while preserving critical image information, in case of medical images. There are various transformation techniques used for data compression. Discrete Cosine Transform (DCT) and Discrete Wavelet Transform (DWT) are the most commonly used transformations. DCT has high energy compaction property and requires less computational resources. On the other hand, DWT is a multi-resolution transformation.**

***Keywords*- Image compression, quantization, DWT, DCT, Huffman encoding, medical image.**

I. INTRODUCTION

A lot of hospitals handle their medical image data with computers. The use of computers and a network makes it possible to distribute the image data among the staff efficiently. X-Ray and CT produce sequence of images. The amount of data produced by these techniques is vast and this might be a problem when sending the data over a network. To overcome this problem image compression has been introduced in the field of medical. There have been numerous compression research studies, examining the use of compression as applied to medical images.

To achieve higher degree of compression we have chosen the hybrid scheme of DWT, DCT and Huffman encoding compression technique. This approach will improve the performance of medical image compression while satisfying medical team who need to use it. There are several types of image compressions available but in case of biomedical images the loss of diagonasability of the image is not tolerable and hence this approach will achieve higher degree of compression without any significant loss in the diagonasability of the image.

The Joint Photographic Expert Group (JPEG) system, based on the Discrete Cosine Transform (DCT), has been the most widely used compression method.

The Discrete Wavelet Transform (DWT), on the other hand, has been emerged as an efficient tool for medical image compression, mainly due to its ability to display image at different resolutions. It also offers higher compression ratio.

The main objectives of this paper are to compare the schemes of compression based on certain objective and subjective parameters.

II. DCT-BASED JPEG IMAGE CODING

A. DCT

A DCT represents the input data points in the form of a sum of cosine functions that are oscillating at different frequencies and magnitudes [1]. There are mainly two types of DCT: one dimensional (1-D) DCT and two dimensional (2-D) DCT. Since an image is represented as a two dimensional matrix, for this work, 2-D DCT is considered. The 2-D DCT for an N x N input sequence an be defined as follows[1]:

$$D_{DCT}(i,j) = \frac{1}{\sqrt{2N}} B(i)B(j) \sum_{x=0}^{N-1} \sum_{y=0}^{N-1} M(x,y) \cos\left[\frac{2x+1}{2N} i\pi\right] \cos\left[\frac{2y+1}{2N} j\pi\right]$$

B. DCT Quantization and Dequantisation

In the DCT compression, almost all of the information is concentrated in a small number of the low frequency coefficients. These low frequency coefficients are also known as DC components and the rest of the components are AC components. The DCT coefficients are then quantized using a 8 x 8 quantization table [2], Q as described in the Joint Photographic Expert Group (JPEG) standard. Further compression can be achieved by applying appropriate scaling factor. In order to reconstruct the output data, the rescaling and the de-quantization should be performed.

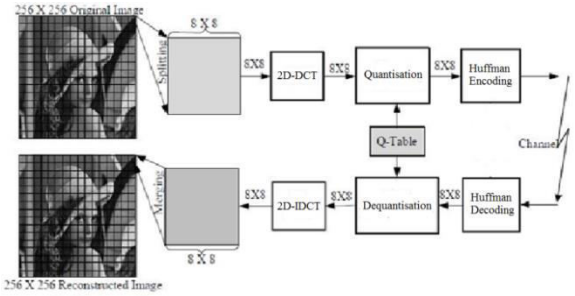

Fig 1: Block diagram of DCT

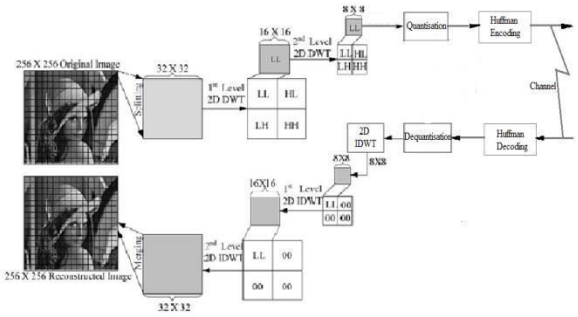

Fig 2: Block Diagram of DWT

III. DWT-BASED JPEG IMAGE CODING

A.DWT

The DWT represents an image as a sum of wavelet functions, known as *wavelets*, with different location and scale [20]. It represents the data into a set of high pass (detail) and low pass (approximate) coefficients. The input data is passed through set of low pass and high pass filters. The Daubechies filter coefficients [3] are used for in this work.

B.Methodology

In this paper, an image is first divided into blocks of 32 x 32. Each block is then passed through the two filters: high pass filter and low pass filter. The first level decomposition is performed to decompose the input data into an approximation and the detail coefficients. After obtaining the transformed matrix, the detail and approximate coefficients are separated as LL, HL, LH, and HH coefficients. All the coefficients are discarded, except the LL coefficients. The LL coefficients are further transformed into the second level. The process continues for one more level. The coefficients are then divided by a constant scaling factor (SF) to achieve the desired compression ratio. Finally, for data reconstruction, the data is rescaled and padded with zeros, and passed through the wavelet filters. The entire process of 2- D DWT compression and reconstruction is shown in Figure 2.

IV. HUFFMAN ENCODING

Huffman coding is a statistical lossless data compression technique. Huffman coding is based on the frequency of pixel in images. It helps to represent a string of symbols with lesser number of bits. In this lossless compression shorter codes are assigned to the most frequently used symbols, and longer codes to the symbols which appear less frequently in the string. This algorithm is an optimal compression algorithm when only the frequencies of individual letters are used to compress the data [4]. Therefore, when Huffman coding when combined with technique of reducing the image redundancies using Discrete Cosine Transform (DCT) helps in compressing the image data to a better level.

V EVALUATION CRITERION

The performance of both DCT and DWT techniques were estimated using compression ratio (CR), peak signal to noise ratio (PSNR) and SSIM (Structural Similarity Index)

- *PSNR* = 10log10 (I / *MSE*) dB
  where I is the maximum intensity level

- Compression ratio (*CR*) is a measure of the reduction of the detail coefficient of the data. It can be defined as,
  CR=Discarded Data / Original Data

- SSIM (Structural Similarity Index): During the data compression, the structures of the reconstructed data

are distorted. This distortion can be analyzed using SSIM index.

VI. SIMULATION RESULTS

The above coding techniques were applied to a medical image (an endoscopic image) and compared based on various parameters.

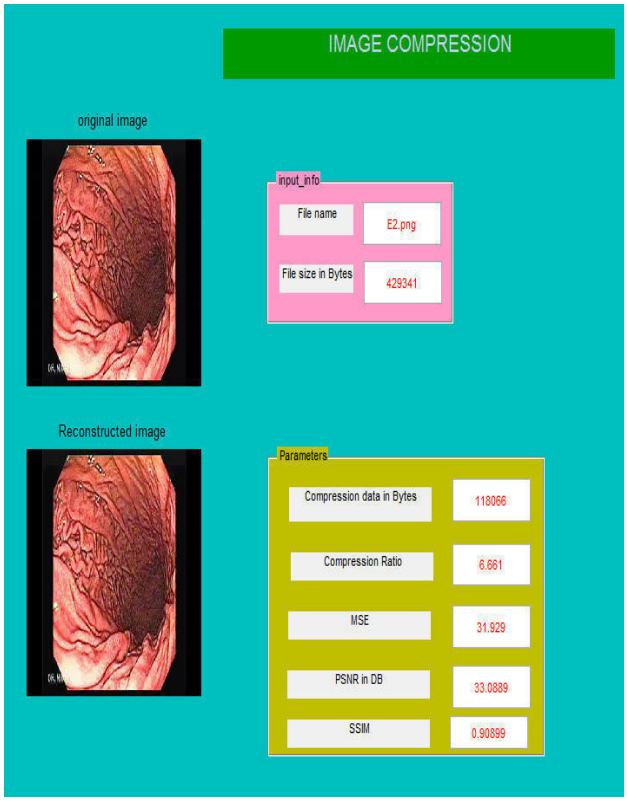

Fig 3: DCT based Compression

Fig 4: DWT based Compression

Table 1: Comparison of Parameters

Image/ Algorithm	**DCT**			**DWT**		
	CR	PSNR (dB)	SSIM	CR	PSNR (dB)	SSIM
Medical Image	6.66	33.08	0.908	27.81	31.512	0.76125

VII. CONCLUSION

It can be concluded that the images compressed using DWT have a better compression ratio compared to those compressed using DCT but at the cost of diagonasability of the image.

VIII. FUTURE SCOPE

Both the mentioned techniques-DCT and DWT in the paper can be combined to achieve still higher compression ratios without compromising the quality of the image.

IX. REFERENCES

[1] R. K. Rao and P. Yip, Discrete Cosine Transform: Algorithms, Advantages and Applications. NY: Academic, 1990.

[2] J. D. Kornblum, "Using JPEG quantization tables to identify imagery processed by software," Digital Forensic Workshop, Elsevier, pp. 21–25, 2008.

[3] I. Daubechies, Ten Lectures on Wavelets. SIAM, 1992.

[4] Image Compression Using DWT, DCT & Huffman Encoding Techniques, Harjeetpal singh, Sakhi Sharma, October 2012.

[5] S.E. Ghrare, M.A.M Ali, M. Ismail , and K. Jumari, " Diagnostic quality of compressed medical images : Objective and Subjective evaluation".

[6] W. B. Pennebaker and J. L. Mitchell, JPEG Still Image Data Compression Standard, 3rd ed. New York: Springer, 1993.

[7] N. Ahmed, T. Natarajan, and K. Rao, "Discrete Cosine Transfom," Computers, IEEE Transactions on, vol. C-23, no. 1, pp. 90 – 93, Jan 1974.

[8] G. Strang and T. Nguyen, Wavelets and Filter Banks. Cambridge Press, 1996.

ENERGY EFFICIENT ROUTING PROTOCOL FOR WBAN

Siddiq Iqbal[1], Dr. Sujatha B R [2]
[1] Dept. of Telecommunication, B.M.S. Institute of Technology & Management, Bengaluru
[2]Assosicate Professor, Dept. of Electronics & Communication, Malnad College Of Engineering, Hassan
[1]siddiq@bmsit.in, [2]brshsn61@gmail.com,

***Abstract*—Wireless body area network is a new emerging field in WSN. WBAN is a wireless network of wearable devices, with computing capability. The most important application of WBAN is health monitoring. In WBANs the wireless sensors are deployed in the human body and these sensors are used to monitor the various human body parameters such as blood pressure, glucose level, heart rate etc. WBANs capture accurate and quantitative data from a variety of sensors. In this work we propose a energy efficient routing protocol for WBANs that uses a combination of multi-hop and single-hop topology. We use the concept of cost function in order to select the forwarder node. The calculation of cost function takes into consideration the residual energy parameter into account thus making sure that the energy consumption of the network is balanced. MATLAB simulations of proposed routing algorithm have been performed to obtain the simulation results. The simulation results show that our proposed protocol increases the network stability and the nodes stay alive for a longer duration, which in turn contributes to higher packet delivery to the sink.**

***Index Terms*— WBAN, cost function, residual energy, stability, network lifetime, path loss.**

I. INTRODUCTION

The Body Area Network field is an interdisciplinary area which could allow continuous health monitoring with a real-time updates of medical records [1]. As sensors are available in various sizes, they can be worn on, attached or implanted into the human body. The main objective of WBANs is to simplify and improve the speed and accuracy of data collection from nodes, thus providing reliable communication. WBANs also control actuators for in-time release of medication. The sensors used in WBANs are battery driven units. These sensor nodes have limited battery resources, due to which the sensor nodes are unable to collect all information stored in the network[3].

The most important application of WBANs is the patient monitoring. The sensors deployed in the human body record the various physiological conditions of the patients under supervision and can provide us real-time feedback. The sensors collect the patient data and then send it to the physician in a hospital through Metropolitan Area Network (MAN) or Local Area Network (LAN).

As frequent charging of the batteries is a tedious process, the deployment of WBANs requires a novel solution towards power-efficient communication. Higher power consumption leads to increase in electro-magnetic radiations, which have negative impacts on the human body. Power efficient communication ensures the significant decrease in the electromagnetic radiations. Thus low power routing is of great importance.

The routing protocols in WBANs are classified as follows [5]-

Temperature Based Routing Protocols: The objective of these protocols is to avoid routing on hot spots by maintaining low temperature among sensor nodes.
Cluster Based Routing Protocols: These protocols divide the various nodes in the WBAN network into different clusters and assigns one Cluster Head for each cluster [8]. Cluster head routes the data from sensor nodes to the sink through Cluster Heads [9].
Cross Layer Routing Protocols: These protocols are mainly reactive and need to gain knowledge of the connectivity of all nodes in the network and their other features which leads to significant overhead.
Cost-Effective Routing Protocols: These protocols introduce the concept of cost function. Periodically the cost function is updated based on the cost-effective information and the node with the minimum cost function is selected for the transmission of data.
QoS-Based Routing Protocols: These protocols provide separate modules for various QoS metrics, hence providing higher reliability, lower end-to-end delay and higher packet delivery ratio.
The rest of the paper is organized in the following order. In section 2 the radio model is presented. Low energy protocol is proposed in section 3. Existing protocols are discussed in section 4. Performance metrics and simulation results are presented in section 5. And finally section 6 presents conclusion.

II. RADIO MODEL

We use first order radio model proposed in [3]. Single-hop communication is used to minimize delay. This radio model considers the separation between transmitter and receiver, d^2

the loss of energy due to transmission channel. We calculate energy consumed in Single-hop communication as:

$$E_{s\text{-}hop} = E_{transmit} \text{ .....(1)}$$

where, $E_{transmit}$ is the transmission energy and is calculated as:

$$E_{transmit} = E_{elec} + E_{amp} \text{ .....(2)}$$

where, E_{elec} is the energy consumed for processing data and E_{amp} is energy consumed by transmit amplifier.

$$E_{transmit} = k(E_{elec} + E_{amp}*d^2) \text{ ..... (3)}$$

Where, k is number of bits in a packet.

The energy consumption during Multi-hop communication can be computed using the following equations:

$$E_{M-HOP} = E_{transmit} + E_{received} \text{ .....(4)}$$

where, $E_{received}$ is the energy consumed for receiving data. If *k*-bits are transmitted to a distance of *n*-hops the transmission energy will be $n*k*E_{transmit}$ and receiving energy will be $(n-1)*k*E_{received}$. So the energy consumed for Multi-hop is:

$$E_{M-HOP} = n*k*E_{transmit} + (n-1)*k*E_{received} \text{ .... (5)}$$

From (3) and (5), taking $E_{received} = E_{elec}$ since the receiving energy is equal to energy consumed to process received data we obtain

$$E_{M-HOP} = n*k*(E_{elec} + E_{amp}*d^2) + (n-1)k*E_{elec} \text{ .....(6)}$$

$$E_{M-HOP} = n*k*E_{elec} + n*k*E_{amp}*d^2 + n*k*E_{elec} - k*E_{elec} \text{ ...(7)}$$

$$E_{M-HOP} = [2*n*k*E_{elec} + n*k*E_{amp}*d^2 - k*E_{elec}] \text{ .....(8)}$$

III. Proposed Protocol

Low Energy Routing Protocol:

1) System Model

In this protocol, sink is placed at center of the human body. Sensor nodes are deployed on a human body; having equal power and computation capabilities. The sensor nodes used to detect ECG and glucose transmits data directly to sink. Single-hop communication is used during emergency conditions [2] and multi-hop scheme is used for normal data delivery as proposed in [4]. The relay nodes are used so that they can easily forward the received data to sink due to higher energy levels.

2) Initial Phase

Three tasks are performed in this phase. Firstly each node is informed about its neighbors; the location of sink on the body is identified and finally all the possible routes to sink are also evaluated. Each of the sensors updates location of neighbors and sink, when each node broadcasts an information packet containing its node ID, its own location and its energy status. Fig 1 shows the flow chart for the implementation of low energy protocol.

3) Selection of forwarder node

The sink node knows the ID, distance and residual energy status of all the nodes in the network. It computes the cost function of all nodes and transmits this value to all members. The cost function is calculated as follows:

$$CF(i) = \frac{\sqrt[4]{d(i)}}{R.E(i)}$$

where d(i) is the distance between the node i and sink, E(i) is the residual energy of node i and is calculated by subtracting the current energy of node from its initial energy.
Forwarder node is selected based on cost function; which ever node has minimum cost function value becomes the forwarder node. All the neighbor nodes stick together with forwarder node and transmit their data to it. Forwarder node aggregates collected data and forward to the sink. Nodes transmitting ECG and glucose do not participate in forwarding the data. Nodes are awake only at the time of transmission.

4) Routing Phase

Consequently, route selection is done using radio model. Only such routes are selected which are at fewer hops to the sink. As the nodes have information of all nodes and sink's location, so selected routes are stead fast and consume less energy. In case of emergency, all the implanted nodes on the body can communicate directly with the sink.

IV. Other Protocols

The existing protocols that will be used for comparison with the proposed protocol are discussed in this section

A. *Mobile-adaptive threshold based thermal aware energy-efficient multi-hop protocol (M-ATTEMPT)*:[6]

In M-ATTEMPT, both single hop communication and multi-hop communication is used. Single hop communication is used for real-time traffic (critical data) or on-demand data while Multi-hop communication is used for normal data delivery. In WBANs it is important to sense the heat generated by the implanted sensor nodes. The M-ATTEMPT protocol is thermal-aware and it senses the link Hot-spot and routes the data away from these links. This protocol considers the

concept of mobility, in order to keep the established links intact.

In this protocol, the sink is placed at the center of human body and the sensor nodes are deployed on the human body. The nodes with high data rate send data directly to the sink node and can easily forward the received data from low data rate sensors.

Initially, all nodes broadcast Hello messages. This Hello message contains neighbors information and distance of sink nodes in the form of hop-counts. In this way all nodes are updated with their neighbors, sink position and available routes to the sink node. Using Radio model, routes with fewer hops to sink are selected from available routes and the selected routes are steadfast and consume less energy.. In case of emergency, all processes are lagged until critical data is successfully received by sink node.

After route selection the sink node assigns Time Division Multiple Access (TDMA) schedule for communication between sink node and nodes. Sink node allocate time-slots to nodes, thus enabling a node to communicate with the sink node at the allotted time. Finally, the sink node receives the data from the nodes and aggregates it.

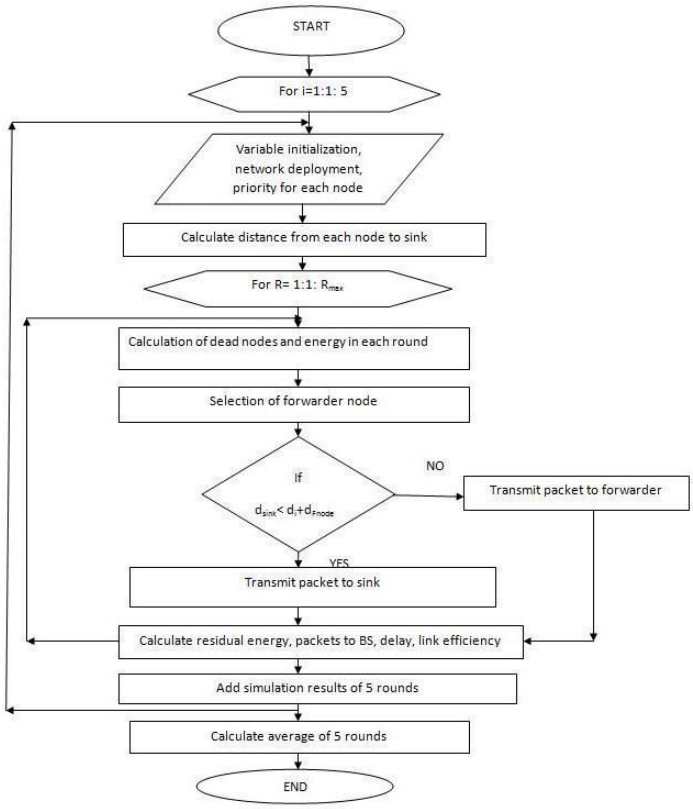

Fig *1*: Flowchart for Low Energy Protocol

B. *Stable Increased-throughput Multi-hop Protocol for Link Efficiency in Wireless Body Area Networks (SIMPLE)*:[7]

In this protocol, the sensors of equal power and computational capabilities are deployed on human body. The sink node is placed at the waist. The sensors carrying the ECG information and the glucose information continuously transmit the data to the sink directly.

Initially, the sink broadcasts a short information packet which contains the location of the sink on the body. After receiving the control packet, each sensor node stores the location of sink. Consequently, sensor node broadcasts an information packet which contains node ID, location of node on body and its energy status. In this way, all sensor nodes are updated with the location of neighbors and sink.

Multi-hop communication scheme is used in order to save energy. In order to balance energy consumption among sensor nodes and to trim down energy consumption of network, this protocol elects a new forwarder in each round. The sink is aware of the ID, distance and residual energy status of the nodes. Thus, this feature enables the sink to compute the cost function of all nodes and transmits this cost function to all nodes. On the basis of this cost function, the forwarder node is elected. The cost function is computed as follows-

$$C(i) = \frac{d(i)}{R.E(i)}$$

Where d(i) is the distance between the node i and sink, R.E(i) is the residual energy of node i and is calculated by subtracting the current energy of node from initial total energy.

A node with minimum cost function becomes the forwarder node. The forwarder node has maximum residual energy and minimum distance to the sink. All the neighbor nodes stick together with forwarder node and transmit their data to it. Forwarder node aggregates collected data and forward to sink. Nodes transmitting ECG and glucose do not participate in forwarding the data. Nodes are awake only at the time of transmission.

The forwarder assigns time slots to the children node with the help of Time Division Multiple Access (TDMA) scheme. The children nodes transmit their sensed data to forwarder node in its own scheduled time slot. This minimizes the energy dissipation of the individual nodes.

V. Simulation Results

We used MATLAB for performance analysis. A network size of 0.8m x 1.6m is considered here, where eight nodes are deployed on the human body and sink node is placed at the co-ordinates location of (0.25m, 1m) of the network. 8000 number of rounds was taken and nodes with initial energy of nodes 0.5J and radio range of 10m selected. The protocol was executed 5 times and the average results with graphs are provided. The simulation results are compared.

The metrics used for performance analysis are:

1. *Stability Period:* The time interval from the start of network operation until the death of the first sensor node.

2. *Residual Energy:* The energy remaining in a sensor node after each round.
3. *Network lifetime:* The time interval from the start of operation of the sensor network until the death of the last node.
4. *Throughput:* The total rate of data sent over the network.
5. *Delay spread*: is a measure of the multipath richness of a communication channel or the arrival time difference between the earliest multipath component and the latest multipath component of the received signal.

Parameters	Value
DC Current (Rx)	18mA
DC Current (Tx)	*10.5*mA
Minimum DC supply voltage	*1.9*V
E_{rx} – elec	36.1 nJ/bit
E_{tx} – elec	16.7 nJ/bit
Amplification energy for long distance *Eamp*	1.97 nJ/bit
EDA	5 nJ/bit
Wavelength (λ)	0.125m
Frequency (f)	2.4GHz
Initial Energy (E_0)	0.5J

Table1: Parameter setting

Fig 2, fig 3, fig 4, fig 5, shows the comparison between M-ATTEMPT, SIMPLE and Low Energy routing protocol. From fig 2 we can conclude that, stability period for Low Energy protocol is much greater than those of SIMPLE and M-ATTEMPT. Increased stability period is seen in Low Energy protocol compared to SIMPLE and M-ATTEMPT is because of non-continuous data transmission. Fig 3 shows that the proposed protocol achieves higher throughput than SIMPLE and M-ATTEMPT protocols. Fig 4 shows that Low Energy protocol has approximately same residual energy when compared to SIMPLE protocol. Fig 5 shows that Low Energy protocol has more delay since number of packets transmitted is more when compared to SIMPLE and M-ATTEMPT protocols.

Table2

Protocol	Stability Period (Rounds)	Propagation delay (Rounds)	Network Lifetime (Rounds)	Throughput (Packets)
M-ATTEMPT	7440	0.9×10^{-8}	2200	1.7×10^4
SIMPLE	7450	1.01×10^{-8}	4400	2.8×10^4
LOW ENERGY PROTOCOL	7450	1.3×10^{-8}	5000	3.4×10^4

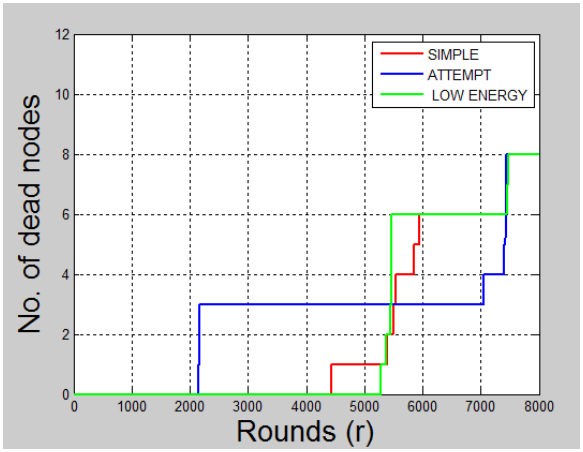

Fig 2: *Network Lifetime*

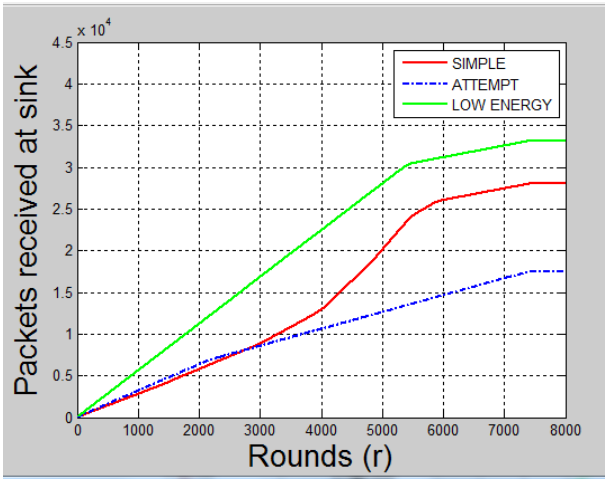

Fig 3: *Throughtput*

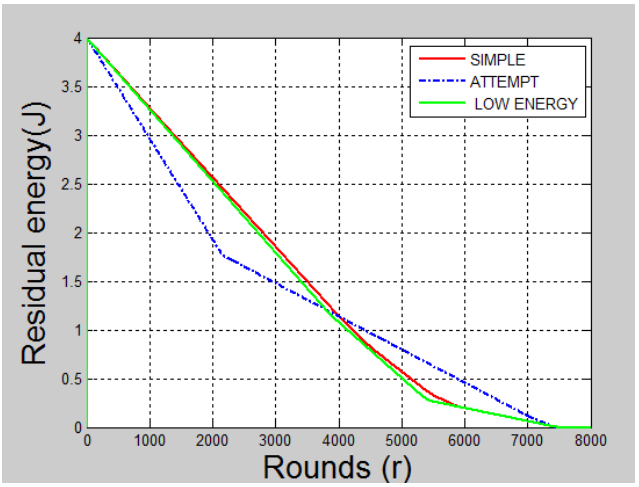

Fig 4: *Analysis of remaining energy*

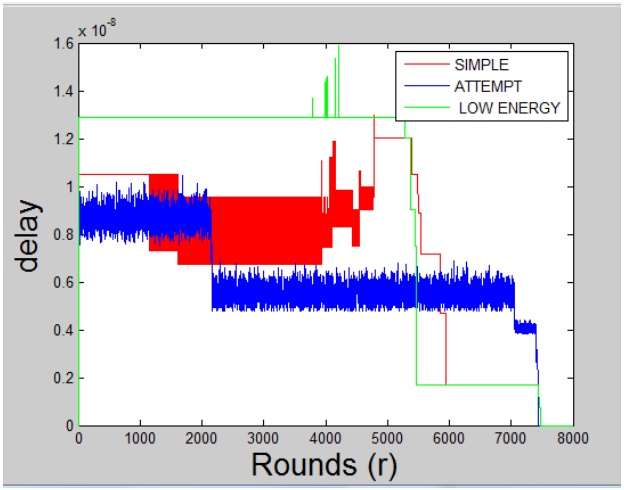

Fig 5: *Delay*

VI. Conclusion

In this paper, we have proposed a mechanism to route data in WBANs in which both the merits of single-hop and multi-hop are utilized. The proposed scheme uses cost function to select the most appropriate route to sink. Our simulation results shows that proposed routing scheme has considerably enhanced the network stability period, it also has increased network lifetime and it reduces the power consumption of the WBAN network thus making it a power efficient protocol. In future work, we shall try to implement a probability function which determines the path through which the packets can be sent successfully to the sink.

References

1. Aashima Arya , Naveen Bilandi, A Review: Wireless Body Area Networks for Health Care International Journal of Innovative Research in Computer and Communication Engineering Vol. 2, Issue 4, April 2014.

2. K. Y. Yazdandoost, K. Sayrafian-Pour, *et al.*, "Channel model for body area network (ban)," *IEEE P802*, vol. 15, 2009.

3. Heinzelman, Wendi Rabiner, Anantha Chandrakasan, and Hari Balakrishnan. "Energy-efficient communication protocol for wireless microsensor networks." System Sciences, 2000. Proceedings of the 33rd Annual Hawaii International conference.

4. N. Javaid, U. Qasim, Z. A. Khan, M. A. Khan, K. Latif and A. Javaid,"On Energy Efficiency and Delay Minimization in Reactive Protocols in Wireless Multi-hop Network", 2nd IEEE Saudi International Electronics, Communications and Photonics Conference (SIECPC 13), 2013, Riyadh, Saudi Arabia.

5. Samaneh Movassaghi, Mehran Abolhasan, "A Review of Routing Protocols in Wireless Body Area Networks", JOURNAL OF NETWORKS, VOL. 8, NO. 3, MARCH 2013.

6. N. Javaid, Z. Abbas, M. Fareed, Z. Khan, and N. Alrajeh, "M-attempt: A new energy-efficient routing protocol for wireless body area sensor networks,"The 4th International Conference on Ambient Systems, Networks and Technologies (ANT 2013), 2013, Halifax, Nova Scotia,Canada, Procedia Computer Science, Volume 19, 2013, Pages 224-231.

7. Q. Nadeem, N. Javaid, S. Mohammad, M. Khan, S. Sarfraz, and M. Gull, "Simple: Stable increased-throughput multi-hop protocol for link efficiency in wireless body area networks," Broadband and Wireless Computing, Communication and Applications (BWCCA), 2013 Eighth International Conference on ,vol., no.pp.221,226, 28-30 Oct. 2013.

8. Hu Junping, Jin Yuhui, Dou Liang, "A Time-based Cluster-Head Selection Algorithm for LEACH", A Time-based Cluster-Head Selection Algorithm for LEACH", Computers and Communications, ISCC 2008, 1172 – 1176, 2008.

9. Qian Liao, Hao Zhu, "An Energy Balanced Clustering Algorithm Based on LEACH Protocol", 2nd International Conference 2012 on Systems Engineering and Modeling.

Interline Unified Power Quality Conditioner for mitigation of Power Quality in two feeder distribution System using Simulink

Dr. Thejaswi. A. H,
Professor
Dept. of E&E Engg.,
JNNCE, Shimoga-577204

Veeresha. K. B,
Research Scholar
Dept. of E&E Engg.,
JNNCE, Shimoga-577204

Email-id: *ahtph711@gmail.com, kbveeresha@gmail.com,*

ABSTRACT: *This paper proposes a modified connection for a UPQC to improve the power quality of two feeders in a distribution system is the Interline Unified Power Quality Conditioner (IUPQC). IUPQC specifically aims at the integration of series VSC and Shunt VSC to provide high quality power supply by means current & voltage harmonic elimination and voltage sag/swell compensation in a of two feeders in a distribution system, so that improved power quality can be made available at the point of common coupling. The structure, control and capability of the IUPQC are discussed in this paper. The efficiency of the proposed configuration has been verified through simulation using MATLAB/ SIMULINK.*

***Index Terms*—Power quality (PQ), Interline Unified Power-Quality Conditioner (IUPQC), Voltage Source Converter (VSC).**

I. INTRODUCTION

Power Electronics has three faces in power distribution, first one that introduces valuable industrial and domestic equipment, a second one that creates problems and finally a third one that helps to solve those problems. Modern semiconductor switching devices are being utilized more and more in a wide range of applications in distribution networks, particularly in domestic and industrial loads. Examples of such applications widely used are Adjustable Speed motor Drives (ASD's), Diode and Thyristor rectifiers, Uninterruptible Power Supplies (UPS), computers and their peripherals, consumer electronics appliances (TV sets for example) and arc furnaces. Complications related to the use of non-linear loads for these systems have been a major issue for a long time for both power providers and users alike. Power problems are partially solved with the help of LC passive filters [1-2].

A Unified Power Quality Conditioner (UPQC) can perform the functions of both DSTATCOM and DVR. The UPQC consists of two Voltage-Source Converters (VSCs) that are connected to a common DC bus. One of the VSCs is connected in series with a distribution feeder, while the other one is connected in shunt with the same feeder. The DC links of both VSCs are supplied through a common DC capacitor [3-5].

This paper presents a modified connection for a UPQC called interline UPQC (IUPQC). The Typical IUPQC connected distribution system is shown in Fig.1. Two feeders, Feeder-1 and Feeder-2, which are connected to two different substations, supply the system loads L-1 and L-2. The supply voltages are denoted $V_{s1}$by V_{s2} and. It is assumed that the IUPQC is connected to two buses B-1 and B-2, the voltages of which are denoted by V_{t1} and V_{t2}, respectively. Further two feeder currents are denoted $i_{s1}$by i_{s2} and while the load currents are denoted by i_{l1} and i_{l2}. The load L-2 voltage is denoted by V_{t2}.

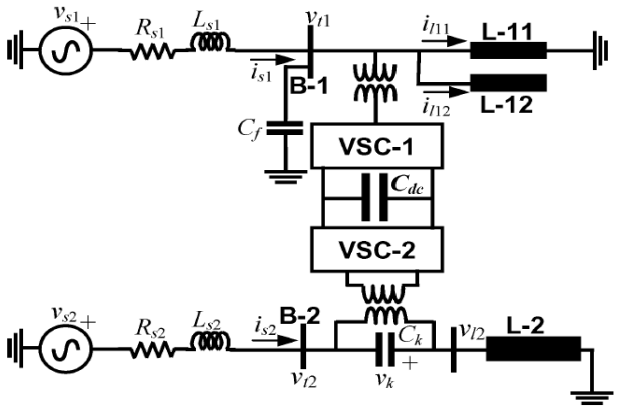

Fig.1 Typical IUPQC connected in a distribution system

The purpose of the IUPQC is to hold the voltages v_{t1} and v_{t2} constant against voltage sag/swell, temporary interruption in either of the two feeders. It has been demonstrated that the IUPQC can absorb power from one feeder (say Feeder-1) to hold v_{l2} constant in case of sag in the voltage v_{s2}. This can be accomplished as the two VSCs are supplied by a common dc capacitor. The dc capacitor voltage control has been discussed here along with voltage reference generation strategy. Also, the limits of achievable performance have been computed. The performance of the IUPQC has been evaluated through simulation studies using SIMULINK.

II. STRUCTURE AND CONTROL

The IUPQC shown in Fig. 1 consists of two VSCs (VSC-1 and VSC-2) that are connected back to back through a common energy storage dc capacitor. Let us assume that the VSC-1 is connected in shunt to Feeder-1 while the VSC-2 is connected in series with Feeder-2. Each of the two VSCs is realized by three H-bridge inverters [9], [10], and each switch represents a power semiconductor device (e.g., IGBT) and an anti-parallel diode. All the inverters are supplied from a common single dc capacitor and each inverter has a transformer connected at its output.

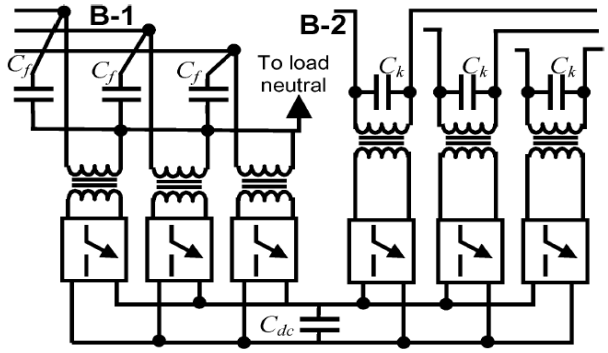

Fig.2. Complete structure of an IUPQC.

The complete structure of a three-phase IUPQC with two such VSCs is shown in Fig.2. The secondary (distribution) sides of the shunt-connected transformers (VSC-1) are connected in star with the neutral point being connected to the load neutral [6-7]. The secondary winding of the series-connected transformers (VSC-2) are

directly connected in series with the bus B-2 and load L-2.

The ac filter capacitors and are also connected in each phase (Fig. 2) to prevent the flow of the harmonic currents generated due to switching. The six inverters of the IUPQC are controlled independently. The switching action is performed by control signal obtained by Space vector PWM [8-9, 11].

III. SYSTEM DESCRIPTION

An IUPQC connected to a distribution system is shown in Fig.1. In this figure, the feeder impedances are denoted by the pairs (R_{s1}, X_{s1}) and (R_{s2}, X_{s2}). It can be seen that the two feeders supply the loads L-1 and L-2. The load L-1 is assumed to have two separate components—an unbalanced part (L-11) and a non-linear part (L-12). The currents drawn by these two loads are denoted by i_{l1} and i_{l2}, respectively.

We further assume that the load L-2 is a sensitive load that requires uninterrupted and regulated voltage. The shunt VSC (VSC-1) is connected to bus B-1 at the end of Feeder-1, while the series VSC (VSC-2) is connected at bus B-2 at the end of Feeder-2.

The voltages of buses B-1 and B-2 and across the sensitive load terminal are denoted by V_{t1}, V_{t2}, and V_{l2}, respectively. The aim of the IUPQC is two-fold:

- to protect the sensitive load L-2 from the disturbances and sag/swell occurring in the system by regulating the voltage V_{l2};
- to regulate the bus B-1 voltage V_{t1} against disturbances in the system.

In order to attain these aims, the shunt VSC-1 is operated as a voltage controller while the series VSC-2 regulates the voltage across the sensitive load.

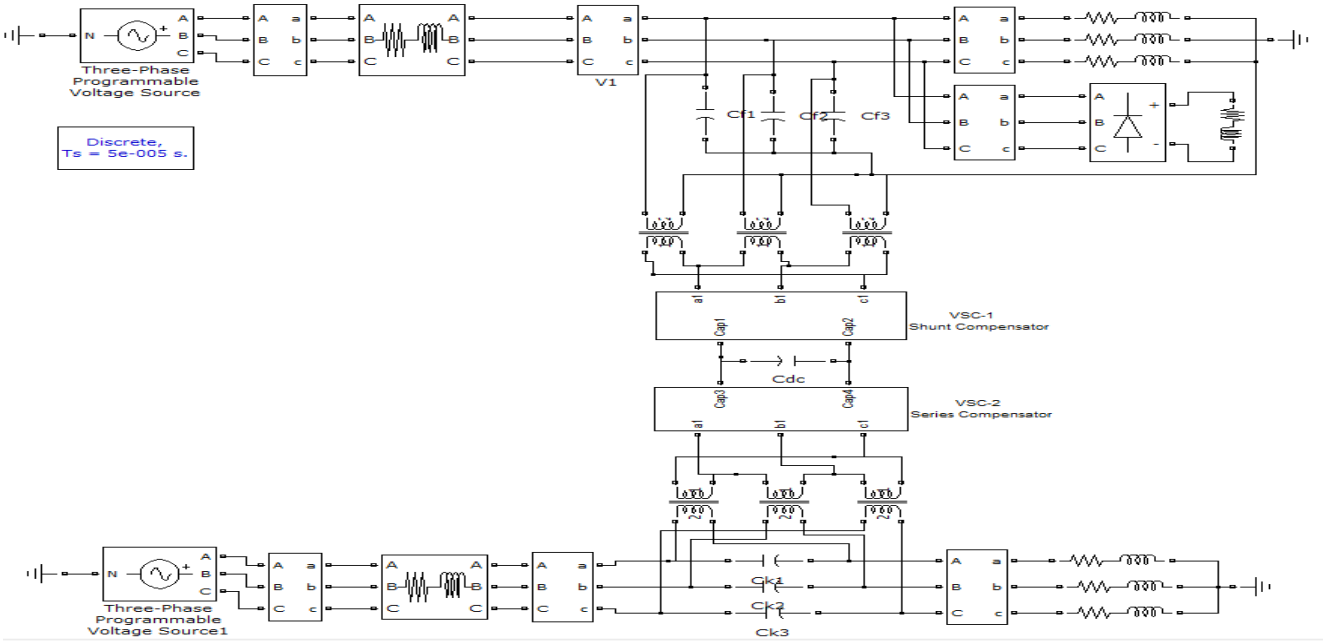

Fig.3. IUPQC Simulation model

The length of Feeder-1 is arbitrarily chosen to be twice that of Feeder-2. The voltage of bus B-1 and load L-1 currents, when no IUPQC is connected to the distribution system, due to the presence unbalanced (L-11) and non-linear load (L-12), the voltages are unbalanced and distorted. Also, the load L-11 causes an unbalance in the current, while load L-12 causes distortion in the current .We shall now demonstrate how these waveforms can be improved using the IUPQC with simulink model shown in fig.3.

V. SIMULATION RESULTS

a) Compensation of current harmonics at feeder-1

Simulation is carried out in this case study under distorted conditions of currents in feeder-1 (consist of unbalanced load and nonlinear load) and supply voltage of feeder 2 (balanced load) as shown in fig.4. The effectiveness of IUPQC's shunt compensator is evident from Fig.5 as the source current becomes sinusoidal and balanced. The Total Harmonic Distortion (THD) of Supply currents decreased from 6.7% to 0.2% and Unbalanced load Currents are decreased from 12.79% to 0.5% respectively.

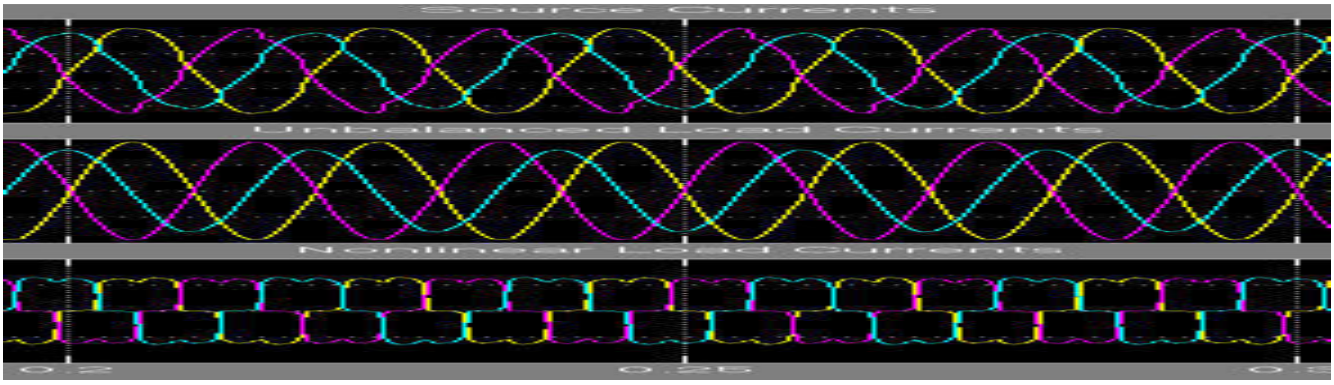

Fig.4. Supply, Unbalanced load and nonlinear load Currents in absence of IUPQC

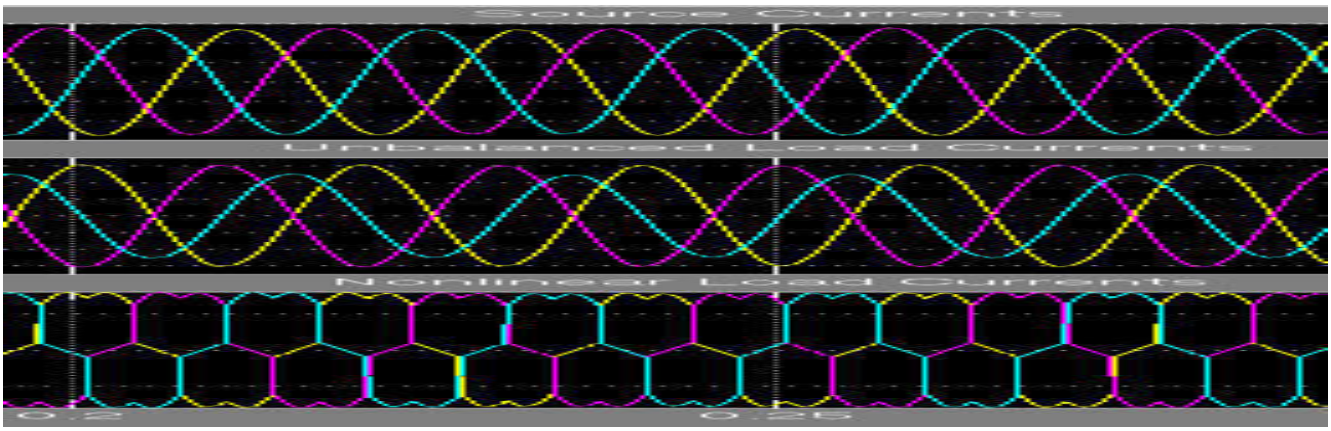

Fig.5. Supply, Unbalanced load and nonlinear load Currents in presence of IUPQC

b) Compensation of voltage harmonics at feeder-2

In this case study supply voltage feeder-2 is distorted by introducing 5th harmonic and 50% sag from 0 to 0.1 s. Fig.6. Shows that IUPQC's series compensator minimizes the voltage distortion and improves load voltage are nearly to sinusoidal.

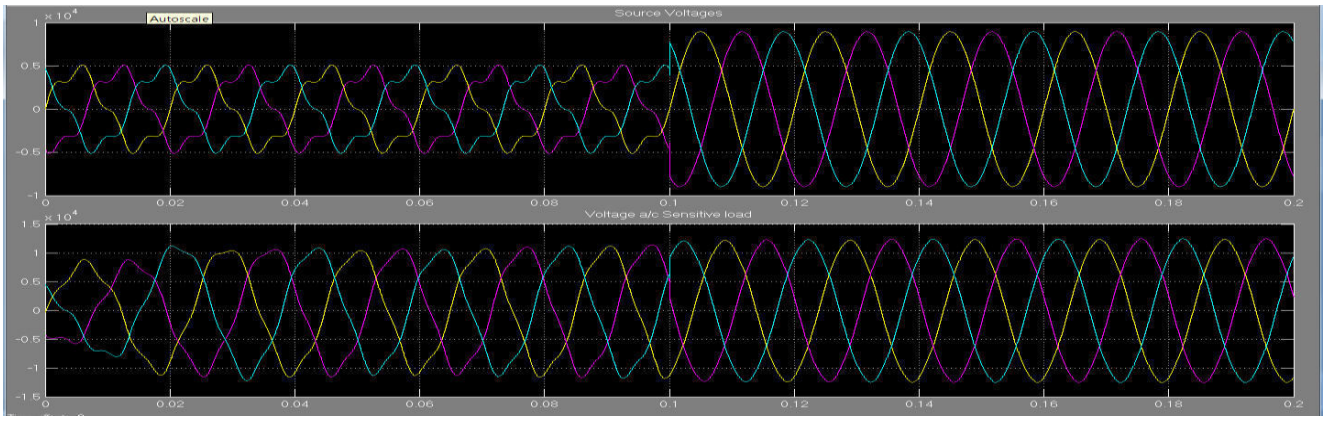

Fig.6. Supply and load voltages of Feeder-2

c) Compensation of Sag and Swell at feeder-2

In this case study supply voltage of feeder-2 is distorted by 20% sag from 0.1 s to 0.15 s and a 20% swell from 0.3 s to 0.35 s. In order to compensate source voltage sag and swell of feeder-2, the series compensator injects corresponding voltages in feeder-2 and minimizes the imperfections as shown in fig.7.

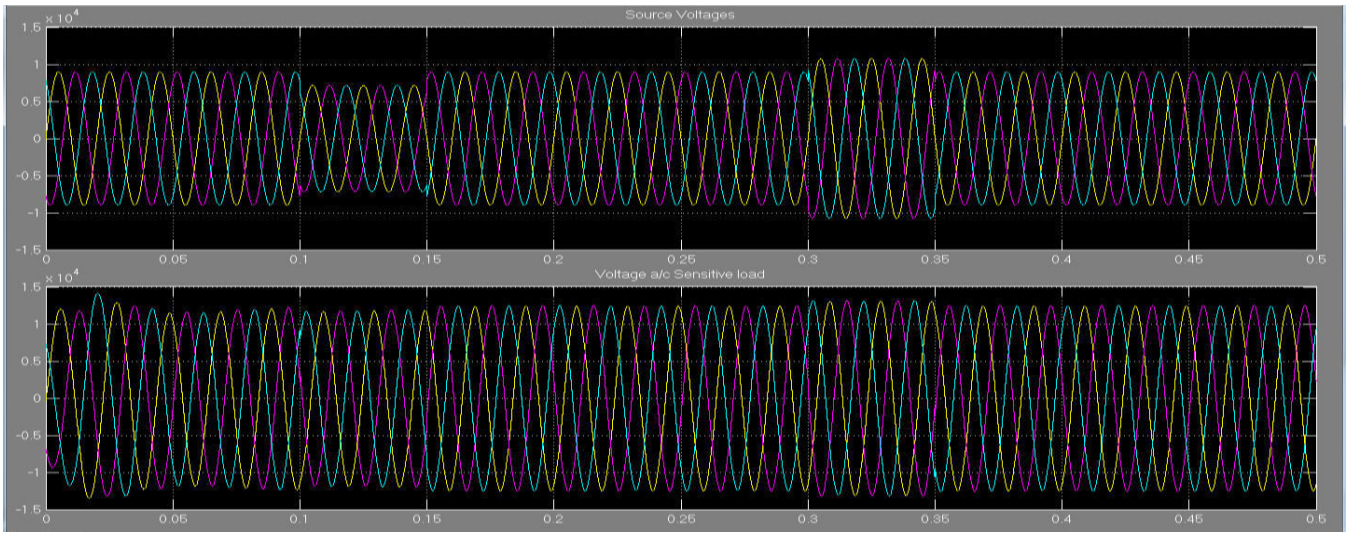

Fig.7. Supply and load voltages of Feeder-2

CONCLUSION

This paper describes the modified connection for unified power quality conditioner (UPQC) to improve the power quality of two feeders in a distribution system. From the simulation study the following conclusions are drawn,

- ✓ With shunt Compensator (VSC-1) at feeder-1 a supply waveform is found to be pure sinusoidal.
- ✓ In the feeder-2, with series compensator about 20% of sag and swell are compensated for balanced load.
- ✓ The performance of the IUPQC connected between feeder shows the improvement of power quality aspect like THD, sag and swell. Results are well within the IEEE standards.

Further work is in progress to study the various issues of power quality in related to IUPQC.

REFERENCES

[1] Ghosh and G. Ledwich, "Power Quality Enhancement Using Custom Power Devices". Norwell, MA: Kluwer, 2002.

[2] A. K. Jindal, A. Ghosh, and A. Joshi, "Interline unified power quality conditioner," IEEE Trans. Power Del., vol. 22, pp. 364–372, 2007.

[3] F. Z. Peng and J. S. Lai, "Generalized instantaneous reactive power theory for three-phase power systems," IEEE Trans. Instrum. Meas., vol. 45, no. 1, pp. 293–297, Feb. 1996.

[4] G. Ledwich and A. Ghosh, "A flexible DSTATCOM operating in voltage and current control mode," Proc. Inst. Elect. Eng., Gen., Transm. Distrib., vol. 149, no. 2, pp. 215–224, 2002.

[5] M. K. Mishra, A. Ghosh, and A. Joshi, "Operation of a DSTATCOM in voltage control mode," IEEE Trans. Power Del., vol. 18, no. 1, pp.258–264, Jan. 2003.

[6] Ghosh, A. K. Jindal, and A. Joshi, "A unified power quality conditioner for voltage regulation of critical load bus," in Proc. IEEE Power Eng. Soc. General Meeting, Denver, CO, Jun. 6–10, 2004.

[7] Ghosh and G. Ledwich, "A unified power quality conditioner (UPQC) for simultaneous voltage and current compensation," Elect Power Syst. Res., vol. 59, no. 1, pp. 55–63, 2001.

[8] N.H. Woodley, A.Sundaram, B. Coulter and D.Moris, "Dynamic voltage restorer demonstration project experience" in Proc. 12th Conf. Elect. Power Supply Ind., Pattaya, Thailand, 1998.

[9] F. Kamran and T. G. Habetler, "Combined deadbeat control of a series parallel converter combination used as a universal power filter," IEEE Trans. Power Electron., vol. 13, no. 1, pp. 160–168, Jan. 1998.

[10] R. C. Dugan, M. F. McGranaghan, S. Santoso, and H. W. Beaty, Electrical Power Systems Quality, 2nd ed. New York: McGraw-Hill, 2003, ch. 8.

[11] Kennedy Aganah, Sosthenes Karugaba and Olorunfemi Ojo, "Space Vector and Carrier-Based PWM Modulation Schemes for Maximum Utilization of Voltage Sources of a Nine-Switch Converter," IEEE Energy Conversion Congress and Exposition (ECCE), pp 2521 – 2528, 2012

Facial Expression Based Human Emotion Recognition with Live Computer Response

Dr. G. Shivakumar, Professor*& Head, Department of E&I Engg., Malnad College of Engineering, Hassan.*
Dr. P.A. Vijaya,*Professor , Department of E & C Engg., BNM Institute of Technology,Bengaluru.*
Dr. H.S. Mohana,*Dean (AA) & Professor, Department of E&I Engg., Malnad College of Engineering, Hassan.*

***Abstract*-Humans are more likely to consider computers to be human-like when those computers understand and display appropriate nonverbal communicative behaviour. Our work presents an approach to automatic visual recognition of expressive face suitable for use in a vision-based affective framework. After describing the feature extraction techniques, classification results from several subjects are presented. Firstly, individual classifiers are trained separately with face features for classification into Face Action Units (FAU). Secondly, the same procedure is applied for classification into labelled emotion categories. A combined Ekman-Frison and Cohn-Kanade face action units are measured to label the emotion class. The five emotion classes like happy, sad, neutral, angry and surprise are considered in our analysis. The Open CV Library functions which are mainly aimed at real time computer vision are used extensively in our work. Depending on the various emotions detected, system responds to it by playing the appropriate audio or video stream. The results obtained using Quasi Newton algorithm and quick propagation are compared and the performance is analyzed.**

***Index Terms*- Emotion, Face Action Units, Quick propagation, Quasi-Newton.**

I. INTRODUCTION

Computer Vision seeks to emulate human vision by analysing digital image inputs. For humans to detect an emotion will not be a difficult job to perform as they are linked with emotions themselves but for a computer detecting an emotion will be difficult job to perform. Computer vision is an area of artificial intelligence that focuses on making computers to emulate human vision, including learning, making inferences and performing cognitive actions based on visual inputs. Computer vision also plays a major role in Human Computer Intelligent Interaction (HCII) which provides natural ways for humans to use computer as aids. Our work presents an approach to automatic visual recognition of expressive face. The same procedure is applied for classification into labelled emotion categories. Recognizing human facial expression and emotion by computer is an interesting and challenging problem. Faces are rich in information about individual identity, and also about mood and mental state. The expression on faces is the most basic form of non-verbal communication. This paper presents an approach for recognizing emotions through facial expressions displayed in live video streams and video sequences. To detect and extract the face and face features like eyes, nose, mouth and eyebrows corresponding Haar classifiers are used. Though facial expressions obviously are not to equate with emotions, in the computer vision community, the term facial expression recognition often refers to the classification of facial features in one of the six so called basic emotions: happiness, sadness, fear, disgust, surprise and anger as introduced by Ekman[1] in 1971. This attempt of an interpretation is based on the assumption that the appearances of emotions are universal across individuals as well as human ethnics and cultures.

II. PROPOSED METHODOLOGY

Our task is to analyze expressive cues within HHI and HCI which mostly take place as dialogues in a sitting position. Hence, we focus on the expressiveness of the upper part of the body in our work. We assume that initially the person is in frontal view, the complete upper body, two hands and the face are visible and not occluding each other. We first extract and analyze face action units (FAUs). The general system framework for uni-modal that is facial expression based emotion recognition is depicted in Figure1. The steps involved in the complete implementation of the work are as follows.

- Face detection.
- Face feature extraction.
- Feature point selection.
- Emotion recognition.
- Feedback from computer.

Face detection is a process that aims to locate a human face in an image. The process is applied on stored image or images from a camera. Human face varies from one person to another. This variation in

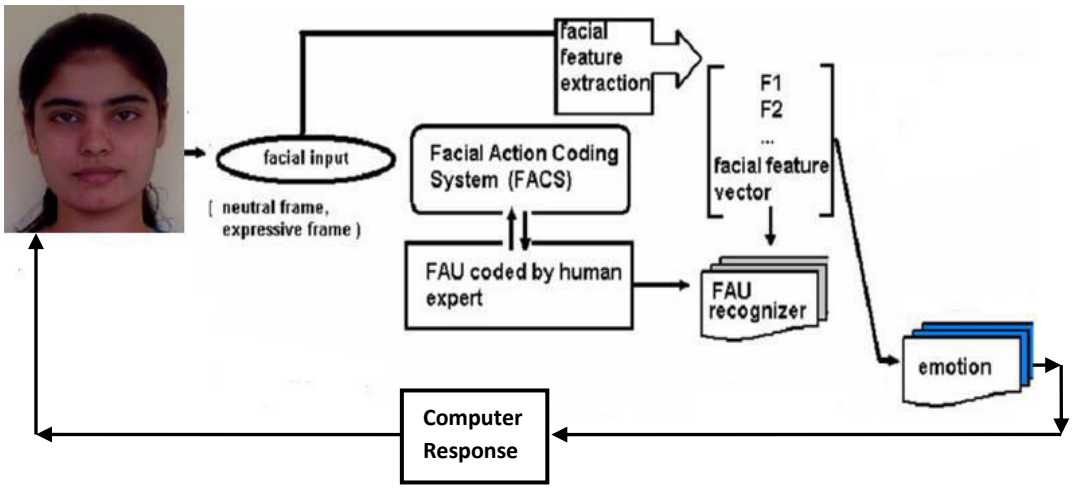

Fig.1 Schematic Diagram of the System.

faces could be due to race, gender, age, and other physical characteristics of an individual. The face is initially located using a face detection algorithm. We use the well known Viola-Jones procedure. Viola and Jones introduced a method to accurately and rapidly detect faces within an image. This technique can be adapted to accurately detect facial features. However, the area of the image being analyzed for a facial feature needs to be regionalized to the location with the highest probability of containing the feature. By regionalizing the detection area, false positives are eliminated and the speed of detection is increased due to the reduction of the area examined. The second step is using the isolated face to detect each feature. Since each the portion of the image used to detect a feature is much smaller than that of the whole image, detection of all three facial features takes less time on average than detecting the face itself.

Detecting human facial features, such as the mouth, eyes, and nose require that Haar classifier first be trained. The simple rectangular features of an image are calculated using an intermediate representation of an image, called the integral image. The integral image is an array containing the sums of the pixels intensity values located directly to the left of a pixel and directly above the pixel at location (x, y) inclusive. In order to train the classifiers, Haar feature algorithms must be implemented. These features, rather than using the intensity values of a pixel, use the change in contrast values between adjacent rectangular groups of pixels. The contrast variances between the pixel groups are used to determine relative light and dark areas. Two or three adjacent groups with a relative contrast variance form a Haar-like feature.

To train the classifiers, two set of images are needed. One set contains an image or scene that does not contain the object, in this case a facial feature, which is going to be detected. These set of images are referred to as the negative images. The other set of images, the positive images, contain one or more instances of the object. The location of the objects within the positive images is specified by: image name, the upper left pixel and the height, and width of the object. For training facial features 5,000 negative images with at least a mega-pixel resolution were used for training.

Although calculating a feature is extremely efficient and fast, calculating all 180,000 features contained within a 24×24 sub-image is impractical .Fortunately, only a tiny fraction of those features are needed to determine if a sub-image potentially contains the desired object. In order to eliminate as many sub-images as possible, only a few of the features that define an object are used when analyzing sub-images. The goal is to eliminate a substantial amount, around 50%, of the sub-images that do not contain the object. This process continues, increasing the number of features used to analyze the sub-image at each stage. The cascading of the classifiers allows only the sub-images with the highest probability to be analyzed for all Haar-features that distinguish an object. It also allows one to vary the accuracy of a classifier. One can increase both the false alarm rate and positive hit rate by decreasing the number of stages. The inverse of this is also true. Using a 2 GHz computer, a Haar classifier could detect human faces at a rate of at least five frames per second.

Fig. 2 Location of feature points on face

III. RESPONSE FROM COMPUTER

In our work, the feedback is a computer's response to the corresponding emotion recognized. It includes displaying the recognized emotion on the screen and as well as taking corresponding action by the computer. For emotion detected, computer plays the appropriate song automatically without any user intervention to make the user to work in a better mood to have a better outcome of it. Table 1 shows the list of detected emotions and the corresponding feedback from the computer. Steps involved in the said process are as follows:

1. Start.
2. Include "windows.h" header file in the main program.
3. Link winmm.dll file.
4. Test for emotion.
5. Play asynchronously, an appropriate music using play sound command.
   Syntax:PlaySound((LPCSTR) "filename", NULL, SND_FILENAME | SND_ASYNC;
6. Continue testing for further emotion.
7. Stop.

TABLE 1. FEEDBACK FROM THE COMPUTER

Detected Emotion	Neutral	Sad	Happy	Surprise	Angry
Audio Played	No music played	Carefree_Time	Driven_to_Success	No music played	Light_Tune, Rhythms_of_Peace

IV. RESULTS

Pairs of input and output vectors are chosen to train the feed forward neural network first. Once training is completed, the weights are set and the network can be used to find outputs for new inputs. Mapping depends on what pair of patterns or vectors are used as exemplaries to train the network, which determine the network weights. Once trained the network gives the image of a new vector under the mapping. Knowing what mapping is expected, the feed forward propagation network to be trained for implies the dimensions of the input space and the output space, so that we can determine the number of neurons to have in the input and output layers. Two algorithms Quasi-Newton and Quick propagation are used in our work. Face images of size 640X480 pixels in JPEG format are made use from a video stream. Ekman and Friesen studies suggested that anger, disgust, fear, happiness, sadness and surprise are the six basic prototypical face expressions recognized universally. However, six universal emotion categories are not sufficient to describe all facial expressions in detail. In order to capture the subtlety of human emotion, recognition of fine grained changes and atomic movements of the face is needed. Ekman and Friesen developed the Facial Action Coding System (FACS) for describing face expressions by face action units (FAUs). 44 face action units (FAUs) are defined. 30 FAUs are anatomically related to the contractions of specific face muscles: 12 are for upper face, and 18 are for lower face. AUs can be classified either individually or in combination.

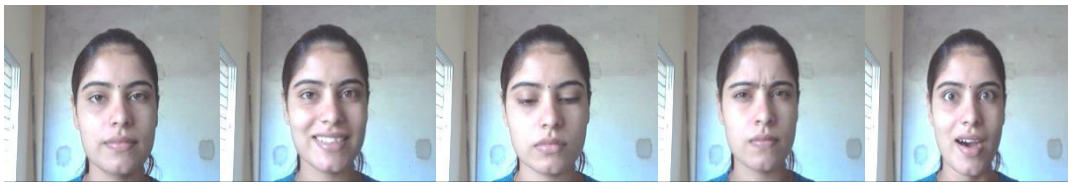

Neutral Happy Sad Angry Surprise

Fig. 3 Different Emotions of an Example Subject

TABLE 2 CONFUSION MATRIX

A. QUICK PROPAGATION

Target Output	Neutral	Angry	Surprise	Happy	Sad
Neutral	**84**	01	00	00	00
Angry	01	**69**	09	04	02
Surprise	00	05	**78**	00	02
Happy	00	04	06	**74**	01
Sad	05	18	01	02	**59**

B. QUASI-NEWTON

Target Output	Neutral	Angry	Surprise	Happy	Sad
Neutral	**82**	02	00	00	01
Angry	04	**76**	02	01	02
Surprise	00	07	**62**	02	14
Happy	00	05	05	**74**	01
Sad	06	20	02	03	**54**

V. CONCLUSIONS

The entire algorithm has been implemented using Dev C++ compiler. The header files of open CV has been used. The results obtained with our dataset is validated using the bentch mark Cohen-Kanade database. The following conclusions are drawn after successfully testing the network.

1. Best performance for quick propagation and Quasi-Newton network was respectively 90% and 85%.Accuracy can be further increased with a still larger dataset.
2. Comparison of the recognition performance with different types of features shows that the quick propagation network is more stable.
3. The increase of training set increases the rate of recognition of the network. Hence increasing number of samples in dataset, accuracy can be increased.
4. By including additional facial and physiological features, we can improve the accuracy of emotion recognition.
5. Using neural network for emotion classification in real time is tedious and time consuming, but it can be accurate. Whereas emotion classification without using neural network in real time is fast but it is relatively less accurate.
6. Recognition accuracy can be further improved with a high resolution camera and a sophisticated data acquisition system.

ACKNOWLEDGEMENTS

The authors express their sincere thanks to the Principal and management of Malnad College of Engineering, Hassan for providing all facilities required to carry out the research work.

REFERENCES

[1] Hess U. and Kleck R. E., "Differentiating emotion elicited and deliberate emotional facial expressions", P. Ekman & E. L. Rosenberg (Eds.), *What the face reveals: Basic and applied studies of spontaneous expression using thefacial action coding system (FACS)*2nd ed., pp. 271-286, Oxford University Press, 2005.

[2] HaticeGunes and Massimo Piccardi, *"Fusing Face and Body Gesture for Machine Recognition of Emotions"*, 2005 IEEE International Workshop on Robots and Human Interactive Communication, pp. 94-99.

[3] G. R. Bradski, *"Computer vision face tracking for use in a perceptual user interface"*, Intel Technology Journal, 2nd Quarter, 1998.

[4] Vinay Kumar, ArpitAgarwal&Kanika Mittal *"Introduction to Emotion Recognition for Digital Images"*, Jaypee University of Information Technology Waknaghat, Himachal Pradesh, inria-00561918, version 1 - 2 Feb 2011

[5] JagdishLalRaheja&Umesh Kumar *"Human facial expression detection from detected in captured image using back propagation neural network"*, Digital Systems Group, Central Electronics Engineering Research Institute (CEERI)/Council of Scientific & Industrial Research (CSIR), Rajasthan,2002.

[6] Phillip Ian Wilson & Dr. John Fernandez "*facial feature detection using haar classifiers*", Texas A&M University, JCSC 21, 4 (April 2006).

[7] Open Computer Vision Library Reference Manual. Intel Corporation, USA, 2001

[9] Ying-li Tian, Takeo Kanade, and Jeffrey F. Cohn, "Recognizing action units for facial expression analysis", IEEE transactions on pattern analysis and machine intelligence, vol. 23, no. 2, February 2001,pp 97-113.

[8] Christian Peter and Antje Herbon, "Emotion representation and physiology assignments in digital systems", *Interacting with Computers(Elsevier),* no.18, pp.139–170, 2006.

[9] Arun Ross and Anil Jain, "Information fusion in biometrics", *Pattern Recognition Letters (Elsevier),* no.24, pp. 2115–2125, 2003.

[10] John G. Taylor and Nickolaos F. Fragopanagos, "The interaction of attention and emotion", *Neural Networks(Elsevier),* no.18 pp.353–369, 2005.

[11] G. Shivakumar and P. A. Vijaya, "Face Recognition System Using Back Propagation Artificial Neural Network",*International Journal of Computer Science and Information Technology*, Volume 1, Issue 1,pp.68-77, 2009.

[12] P. A. Vijaya and G. Shivakumar, "Galvanic Skin Response: A Physiological Sensor System for Affective Computing", *IEEE International conference on Machine Learning and Computing (ICMLC)*, Singapore, pp. 01-05., Feb. 2011.

A MATLAB based Face Recognition System using Image Processing and Neural Networks

NamrathaGanesh , Annapoorna S N, Mrs. Rubeena Muheeb
B.E student Dept. of TelecommunicationEngineering, B.E student Dept. of TelecommunicationEngineering, Asst. Prof, Dept. of Telecommunication GSSSIETW, Mysore, India
rubeena.muheeb@gmail.com, namrathaganesh166@gamil.com, annapoornasuma@gmailcom

Abstract— ***Face recognition (FR) is a challenging issue due to variations in pose, illumination, and expression. Automatic recognition of people is a challenging problem which has received much attention during recent years due to its many applications in different fields. In modern times, face recognition has become one of the key aspects of computer vision. Face recognition is one of those challenging problems and up to date, there is no technique that provides a robust solution to all situations. In this paper some of the most common techniques available including applications of neural network in facial recognition are Studied and compared with respect to their performance.***

Keywords*: Face Recognition, PCA, MPCA, discrete cosine transform, self-organizing map, Neural Network.*

INTRODUCTION

Designing a system for automatic image content recognition is a non-trivial task that has been studied for a variety of applications. Computer recognition of specific objects in digital images has been put to use in manufacturing industries, intelligence and surveillance, and image database cataloging to name a few. [1]

Face recognition has become a very active area of research in recent years mainly due to increasing security demands and its potential commercial and law enforcement applications.

Although a trivial task for the human brain, face recognition has proved to be extremely difficult to imitate artificially, since although commonalities do exist between faces, they vary considerably in terms of age, skin, color and gender. The problem is further complicated by differing image qualities, facial expressions, facial furniture, background, and illumination conditions [3]. Since skin color in humans varies by individual, research has revealed that intensity rather than chrominance is the main distinguishing characteristic.

Face detection and recognition has many real world applications, like human/ computer interface, surveillance, authentication and video indexing.

We do face recognition almost on a daily basis. Most of the time we look at a face and are able to recognize it instantaneously if we are already familiar with the face. This natural ability if possible imitated by machines can prove to be invaluable and may provide for very important in real life applications such as various access controls, national and international security and defense etc. Presently available face detection methods mainly rely on two approaches. The first one is local face recognition system which uses facial features of a face e.g. nose, mouth, eyes etc. to associate the face with a person. The second approach or global face recognition system use the whole face to identify a person.

The recent development of artificial neural network and its possible applications in face recognition systems have attracted many researchers into this field. The intricacy of a face features originate from continuous changes in the facial features that take place over time. Regardless of these changes we are able to recognize a person very easily. Thus the idea of imitating this skill inherent in human beings by machines can be very rewarding.

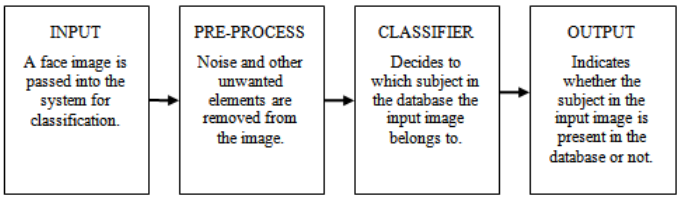

Fig.1. Generic representation of a face recognition system

Considering all the above mentioned points and their implications we would like to gain some experience with some of the most commonly available face recognition algorithms and also compare and contrast the use of neural network in this field.
Some of the common methods described by the researchers of the respective fields are:

Principal Component Analysis (PCA):

In high-dimensional data, this method is designed to model linear variation. Its goal is to find a set of mutually orthogonal basis functions that capture the directions of maximum variance in the data and for which the coefficients are pair wise decorrelated [3]. For linearly embedded manifolds, PCA is guaranteed to discover the dimensionality of the manifold and produces a compact representation. The Eigen face algorithm uses the Principal Component Analysis

(PCA) for dimensionality reduction to find the vectors which best account for the distribution of face images within the entire image space [14]. These vectors define the subspace of face images and the subspace is called face space. All faces in the training set are projected onto the face space to find a set of weights that describes the contribution of each vector in the face space. To identify a test image, it requires the projection of the test image onto the face space to obtain the corresponding set of weights. By comparing the weights of the test image with the set of weights of the faces in the training set, the face in the test image can be identified.

Multilinear principal components analysis (MPCA):

One extension of PCA is that of applying PCA to tensors or multilinear arrays which results in a method known as multilinear principal components analysis (MPCA) [5]. Since a face image is most naturally a multilinear array, meaning that there are two dimensions describing the location of each pixel in a face image, the idea is to determine a multilinear projection for the image, instead of forming a one- dimensional (1D) vector from the face image and finding a linear projection for the vector. It is thought that the multilinear projection will better capture the correlation between neighborhood pixels that is otherwise lost in forming a 1D vector from the image [2].

Independent Component Analysis (ICA):

The ICA separates the high-order moments of the input in addition to the second-order moments utilized in PCA. Both the architectures lead to a similar performance. Specifically, we maximize the variance between pixels to separate linear dependencies between pixels. ICA is a generalization of PCA in that it tries to identify high-order statistical relationships between pixels to form a better set of basis vectors. In [8], where the pixels are treated as random variables and the face images as outcomes.

In a similar fashion to PCA and LDA, once the new basis vectors are found, the training and test data are projected into the subspace and a method such as NN is used for classification. The code for ICA was provided by the authors for use in face recognition research [8].

2D-DCT (Discrete Cosine Transform):

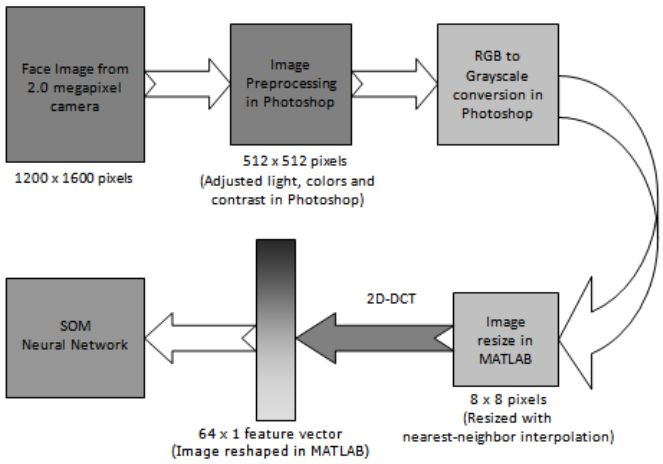

Fig (a): Face image fabrication process

Nearest-neighbor interpolation is performed using the MATLAB Image Processing Toolbox to resize preprocessed images from size 512 × 512 pixels to image blocks of size 8×8 pixels as shown in fig (a) The proposed design technique calculates the 2D-DCT of the image blocks of size 8 × 8 pixels using '8' out of the 64 DCT coefficients for masking. The other 56 remaining coefficients are discarded (set to zero). The image is then reconstructed by computing the 2D-IDCT of each block using the DCT transform matrix computation method. Finally, the output is a set of arrays. Each array is of size 8 × 8 pixels and represents a single image. These steps are represented in Fig (b) for a sample image. Empirically, the upper left corner of each 2D-DCT matrix contains the most important values, because they correspond to low-frequency components within the processed image block [2].

Overview of 2D-DCT:

The discrete cosine transform is an algorithm widely used in different applications. The most popular use of the DCT is for data compression, as it forms the basis for the international standard loss image compression algorithm known as JPEG [5]. The DCT has the property that, for a typical image, most of the visually significant information about the image is concentrated in just a few coefficients. Extracted DCT] coefficients can be used as a type of signature that is useful for recognition tasks, such as face recognition [6, 7]. Face images have high correlation and redundant information which causes computational burden in terms of processing speed and memory utilization. The DCT transforms images from the spatial domain to the frequency domain. Since lower frequencies are more visually significant in an image than higher frequencies, the DCT discards high-frequency coefficients and quantizes the remaining coefficients. This reduces data volume without sacrificing too much image quality [3]. The 2D-DCT of an M × N matrix A is defined as follows:

$$B_{pq} = \alpha_p \alpha_q \sum_{m=0}^{M-1} \sum_{n=0}^{N-1} A_{mn} \cos\left[\frac{(\pi(2m+1)p)}{2M}\right] \cos\left[\frac{(\pi(2n+1)p)}{2N}\right], 0 \le \mathrm{p} \le \mathrm{M}-1 \quad 0 \le \mathrm{q} \le \mathrm{N}-1 \tag{2.1}$$

The values B_{pq} are the DCT coefficients. The DCT is an invertible transform, and the 2D-IDCT (2D Inverse-DCT) is defined as follows:

$$A_{mn} = \sum_{p=0}^{M-1} \sum_{q=0}^{N-1} \alpha_p \alpha_q B_{pq} \cos\left[\frac{(\pi(2m+1)p)}{2M}\right] \cos\left[\frac{(\pi(2n+1)p)}{2N}\right], 0 \le \mathrm{m} \le \mathrm{M}-1 \quad 0 \le \mathrm{n} \le \mathrm{N}-1 \tag{2.2}$$

The values α_p and α_q in (2.1) and (2.2) are given by:

$$\alpha_p = \begin{cases} \sqrt{\frac{1}{M}}, & p = 0 \\ \sqrt{\frac{2}{M}}, & 1 \le \mathrm{p} \le \mathrm{M}-1 \end{cases}$$

$$\alpha_q = \begin{cases} \sqrt{\frac{1}{N}}, & q = 0 \\ \sqrt{\frac{2}{N}}, & 1 \le \mathrm{q} \le \mathrm{N}-1 \end{cases} \tag{2.3}$$

The proposed technique uses the DCT transform matrix in the MATLAB Image Processing Toolbox. This technique is efficient for small square inputs such as image blocks of 8 × 8 pixels. The M × M transform matrix T is given by:

$$T_{pq} = \begin{cases} \sqrt{\frac{1}{M}}, & p = 0, 0 \le \mathrm{q} \le \mathrm{M}-1 \\ \sqrt{\frac{2}{M}} \cos\left[\frac{(\pi(2q+1)p)}{2M}\right], & 1 \le \mathrm{p} \le \mathrm{M}-1 \end{cases} \tag{2.4}$$

Overview of the paper:

For the commonly available algorithms it is important to gain some theoretical knowledge before their implementation and their pros and cons. Based on the continuous reading of related scientific papers, some of the implementation might not be pragmatic in time permitted. Because there are a lot of issues associated with this. For example, to get an understandable working simulation the tools needed may not be available freely i. e. the tools might be offered by some vendors. In that case their implementations already done by researchers will be needed to take into account. Even in that case I'll try to get a through understanding of how it can be implemented in future, what are the things that are assumed or variables fixed for the implementation etc.

There are mainly two approaches face recognition algorithms. One way is general algorithmic (PCA, LDA, ICA etc.) and another one is AI centric (e.g. Supervised and unsupervised learning methods such as SVM, Neural Networks etc.). One way to gain a rough understanding of these two approaches would be to select any two algorithms of these and then run algorithms on some sample data. There are many databases freely available online for these purpose. After going through some of the available methods and tools it became apparent that some of these would be too time consuming to actually go through them in depth. MATLAB seemed to be a good choice in this respect. This is a fourth generation programming language and a numerical computing environment widely used by educational and research organization throughout the whole world.

Though is a proprietary software released by Math Works, it has a fairly strong user groups all around the world. The algorithms generally proposed to use for face recognition are many times implemented by experienced researchers and users. Sometimes they share the actual implementation with other users. In order to reduce the implementation time, two of these were chosen to be implemented in this paper. As the implementation tool, the latest release of MATLAB R2011b is chosen. To implement the experiments, there are also two toolboxes that are necessary along with the main environment of Mat lab: image processing toolbox and neural network toolbox. The first toolbox is needed in order to implement the first part i.e. face recognition based on Eigen faces and neural network toolbox is needed to test the neural network based implementation of face recognition technique.

Challenges in Face Recognition:

Pose, Illumination, Facial expression, Image condition, Face size. Classification of Face Recognition Face recognition scenarios can be classified into two types Face verification (or authentication) and Face identification (or recognition).

1) Face verification: It is a one-to-one match that compares a query face image against a template face image whose identity is being claimed. To evaluate the verification performance, the verification rate (the rate, at which legitimate users are granted access) vs. false accepts rate (the rate at which imposters are granted access) is plotted, called ROC curve. A good verification system should balance these two rates based on operational needs.

2) Face identification: It is a one-to-many matching process that compares a query face image against all the template images in a face database to determine the identity of the query face. The identification of the test image is done by locating the image in the database that has the highest similarity with the test image [4]. The identification process is a "closed" test, which means the sensor takes an observation of an individual that is known to be in the database. The test subject's (normalized) features.

Scope in India:

1) In order to prevent the frauds of ATM in India, it is recommended to prepare the database of all ATM customers with the banks in India & deployment of high resolution camera and face recognition software at all ATMs. So, whenever user will enter in ATM his photograph will be taken to permit the access after it is being matched with stored photo from the database.
2) Duplicate voter are being reported in India. To prevent this, a database of all voters, of course, of all constituencies, is recommended to be prepared. Then at the time of voting the resolution camera and face recognition equipped of voting site will accept a subject face 100% and generates the recognition for voting if match is found.
3) Passport and visa verification can also be done using face recognition technology as explained above.
4) Driving license verification can also be exercised face recognition technology as mentioned earlier.
5) To identify and verify terrorists at airports, railway stations and malls the face recognition technology will be the best choice in India as compared with other biometric technologies since other technologies cannot be helpful in crowdie places.
6) In defense ministry and all other important places the face technology can be deployed for better security.
7) This technology can also be used effectively in various important examinations such as SSC, HSC, Medical, Engineering, MCA, MBA, B- Pharmacy, Nursing courses etc. The examinee can be identified and verified using Face Recognition Technique.
8) In all government and private offices this system. Can be deployed for identification, verification and attendance.
9) It can also be deployed in police station to identify and verify the criminals.
10) It can also be deployed vaults and lockers in banks for access control verification and identification of authentic users.
11) Present bar code system could be completely replaced with the face recognition technology as it is a better choice for access & security since the barcode could be stolen by anybody else.

Conclusion and future Work:

Face recognition is a both challenging and important recognition technique. Among all the biometric techniques, face recognition approach possesses one great advantage, which is its user-friendliness (or non-intrusiveness). In this paper, we have given an introductory survey for the face recognition technology. We have covered issues such as the generic framework for face recognition, factors that may affect the performance of the recognizer, and several state-of-the-art face recognition algorithms. We hope this paper can provide the readers a better understanding about face recognition, and we encourage the readers who are interested in this topic to go to the references for more detailed study.

Face recognition technologies have been associated generally with very costly top secure applications. Today the core technologies have evolved and the cost of equipment is going down dramatically due to the integration and the increasing processing power. Certain applications of face recognition technology are now cost effective, reliable and highly accurate. As a result there are no technological or financial barriers for stepping from the pilot project to widespread deployment. Though there are some weaknesses of facial recognition system, there is a tremendous scope in India. This system can be effectively used in ATM"s, identifying duplicate voters, passport and visa verification, driving license verification, in defense, competitive and other exams, in governments and private sectors.

Government and NGOs should concentrate and promote applications of facial recognition system in India in various fields by giving economical support and appreciation.

There are a number of directions for future work. The main limitation of the current system is that it only detects upright faces looking at the camera. Separate versions of the system could be trained for each head orientation, and the results could be combined using arbitration methods similar to those presented here. Preliminary work in this area indicates that detecting pro files views of faces is more difficult than detecting frontal views, because they have fewer stable features and because the input window will contain more background pixels.

OUTPUT RESULTS:

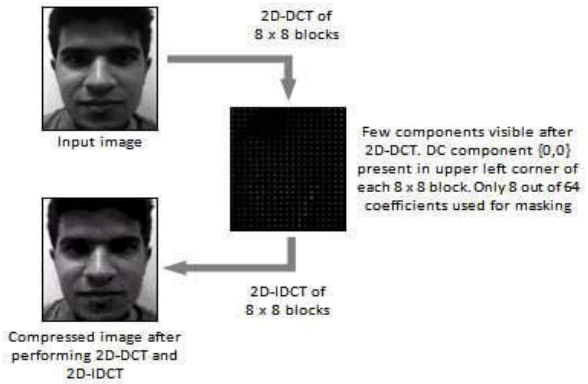

Fig (b): 2D-DCT computation of face image

Acknowledgement

The work described in this paper is supported by President, Hon. Secretary and CEO Geetha Shishu Shikshana Sangha (R),Mysuru. Authors would like to thank Principal, AAO GSSS Institute of Engineering and Technology for women, Mysuru for their guidance and constant support.

REFERENCES

1. Abdallah, M. Abou El-Nasr, and A. Lynn Abbott, "A New Face Detection Technique using 2D DCT and Self Organizing Feature Map" in Proc. of World Academy of Science, Engineering and Technology, Vol. 21, May 2007, pp. 15-19.
2. J. Nagi, "Design of an Efficient High-speed Face Recognition System", Department of Electrical and Electronics Engineering, College of Engineering, Universiti Tenaga Nasional, March 2007.
3. E. Ifeachor and B. Jervis, Digital Signal Processing: A Practical Approach. Prentice Hall, 2001.
4. L. Ma, Y. Xiao, and K. Khorasani, "A new facial expression recognition technique using 2D DCT and k-means algorithm", in Proc International Conference on Image Processing, Oct. 2004, pp. 1269-1272.
5. L. Ma and K. Khorasani, "Facial expression recognition using constructive feed forward neural networks", IEEE Transactions on Systems, Man and Cybernetics, Part B, Vol. 34, No. 3, June 2004, pp.1588-1595.
6. E. Hjelmås, and B. K. Low, "Face detection: A survey", Computer Vision and Image Understanding, Vol. 83, No. 3, Sept. 2001, pp. 236-274.
7. Harguess, J., Aggarwal, J.K.; A case for the average-half-face in 2D and 3D for face recognition, IEEE Computer Society Conference on Computer Vision and Pattern Recognition Workshops, pp. 7-12, 2009
8. Xiaofei He; Shuicheng Yan; Yuxiao Hu; Niyogi, P.; Hong-Jiang Zhang; , IEEE Transactions on Pattern Analysis and Machine Intelligence, pp. 328 – 340, 2005
9. M. Turk and A. Pentland. Eigenfaces for recognition, Journal of Cognitive Neuroscience, 3(1), pp. 71–86, 1991
10. H. Lu, K. N. Plataniotis, and A. N. Venetsanopoulos. Mpca: Multilinear principal component analysis of tensor objects. IEEE Trans. on Neural Networks, 19(1):18–39, 2008.
11. Martinez, A.M. ; Kak, A.C. ; IEEE Transactions on Pattern Analysis and Machine Intelligence, Volume : 23 ,Issue:2, pp. 228 – 233, Feb 2001.
12. M. S. Bartlett, J. R. Movellan, and T. J. Sejnowski; Face recognition by independent component analysis., IEEE Transactions on Neural Networks, 13:1450–1464, 2002
13. Fan X. ; Verma, B. ; A comparative experimental analysis of separate and combined facial features for GA-ANN based technique, Sixth International Conference on Computational Intelligence and Multimedia Applications, 2005.
14. Shaoning Pang; Daijin Kim; Sung Yang Bang; Face membership authentication using SVM classification tree generated by membership-based LLE data partition, IEEE Transactions on Neural Networks, Volume: 16 , Issue: 2 ,pp. 436 – 446, 2005
15. Ke Lu, Xiaofei He, Jidong Zhao; Semi-supervised Support Vector Learning for Face Recognition, Lecture Notes in Computer Science, pp. 104-109, 2006
16. Jamil, N. ; Iqbal, S. ; Iqbal, N. ; Face recognition using neural networks, Technology for the 21st Century, pp. 277 – 281, IEEE INMIC, 2001
17. P. Latha, Dr. L. Ganesan & Dr. S. Annadurai; Face Recognition using Neural Networks, Signal Processing: An International Journal (SPIJ) Volume (3): Issue (5). 153, 2009
18. http://www.mathworks.com/matlabcentral/fileexchange/4408
19. AT&T Laboratories Cambridge. The ORL face database, Olivetti Research Laboratory available at http://www.uk.research.att.com/pub/data/att_faces.zip
20. Encyclopaedic, ©1993-2002 Microsoft Corporation, Collection Microsoft® Encarta® 2003.

ENERGY MANAGEMENT THROUGH SMART HOME

MANJUNATHA H M
Department of Electrical & Electronics Engineering,
RIT, Hassan, Karnataka
manjunath.hm1986@gmail.com

PURUSHOTHAMA G K
Department of Electrical & Electronics Engineering,
MCE, Hassan, Karnataka
gkuttama@gmail.com

Abstract: Present electricity network will increasingly rely upon a set of intelligent communication and control technologies like home area network. Within the smart grid network, Home Area Network (HAN) help develop the demand response and demand side management. Distribution generation opportunities such as Rooftop PV systems and Diesel generation are also closely linked to the development of HAN and Demand Response. Home Energy Management (HEM) describes a class of technologies including sensors, smart thermostats, and feedback devices seeking to manage residential energy consumption profiles to reduce peak electric demand and consumers' electric bills.

Key point: ***Smart grid, HAN and HEM***

I. INTRODUCTION

Power system is a mechanism of generation, transmission, distribution and at the end utilization of energy by end users. With the continued increase in the energy consumption, the electrical power systems all over the world are becoming more and more complex and expensive. Hence there is a need of Total Quality Management (TQM) strategy in all sector of power system to improve their operation.TQM approach should include any energy management component to improve the efficiency of the power system and reducing the energy use their by cost. Energy management system (EMS) concentration towards energy conservation, by adopting different activities to get largest saving in terms of energy their by cost. EMS improves the national economic condition, energy production, national competitiveness and minimizes the reliance on imported fuel. EMS aims to provide mutual benefits to consumer and utility[1].

This paper focus on HEM system because of its potential to conserve resources. Residential energy consumption currently accounts for approximately 22% of the nation's total energy demand. HEM adapts the energy management program to achieve efficient home automation for conserve energy. Such a home is termed as Smart home and is shown in Figure1.

Smart home is the integration of technology and services through home networking for a better quality of living. Smart homes have the potential to improve home comfort, convenience, security and energy management. HEM systems enable Demand Side Management (DSM) and Demand Response (DR) programs. DSM is more related to planning, implementing and evaluating techniques and policies which are designed to modify the electricity consumption of consumers. Whereas DR programs are used to manage and alter energy consumption based on supply. Continuous efforts from research community are underway to design new protocols, standards and optimization methods to coordinate Distribution Energy Generation (DER) and residential appliances efficiently in order to reduce peak demand and energy consumption charges of consumers.

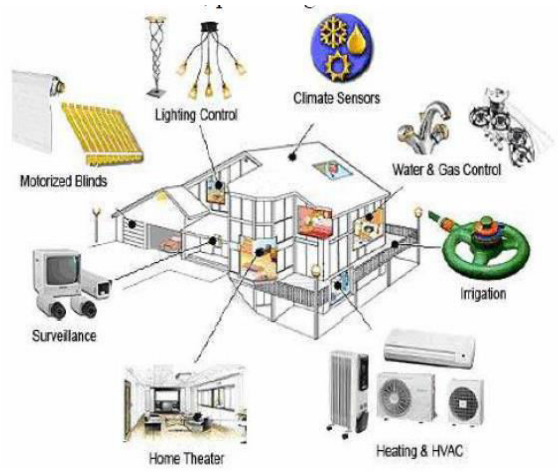

Fig.1: A Smart home Integration services.

In this paper, a HEM technique based on a set of sensors is presented that can be adapted according to habitant's requirements. In the remaining part of this article, Section II describes technologies used in a smart home. Section III presents how smart home can reduce the energy consumption via home energy management. In section IV, an experimental set up and results are reported.

II. SMART HOME TECHNOLOGY

At consumption level, HEM employs HANs for inter networking of smart loads, energy management units and smart meters. A HAN is a dedicated network connecting devices in the home such as displays, load control devices and ultimately "smart appliances" seamlessly into the overall smart metering system. It also contains turnkey reference designs of systems to monitor and control these networks. Most of our high energy use today comes from heating/cooling, cooking, lighting, washing and drying. These home appliances are beginning to become smart with connectivity features that allow them to be automated in order to reap benefits that smart metering and variable tariffs bring[2]. Figure 2. shows how smart appliances are interconnected within a HAN.

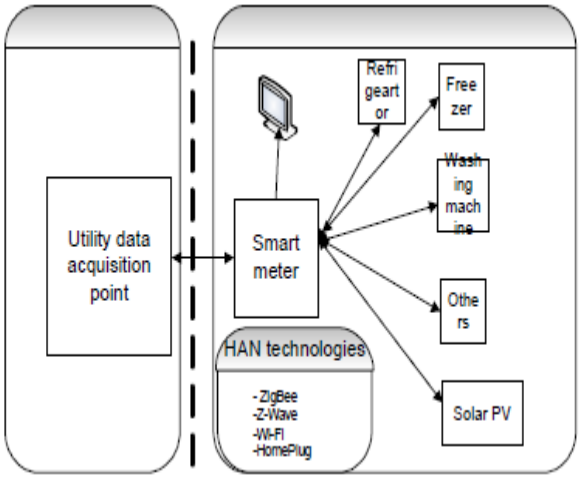

Fig.2: Home area network

The key challenge in implementing a HAN solution is to connect the entire house/building network to the "external world" for remote monitoring and control, and simultaneously to connect objects inside houses/ buildings to offer smart interoperability features. A key challenge from the consumer's perspective is remote controlling and monitoring for surveillance companies, while the challenge from the service provider's perspective is remote metering for utility companies and security monitoring for surveillance companies.

One such example is connecting PIR sensors to heating, ventilation and air-conditioning (HVAC) and lighting systems to turn off heating when windows are open, or turn lights off when no presence is detected. Summing up, the challenge in implementing a HAN solution is to interconnect different technologies to offer smart services for: Comfort, Automation, Security ,Energy management and Health.

Various communication technologies both wired and wireless have been proposed for bidirectional communication in smart home. Many home automations are connected through wiring system such as new wire (twisted pair, optical fiber), Power line, Bus line, etc. An example of outstanding technology is X10, which is open standard for home automation. X10 transmits binary data using the Amplitude Modulation (AM) technique, and X10 controllers send signals over existing AC wiring to receiver modules.

The wireless system must have two main elements: sender and receiver. Many new appliances use wireless technology to communicate with other devices. The example of wireless communication system are microwaves, Infrared (IR), radio frequency (RF), Wi-Fi, Bluetooth, IEEE 802.11, and so on. Furthermore, some of smart home network standard can work using both wiring system and wireless system. An example of wireless communication system for smart home is Z-wave, which is a reliable and affordable wireless home automation solution[3].

In this paper, we evaluate different technologies used in HAN technologies like– ZigBee, Wi-Fi, Ethernet, Z-Wave, HomePlug, Wireless M-Bus etc.

ZigBee[4]:

- Wireless mesh proprietary networking solution (from Layer 3 to the application layer) built on the IEEE 802.15.4 media standard.
- In a mesh network, nodes are interconnected with other nodes so that at least two pathways connect each node. Connections between nodes are dynamically updated and optimized. Mesh networks are decentralized in nature; each node is self-routing and able to connect to other nodes as needed. The characteristics of mesh topology and ad-hoc routing provide greater stability in changing conditions or failure at single nodes.
- The low power network must exclusively be made of devices interconnected by IEEE 802.15.4 links. The raw, over-the-air data rates are:
  - 250 kbps per channel in the unlicensed 2.4 GHz band (Worldwide)
  - 40 kbps per channel in the unlicensed 915 MHz band (Australia and US)
  - 20 kbps in the unlicensed 868 MHz band (Europe)
- Distance covered is 10-100 metres point to point, typically 30 metres indoors; unlimited with mesh networking.

- Low cost allows wide deployment in wireless control and monitoring applications;
- Low power usage allows longer life with smaller batteries (up to 10 years) and the mesh networking provides high reliability and broader range.
- Provides secure connections between devices through 128-bit AES encryption.

Z-wave[5]:

- Z-Wave is a proprietary wireless communications standard designed specifically to remote control applications in residential and light commercial environments.
- Due to an impressive eco-system community Z-Wave is widely spread although it is not open and is available only to Zensys customers. Zensys is now a division of Sigma Designs.
- The Z-Wave Radio uses the unlicensed 900 MHz ISM (Industry, Scientific and Medical) band. 900MHz is unlicensed radio frequency band used in Australia, Israel and North America, while 2.4Ghz is unlicensed band used worldwide including India. Generally, 900MHz solutions provide significantly longer range and lower power than those operating in 2.4GHz.
- Distance covered is approx 30 metres point to point open-air, reduced indoor; unlimited with mesh networking and bandwidth 40kbps.
- Optimized for low-overhead commands such as on-off (as in a light switch or an appliance) and raise lower (as in a thermostat or volume control), with the ability to include device metadata in the communications.
- The freedom from household interference (WiFi, Microwave, Cordless Phone) allows for a standardized low bandwidth control medium that can be reliable alongside common wireless devices.

HomePlug[6]:

- HomePlug is a power line communication technology. It uses the existing home electricity wiring to communicate.
- To create a network, a user connects two or more adapters to the power outlets in the home. The user can then connect devices to the network via the adapter.
- Alternatively, devices may already have HomePlug adapters built in, and therefore it is just a manner of connecting the devices to the home power outlet to enable network connectivity.
- Several HomePlug specifications exist. HomePlug 1.0 supports speeds up 14 Mbps while HomePlug AV supports speeds up to 200 Mbps. A standard also exists currently in draft: IEEE P1901.
- Security with HomePlug AV is provided via 128-bit AES Encryption.
- HomePlug Command & Control (HPCC) is an alternative to the AV version and is designed for lower speed, very low-cost applications. Supports a number of protocols including IP.
- Setup and configuration may take a level of skill.

Ethernet:

- Ethernet is a very common communication technology standard primarily used within the LAN but can also be used on the WAN.
- Devices can connect to the Ethernet network in a variety of ways including copper “twisted-pair” cabling or fibre optics.
- Predominantly, copper cabling is used in Home LAN’s. With the copper cabling connecting to a hub or switch in a star topology. This hub or switch may also serve as a gateway providing DSL/Cable/3G access to an ISP.
- A variety of speeds can be achieved including: 10 Mbps, 100 Mbps, 1000 Mbps and 10000 Mbps. 100 Mbps is the most common speed found in the Home LAN although 1000 Mbps is making an appearance as high bandwidth media such as Video and Network Attached Storage (NAS) becomes more prevalent. The NBN proposes 100 Mbps.
- The majority of network attached devices today come with Ethernet interfaces, including personal computer, laptops, servers, printers, AV equipment, media console, game consoles. Being standards based setup and configuration is very easy.
- Ethernet may not be appropriate for connecting all devices in the HAN (especially appliances) due to the high cost and power requirements plus the need for separate cabling back to a central point.

Wi-Fi[7]:

- WiFi is a popular wireless technology used in home networks, mobile phones, video games and other electronic devices.
- Based on mature IEEE 802.11 standards: 802.11n (~ 300 Mbps); 802.11b (11 Mbps); 802.11g (54 Mbps); 802.11a (54 Mbps)
- Support is wide spread with nearly every modern personal computer, laptop, game console and peripheral device provides a means to wirelessly access the network via WiFi.
- WiFi is generally upper layer protocol agnostic with IP being the most predominate protocol.
- Setup and configuration may take some level of skill.

IP:

- IP is a protocol used for communicating data within a packet switched internetwork. It is responsible for delivering data from source to destination based on a IP address.
- IP is the foundation on which the Internet is built and communication is achieved.
- IP is a single layer within a multi-layer suite known as the TCP/IP stack. Due to this abstraction, IP can be used across a number of different heterogeneous network technologies, including: Ethernet, WiFi, HomePlug without translation.
- The design of IP infuses the view that the underlying network is inherently unreliable and therefore is a "best effort" delivery mechanism. It is the responsibility of the upper layer protocols to provide reliability.
- Due to the ease of interoperability, ubiquitous nature, wide spread adoption and work being performed to create a lightweight interface (6LoWPAN), IP is being seen as essential to the success of HAN and Smart Grid development.
- It supports networking over power lines, phone lines and coaxial cables.
- Expected data rates up to 1Gbps.
- Provides secure connections between devices through 128-bit AES encryption. Authentication and key exchange is done following ITU-T Recommendation X.1035.
- G.hn natively supports popular protocols like Ethernet, IPv4 and IPv6 and as a result G.hn-based Energy Management networks can easily be integrated with IP-based SmartGrids.
- Availability of G.hn-compliant chips is expected during CY2010.
- Key advantages are ability to connect to any room regardless of wiring type, consumer self-install, built-in diagnostic information and self management as well as multiple equipment suppliers.

Wireless M-Bus[8]:

M-Bus (Meter-Bus) is a European standard for the remote reading of gas or electricity meters. M-Bus is also usable for other types of consumption meters. The M-Bus interface is made for communication on two wire, making it very cost effective. A radio variant of M-Bus (Wireless M-Bus) is also specified in EN 13757-4. The M-Bus was developed to fill the need for a system for the networking and remote reading of utility meters, for example to measure the consumption of gas or water in the home. This is suitable for- large number of connectable devices, possibility for network expansion, Fail-safe characteristics / robustness, minimum cost, minimum power consumption in the meters and acceptable transmission speed.

III. ENERGY MANAGEMENT SYSTEM

One of the major benefits of smart home to consumers is their ability to incorporate energy management features through utility supply, Distribution generations (solar, wind and small turbo generators) lighting, HVAC and home appliances.

A. Supply

Selection of supply is a key energy conservation activity in the home energy management system. Usually supply is from utility or from distribution generation. In the present work, supply for the smart home is intelligently selected based on cost of generation. Hence, priority is given to the different types of supply based on cost of generation.

B. Lighting

Lighting is an essential load in home, highest priority is given to the light in darkness. It necessitates the sensor to control lighting loads to turn ON and turn OFF based on light intensity to minimize the energy consumption by light loads.

C. HCAC

HVAC loads are also major loads in home. Controlling of HVAC loads gives better energy conservation in smart home. This necessitates different types of heating, cooling and air volume sensors(PIR sensors) to actuate HVAC system to operate effectively to conserve energy.

D. Home appliances

Smart homes can even go further in energy management by keeping track of the energy usage of each and every appliance in the house. The smart house controllers could schedule the operation of heavy power consuming appliances (such as dishwashers and electric water heaters) to take maximum advantage of off peak electric rates.

IV. EXPERIMENTAL SETUP AND RESULTS

The proposed architecture use ARM processor, GSM protocol to communicate with the control unit and sensors constitutes a intelligent controller for HAN. It will control the selection of supply based on cost of generation, availability of amount of power and amount of load consumption without interrupting the consumer needs. And also controls the loads based on priority to minimize the energy consumption to take maximum advantage of off peak electric rates. The operational flow charts of proposed smart home energy management system is shown in Figure.4.

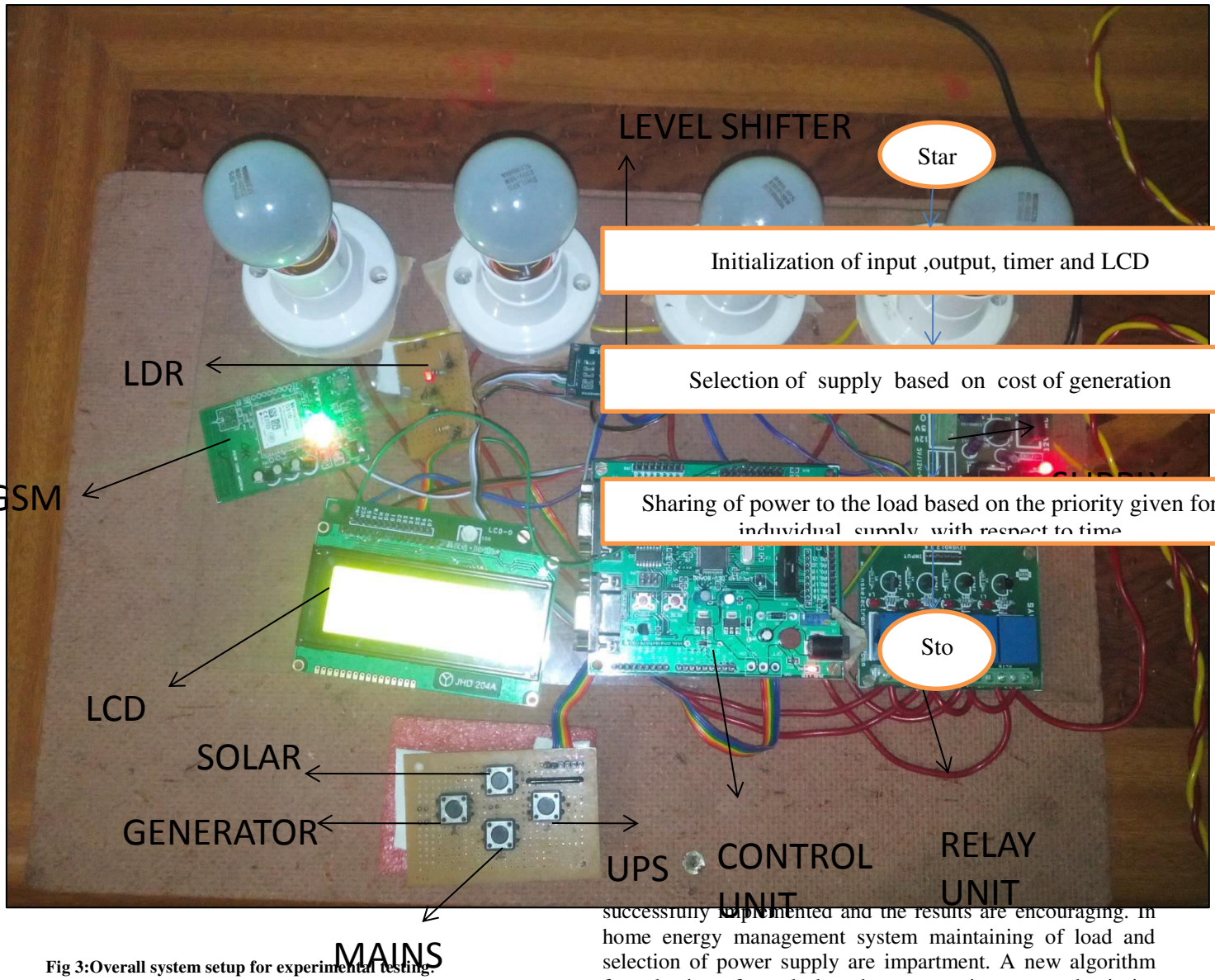

Fig 3:Overall system setup for experimental testing.

Experiments are carried out for smart home to study the different performance characteristics of the system. At each stage of operation we observed the selection of the supply and priority based sharing of the load. In this work, switching of different supply is based on cost of each unit of supply. The utility supply cost varies based on generating cost and DG cost based on fuel rate. DG supply unit cost can be fixed by the consumer. When DG supply unit cost become less than the utility supply cost, HAN switches to DG supply together with solar energy, then load sharing priority is set based on time and conservation plan to take the advantages of off peak electric rates. when utility supply cost reduce to less then DG supply cost, HAN automatically switches to utility supply together with solar energy, then load sharing priority is set

successfully implemented and the results are encouraging. In home energy management system maintaining of load and selection of power supply are impartment. A new algorithm for selection of supply based on generating cost and priority based load sharing has been proposed. In addition to proposed load sharing we could include time based and severity based load sharing among home appliances.

REFERENCES

[1]. Barney L.Capehart " Guide to energy management" Fourt edition ,The Fairmont Press,Inc.

[2]. Md. Zahurul Huq and Prof. Syed islam "Home area network technology assessment for demand Response in smart grid environment"

[3]. Tiago D. P. Mendes and Radu Godina " Smart Home Communication Technologies and Applications: Wireless Protocol Assessment for Home Area Network Resources" *Energies* 2015, *8*, 7279-7311; doi:10.3390/en8077279

[4]. Zigbee Alliances- Whitepapers http://www.zigbee.org/LearnMore/WhitePapers.aspx

[5]. ZWave homepage - http://www.zwave.com

[6]. HomePlug homepage - http://www.homeplug.org/home/

[7]. WiFi Alliances Homepage - http://www.wifi.org/

[8]. M-Bus documents homepage - http://www.mbus.com/files/

A Double Fuzzy based torque ripple minimization for DTC Induction motor drives

Mohana Lakshmi J., Purushothama G.K.
Department of EE Engg., Malnad College of Engineering, Hassan, KA, India

Abstract: ***Recent developments in control strategies have formulated many control methodologies for the improvement in performance of the induction motor (IM) drives. Among all the control methods, the Direct Torque Control (DTC) method is considered as the most efficient control scheme. DTC allows good torque control in steady state and transient operating conditions. However, the presence of hysteresis for flux and torque may introduce torque and current ripple and variable switching frequency operation for the voltage source inverter. In this paper, an advanced control strategy for the DTC of the IM using Double Fuzzy technique is proposed. In this Double Fuzzy technique, the parameters of the Proportional-Integral (PI) controller are controlled using one fuzzy logic controller while the optimal selection of voltage vectors is performed using the second fuzzy controller. The integrated controller using both these aspects is then applied to the IM drive. Simulation in MATLAB shows that the proposed approach improves not only the speed response, overshoot and steady state speed precision, but also the ripples in torque, flux and stator current have been effectively decreased at low speed.***

Keyword- Double-Fuzzy Logic Technique, Induction Motor Drive, Fuzzy PI controller

I. INTRODUCTION

Induction motor is a multi-variable, non-linear and closed coupled subject, and hence intensive research studies are made in order to acquire its excellent speed regulation capability. Subsequent to the conventional vector-control technology, DTC, proposed by M. Depenbrock and I. Takahashi [1-2], is a new approach with high performance AC speed regulation technology, which discards the concept of decoupling in the vector-control technology, and adopts the orientation of stator flux and transient space vector theory.

In traditional DTC system, speed regulator is widely based on conventional PI regulator [3-4], which has to depend on precise math-model of the subject. Since DTC technology does not decouple the IM model, it is difficult to confirm the relationship between set speed and torque, when the induction motor variables have changed or environment disturbances have occurred. Furthermore, the conventional parameter fixed speed regulator cannot easily achieve swift response, small over shooting and fine speed control precision in a wide speed range. In order to resolve this problem, reference [5] states that improved neural network self-recognition PID regulator can improve the simulation results remarkably.

However, neural network system which needs offline training is quite complicated, and has great difficulty in real-time control. To reduce torque ripple, Peter Vas [6] used higher switch frequency of inverter to decrease torque ripple. The method increases power loss and deceases efficiency of inverter, at the same time needs a high frequency inverter. Reference [7] introduced a parallel three-phase PWM inverters method. The method can decrease torque ripple to a certain extent, but it makes the system more complex, reduces the systemic dependability and increases the cost. Therefore, in this work, an advanced control strategy for the DTC of the IM using double fuzzy technique is attempted. In this double fuzzy technique, the parameters of the PI controller are controlled using one fuzzy logic controller while the optimal selection of voltage vectors is performed using the second fuzzy controller. The integrated controller using both these aspects is then applied to the IM drive.

II. BASIC DTC SCHEME FOR INDUCTION MOTOR

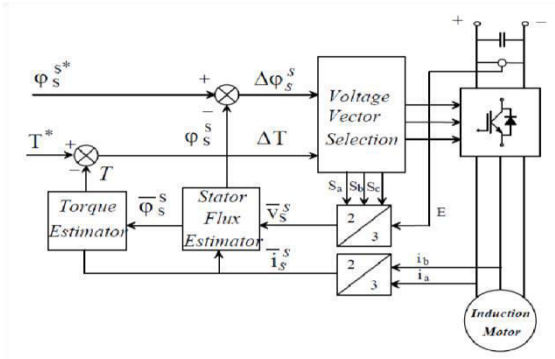

Fig. 1 Basic DTC scheme for induction motor

A method of implementing the DTC induction motor drive with voltage source inverter is shown in Figure 2.2. This method uses feedback control of torque and stator flux, which are computed from the measured stator voltages and currents. As the method does not use a position or speed sensor to control the machine and uses its own electrical output currents and resulting terminal voltages, this method is also referred as the direct self-control scheme [14]. The method uses a stator reference model of the induction motor for its implementation, thereby avoiding the trigonometric operations in the co-ordinate transformations of the synchronous reference frames. This is one of the key advantages of the control scheme. The scheme uses

stator flux linkages control. That enables the flux weakening operations of the motor to be straight forward compared to rotor flux weakening, in that the stator flux is directly proportional to the induced e.m.f, whereas the rotor flux does not have the same relationship. This reduces the dependence of the scheme on many motor parameters, thus making it a robust scheme in the flux weakening region. The scheme depends only on stator resistance and no other parameters. For its flux and torque control, this control scheme requires the position of the flux phasor, which is difficult to obtain at low and zero speeds. At such low speeds, these signals are very small, making scaling and accuracy problematic: also, the stator resistance variations introduce significant errors in the flux phasor computation. Invariably the low speed operation suffers with this scheme without stator resistance compensation. The implementation of the scheme requires flux linkages and torque computations plus generation of switching states through feedback control of the torque and flux directly without inner current loops.

The stator q and d-axes flux linkages are

$$\lambda_{qs} = \int \left(v_{qs} - R_s i_{qs}\right) dt \quad (1)$$

$$\lambda_{ds} = \int (v_{ds} - R_s i_{ds}) dt \quad (2)$$

Where the direct and quadrature axis components are obtained from the abc variables by using the transformation:

$$i_{qs} = i_{as} \quad (3)$$

$$i_{ds} = \frac{1}{\sqrt{3}}(i_{cs} - i_{bs}) \quad (4)$$

This transformation is applicable for voltages and flux linkages as well. To obtain uniformly rotating stator flux, the motor voltages have to be varied uniformly without steps too. This imposes a requirement of continuously variable stator voltages with infinite steps, which is not usually met by the inverter because it has only finite switching states [15]. The Space Vector PWM (SVPWM) generation module accepts modulation index commands and generates the appropriate gate drive waveforms for each PWM cycle.

III. IMPLEMENTATION

A. *Structure of the proposed system*

For the reduction of ripple in torque and flux in an induction motor drive it is necessary to have an effective means of control strategy. The concept of double fuzzy logic technique is an efficient method in order to reduce ripple in torque and flux and improve the systems response to a greater extent. It consists of two fuzzy logic controllers, one for optimizing the parameters of K_P and K_I and other for selecting proper voltage vectors to the inverter supplying the motor drive.

The integrated system consists of fuzzy self-adaptation speed PI regulator, stator flux and torque observation,

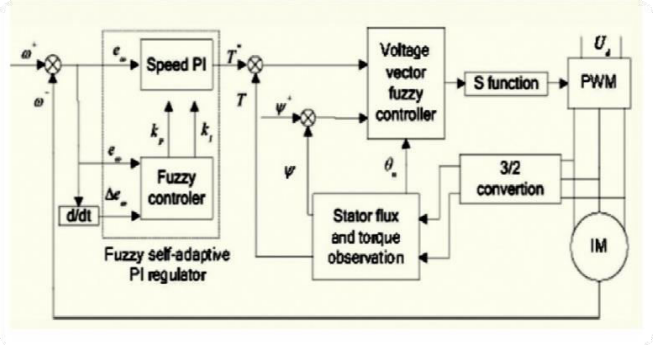

Fig. 2. Overall structure of the proposed Fuzzy DTC system with fuzzy self- adaptation speed PI Regulator

voltage vector fuzzy control, PWM inverter voltage and current sensors. The fuzzy self-adaptation PI speed regulator, composed of PI speed regulator and fuzzy-parameters controller, can adjust and optimize the real-time parameters of K_P and K_I through fuzzy inference mechanism. The stator flux linkage and electromagnetic torque are observed by flux linkage and torque observers. According to electromagnetic torque error and stator flux linkage error as well as flux-angle, the system is controlled through the approach that voltage vectors, selected properly by fuzzy controller, are exported to inverter. The error signals of torque and flux photoelectrical encoder feeds back the speed signal to the system.

B. *Design of Fuzzy Speed Regulator*

In the DTC system, the discrete expression of the conventional speed PI regulator is showed as Equation (5)

$$T_d^*(k) = K_P e_\omega(k) + K_I \int_0^t e_\omega(t) dt \quad (5)$$

Where, T is sampling period, $e_\omega(k)$ is speed error single, $T_d^*(k)$ IS set value of torque output, K_P is proportional coefficient, and K_I is integral coefficient. Equation (5) infers that control effects can easily be acquired at different speed demand, by dynamically adjusting K_P and K_I according to input speed variable.

C. *Selection of Fuzzy Subsets*

The fuzzy controller is a system with 2-input, 2-output system. $\Delta e_\omega(k)$ and $e_\omega(k)$ are input variables, K_P and K_I are output variables. The values of $e_\omega(k)$ and $\Delta e_\omega(k)$ are as equation (6) and (7) respectively:

$$e_\omega(k) = \omega^*(k) - \omega(k) \quad (6)$$

$$\Delta e_\omega = e_\omega(k) - e_\omega(k-1) \quad (7)$$

The range of K_P and K_I are [0, 1] and [0, 1] respectively. $e_\omega(k)$ is fuzzified into E ω including 7 fuzzy subsets

{NB(negative large), NM(negative middle), NS(negative small), ZE(zero), PS(positive small), PM(positive middle), PB(positive large)}, and its membership function is shown in Fig.(3). The nearer the fuzzy subset leans zero, the higher its resolution and control sensibility. Because ΔEω changes quickly in DTC system, it is not necessary to subdivide it. ΔEω includes 3 fuzzy subsets {N (negative), Z (zero), P (positive)}. K_P and K_I are fuzzified into K_P' and K_I' respectively. They both include 4 fuzzy subsets {Z, S, M, and B}.

Fuzzy control rule is regarded as the core of the whole fuzzy control. The proposed fuzzy control rules are based on the step response of conventional PI regulator, together with the characteristics of the DTC of induction motor. According to the different speed error $e_\omega(k)$ and its rate of change $\Delta e_\omega(k)$, the principles about the self-adjustment of K_P and K_I are listed as follows:

- When $e_\omega(k)$ takes a relatively big number, a big number should also be assigned to K_P in order to accelerate the system speed response, but K_I must take a quite small number or even zero in order to prevent integral saturation and distinct speed overshooting.
- When $e_\omega(k)$ takes a moderate number, K_P must take a relatively small number and K_I must take a moderate one, in order to decrease the overshooting and ensure the swift speed response.
- When $e_\omega(k)$ takes a relatively small number, the system usually runs in steady state, thus a moderate K_P and a big K_I, should be assigned to decrease static error and ensure the stability of the system.

According to the different speed error$e_\omega(k)$ and its rate of change, fuzzy control rules of K_P and K_I at different states can be acquired as shown in Table I.

Table I. Fuzzy control rule table

$\Delta e_\omega(k)$ \ $e_\omega(k)$	NB	NM	NS	ZE	PS	PM	PB
N	Z/B	M/S	S/M	M/B	S/S	M/S	B/B
Z	Z/B	M/S	B/M	Z/B	B/B	M/S	B/B
P	Z/B	M/M	B/M	Z/B	B/B	M/M	B/B

The advantage of maximum membership function method is taken into consideration, which regards the maximum value of the membership function as output value. Then the actual value can be acquired by using linear transform to the output value. The linear transform formula of proportional coefficient K_P and integral coefficient K_I is as in equation (8) and (9).

$$K_P' = 0.06 + 0.04K_P \quad (8)$$

$$K_I' = 0.3 + 0.2K_I \quad (9)$$

D. SVM based Voltage Vector

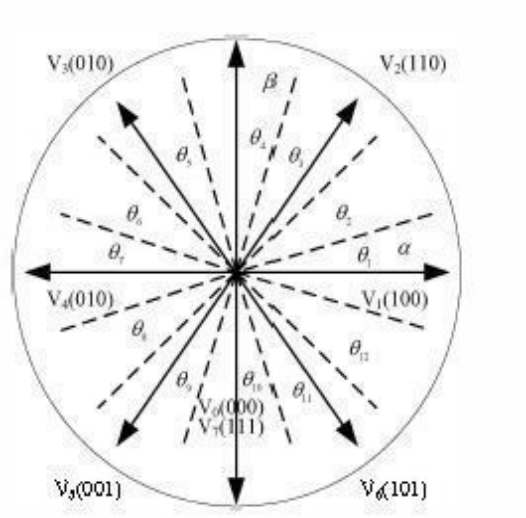

Fig. 3 Voltage Vector Fuzzy Controller

The conventional DTC is based on two discrete hysteretic comparators, in which the torque and the stator flux are controlled directly. Because its selective range is too small, it is easy to select the same voltage vector, when the error of torque and the stator flux are big or small. So it will lead to high torque ripple and reduce torque response. In order to improve static and dynamic torque response performance of DTC, and decrease torque ripple, a fuzzy logic idea was bring into DTC. The stator flux phase angle, the stator flux error, and the torque error are reasonably fuzzified into several fuzzy subsets to optimize selection of the voltage vector. In 3-phase voltage source inverter, "1" denotes to turn-on in above bridge, and "0" denotes to turn-on in below bridge, so 8 voltage vectors can be got, u1 ~ u6 is 6 nonzero voltage vector, and u0 ~ u7 is two zero voltage vector in the origin, as in Fig.3.

The voltage-vector fuzzy controller is a system with 3-input and 1-output e_Ψ, e_T *and* θ_N are input variables, voltage vector u_S is the output variable. e_Ψ is fuzzified into E_Ψ including 3 fuzzy subsets {P,N,Z}, e_T is fuzzified into E_T, including 5 fuzzy subsets {PL,PS,ZE,NS,NL}. θ_n has 12 components in 2π range, it is fuzzified into 12 fuzzy subsets $\{\theta_1, \theta_2, \ldots\ldots\ldots, \theta_{12}\}$. As u_S the output variable has only 7 selective voltage vectors, it isn't essential to subdivide fuzzy sets, so it is fuzzified into point fuzzy subsets {u0,u1,u2,u3,u4,u,5,u6}. The fuzzy control rule R_i is as in equation (10):

$$R_s: if\ e_\Psi\ is\ A_i, e_T\ is\ B_i\ and\ \theta\ is\ \theta_i\ then\ U_n\ is\ u_i \quad (10)$$

Where variablesA_i,B_i ,θ_i,u_i are fuzzy subsets of flux error, torque error, flux phase angle and the voltage vector, i=1~180, j=1~12 and k=0~7. There are 180 rules in the

strategy. According to the all rules and Mamdani's organon, and all the variable membership function, a fuzzy control table can gain, as shown Table II.

Table II. Fuzzy Control Rules of Voltage Vector

E_ψ	E_t	θ_1	θ_2	θ_3	θ_4	θ_5	θ_6	θ_7	θ_8	θ_9	θ_{10}	θ_{11}	θ_{12}
N	NS	5	6	6	1	1	2	2	3	3	4	4	5
	NL	5	5	6	6	1	1	2	2	3	3	4	4
	ZE	0	0	0	0	0	0	0	0	0	0	0	0
	PS	3	4	4	5	5	6	6	1	1	2	2	3
	PL	3	3	4	4	5	5	6	6	1	1	2	2
Z	NS	6	6	1	1	2	2	3	3	4	4	5	5
	NL	0	0	0	0	0	0	0	0	0	0	0	0
	ZE	0	0	0	0	0	0	0	0	0	0	0	0
	PS	3	3	4	4	5	5	6	6	1	1	2	2
	PL	2	3	3	4	4	5	5	6	6	1	1	2
P	NS	6	1	1	2	2	3	3	4	4	5	5	6
	NL	6	1	1	2	2	3	3	4	4	5	5	6
	ZE	0	0	0	0	0	0	0	0	0	0	0	0
	PS	2	2	3	3	4	4	5	5	6	6	1	1
	PL	2	2	3	3	4	4	5	5	6	6	1	1

IV. SIMULATION RESULTS

The control technique of the proposed work is implemented using Simulink. The Simulink model of induction motor employing DTC is realized using Simulink and Sim Power System blocks. The results for DTC employing conventional methods and the proposed method are obtained through simulation. Stator flux trajectory is developed in which the trajectory response shows the presence of ripple in the stator flux.

A. Control of Induction Motor Drive Using Conventional DTC

The model in conventional scheme is developed using SIMULINK. The rotor speed, the electromagnetic torque, the DC bus voltage, the stator flux and the stator current of the motor are observed on the scope as in Fig. 5. The Fig. 5 shows the response of the electromagnetic torque in an induction motor drive using DTC without fuzzy PI controller. It is observed that the responses of current and torque is not symmetric and fluctuations are present. The torque pulsations are also very high. Fluctuations are observed in speed as well. The responses of torque and speed increase and suddenly decrease yielding dips in the response as shown in Fig. 5 when the speed is controlled without fuzzy logic PI controllers.

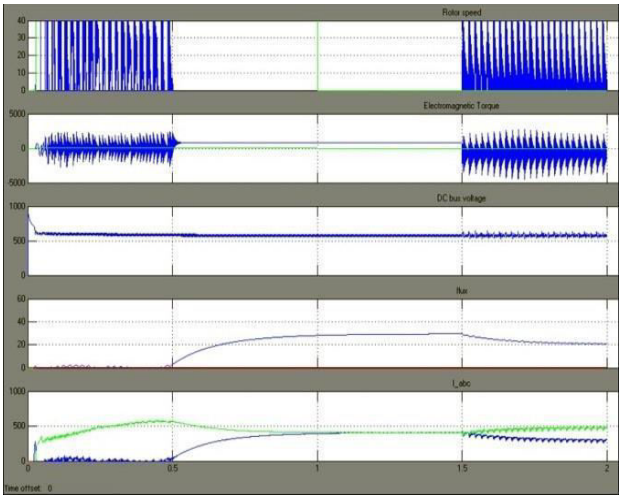

Fig. 5. Output waveforms of Speed, Electromagnetic Torque DC Bus Voltage, Flux and current using a Conventional Controller.

B. Control of Induction Motor Using Single Fuzzy Controller

The model is developed with a single fuzzy logic controller for the control of the induction motor drive employing DTC. The tuning process of the circuit is done by the use of PI controller which reduces the steady state error and increases stability of the system. The voltage vectors are selected in the switching operation of the inverter. The simulated results are viewed which comprises the speed, electromagnetic torque, voltage and current responses as shown in Fig. 6.

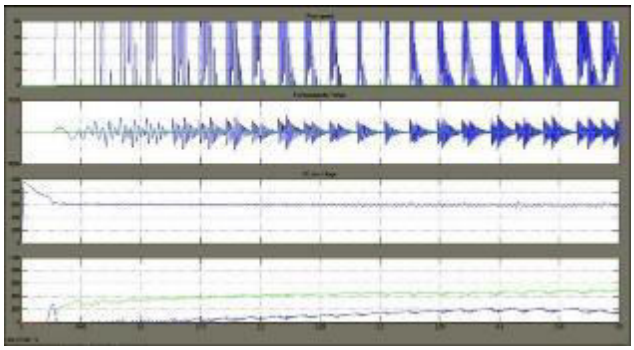

Fig.6. Output Waveforms of Stator current, rotor speed, electromagnetic torque and voltage employing a simple fuzzy logic controller.

From the results obtained as shown in Fig. 6, it is clear that using a fuzzy logic controller the ripple in torque is reduced and the performance of the system has also improved with lower ripples in speed too. The response of the current has also improved. Although the results are better compared to the conventional DTC method there are high distortions in torque and speed. The ripple content in torque is higher during start up. There are

sudden dips in the electromagnetic torque with ripple during the speed control of the motor.

C. Control of Induction Motor Drive Using Double Fuzzy Logic Technique

The concept of double fuzzy logic technique involves two fuzzy logic controllers .One is the fuzzy speed PI regulator used to adjust the parameters of the conventional PI regulator and improve speed self-adaptation performance. The second fuzzy logic controller is adopted to optimize selection of the voltage vector and improve dynamic response performance by reducing torque and flux ripple. Apart from this the parameters are optimized separately using fuzzy logic controllers for each. Both the parameters are tuned in order to improve the steady state response of the system and reduce the error in speed response there by stabilizing the system. The use of voltage vector fuzzy logic controller provides a constant inverter switching frequency. The control of stator flux employs the tuning of parameters for improving the steady state characteristics of flux.

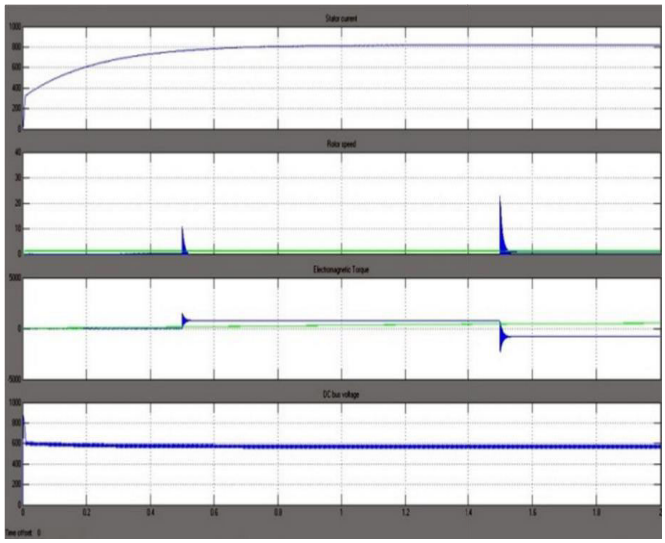

Fig.7 Waveforms of stator current, rotor speed, electromagnetic torque and voltage a Double fuzzy logic controller

Fig. 7 and Fig. 8 shows the simulated results using double fuzzy logic controller. The use of fuzzy logic controllers permits a fast response and more robustness. The use of voltage vector fuzzy controller provides a constant inverter switching frequency that results in small torque and flux ripples, and current distortions as shown in Fig 7 and 8 respectively. Although there are sudden dips observed in the electromagnetic torque, the response is seen ripple free. The Fig. 8 represents steady state characteristic of flux without any distortions. The response of current and voltage is also free from fluctuations and distortions. Thus, the overall performance of the system is enhanced.

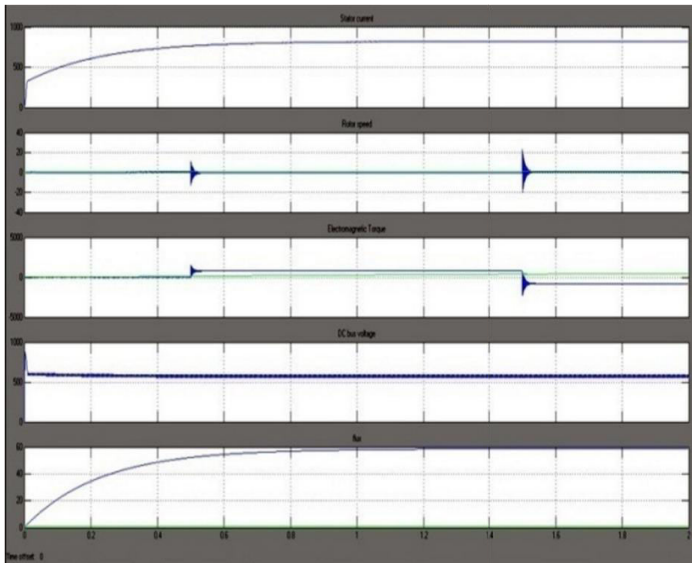

Fig. 8. Output Waveforms for Flux Using a Double Fuzzy logic Controller

D. Trajectory Analysis

Trajectory responses for each condition employing conventional DTC, simple fuzzy logic control technique and the double fuzzy logic control technique is obtained.

**Stator Flux Trajectory employing Conventional DTC*

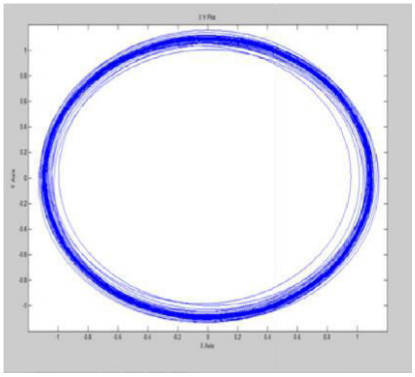

Fig.9 Stator flux trajectory Employing Conventional DTC

Fig. 9 shows the stator flux trajectory of the induction motor without using fuzzy PI controller i.e. employing the conventional DTC. From the trajectory response it is observed high ripples are created in the trajectory when the speed is controlled.

** Stator Flux Trajectory Employing Simple Fuzzy Logic Technique*

It is observed that the model employing a simple fuzzy logic controller as in Fig.10 has almost a circular

trajectory for stator flux indicating the minimization of ripples or distortions in the flux trajectory when compared to the DTC without using a fuzzy controller.

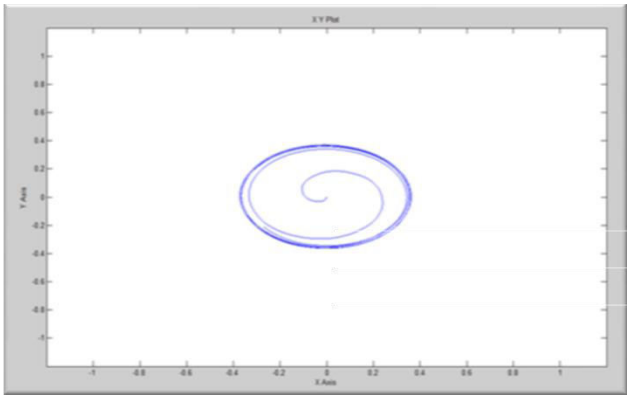

Fig.10 Stator flux trajectory using simply fuzzy Controller

** Stator flux trajectory using double fuzzy logic technique*

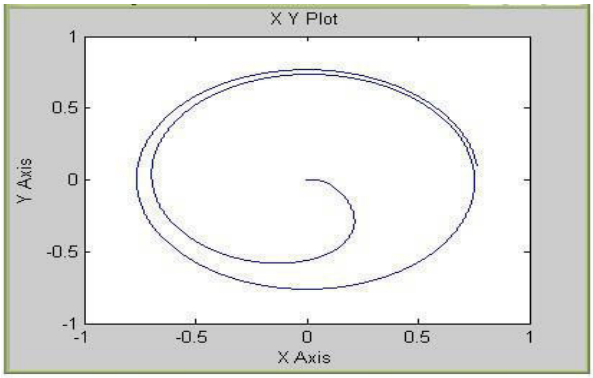

Fig. 11 Stator flux trajectory using double fuzzy logic technique

Fig. 11 shows stator flux trajectory employing double fuzzy logic technique. The trajectory is a smooth curve which shows minimized ripple and distortions compared with the model employing conventional and simple fuzzy technique.

V. CONCLUSIONS

DTC is employed for an efficient control of the torque and flux without changing the motor parameters and load. Also the flux and torque can be directly controlled with the inverter voltage vector in DTC.

Fuzzy adaptive PI controller has been used as DTC speed regulator and the fuzzy reasoning rules are optimized so that the parameters can be dynamically adjusted in real-time. The double fuzzy logic technique along with the voltage vector fuzzy controller is analyzed in comparison to the conventional hysteresis controller connected to DTC. The results obtained through numerical simulations are presented. The work proposed can be improved by developing a completely auto adaptive controller not only for torque ripple reductions but also for reducing EMI for increasing energy savings from mains.

References

[1] Jun Liu, Pusheng Wu, "Application of fuzzy control in direct torque control of permanent magnet synchronous motor", *Proceeding of the 5th World congress on intelligent control and automation*, 2004, pp. 4573-4576.

[2] F. Barrero, A. Gonzalez, Torralba, E. Galvan, and L. G. Franquelo, "Speed control of induction motors using a novel fuzzy sliding mode structure", *IEEE Transactions on Fuzzy systems*, No. 10,2002, pp. 375-383.

[3] Anitha Paladugu, Badrul H. Choedhury, "Sensorless control of inverter fed induction motor drives", *Electric Power Systems Research*, No. 77, 2007, pp. 619-629.

[4] Y.S. Lai, J.H. Chen, "A new approach to direct torque control of induction motor drives for constant inverter switching frequency and torque ripple reduction", *IEEE Transactions in Energy Conversion*, No. 16,2001, pp. 220-227.

[5] F. Herrera, "Genetic Fuzzy Systems: Status, Critical Considerations and Future Directions", *International Journal of Computational Intelligence Research*, Vol. I, No. 1, 2005, pp. 59-67.

[6] Chang-liang Xia, Pei-jian Guo, Ting-na Shi, and Ming-chao Wang, "Control of Brushless DC Motor using Genetic Algorithm based Fuzzy Controller", *Proceedings of the CSEE*, Vol. 25, No. 11, June 2005, pp. 129-133.

[7] I. K. Bousserhane, A. Hazzab, M. Rahli, M. Kamli, and B. Mazari, "Adaptive PI Controller using Fuzzy System Optimized by Genetic Algorithm for Induction Motor Control", *IEEE Transactions in Industrial Electronics* , 2006.

FEW ASPECTS OF MICROGRID

VIMA MALI[1], K. S. APRAMEYA[1*], R. L. CHAKRASALI[2]
[1]Electrical and Electronics Engineering Research Centre, University B.D.T. College of Engineering, Davanagere, India.
[2]Department of Electrical and Electronics Engineering, SDM College of Engineering and Technology, Dharwad, India.

Abstract— ***With demands for electric power in India growing at a faster pace than the construction of electric power infrastructure and new generation sources, many Indian companies are apprehensive about their ability to obtain enough reliable, ready energy from the grid so that they can effectively run their businesses and the electricity supply to the rural village is also not economically advantageous for government, because of minimal power consumption and high cost of distribution and transmission for the electricity supply, apart from that grid failure will add more trouble to the electricity then there is a hope of innovation, Microgrid. It is the only effective solution to overcome the problems of not only India but also many developing countries, so this paper explains about importance of microgrid, its types, operation, concept of renewable energies, benefits and problems of microgrid, its energy storage benefits, simulation tools and lastly effect of microgrid on society.***

I.INTRODUCTION

In Jan 2012, over 300 million Indian citizens had no access to electricity. Over one third (33%) of India's rural population lacked electricity, as did 6% of the urban population. Of those who did have access to electricity in India, the supply was intermittent and unreliable. The North India blackout is one of the greatest examples of Indian electricity grid failure. To all these problems Micro-grid possibility in Indian scenario is a light of hope. Micro -grid is small power generation grid near to the consumers. The concept of microgrid (MG) is proposed by the Consortium for Electric Reliability Technology Solutions (CERTS) so as to enhance the local reliability and flexibility of electric power systems, which may consist of multiple distributed energy resources (DERs), customers, energy storage units, small electric power system being able to operate physically Islanded or interconnected with the utility girds [1]. The main benefit of microgrid is that the ability to operate if access to the central grid is unavailable.

The demand for electrical energy consumption is expected to grow rapidly throughout the world, particularly in developing countries. Residential electrical energy consumption is about 30-40% of the total energy use in different countries [2]. Total identified microgrid capacity has grown from 4,393 megawatts (MW) in the second quarter of 2014 to more than 12,000 MW today, according to Navigant Research. North America continues to be center

of worldwide microgrid activity, particularly for grid-connected microgrids. Meanwhile grid-deficient Africa, India & the Island nations spur a market for remote microgrids. The need of reducing CO_2 emissions in the electricity generation field, recent technological developments in the microgeneration domain, and electricity business restructuring are the main factors responsible for the growing interest in the use of microgeneration [3, 4].

The United States Department of Defense (DoD), Department of Energy (DoE), Northeast states and utilities are the primary drivers behind a projected $26 billion/5.9 gigawatts (GW) annual microgrid market. The DoD is establishing a network of microgrids at over 40 military bases, and are investigating the deployment of mobile microgrids at its 600 + forward operating bases. The DoD is hoping microgrids can reduce their $4 billion annual energy bill, while improving the reliability of mission-critical operations running during grid outages. Nowadays, a considerable research has been undertaken on the microgrid technology. As part of the research, a series of microgrid test facilities, such as CERTS microgrid test bed, GE microgrid in America [5, 6], Aichi, Kyoto, Sendai microgrid in Japan [7, 8], Labein, Kythnos, CESI microgrid in Europe [3,9], have been built for possible demonstrations of advanced distributed generation system[10].Even Nanyang Technological University Singapore (NTU Singapore) has integrate multiple large-scale renewable energy sources such as solar, wind, tidal-current, diesel, storage and power-to-gas technologies, and ensure these energy sources operate well together.

A microgrid is a better alternative to over-come the challenges of integrating distributed energy resource units, including renewable energy, into power systems [11]. Microgrid efficiently generate, store & use either AC or DC electricity locally without the need for long range transmission & distribution network. Multiple source microgrids such as solar, wind, biomass & energy storage batteries is found to give better solution than single source; microgrid. But challenge lies in integration of all such resources based generations to meet consumer demand with reliability, security and best of quality [12]. The micro grid is divided into ac micro grid and dc micro grid, which is classified by whether, distributed sources and loads are connected on the basis of ac or dc grid. Ac micro grid has a benefit to utilize existing ac grid technologies, protections

and standards but stability and requirement of reactive power are the inherent demerits of it. On the other hand, dc microgrid has no such demerits of ac micro grid and assures reliable implementation of environment-friendly distributed generation sources [13, 14].

II.IMPORTANCE OF MICROGRID

1. Transmission and Distribution over capacity an expensive to fix or extend it (US businesses lose $80B to $150B per year in revenues due to power outages).
2. Due to Electric and gas prices fluctuations.
3. Need of power quality, efficiency and reliability.
4. Cyber and physical security.
5. Increase in energy demand due to standard of living.
6. Power demand in remote areas can be met, where the grid supply is not reliable & efficient.
7. Fuel is available free of cost.
8. Environmental friendliness.
9. Higher energy efficiency
10. Improved service quality and reliability.
11. Reduced greenhouse gases and pollutant emissions.
12. Emergency power can be provided during power shortage or interruption in the main grid.
13. In case of grid-interconnected mode bi-directional or import and export of power is possible.
14. Microgrids can reduce economic losses from outages.
15. To maintain the supply-demand balance. Microgrid control systems manage supply and demand in real time to maintain balanced and stable operation.

III.TYPES OF MICROGRID

According to the survey of 265 U.S. electric utility and independent power producer executives, an overwhelming 97% of respondents see microgrids as a business opportunity for them over the next decade. More than half of utilities surveyed see themselves in the microgrid market even earlier - within five years. Navigant Research has divided up the microgrid market into five categories based on the end-user [2, 15].

1. Island and Remote "off-grid" microgrids: An "off-grid" microgrid is usually built in areas that are far distant from any transmission & distribution. These microgrids including islands, remote sites, mining camps and other microgrid systems not connected to a local utility network. Due to this, such a microgrid must have black start capacity.

2. Institutional or campus microgrids: It is fully interconnected with a local grid, but they also maintain some level of service in isolation from the grid, such as during a utility outage. Campus microgrids do not cross public rights of way or incorporate public utility infrastructure. Typical examples serve university and corporate campuses, prisons & military bases. As all the buildings in the particular organization belong to single group, this kind of structure makes decisions fast.

3. Community & Utility microgrids: These are integrated into utility networks. Such microgrids serve multiple customers or services within a community, generally to provide resilient for vital community assests. There can be a wide variety of renewable or fossil-fueled distributed energy resources within this type of microgrid. Due to high number of participants, decisions will be lengthy as compared to other microgrid structures.

4. Commercial & Industrial microgrids: Main reasons for the installation of an industrial microgrid are power supply security & its reliability. There are many manufacturing processes in which an interruption of the power supply may cause high revenue losses and long start-up times. Typical examples are chip manufacturing, the chemical industry, the paper & foodstuff industries etc.

5. Nanogrids: Nanogrids comprised of the smallest discrete network units with the capacity to operate independently. A nanogrid can be defined as a single building or a single energy domain such as a commercial, industrial or residential facility or serving a dedicated system, such as a water treatment or pumping station. The figure 1 below shows microgrid types and there capacity in MW contribution according to Navigant Research 2013.The Institutional/campus has contributed highest power generation of 1021 MW and the lowest contribution is by commercial/industrial by 433 MW.

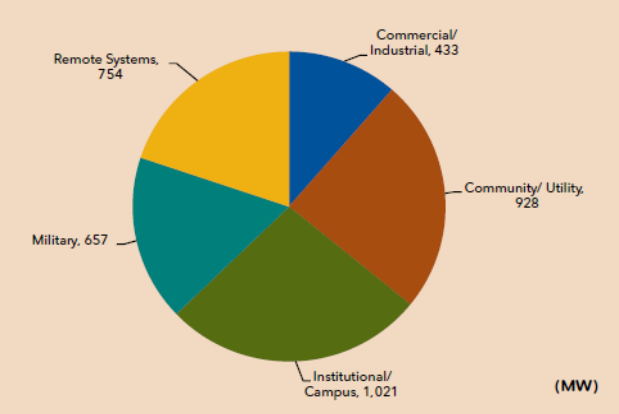

Figure 1: Microgrid capacity by segment, world markets: 2nd Quarter 2013.

IV. MODERN MICROGRID OPERATION

Microgrid can continuously run in off –grid mode, as well as in dual mode by changing the grid status. The microgrid can be operated in two ways:

1. Islanded mode: In islanded mode, the renewable energies such as solar, biomass & wind are used. It is situated in remote areas away from the large centralized grid. Especially in winter and rainy season, when the solar panels will be producing very poor level of power, that

amount of power is compensated by wind & biomass generators used.

2. Grid connected mode: In grid-connected mode, the renewable energies such as solar, biomass & wind are used; the microgrid operator can take economic decisions-such as to sell or buy energy depending on site generation capability, its cost & the current prices on the energy market. In case of the utility power system outage, the point of common coupling breaker will automatically open & own generators will continue to supply power to loads within the microgrid [16].

V.RENEWABLE ENEGRGIES

Renewable energy in India comes under the purview of the Ministry of New and Renewable Energy. India was the first country in the world to set up a ministry of non-conventional energy resources, in early 1980s. India's cumulative grid interactive or grid tied renewable energy capacity (excluding large hydro) has reached 29.9 GW, of which 68.9% comes from wind, while solar PV contributed nearly 4.59% of the renewable energy installed capacity in India[8,9]. The Indian electricity grid faces significant challenges to reliability, cost effectiveness, and expansion. It is often too far and too expensive to feasibly connect rural towns to the grid. Solar, wind and other renewable may be the only way to provide these areas with electricity (US Dept of Energy 2010).

Indian Electrical and Electronics Manufacturers Association (IEEMA) Plays a major role in Renewable Energy.Due to the lack of the electricity generation from the conventional sources and the huge demand for the current environment the role of electricity generation from the renewable sources are increasing day to day[17,18,19,20]. These renewable energy sources have a plenty of advantages like the infinite availability, the zero percentage generation of harmful emissions [19, 20, 21, 22, 23]. The main disadvantages of these sources are the instability or the fluctuations in the energy generation and the high system cost [19, 24, 25, 26].

The Indian Solar Loan Programme, supported by the United Nations Environment Programme has won the prestigious Energy Globe World award for Sustainability for helping to establish a consumer financing program for solar home power systems. Over the span of three years more than 16,000 solar home systems have been financed through 2,000 bank branches, particularly in rural areas of South India where the electricity grid does not yet extend [53,54].

In its 12th Five Year Plan (2012-2017), the Indian Government has set a target of adding 18.5 GW of renewable energy sources to the generation mix out of which 11 GW is Wind Energy. Indian Wind Energy Alliance (IWEA) is the apex body for the wind energy industry in India. It was launched in December 2014 and Mr. Sumant Sinha is the chairman of IWEA [27]. Table 1 below shows total renewable energy installed capacity.

Table 1. Total Renewable Energy Installed Capacity in India (31 Dec 2014) [28]

Sl.no	*source*	*Total Installed Capacity(MW)*
1.	***Wind Power***	22,465.03
2.	***Solar Power (SPV)***	3,062.68
3.	***Small Hydro Power***	3,990.83
4.	***Biomass Power***	1,365.20
5.	***Bagasse Cogeneration***	2,800.35
6.	***Waste to Power***	107.58
Total		**33,791.74**

VI. BENEFITS AND PROBLEMS OF MICROGRID

Benefits of microgrid power plants in India are enormous:

1. The generation of power for these micro grids are mostly based on renewable energy source such as solar, wind, biomass. Some of the micro-grids is also depend upon mini-hydro Plants.
2. The power supply from these grids is 50% cheaper than the diesel price, which is the most dependable source for any small scale industry/telecom tower/small business owners.
3. The microgrid model also brings growth to the area with employment, industrialization and advantage to health and education.

But the future of Micro-grid is not lucrative. Many ***problems*** in this business model create a question mark to the investor and entrepreneur to take further steps in this field; Such as

1. Low Return on capital investment due to unpredictable revenue, as there is no reliable non-residential consumer.
2. Variable energy of sun and wind creates instability.
3. Demand for electricity is high in night time and generation is high in day time, so demand supply mismatch creates loss to the micro-grid operator.
4. Overloading is another problem. Hooking up an additional light or a mobile charger robs the companies of revenue and also often trips the system and brings the whole village to darkness.
5. Large battery banks are required which needs more space and maintenance.
6. Implementation of microgrids is an important challenge faced during microgrid protection.
7. Last but not the least the amount of electricity generation is very random, which varies from -50% to +50%. It may be one of the reasons not to go for PPA (Power purchase agreement) model for any industrial consumer.

VII. BENEFITS OF STORAGE SOLUTIONS IN MICROGRID

1. PV plants become "dispatchable".
2. Capacity of backup power-plants can be reduced while still securing supply security.
3. Expensive roll-out of transmission grid can be reduced while still securing power quality.
4. Distribution grids are stabilized and relieved from heavy energy shifting.
5. Energy self-consumption on-site can significantly be increased.

VIII.SIMULATION AND OPTIMIZATION SOFTWARE TOOLS FOR MICROGRID

There are different simulation tools used to simulate power system model by comparing the feasible system design, list of cost effectiveness etc. The lists of the software are:

1. HOMER (Hybrid Optimisation Model for Electric Renewable): It was developed by NREL (National Renewable Energy Laboratory, USA). HOMER, the micropower optimization model simplifies the task of evaluating designs of both off-grid and grid –connected power systems for a variety of applications. The different functions performed by HOMER are:

a. Homer is convenient and fast to be programmed, simple to be learned [29].

b. It simulates the operation of a system by making energy balance calculations for each of the 8760 hours in a year.

c. For each hour calculates the flows of energy to and from each component of the system.

d. It performs these energy balance calculations for each system configuration that you want to consider.

e. It then determines whether a configuration is feasible, i.e whether it can meet the electric demand under the conditions that you specify.

f. It estimates the cost of installing and operating the system over the lifetime of the project.

g. The load can be AC, DC & or hydrogen loads, as well as thermal loads. Depending on the number of variables used, the simulation can take a long time [30, 31].

h. The version is available free of charge is sufficient for most applications.

2 .HYBRID2: Hybrid2 was developed by the Renewable Energy research laboratory (RERL) of the University of Massachusetts. Hybrid2 is very flexible and easy to use computer software to help with the long term prediction of hybrid power system performance. It will allow industry, government and other non-government agencies interested in the electrification of rural areas but who may have limited knowledge of hybrid power systems to evaluate hybrid alternatives to standard petroleum-based generators. The hybrid systems include three types of electrical loads, multiple diesel generators, multiple wind turbines of different types, PV generators and battery storage, four types of power conversion devices and fuel cell or electrolyzers can be modelled in the software [32].

3. HOGA(Hybrid Optimization by Genetic Algorithm): Hoga is a simulation & optimization program developed in C++ by Jose L. Bernal-Agustin and Rodolfo Dufo-Lopez, University of Zaragoza, Spain, for hybrid renewable systems for generation of electrical energy and/or hydrogen. The hybrid system is comprised of photovoltaic (PV) panels, wind turbines, hydroelectric turbines, fuel cells, H2 tanks, and electrolyzers, as well as batteries, battery charge regulators, inverters, rectifiers & AC generators. HOGA uses of genetic algorithms (GA) for optimization, both for the system components (main GA), and for the control strategy (secondary GA). They may produce adequate solutions when applied to highly complex problems [33].

4. PHOTOV-III: Photov – III is a numerical code which used to generate PV- BAT configurations able to Guarantee Zero load rejection (100% energy autonomy) for a given area and time period examined. The computational algorithm PHOTO-III is used in [34].

5. LINDO (Linear, Interactive, Discrete Optimizer): is an interactive linear, quadratic, and integer programming system useful to a wide range of users. LINDO can be used

a. To solve interactive linear, quadratic, general integer and zero-one integer programming programs up to 500 rows and 1,000 columns

b. To perform sensitivity analysis and parametric programming.

IX.EFFECT OF MICROGRID ON SOCIETY

1. Change in the structure of energy economy.
2. Availability to new facilities & lifestyle.
3. Viable for regions with underdeveloped transmission infrastructure, for example remote villages & islands.
4. Suitable alternative for replacing Diesel Generators & also reduced dependency on diesel subsidy.
5. Micro-Grid enables remote locations to access pollution free energy.
6. Use of micro grid gives impetus to the use of Renewable sources of energy.
7. In an event of Power Grid failure Micro-Grid is one of the best alternatives.

X.CONCLUSION

The microgrid plays an important role in overcoming and solving energies crisis problems of many developing countries such as green house effect, crude oil, natural gas, rural electrification, minimizing the cost of far transmission and distribution lines. For different applications many types of microgrid are available As microgrid mainly uses renewable energy sources to provide electrical power to the consumers & also use batteries as a backup in case of lack of primary source & to provide power without interruptions from this world-wide, many countries have benefitted from it. Lastly having awareness about its overall criteria helps in benefitting the society.

REFERENCES

1. Saurabh M I, A.P chaudhari, G. K Mahajan "A Review on advance energy storage technology for microgrid and smart grid", International Journal of Science, Engineering and Technology Research (IJSETR).
2. Rakesh Sahu et al., "Hybrid Power Model of Renewable Energy Sources For On Grid Power Suppy", International Journal of advanced Research in Electrical, Electronics & Instrumentation Engineering, Vol. 2, Issue 11, Nov 2013.
3. European Research Project More Microgrids. [Online]. Available: http://Microgrids.power.ece.ntua.gr/.
4. R. Lasseter et al., White Paper on Integration of Distributed Energy Resources—The CERTS MicroGrid Concept. [Online]. Available: http://certs.lbl.gov/pdf/LBNL_50 829.pdf.
5. R.H. Lasseter and P. Piagi, "Control and Design of Microgrid Components, Final project report," PSERC publication 06-3, [Online]. Available: http://certs.aeptechlab.com/.
6. Department of Energy Electricity Distribution Programme, Advanced Distribution Technologies and Operating Concepts - Microgrids, [Online]. Available: http:// www.electricdistribution.ctc .com/Microgrids .htm.
7. Toshihisa Funabashi and Ryuichi Yokoyama, "Microgrid Field Test Experiences in Japan," Power Engineering Society General Meeting, pp. 1-2, 2006.
8. S. Morozumi, "Micro-grid demonstration projects in Japan," IEEE Power Conversion Conference, pp.635-642, April, 2007.
9. Oleg Osika, Aris Dimeas and Mike Barnes et al, "DH1_Description of the laboratory micro grids," Tech. Rep. Deliverable DH1, 2005.
10. Yanbo CHE et al; "Research on Design and Control of Microgrid System", PRZEGLĄD EKTROTECHNICZNY (Electrical Review), ISSN 0033-2097, R. 88 NR 5b/2012.
11. A. Mehrizi- Sani, A.H Etemadi, D.E. Olivares, and R. ravani, " Trends in microgrid control", IEEE Trans.Smart Grid, to be published.
12. Palak Kalra, "Hybrid Micro Grid Systems - Drivers & Challenges", Journal of Energy Technologies and Policy, ISSN 2224-3232 (Paper) ISSN 2225-0573 (Online) Vol.3, No.12, 2013.
13. J. Lee, B. Han, H. Cha, ―Operational analysis of DC micro grid using detailed model of distributed generation‖, IEEE Transl. Transmission & Distribution Conference & Exposition: Asia and Pacific, DOI: 10.1109/TD-ASIA.2009.5356839, October 2009.
14. Syed Enam Reza et al; " A Novel Load Distribution Technique Of Dc Micro-Grid Scheme On Pv-Diesel Hybrid System For Remote Areas Of Bangladesh" , International Journal Of Scientific & Technology Research Volume 2, Issue 1, January 2013 Issn 2277-8616.
15. Navigant Research, 2013.
16. Microgrids white paper, Seimens 2011.
17. Ward Bower, Scott Kuszmaul, Sigifredo Gonzalez, "Solar Energy Grid Integration Systems (Segis) Proactive Intelligent Advances for Photovotaic Systems", IEEEConf. of Photovoltaic specialists, Honolulu , June 2010.
18. R. W. Wies, R. A. Johnson, John Aspnes, "Design of an Energy-Efficient Standalone Distributed Generation System Employing Renewable Energy Sources and Smart Grid Technology as a Student Design Project", IEEE Photo Voltaic Specialist Conf., Minneapolis, June 2010.
19. A.M. van Voorden, J.G. Slootweg, G.C. Paap, L. van der Sluis "Potential for renewable energy generation in an urban distribution network" , IEEE 16th International Conference and Exhibotion, Amsterdam, June 2011.
20. Ahmed Yousuf Saber, Ganesh Kumar Venayagamoorthy, "Plug-in Vehicles and Renewable Energy Sources for Cost and Emission Reductions", IEEE Transactions on Industrial Electronics, Vol. 58, No. 4, April 2011.
21. Matthew Wells, Stony Brook, "Model of Smart Solar PV Charge Controller", IEEE Conference on Systems, Applications and Technology, Farmingdale, May 2011.
22. Lars Gertmar, Per Karlsson, Olof Semuelsson, "On DC Injection to AC Grids from Distributed Generation", IEEE Conference on Power electronics and applications, Dresden, 2005
23.B. Azzopardi, J. Mutale, "Smart Integration of Future Grid-Connected PV Systems", IEEE Photovoltaic Specialist Conference, Philadelphia, June 2009.
24.Bower, Scott Kuszmaul, Sigifredo Gonzalez, "Solar Energy Grid Integration Systems (Segis) Proactive Intelligent Advances for Photovotaic Systems", IEEEConf. of Photovoltaic specialists, Honolulu , June 2010.
25.Lars Gertmar, Per Karlsson, Olof Semuelsson, "On DC Injection to AC Grids from Distributed Generation", IEEE Conference on Power electronics and applications, Dresden, 2005.
26. Junichi Arai, Kenji Iba, Yosuke Nakanishi, Kaoru Koyanagi, Ryuichi Yokoyama, "Power electronics& its Application to Renewable energy in Japan", IEEE Circuits and Systems Magazine, July 2008.
27. "Announcing The Launch of The Indian Wind Energy Alliance (IWEA)". *Business Wire India*. 3 December 2014. Retrieved 20 May 2015.
28. Cumulative deployment of various Renewable Energy Systems/ Devices in the country, http://www.mnre.gov.in/.
29. Lilienthal, P.D. Lambert, T.W. Gilman, P. (2011) Getting started guide for Homer Legacy (version 2.68). Homer Energy, Boulder, CO; National Renewable Energy Laboratory (NREL) of the USDOE, Golden, CO; 28p.
30. Silva .S.B, M.M.Severino, M.A.G.de Oliveira, " A stand alone hybrid photovoltaic, fuel cell and battery system: a case study of Tocantins, Brazil", In: Renewable Energy, (2013), vol.57,p. 384-389.
31.Khan. MJ, Iqbal.MT, " Pre-feasibility study of stand alone hybrid energy systems for application in Newfoundland", In: Renewable Energy, (2005), Vol.30, issue6, p.835-854.
32. Salima Kebaili et al; "Optimal Sizing Of Stand Alone Photovoltaic Systems: A Review", *Journal of Electrical Engineering, www.jee.ro*.
33. HOGA (Hybrid Optimization by genetic algorithms). Online Available http://www.unizar.es/rdufo.hoga-eng.htm.
34. J.K. Kaldellis, D. Zafirakis, E.Kondili, "Optimum autonomous stand alone photovoltaic system design on the basis of energy pay-back analysis" , In: Energy, (2009), Vol,34,p.1187-1198.

Moment Method approach to evaluate error induced by dipoles connected in a crossed structure used as near field sensors

Suma.M
Department of Electronics and Communication
Adichunchanagiri Institute of Technology, Chikmagalure, India
Suma.aug13@gmail.com

Vani. H.R
Department of Electronics and Communication
Adichunchanagiri Institute of Technology, Chikmagalure,
IndiaVanisrinivas2002@yahoo.co.in

Paramesha
Department of Electronics and Communication
Government Collage of Engineering
Hassan
prm.ait@yahoo.com

Goutham.M.A
Department of Electronics and Communication
Adichunchanagiri Institute of Technology, Chikmagalure, India
magoutham@yahoo.co.in

Abstract— Three dipoles connected in a crossed structure are used as near field measuring probe of a waveguide radiator in an infinite ground plane. The Moment Method is used to estimate the error induced by the probe in the near field. Probe measures both co-pole (along y-axis), cross- pole (along x-axis) and z-axis component components simultaneously. However, due to multiple reflections between radiator and dipoles, near field values are changed. Computation has been carried out to compare the relative sampled co-pole voltage pattern to the relative sampled electric field (without probe) pattern in the scan plane, and the error induced by the dipoles is determined. The waveguide reflection coefficients and radiation admittances with the probe are altered with respect to the corresponding values when there is no probe in the near-field.

Keywords—Basis Functions; Co-pole; Cross pole; EM wave; MoM; Waveguides.

I. INTRODUCTION

The rectangular aperture in an infinite ground plane fed by a waveguide being used as a radiating element is assumed excited in the dominant TE_{10} mode. The three dipoles i.e. along y-axis (co-pole), along x-axis (cross-pole) and dipole in z-axis are connected in crossed structure are used as a near-field probe. The method of moments can be used to solve boundary value problems. The waveguide aperture electric field is described by the weighted sinusoidal entire domain basis functions, and induced currents on co-pole, crossed pole and z-axis directed dipole are described by pulse basis functions. The boundary conditions at the waveguide aperture are imposed simultaneously at the plane of a transmitting waveguide aperture and on the axis of co-pole, cross pole and z-axis directed dipole by taking multiple reflections and effects of the mutual coupling automatically. Computation has been carried out to compare the relative sampled co-pole voltage pattern to the relative sampled electric field (without probe) pattern in the scan plane, and error induced by the probe is determined. The waveguide radiator reflection coefficient and admittances with the probe are altered with respect to the corresponding values when there is no probe in the near field.

Basic radiating element is the open end of the waveguide, generally terminated by an infinite metallic structure. Many authors using different approaches such as the variational, correlation matrix, and integral equation methods have studied this topic [1], [2]. The number of methods has been developed for the determination of the mutual and self admittance between radiating elements [2], [3]. Many authors used the method of moment technique to solve the waveguide problems [3], [4], [5]. In MoM, the aperture electric field is described by a summation of a number of weighted basis functions, the weights being unknown [6]. An EM wave in free space incident on a thin, finite, perfectly conducting wire was analyzed by [7]. MoM analysis of waveguide radiator and dipole, crossed dipole as the near field sensor is given by many authors [8], [9].

II. PROBLEM FORMULATION

The three dipoles i.e. along y-axis (co-pole), along x-axis (cross-pole) and along z-axis in the near field of an open ended waveguide radiator of aperture dimension 2a×2b in an infinite ground plane, is shown in Figure 1.The rectangular waveguide feeding the aperture is excited in the dominant TE_{10} mode

The incident magnetic field at the waveguide aperture for the dominant mode is given by:

$$H_x^{inc1} = -Y_0 \cos\left(\frac{\pi x}{2a}\right) e^{-j\beta z}$$

The induced current on the surface of the co-pole (parallel to y-axis) of the near-field probe is described by:

$$I = \hat{u}_y \sum_{p=1}^{M} I_{yp}\, i_{yp}$$

Where the Pulse basis function i_{yp}(p=1, 2, 3.. M) are defined by

$$i_{yp} = \begin{cases} 1 & y_{p-1} \le y \le y_p \\ 0 & elsewhere \end{cases}$$

I_{yp} is the coefficients of the pulse basis function for the co-pole

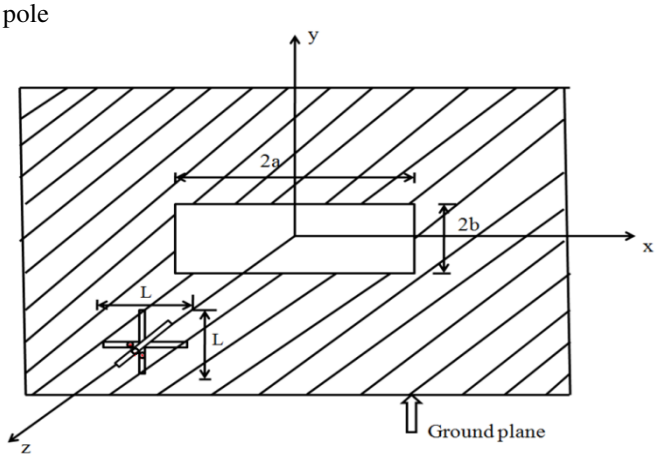

Fig.1 Dipoles connected in crossed structure as probe at the near-field of the waveguide radiator

Similarly induced current on the surface of the cross-pole (parallel to x-axis) of the near-field probe is described by:

$$I = \hat{u}_x \sum_{p=1}^{M} I_{xp}\, i_{xp}$$

Where the Pulse basis function i_{xp}(p=1, 2, 3,. M) are defined by

$$i_{xp} = \begin{cases} 1 & x_{p-1} \le x \le x_p \\ 0 & elsewhere \end{cases}$$

Similarly induced current on the surface of the z-axis directed dipole of the near-field probe is described by:

$$I = \hat{u}_z \sum_{p=1}^{M} I_{zp}\, i_{zp}$$

Where the Pulse basis function i_{zp}(p=1, 2, 3, ..., M) are defined by

$$i_{zp} = \begin{cases} 1 & z_{p-1} \le z \le z_p \\ 0 & elsewhere \end{cases}$$

Where I_{yp} , I_{xp} and I_{zp} are the coefficients of the pulse basis function for the co-pole, cross pole and z-directed dipole

The radiated magnetic field at the plane of the waveguide aperture is evaluated using the plane-wave spectrum approach and given

$$H_x^{ext} = -\frac{ab}{\pi^2 k\eta} \sum_{P=1}^{M} E_P^1$$

$$\int_{-\infty}^{\infty}\int_{-\infty}^{\infty} \frac{k^2 - k_x^2}{(k^2 - k_x^2 - k_y^2)^{\frac{1}{2}}}\, sinc\,(k_y b)\, \frac{\left\{\begin{matrix} jsin(k_x a) & p\ even \\ \cos(k_x a) & p\ odd \end{matrix}\right\}}{\frac{p\pi}{2}\left\{1 - \left(\frac{2ak_x}{p\pi}\right)^2\right\}}\, e^{j(k_x x + k_y y)}\, dk_x\, dk_y$$

The radiated electric field at the near-field probe also evaluated using the plane-wave spectrum approach give the electric field components at the probe as below:

$$E_y = -\frac{ab}{\pi^2} \sum_{P=1}^{M} E_p$$

$$\int_{-\infty}^{\infty}\int_{\infty}^{\infty} sinc\,(k_y b)\, \frac{\left\{\begin{matrix} jsin(k_x a) & p\ even \\ \cos(k_x a) & p\ odd \end{matrix}\right\}}{\frac{p\pi}{2}\left\{1 - \left(\frac{2ak_x}{p\pi}\right)^2\right\}}\, e^{j(k_x x + k_y y - k_z z)}\, dk_x\, dk_y$$

$$E_z = -\frac{ab}{\pi^2} \sum_{P=1}^{M} E_p$$

$$\int_{-\infty}^{\infty}\int_{\infty}^{\infty} \frac{k_y}{k_z} sinc\,(k_y b)\, \frac{\left\{\begin{matrix} jsin(k_x a) & p\ even \\ \cos(k_x a) & p\ odd \end{matrix}\right\}}{\frac{p\pi}{2}\left\{1 - \left(\frac{2ak_x}{p\pi}\right)^2\right\}}\, e^{j(k_x x + k_y y - k_z z)}\, dk_x\, dk_y$$

Internally scattered field obtained by using the modal expansion approach, gives the x-component of the internally scattered magnetic field:

$$H_x^{int} = \sum_{P=1}^{M} E_p\, Y_{po}^e \sin\left\{\frac{\mathrm{m}\pi}{2\mathrm{a}}(\mathrm{x} + \mathrm{a})\right\}$$

At any observation point, on the axis of co pole, the y-component of the electric field scattered by the induced current on the co-pole given by:

$$E_y^s = \frac{\lambda\sqrt{\frac{\mu}{\varepsilon}}}{8\pi^2 j}\int_{-l/2}^{l/2} I_{yp}\frac{e^{-jkR_1}}{R_1^5}\,[(1 + jkR_1)(2R_1^2 - 3a_w^2) + k^2 a_w^2 R_1^2]\, dy'$$

Where $R_1 = \sqrt{a_w^2 + (y - y')^2}$

The field at the axis of the cross-pole (oriented along x-axis) scattered by the induced current on that pole is given by:

$$E_x^s = \frac{\lambda\sqrt{\frac{\mu}{\varepsilon}}}{8\pi^2 j}\int_{-l/2}^{l/2} I_{xp}\frac{e^{-jkR_1}}{R_1^5}\,[(1 + jkR_2)(2R_2^2 - 3a_w^2) + k^2 a_w^2 R_2^2]\, dx'$$

Where $R_1 = \sqrt{a_w^2 + (x - x')^2}$

Similarly the field at the axis of the cross-pole (oriented along x-axis) scattered by the induced current on that pole is given by:

$$E_z^s = \frac{\lambda\sqrt{\frac{\mu}{\varepsilon}}}{8\pi^2 j}\int_{-l/2}^{l/2} I_{xp}\frac{e^{-jkR_1}}{R_1^5}\left[(1+jkR_2)(2R_2^2-3a_w^2)+k^2\,a_w^2\,R_2^2\right]dz'$$

Where $R_1=\sqrt{a_w^2+(z-z')^2}$

The electric field on the co-pole due to current on the cross-pole (mutual coupling effect) is obtained as

$$E_y^{mx} = \frac{\lambda\sqrt{\frac{\mu}{\varepsilon}}}{16\pi^3 j}$$

$$\int_{x'=-l/2}^{l/2}\int_{\phi'=0}^{2\pi} I_{xp}\frac{e^{-jkR_4}\,(x-x')(y-y')(3+3jkR_4-k^2R_4^2)}{R_4^5}\,dx'\,d\phi'$$

Where $R_4=\sqrt{\rho^2+a_w^2-2\rho a_w cos\phi'(x-x')^2}$

The field on the cross-pole due to current on the co-pole is given by:

$$E_x^{my} = \frac{\lambda\sqrt{\frac{\mu}{\varepsilon}}}{16\pi^3 j}$$

$$\int_{y'=-l/2}^{l/2}\int_{\phi'=0}^{2\pi} I_{yp}\frac{e^{-jkR_5}\,(x-x')(y-y')(3+3jkR_5-k^2R_5^2)}{R_5^5}\,dy'\,d\phi'$$

The field on the z-directed dipole due to current on the cross-pole is given by:

$$E_z^{mx} = \frac{\lambda\sqrt{\frac{\mu}{\varepsilon}}}{16\pi^3 j}$$

$$\int_{x'=-l/2}^{l/2}\int_{\phi'=0}^{2\pi} I_{xp}\frac{e^{-jkR_3}\,(x-x')(z-z')(3+3jkR_3-k^2R_3^2)}{R_3^5}\,dx'\,d\phi'$$

Where $R_3=\sqrt{a_w^2+(z-z')^2}$

The field on the z-directed dipole due to current on the co-pole is given by:

$$E_z^{my} = \frac{\lambda\sqrt{\frac{\mu}{\varepsilon}}}{16\pi^3 j}$$

$$\int_{y'=-l/2}^{l/2}\int_{\phi'=0}^{2\pi} I_{yp}\frac{e^{-jkR_3}\,(y-y')(z-z')(3+3jkR_3-k^2R_3^2)}{R_3^5}\,dy'\,d\phi'$$

Where $R_3=\sqrt{a_w^2+(z-z')^2}$

Imposition of Boundary Condition

In this analysis the co-pole axis is parallel to the y-direction and the cross-pole axis is parallel to the x-direction and another dipole parallel to z-axis is considered.

The boundary conditions are imposed at the plane of the waveguide aperture, on the axis of the co-pole, on the axis of the cross-pole and on the axis of z-directed dipole. The boundary condition at the region of the waveguide aperture is the tangential component of the magnetic field both inside and outside the waveguide is identical. The boundary condition on the axis of the pole is the total tangential component of the electric field is zero.

At the region of the aperture, we consider four sources producing the fields – (1) the source in the waveguide exciting the mode, (2) the magnetic current source at the aperture, (3) the electric current source on the surface of the co-pole (4) electric current source on the surface of the cross-pole and (5) electric current source on the surface of the z-directed dipole. Using the principle of superposition, the x-component of the magnetic field at the plane of the aperture is derived.

At the z=0 plane, using superposition,

$$2H_x^{inc}+2H_x^{int1}=H_x^{ext1}+H_x^{extco}+H_x^{extcr}+H_x^{extzd} \qquad (A)$$

Along the axis of the co-pole and cross-pole and z-axis, the fields are respectively given by

$$E_y^{inc}+E_y^{mx}+E_y^{scat}+E_y^{mz}=0 \qquad (B)$$

$$E_x^{inc}+E_x^{my}+E_x^{scat}+E_x^{mz}=0 \qquad (C)$$

$$E_z^{inc}+E_z^{mx}+E_z^{scat}+E_z^{my}=0 \qquad (D)$$

The weighting functions and the moment of the field are defined as follows:

$$w_q^1=\left\{\sin\left\{\frac{q\pi}{2a}(x+a)\right\}\right\}\quad\begin{cases}-a\le x\le a\\-b\le y\le b\end{cases}$$

0 elsewhere

$$\langle H,w_q^1\rangle=\iint_{surface} H,w_q^1\,dx\,dy \qquad (E)$$

In addition, since the current on the pole of the probe is described by *M* basis functions, *M* unknowns are to be determined from the boundary condition. The weighting functions and the moment of the field is defined as follows:

$$w_q^2=\left[\delta(h-h_q)\right]=[\delta(h-h_1),\delta(h-h_2),\dots\dots]$$

Where h specifies a position with respect to some reference (origin), and h_q represents a point at which the boundary condition is enforced.

$$\langle E,w_q^2\rangle=\iint_{surface} E,w_q^2\,ds \qquad (F)$$

Using the boundary conditions given by Equations (A), (B), (C) and (D) and definition in Equations (E) and (F) and converting into matrix form,

RESULTS

The aperture in an infinite ground plane fed by a standard X-band WR-90 rectangular waveguide is used as a radiator and three dipoles, each of length 0.47λ and radius 0.005λ, connected in crossed configuration are used as a near-field probe. The lumped load of 50Ω is connected at co-pole, cross-pole and z-axis directed dipole at a distance of one segment (one pulse basis function) away from the centre of the poles as shown in Figure.1. For the determination of the coefficients of the basis functions, the program written in MATLAB 12 was

run on a 3 GHz Pentium 4 computer. The computation has been carried out to sample the co-pole voltage and electric field (without probe) in transverse (x-y) scanning plane at 10 GHz to compare the normalized (relative) sampled co-pole voltage pattern with the normalized (relative) sampled electric field pattern (without probe). Since the normalized sampled co-pole voltage (as co-pole voltage has dominant effect than the cross pole and z-directed dipole voltages) and field are compared, zero error is enforced at the center of the scan plane. These plots are shown in Figure 2, Figure 3 and Figure 4 in the scanning plane at x=0, and z=0.15λ, 0.25 λ and 0.5 λ respectively. The error in the normalized voltage pattern with respect to the normalized electric field (without probe) pattern is determined. The sampled co-pole voltage phase and sampled electric field phase (without probe) in the scanning plane at x=0, and z=0.15λ, 0.25λ and 0.5λ are shown in Figure 5, Figure 6 and Figure 7 respectively. The radiator absolute reflection coefficients in the presence of the near-field measuring probe with each pole length L =1.41 cm and radius a_w =0.015 cm, (designed at 10 GHz) at x=0, y=0 and z= 0.75 cm, 1.5cm, 3.0cm, and in the absence of the probe, over 8 to 12 GHz, are plotted in Figure 8. The corresponding reflection coefficient phases are shown in Figure 9. The computation for radiation conductance and susceptance has been carried out in the presence three dipoles connected in a crossed-structure used as a probe with each pole length L =1.41 cm and radius a_w =0.015 cm, at x=0, y=0 and z=0.75cm, 1.5cm, 3.0cm, and in the absence of the probe over 8 to 12 GHz, and is shown in Figure 10 and Figure 11.

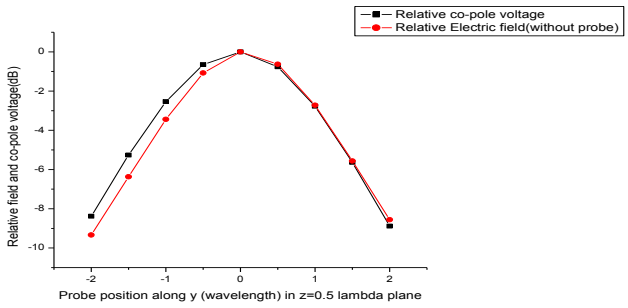

Fig.2

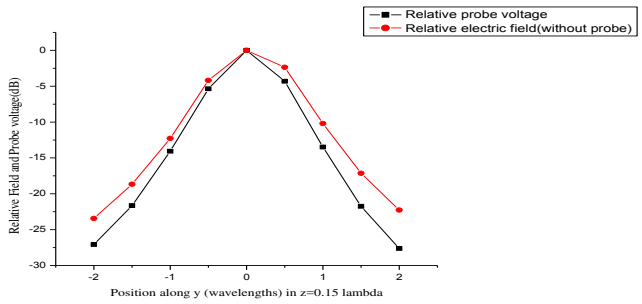

Fig.3

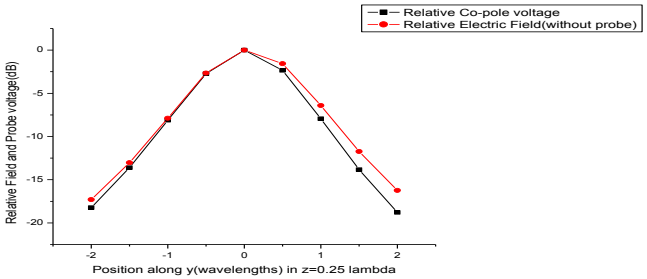

Fig. 4

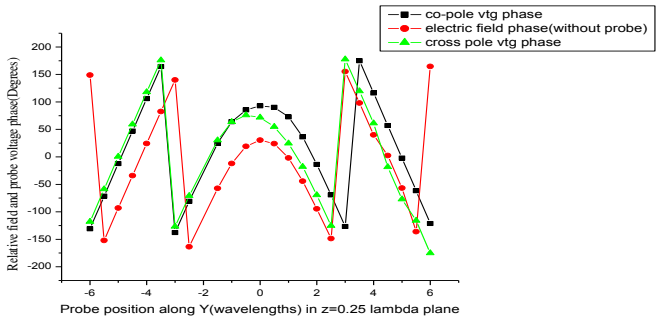

Fig.5

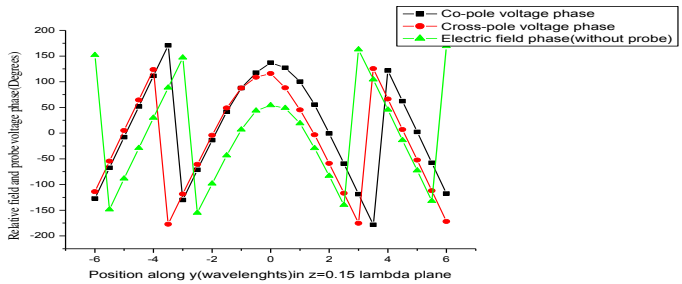

Fig.6

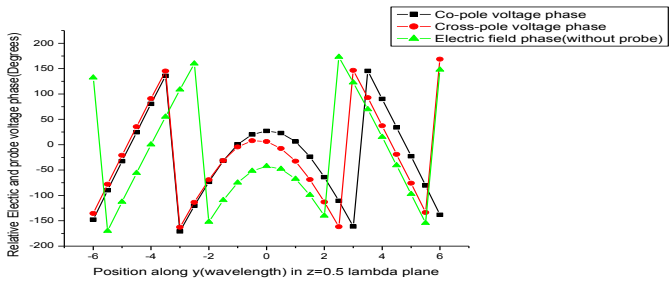

Fig.7

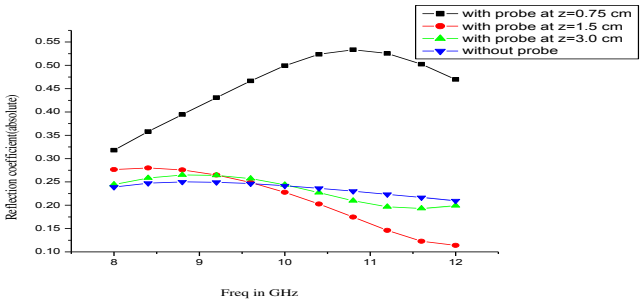

Fig.8

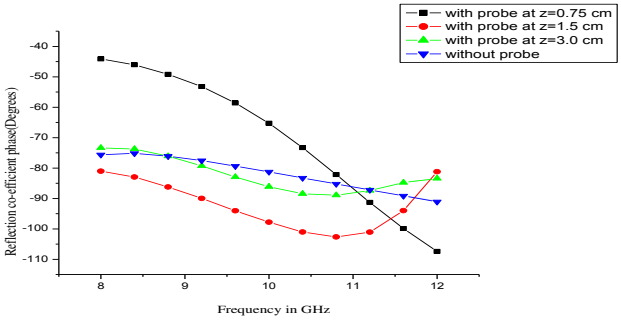

Fig.9

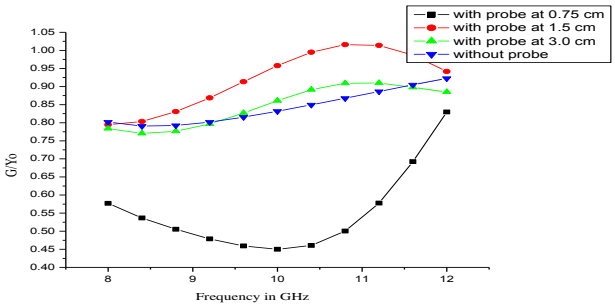

Fig.10

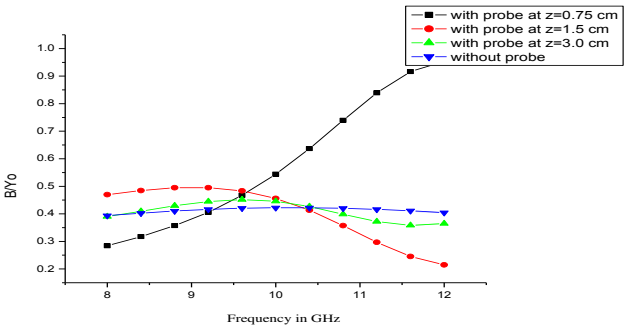

Fig.11

CONCLUSION

The three dipoles connected in crossed structure, which are used as a near-field measuring probe induces error in the near-field, because of multiple reflections between radiator and probe, and effects of mutual coupling between poles of the probe. The error in the relative sampled co-pole voltage pattern with respect to the relative sampled electric field (without probe and in co-pole direction) pattern is presented in Figures 2, 3 and 4. As the probe approaches the radiator, the error induced by the probe is increased. Figure 5, 6 and 7 show the variation of the co-pole voltage phase with respect to electric field phase (co-pole direction) in the scan plane. In the presence of the near-field measuring probe, the radiator reflection coefficient and admittance are changed and presented in Figure 7, 8, 9 and 10. When the separation between radiator and probe is small, the deviations of the reflection coefficient and admittance are larger with respect to the corresponding values than when there is no near-field probe. As the separation increases, the deviation is smaller, and for larger separation, the reflection coefficient and admittance values approach the values obtained, when there no probe in the near-field. However, due to multiple reflections between radiator and probe, near-field values and radiation characteristics of the waveguide radiator are changed.

REFERENCES

[1] G.V.Borgiotti, “Fourier transform method in aperture antenna problems,” Alta Frequenza, vol. 32, Nov. 1963.

[2] R. J. Mailloux, “Radiation and near-field coupling between two collinear open-ended waveguides,” IEEE Trans. On Antennas and Propagation, vol. AP-17, Jan. 1969.

[3] J. Luzwick and R. F. Harrington, “Mutual coupling analysis in a finite planar rectangular waveguide antenna array,” Electromagnetics, vol. 2, pp. 25-42, January- March 1982

[4] R F. Harrington, and J. R. Mautz, “A generalized network formulation for aperture problems,” IEEE Trans. on Antennas and Propagation, vol. AP-24, pp. 870-873, Nov. 1976.

[5] H. Baudrand, Jun-Wu Tao and J. Atechian, “Study of radiating properties of open-ended rectangular waveguides,” IEEE Trans. on Antennas and Propagation, vol. AP-36, pp. 1071-1077, Aug. 1988.

[6] R. F. Harrington, Field computation by moment methods. USA: Roger E. Krieger Publishing Company.

[7] K. K. Mei, “On the integral equations of thin wire antennas,” IEEE Trans. on Antennas and Propagation, vol. 13, issue 3, pp. 374-378, May 1965.

[8] Paramesha and A. Chakrabarty, “Near-Field Distraction due to the Probe,” International conference on Antenna and Technology, Feb. 2005, Space Application Center, ISRO, Ahmedabad.

[9] Paramesha and A. Chakrabarty, “Near-Field Measurement Using Crossed-Dipole,” International Radar Symposium India, IRSI-05, December 2005, Bangalore.

Power Quality Enhancement using ANN-based Optimal Placement of D-STATCOM in a Radial Distribution System

Bharath Y.K.
Dept. of EE Engg., Malnad College of Engineering, Hassan, KA, India
bharath99yk@gmail.com

Purushothama G.K.
Dept. of EE Engg., Malnad College of Engineering, Hassan, KA, India
gkuttama@gmail.com

***Abstract*— This paper presents an ANN-based technique to find an optimal location for the placement of Distribution Static Compensator (D-STATCOM) in a radial distribution system. This method proves to be suitable for both interconnected as well as radial distribution systems. The main feature of this technique is that the optimal bus in which the D-STATCOM is to be placed can be found just by knowing the system parameters, without the need of practical experimentation causing transient conditions. The system is modeled in Matlab/Simulink environment and case studies are performed on it. ANN is trained offline and optimal bus is identified using the training performance. The implementation on a radial feeder situated in Hunsinkere, Hassan illustrate the effectiveness of the proposed technique.**

***Index Terms*—Power quality, Voltage sag mitigation, D-STATCOM, ANN.**

I. INTRODUCTION

The Power Quality is gaining greater importance in distribution systems because of the increased sophisticated loads. Voltage sag is one of the problems related to power quality. This phenomenon happens continuously in transmission and distribution systems. According to IEEE Std. 1159-1995, voltage sag (also known as voltage dip) has been defined as reduction in the Root Mean Square (RMS) voltage in the range of 0.1 to 0.9 per unit (p.u.) for duration greater than half a cycle and less than one minute [1]. Short circuits, transformer energizing, capacitor bank charging are some of the causes of voltage sag. Voltage sag has been considered to be a serious power quality problem faced by many utilities as it may significantly affect industrial production as well as consumer equipments.

Apart from other factors, the load in a distribution system varies with the time of the day as well as seasons. In deregulated environment the generation pattern also continuously changes. Hence, the power flow in distribution system varies even under steady state condition. But, the occurrence of a fault anywhere in the power system may overload the lines and can become a threat to the system security. If a system is operating close to the security limits, even a small disturbance also can lead to power swings and cascade tripping of circuit breakers and tripping of distribution lines. The increase in the loading of distribution lines sometimes can lead to congestion in the network as well as voltage collapse. Such problems can be resolved by means of custom power devices, which have fast and dynamic control over real and reactive power.

Development of compensators to enhance power quality has been an area of active research for the past few decades. Passive compensators like shunt reactors and capacitors are uncontrolled devices and are inadequate for continuous variation in parameters. With the advancement in power electronics, new controllers known as Flexible AC Transmission System (FACTS) have been developed. These controllers are effective in power flow control, reactive power compensation and enhancement of stability margin in AC networks. Power electronics based controllers used in distribution systems are known as custom power devices [2]. Placement of custom power devices like Distribution Static Compensator (D-STATCOM) proves to be an effective remedy for solving power quality problems.

The cost of D-STATCOM is high and their control is found to be effective when they are optimally placed, hence optimal placement of D-STATCOM is necessary in a distribution network.

There are different strategies to optimally place the FACTS devices for transmission lines and for distribution systems. Both mathematical and meta-heuristic (Artificial Intelligent) methods are used for this optimal placement. Among the AI methods, the Artificial Neural Network (ANN) based methodology has been successfully used for the distribution networks to find the optimal location for the placement of D-STATCOM [3].

ANN technique suits to be effective in this case there are a number of parameters that are required to be considered, and ANN is capable of handling huge amount of data efficiently. In this work, an ANN based method is developed and implemented to place a D-STATCOM in a radial distribution system, optimally.

II. D-STATCOM AND ITS MODELING

A STATCOM is a static VAR generator, whose output is varied so as to maintain or control specific parameters of the electric power system. Controllable reactive power can be generated using dc to ac converters. The basic principle of reactive power generation by a voltage-source converter is akin to that of the conventional rotating synchronous condenser.

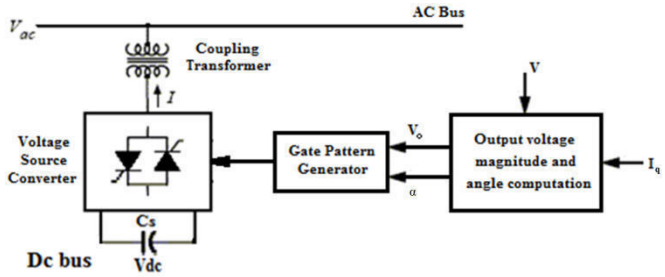

Fig. 1. STATCOM with main functions of the internal converter control.

A STATCOM comprises of a large number of gate-controlled semiconductor power switches. The gating commands for these devices are generated by the internal converter control in response to the demand for reactive and/or real power inference signals. The STATCOM with main functions of the internal converter control is shown in Fig.1. The VAR rating of STATCOM can be found using the empirical formula,

$$VAR = 314.2 \times C_{DC} \times V_{L-L}^2 \qquad (1)$$

Where C_{DC} is the capacitance of the capacitor used [2].

D-STATCOM is a reactive shunt compensator. A STATCOM when installed in a distribution system with reduced rating is known as D-STATCOM.

In the present work, the D-STATCOM is modeled in Matlab/Simulink environment and has been represented as a three-phase programmable voltage source [4] injecting reactive power to the three-phases at the point of coupling (the load bus at which D-STATCOM is placed).

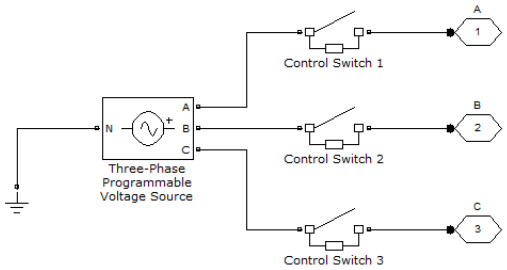

Fig. 2. Proposed D-STATCOM Simulink Model.

The D-STATCOM model is shown in Fig.2. The control scheme consists of three control switches which can be set on/off as per compensation requirement. The three switches remain open during pre-fault condition and are closed upon occurrence of faults. This permits the injection of reactive power under fault to the three-phases of D-STATCOM bus. A delay of 1 millisecond for the switching of the control switches after the occurrence of fault is given to simulate delayed response of D-STATCOM to the fault. The switches are set to open after the clearance of fault. Referring to equation (1), the maximum and minimum reactive power injection limit of D-STATCOM has been taken as +100 kVAR and -100 kVAR.

III. CASE STUDIES

The present work also involves modeling the power system network, conducting case studies on it, collection of voltage database, building and training ANN, obtaining the Mean Square Errors (MSEs), locating the optimal bus, placement of D-STATCOM and verify the field results.

The Hunsinkere radial feeder located in Hassan city is considered for case study. The feeder is drawn from a 66/11kV Master Unit Sub Station (MUSS) of Hassan. Fig.3. shows the single line diagram of Hunsinkere radial feeder. It consists of 9 load buses and the net real and reactive power demand on the feeder is 1721.5 kW and 1066.88 kVAR [7].

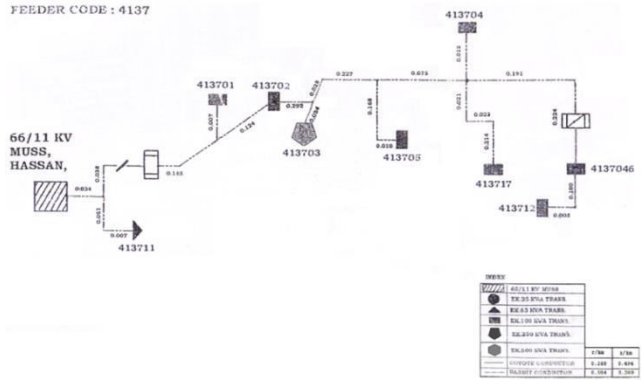

Fig. 3. Single line diagram of the radial feeder.

The simulation model of the radial distribution network under study is developed in Matlab/Simulink environment (see Fig.7.). The model is analyzed by conducting short circuit studies on it. Different types of short circuit faults viz. single line to ground (L-G), line to line (L-L), double line to ground (L-L-G) and three phase (L-L-L or L-L-L-G) faults are created in each bus for a duration of 60 milliseconds. The voltage profiles under fault conditions are tabulated in p.u. values.

For building and training ANN, train data set and target data set are required. The tabulated p.u. voltage database is given to ANN as train dataset. Target dataset is prepared to have the voltage profiles of the system under normal operating condition i.e. 1 p.u. in this case.

IV. ANN AND ITS APPLICATION

In this work, feed forward ANN with back propagation algorithm has been used to find optimal location for D-STATCOM. The architecture of this network is shown in Fig.4.

The input data p_1, p_2, …… p_R flow through the synapses weights w_{ij}. These weights amplify or attenuate the input signals before being added at the node represented by sigma. The summed data flows to the output through an activation function f. the neurons are interconnected creating different

layers. An elementary neuron with R inputs has been shown in Fig.4. Each input is weighted with an appropriate weight w. the sum of the weighted inputs and the bias b forms the input to the transfer function *f*.

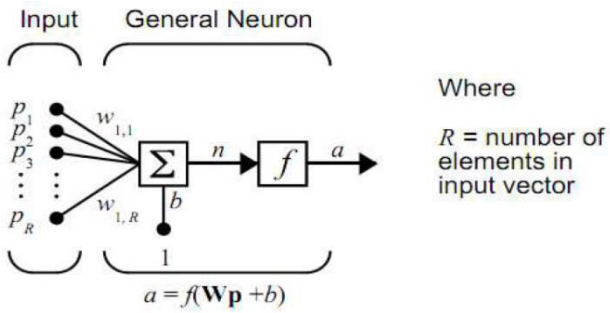

Fig. 4. Artificial Neural Network architecture

Once the network weights and biases are initialized, the network is ready for training. The training process requires a set of examples of proper network behavior, network inputs and target outputs. During training the weights and biases of the network are iteratively adjusted to minimize the network performance function. The default performance function for feed forward networks is Mean Square Error (MSE). The gradient is determined using a technique called back propagation, which involves performing computations backward through the network [5].

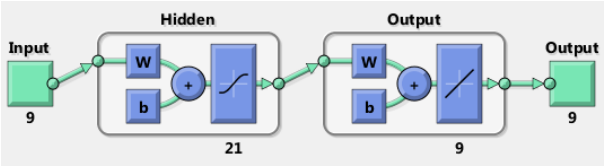

Fig. 5. ANN Structure for Hunsinkere radial feeder case.

Neural network fitting tool in neural network toolbox by Matlab is used to build the ANN [6]. When train and test datasets are presented to the network, initial weights and biases are set. The datasets are divided for training testing and validation. The number of neurons in the hidden layer is arbitrarily selected, according to a rule of thumb it must be between one to three times the numbers of the input neurons. The Multilayer Perceptron is created with one input, output and hidden layer each. The hidden layer uses tan sigmoid transfer function and the output layer uses purelin transfer function as shown in Fig.5.

The network is trained using Levenberg-Marquardt Backpropagation algorithm, which results in error and output profiles, the error represents the degree of deviation of the inputs with respect to the target outputs. The MSEs are computed from the error profile.

The bus which has the highest MSE is considered as the optimal location for the placement of D-STATCOM.

V. Results and Discussions

After the network is trained, MSEs are computed and tabulated as shown in Table I. Fig.6. shows the training performance of ANN for each bus.

TABLE I

MSEs for 9-buses

Bus	MSE
1.	0.0015
2.	0.0268
3.	0.0363
4.	0.0536
5.	0.0625
6.	**0.1223**
7.	0.0321
8.	0.0005
9.	0.0019

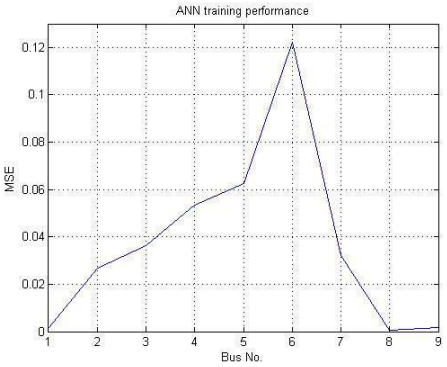

Fig. 6. ANN training performance for the radial feeder case.

The Fig. 6 indicates that bus 6 has highest MSE, hence it is the most vulnerable bus in the radial feeder. This infers that, irrespective of the bus in which a fault occurs, bus 6 experiences severe voltage sags and if a D-STATCOM is placed in bus 6, the degree of voltage sag mitigation will be higher in the system.

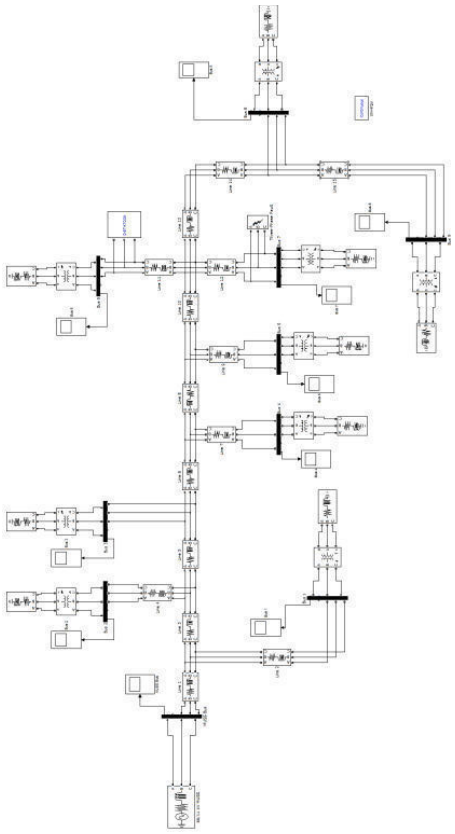

Fig. 7. Simulink model of the radial feeder with D-STATCOM

As shown in Fig.7, the D-STATCOM is placed in bus 6 with reference to ANN training performance. Different types of faults are created on bus 7, as it is the nearest bus to the D-STATCOM bus, and time domain simulations are performed. The waveforms of voltages during the occurrence of faults, with and without D-STATCOM in the radial feeder are as shown in Fig. 8-11.

Buses, which are quite far from the faulty bus, experience a relatively less magnitude of sag compared to the buses that are nearer to the faulty bus. The distance between the buses is accounted from the impedance of the lines connecting them. It can be noted from the figures that the voltage sags are efficiently mitigated by placing the D-STATCOM in the optimal bus.

D-STATCOM is placed at other buses in the radial feeder and time domain simulations with faults are performed. It was found that the performance of the compensator in mitigating the sag is relatively less in these cases compared to when the D-STATCOM is placed in optimal bus.

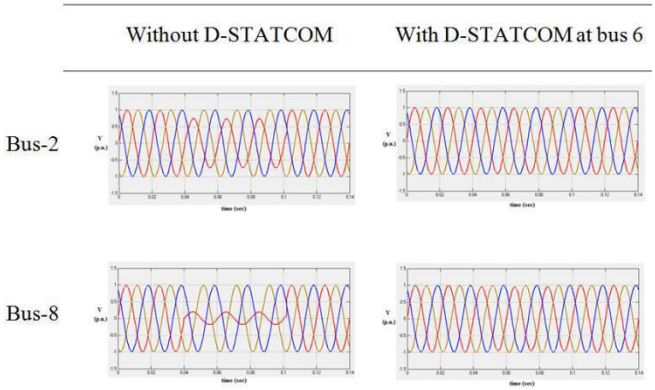

Fig. 8. Voltage profiles of Bus 2 and Bus 8 with L-G fault at Bus 7

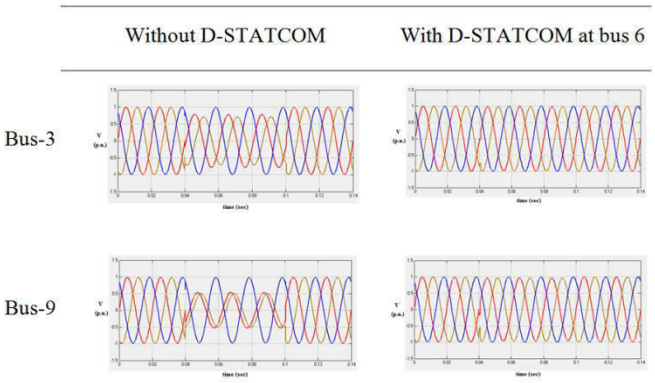

Fig. 9. Voltage profiles of Bus 3 and Bus 9 with L-L fault at Bus 7

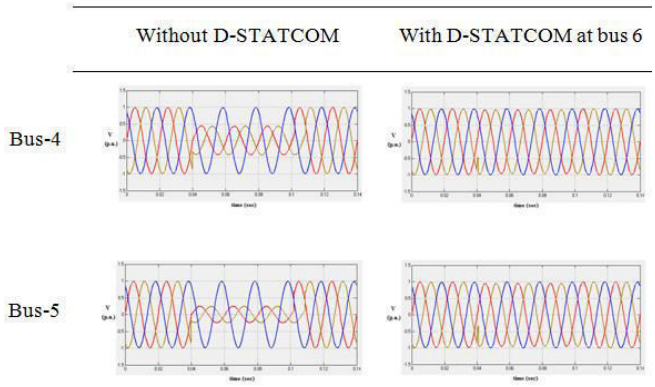

Fig. 10. Voltage profiles of Bus 4 and Bus 5 with L-L-G fault at Bus 7

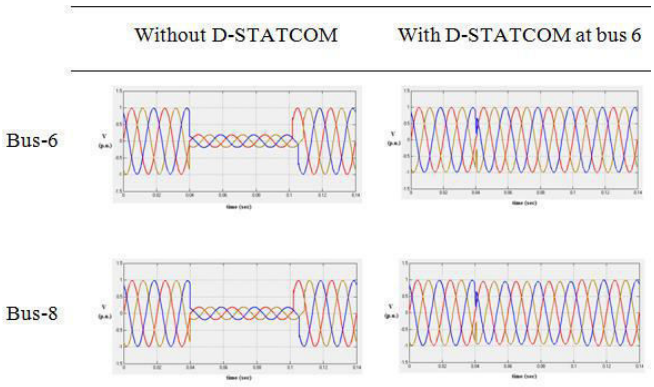

Fig. 11. Voltage profiles of Bus 6 and Bus 8 with L-L-L-G fault at Bus 7

VI. REFERENCES

[1] Roger C. Dugan, Mark F. McGranaghan, Surya Santoso, H. Wayne Beaty, Electrical Power Systems Quality, Second Edition.

[2] Narain G. Hingorani, Laszlo Gyugyi, Understanding FACTS concepts and technonogy of Flexible AC Transmission Systems, Standard Publishers Distributors, 2001.

[3] D.K. Tanti, Brijesh Singh, Dr. M.K. Verma and Dr. O.N. Mehrotra, "An ANN Based Approach for Optimal Placement of DSTATCOM for Voltage Sag Mitigation", *International Journal of Engineering Science and Technology,* vol. 3 No. 2 Feb 2011.

[4] Pooja Prasad Kulkarni, Nitin D. Ghawghawe, "A Review Paper on Optimal Location and Parameter Setting of FACTS to Improve the Performance of Power System", *International Journal of Electrical, Electronics and Data Communication,* vol. 1, Issue 4.

[5] Simon Haykin, Neural Networks a Comprehensive Foundation, Second Edition, Pearson, 2005.

[6] MATLAB 7.0 User's Guides for SimPower Systems and Neural Network Toolbox.

[7] Data sheets of Hunsinkere feeder line from KPTCL.

Solving Discrete Logarithm Problem using Modified Index Calculus

***Jayanth Jain*[1], *Akarsh Mohan*[2] *and Dr. B.R.Sujatha*[3]**

[1] *Software Developer – Security Services, Novell Software, Bangalore, India, jain98366@gmail.com*
[2] *Systems Engineer – Application Development and Maintenance, Infosys Limited, Mysore, India, akarshphenom@gmail.com*
[3] *Associate Professor, Department of E&C Engineering, Malnad College of Engineering, Hassan, India, brshsn61@gmail.com*

***Abstract*— The Discrete Logarithm Problem (DLP) has acquired additional importance in recent years due to its applicability in cryptography. Several cryptographic systems would become insecure if an efficient discrete logarithm algorithm were discovered. The difficulty of the DLP lies in the fact that it has a "one-way" property. Its computational complexity is measured by the computing time of the algorithm used to solve this mathematical problem. In this paper, we describe a method that will enhance the computational speed of solving a DLP by modifying the Index Calculus method with virtually no added implementation complexity.**

Keywords— Integer Factorization; Discrete Logarithm Problem (DLP); Rivest-Shamir-Adleman (RSA); Diffie–Hellman Key Exchange (D-H); Elliptic Curve Cryptography (ECC);

I. INTRODUCTION

Most cryptographic algorithms which are based on complex mathematical problems are designed around computational hardness assumptions, making them hard to break in practice by any adversary. Hence the algorithms such as Integer Factorization and Discrete Logarithm Problem are termed computationally secure.

A. An Overview of Integer Factorization

Integer Factorization is the decomposition of a composite number into a product of smaller integers. If the integers are prime numbers, the process is called Prime Factorization. The problem of finding the prime factors of large composite numbers has always been of mathematical interest. With the advent of public key cryptosystems it is also of practical importance, because the security of some of the cryptosystems such as the Rivest-Shamir-Adleman (RSA) depends on the difficulty of factoring the public keys [1].

Let P & Q be two large integers and N be the product of these two numbers. The Integer Factorization is the problem of finding the decomposed integers P & Q.

$$N = P \times Q \qquad (1.1)$$

Integers P & Q are called Integer factors of N.

B. An Overview of Discrete Logarithm Problem

Discrete Logarithm Problem is a mathematical problem that arises mainly during key generation process of Diffie–Hellman Key Exchange (D-H) algorithm and in Elliptic Curve Cryptography (ECC).

Let F_p be a finite field of prime numbers, p be a large prime, g be a primitive root for F_p and h be a non-zero element of F_p. The Discrete Logarithm Problem is the problem of finding an exponent x such that

$$g^x = h \ (mod\ p) \qquad (1.2)$$

The number x is called the discrete logarithm of h to the base g and is denoted by $log_g(h)$.

It is a well-posed problem to find an integer exponent x such that $g^x = h$. However if there is one solution, then there will be infinitely many solutions because $g^{p-1} = 1 \ (mod\ p)$. Hence if x is a solution to $g^x = h$, then $x+k(p-1)$ is also a solution for every value of k [2].

C. Smooth Numbers

If all the prime factors of a number N is less than or equal to an integer B, then that integer N is called *B-smooth* number.

For example, 5544 has prime factorization $2^3 \times 3^2 \times 7 \times 11$; therefore 5544 is *11-smooth* because none of its prime factors are greater than 11.

The function $\Psi(X, B)$ counts *B-smooth* numbers.
$\Psi(X, B)$ = *number of B-smooth integers n such that* $1 < n \leq X$

For Example, $\Psi\ (30, 5) = 17$, since the count of 5-smooth numbers between 1 and 30 is 17.

2, 3, 4, 5, 6, 8, 9, 10, 12, 15, 16, 18, 20, 24, 25, 27, 30

The total number of prime numbers less than or equal to B is called factor base of B. For example, factor base of 5 is 3 since the total number of prime numbers less than or equal to 5 is 3 (2, 3 & 5).

D. Safe Prime

An integer P is called safe prime if it is of the form 2q+1 where q is a prime number. For example, 227 is a safe prime because 227 can be written in the form 2(113) + 1.

Safe prime plays an important role in cryptography because it is used in algorithms like RSA and D-H as integer factorization becomes difficult if 2q+1 is a safe prime.

E. Chinese Remainder Theorem

The Chinese remainder theorem, describes the solutions to a system of simultaneous linear congruences. The simplest situation is a system of two congruences,

$$x \equiv a \pmod{m} \text{ and } x \equiv b \pmod{n}, \quad (1.3)$$

with *gcd (m,n) = 1*, in which case the Chinese remainder theorem says that there is a unique solution modulo *mn* [3].

Let $m_1, m_2, \ldots, m_k$ be a collection of pairwise relatively prime integers. i.e.,

$$\gcd(m_i, m_j) = 1 \text{ for all } i \neq j$$

Let $a_1, a_2, \ldots, a_k$ be arbitrary integers. Then the system of simultaneous congruences

$$x \equiv a_1 \pmod{m_1},\ x \equiv a_2 \pmod{m_2}, \ldots,\ x \equiv a_x \pmod{m_k} \quad (1.4)$$

has a solution $x = c$. Further, if $x = c$ *and* $x = c'$ are solutions, then

$$c \equiv c' \pmod{m_1 m_2 \ldots m_k} \quad (1.5)$$

The Chinese remainder theorem has many applications in number theory and other areas of mathematics, especially in solving certain instances of Discrete Logarithm Problem.

Example to describe Chinese remainder theorem:

$x \equiv 1 \pmod{5}$ and $x \equiv 9 \pmod{11}$

Since *gcd (5,11) =1*, there is a unique solution *x=31*, such that

$31 \equiv 1 \pmod{5}$ and $31 \equiv 9 \pmod{11}$

II. ALGORITHMS TO SOLVE INTEGER FACTORIZATION

A. Pollard's p-1 Factorization Algorithm

Pollard's p-1 factorization algorithm is a method to factorize large integers. Although not useful for all numbers, there is a certain type of numbers for which it is quite efficient. In Integer factorization, focus is to determine two prime factors *p & q (N=pq).* This algorithm is based on a method to find an integer L with a property *p-1* divides L and *q-1* does not divides L i.e., there are integers *i, j* and *k* with $k \neq 0$; such that

$$L = i(p-1) \text{ and } L = j(q-1) + k$$

Suppose we take a random integer *a* and compute a^L, then

$$a^L = a^{i(p-1)} = (a^{p-1})^i = 1^i = 1 \pmod{p}$$

$$a^L = a^{j(q-1)+k} = a^k (a^{q-1})^j = a^k = a^k \pmod{p} \quad (2.1)$$

We can recover *p* through simple GCD computation.
i.e., $p = gcd(a^L - 1, N)$. Hence $q = N/p$

B. Factorization via Difference of Squares

Factorization via Difference of Squares is based on simple mathematical formula

$$a^2 - b^2 = (a + b)(a - b)$$

In order to factor a number N, we look for an integer *b* such that the quantity $N + b^2$ is a perfect square and equal to a^2.
$N + b^2 = a^2$, so

$$N = a^2 - b^2 = (a + b)(a - b) \quad (2.2)$$

Then the factors of N can be recovered by computing *gcd (N, a+b)* and *gcd (N, a-b)* [1].

III. ALGORITHMS TO SOLVE DLP

Discrete Logarithm Problem is quite impossible to attack by brute-force method. Hence we must use mathematics to have any chance of finding logarithms in large groups. Different types of algorithms to attack DLP have been formulated over several decades. The most prominent one is Index Calculus.

A. Index Calculus

Index Calculus algorithm can be employed to solve DLP using smooth numbers and is based on the idea that if we can find Discrete Logarithm of a small and independent element, then we should be able to determine discrete logarithm of almost any element in the group as most of the elements can be expressed in terms of small independent elements whose logs are known [4].

The idea behind the Index Calculus is fairly simple – to solve DLP.

$$g^x = h \pmod{p}$$

where the prime *p*, integer *g* and *h* are known. For simplicity, we assume *g* is a primitive root modulo *p*, so its power gives all of F_p^*.

Index Calculus rely on finding a value *B* (Smooth Number) and obtaining it's factor base and solving the discrete logarithm problem for its factor base, i.e.,

$$g^x = l \pmod p \text{ for all primes } l \le B$$

In other words, we are computing the discrete logarithm $log_g l$ for each prime $l \le B$. After finding the discrete logarithm of factor base of B, we then compute the quantities

$$h \times g^{-k} \pmod p \text{ for } k = 1,2,...$$

until we find the value of k such that $h \times g^{-k}$ is *B-smooth*. For this value of k, we have

$$h \times g^{-k} = \prod_{l \le B} l^{e_l} \pmod p \quad (3.1)$$

for certain exponents e_l Equation 3.1 can be re-written as

$$log_g(h) = k + \sum e_l log_g l \pmod{p-1} \quad (3.2)$$

since $log_g l$ has already been computed and value of h is known, $log_g h$ can be easily found which in turn solves discrete logarithm problem [5].

B. Known Challenges in Index Calculus

1. *Choosing appropriate B:* It is difficult to find optimized value of B who's factor base contains all factors of $h \times g^{-k}$
2. *Solving $log_g l$:* In current index calculus algorithm, we obtain linear equations for all prime numbers in factor base of B and solve $log_g l$ for all these prime numbers which is computationally expensive.

After computing $log_g l$ for all factor base of B, if we cannot find $h \times g^{-k}$ whose factors are not in factor base of B, we have to increase the value of B and solve $log_g l$ for all the prime numbers in factor base of new value of B [6] [7].

IV. MODIFIED INDEX CALCULUS

To overcome the challenges faced in the original Index Calculus method, in this paper we describe a method to solve DLP by modifying Index Calculus such that it does not rely on finding discrete logarithm of all the prime numbers in the factor base of B.

The idea behind the modified index calculus is to factorize

$$h \times g^{-k} \pmod p \text{ for } k = 1,2,3.....$$

and look for an optimized value of k i.e..,

$$h \times g^{-k} \pmod p = R \quad (4.1)$$

where R is divisible by a small prime number n such that R/n should not be a safe prime (should not be of the form $2q+1$, where q is a prime number). This ensures that it can be integer factorized to a small prime factor using algorithms such as *Pollard's p-1 factorization algorithm* and *Factorization via difference of squares*. Hence, on integer factorization of R, we obtain

$$R = n \times l_1^{e_1} \times l_2^{e_2} \times .....\times l_m^{e_m} \quad (4.2)$$

The modified index calculus relies on finding discrete logarithm of only the factors of R i.e.,

$$g^{x_i} = n^{a_i} \times l_1^{e_{i1}} \times l_2^{e_{i2}} \times .....\times l_m^{e_{im}} \pmod p \; i \text{ from } 1 \text{ to } m \quad (4.3)$$

Applying log_g to Equation 4.3, we get

$$x_i = a_i log_g n + e_{i1} log_g l_1 + e_{i2} log_g l_2 + \ldots\ldots + e_{im} log_g l_m \quad (4.4)$$

solving for $log_g l$ in terms of linear equations,

$$\begin{pmatrix} a_1 & e_{11}\ldots\ldots e_{im} \\ a_2 & e_{12}\ldots\ldots e_{2m} \\ . & . \quad . \\ . & . \quad . \\ . & . \quad . \\ a_m & e_{1m}\ldots\ldots e_{mm} \end{pmatrix} \begin{pmatrix} log_g n \\ log_g l_1 \\ . \\ . \\ . \\ log_g l_m \end{pmatrix} = \begin{pmatrix} X_1 \\ X_2 \\ . \\ . \\ . \\ X_m \end{pmatrix}$$

From Equation 4.1 and Equation 4.2, we have

$$h \times g^{-k} \pmod p = R = n \times l_1^{e_1} \times l_2^{e_2} \times \ldots \times l_m^{e_m} \pmod p \quad (4.5)$$

Applying log_g and re-arranging Equation 4.5, we get:

$$log_g h = k + log\ n + e_1 log\ l_1 + ...+ e_m log\ l_m \pmod p \quad (4.6)$$

Since the values of $log\ n$, $log\ l_1 \ldots\ldots log\ l_m$ are obtained from the above matrix, $log_g h$ can be easily computed which is the solution of discrete logarithm problem.

A. Advantages of Modified Index Calculus

1. *Choosing appropriate B is not required:* There is no need to find the optimized value of B who's factor base contains all factors of $h \times g^{-k}$
2. *Solving $log_g l$ for all the factor base of B is not required:* Since we first factorize $h \times g^{-k}$ and take the optimized value, it is sufficient to find $log_g l$ for only the factors of $h \times g^{-k}$ and not for the entire factor base of B.

The above advantages have a huge impact on solving DLP using Index Calculus algorithm as it reduces the computation overhead of finding B and obtaining it's factor base and finding $log_g l$ for all primes in factor base although most of them are not used in solving Discrete Logarithm Problem.

V. CONCLUSION AND FUTURE WORK

Increasing the speed of solving discrete logarithm problem will have a huge impact on applications that rely on discrete

log problem. In this paper, we described a method that will enhance the computational speed of solving a DLP by modifying the Index Calculus method.

We believe that this initial work can be further extended to efficiently solve Elliptic Curve Discrete Logarithm Problem [ECDLP]. Since Elliptic Curve Digital Signature Algorithm [ECDSA] which is the elliptic curve analogue of DSA relies on the speed of solving discrete logarithm in elliptic curve, our proposed method can further enhance the speed of solving ECDLP.

VI. REFERENCES

1. Jeffrey Hoffstin, Jill Pipher and Joseph Silverman, *An Introduction to Mathematical Crytography,* Springer Publications, 2008.

2. Pohlig, S and Hellman, M, "An improved algorithm for computing logarithms over GF (p) and its cryptographic significance", IEEE Transaction on Information Theory, Vol.24, pp.106-110, 1978.

3. Diffie, W, and Hellman, M. E., "New directions in cryptography", IEEE Trans. Inform. Theory, Vol.22, No.6, pp.644-654, 1976.

4. J.-Ch. Faugere, L. Perret, Ch. Petit, and G. Renault, "Improving the complexity of index calculus algorithms in elliptic curves over binary fields", in EUROCRYPT 2012, LNCS 7237, pp.27-44, Springer 2012.

5. Padmavathy, R and Bhagvati, C, "Methods to Solve Discrete Logarithm Problem for Ephemeral Keys", Advances in Recent Technologies in Communication and Computing, pp.704–708, Oct 2009.

6. Ming-deh Huang, Wayne Raskind, "Signature calculus and discrete logarithm problems", ANTS VII, LNCS 4076, 2006.

7. Oliver Schirokauer, Damian Weber, Thomas Denny, "Discrete Logarithms: the Effectiveness of the Index Calculus Method", 1996.

8. Pierrick Gaudry, "Index Calculus for Abelian Varieties and the Elliptic Curve Discrete Logarithm Problem", 2004.

ARIMA Model to Forecast Future Points in the Dataset of Partial Discharge

N. S. Jyothi
Department of Electrical & Electronics Engineering,
Malnad College of Engineering, Hassan, India

ABSTRACT

The overall reliability of a power transformer depends largely on the smooth operation of the transformer bushings. In the recent past, a revolutionary new class of insulating materials called resin impregnated paper (RIP) with superior thermal and electrical performance has introduced and has now become the insulation of choice. However, their long time electrical and thermal performances need to be carefully assessed. The performance and life of a bushing depends on the parameters like partial discharge, dissipation factor, degree of polymerization and breakdown voltage. This paper, considering the measured values of partial discharge data over a period as a non-stationary stochastic process, proposes a well-found methodology in classical time series analysis known as Box-Jenkins methodology to forecast its future values. This method proposes a set of rules that guides the analyst in the process of deriving a suitable model from a family of parametric and linear time series models, namely Autoregressive Integrated Moving Average (ARIMA) models.

Index Terms – **Time series, autoregressive integrated moving average processes, epoxy resin impregnated insulation, EHV insulation.**

1 INTRODUCTION

A time series is a sequence of observations taken sequentially in time. Many sets of data appear as time series and examples of time series abound in fields such as economics, business, social sciences, natural sciences and engineering. An intrinsic feature of a time series is that the adjacent observations are dependent. The analysis of this dependence among observations of a time series requires the development of stochastic and dynamic models for time series data. New developments in time series analysis can be used to determine a better representation for stochastic processes. The three model types in the time series are autoregressive (AR), moving average (MA) and the combined ARMA models. Many time series exhibit homogeneity in the sense that apart from local level, or local level and trend, one part of the series behaves much like any other part. Models that describe such homogeneous non-stationary behavior can be obtained by supposing some suitable difference of the process to be stationary and the class of models for which the d^{th} difference is a stationary ARMA process are called autoregressive integrated moving average (ARIMA) processes. In theory, time series models present an excellent solution if the model type and model order are known.

Numerous successful applications of ARIMA models in manufacturing, marketing, medical informatics, climatic predictions, travel time etc. have been reported in the literature. In power systems, ARIMA techniques have been used for forecasting [1-5] with good results.

Transformer bushings, until recently, employed Oil Impregnated Paper (OIP) as the main insulation. The points in favor of OIP among others are that it is relatively cheap, its behavior under various conditions of operation is well understood and, in general, its overall dielectric and thermal performance is satisfactory. In the recent past, a new class of insulating materials called Resin Impregnated Paper (RIP) has used as main insulation in the high voltage transformer bushings. In the RIP structure, being an all-solid system, the oil phase is completely eliminated. The RIP technology preserves all the essential advantages of OIP and at the same time is free from nearly all its drawbacks. The resin-paper systems are highly reliable and it has become the dielectric of choice in, for example, medium and high voltage transformer bushings, lead-ins and wall bushings.

The temperature rise in RIP bushings under normal operating conditions is seen to be a difficult parameter to control in view of the limited options for effective cooling. With this in view, the Author have already reported the development of a heat balance and continuity equations for assessing the permissible loading of RIP bushings based on the maximum thermal voltage [6]. A thermal stress model based on inverse power law to estimate the life of RIP insulation is also reported [7]. Data originating from failure time distributions were considered for this analysis. More often, in insulation engineering, data on non-destructive testing needs to be considered. Partial discharge data, a non-destructive property, is a good proposal for this purpose. Partial discharges have long been used as a diagnostic tool for identifying internal defects in power equipment. However, measurement of PD

data for life estimation analysis is a very lengthy process. Hence, it may be better to extend this data points after making measurements for a considerably long time.

This paper suggests a method to forecast the future values of partial discharge from a measured set of data. For this, a suitable ARIMA model is derived from the available data and the well-known Box-Jenkins methodology [8] is used to forecast future values.

2 THEORETICAL ASPECTS OF ARIMA APPROACH

2.1 GENERAL

The first step in the analysis of a time series is the selection of a suitable mathematical model for the data. To allow for the possibly unpredictable nature of future observations, it is natural to suppose that each observation x_t is a realized value of a certain random variable X_t. If the data exhibits no apparent deviations from stationarity and has a rapidly decreasing autocorrelation function, a suitable autoregressive moving average (ARMA) process can represent the mean-corrected data. Failure of the estimated autocorrelation function (ACF) to die out rapidly suggests non-stationarity [8]. Then, we shall first look for a transformation of the data, which generates a new series with the above-mentioned properties. Box and Jenkins [8] recommend the differencing approach to achieve stationarity, leading to consider the class of autoregressive integrated moving average (ARIMA) processes represented by ARIMA(p,d,q). The first difference is denoted as $\nabla x_t = x_t - x_{t-1} = (1 - B)x_t$; where B is the backshift operator defined by $Bx_t = x_{t-1}$. The differences of order d is defined as $\nabla d = (1 - B)d$. The degree of differencing d, necessary to achieve stationarity, has been reached when the autocorrelation function of differenced series dies out fairly quickly. Once the data has been suitably transformed, the problem becomes one of finding a satisfactory ARMA(p,q) model, and in particular of choosing p and q. The mathematical description of ARMA(p,q) model can be expressed as [8-11]

$$x_t = \sum_{i=1}^{p} \phi_i x_{t-i} + \sum_{i=1}^{q} \theta_i w_{t-i} + w_t$$

where p and q are the orders of autoregressive part and moving average part respectively; ϕ_i and θ_i are respectively the coefficients of autoregressive model and the coefficients of moving average model; wt is a normal white noise with zero mean and variance greater than zero.

Box-Jenkins method of model identification, which is based on the tailing property and truncation property of the autocorrelation function and partial autocorrelation function, can be used to estimate a reasonable model and then Akaike Information Criterion (AIC) to get the appropriate values of p and q.

The AIC is a test between models – a tool for model selection. Given a data set, several competing models may be ranked according to their AIC, with the one having the lowest AIC being the best [8-11]. In general, the AIC is determined by

$$AIC = 2k - 2\ln(L)$$

where k is the number of parameters in the statistical model, and L is the maximized value of the likelihood function for the estimated model. After determining order of the model, the coefficients of the ARMA model can be estimated using Method of Moments, Least Square method, Yule-Walker estimates or Maximum Likelihood Estimation (MLE).

In this paper, MLE is used for all estimations. The exact likelihood is computed via a state-space representation of the ARIMA process, and the innovations and their variance found by a Kalman filter. The initialization of the differenced ARMA process uses stationarity and is based on Gardner et al. [12]. For a differenced process, the non-stationary components are given a diffuse prior. Observations, which are still controlled by the diffuse prior (determined by having a Kalman gain of at least 1e4) are excluded from the likelihood calculations. The optimization is done using an alternative parameterization, which is a variation on that suggested by Jones [13], and ensures that the model is stationary. For an AR(p) model, the parameterization is via the inverse tanh of the partial autocorrelations. The MA terms are not constrained to be invertible during optimization, but they will be converted to invertible form after optimization.

Once the model is established, the residual analysis is used to check the appropriateness of the model. If the residual series is white noise, the model is reasonable, otherwise, further improvement is required for the model [9,10].

2.2 MODEL IDENTIFICATION

Measurement of partial discharge data is made on a daily basis for 480 days and this data is arranged as a time series. The first 400 days data is used for the analysis and the remaining 80 days data is preserved for the verification. The basic steps to fit ARIMA models to time series data are plotting the data, if possible transforming the data, identifying the dependence orders of the model, parameter estimation, diagnostics and model choice.

The aim of this analysis is to develop a method to extend the data set, if necessary, for the estimation of life based on the diagnostic data. The time series plot of Partial Discharge and its sample ACF are shown in Figure 1 and Figure 2. The Figure 1 shows a very evident increasing trend and suggests a non-stationarity of the data. From Figure 2, it can be observed that the ACF dies out very slowly which confirms the non-stationarity of the data. Hence, the differencing is called for and the time plot of the differenced data, its sample ACF and PACF is shown in Figure 3. Inspecting the sample ACF and PACF, it can be concluded that the ACF is cutting off at lag 2 and the PACF is tailing off. This would suggest a MA(2) process or the PD data follows an ARIMA(0,1,2) model. Rather than focusing on one model, it can also be observed that, as it appears, the ACF is tailing off and the PACF is cutting off at lag 2. This suggests an AR(2) model or ARIMA(2,1,0) for the data. Hence, an ARIMA(2,1,2), a mixed model, will be a good guess. Since PACF at higher lags (say at lag 4, 8, etc.) shows

little above the 10% limit, model with higher AR order, an ARIMA(3,1,2) is also considered.

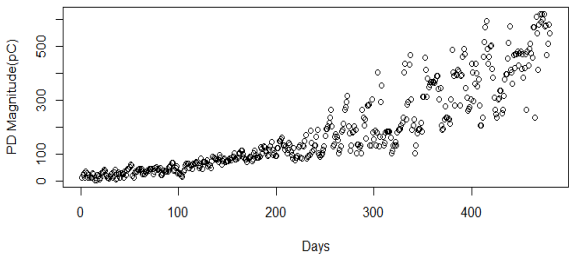

Figure 1: Plot of Partial Discharge Data

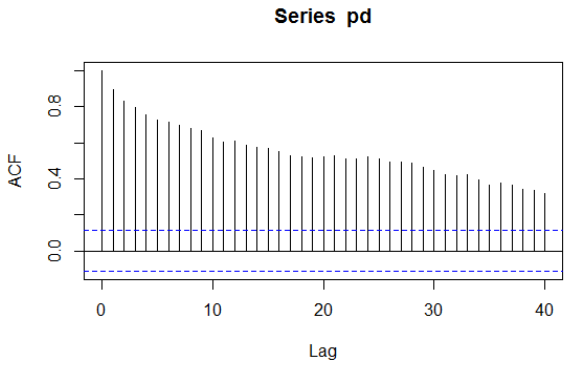

Figure 2: Sample ACF of Partial Discharge Data

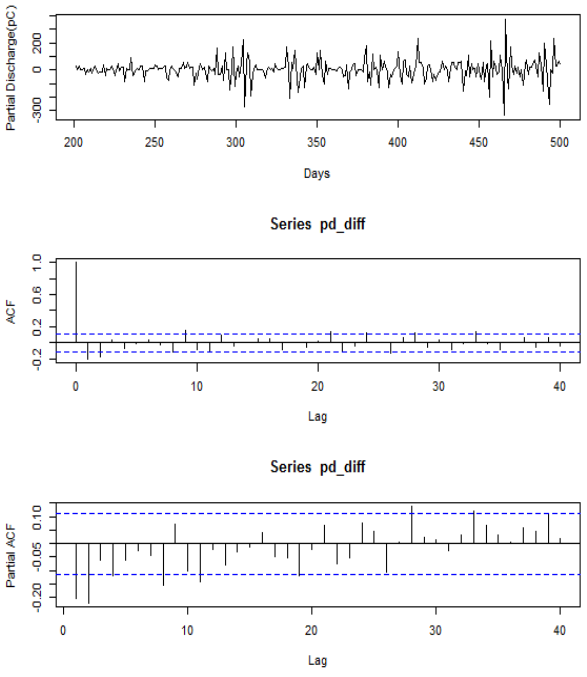

Figure 3: Time series plot of differenced Partial Discharge Data, its ACF and PACF

The AIC is determined for all the four models using statistical software R is as follows. AIC for ARIMA(0,1,2) is 5160.6, for ARIMA(2,1,0) is 5174.53, for ARIMA(2,1,2) is 5146.78 and for ARIMA(3,1,2) is 5135.19. Hence, the ARIMA(3,1,2) model is selected as it has minimum AIC. Using maximum likelihood estimation (MLE) to fit ARMA(3,2) differenced model for the PD data, x_t, the estimated model is

$$x_t = 1.054 - 0.2104x_{t-1} + 0.4293x_{t-2} + 0.1159x_{t-3} - 0.1727w_{t-1} - 0.7634w_{t-2} + w_t$$

with variance σ^2 = 2511, log likelihood = -2560.59, BIC = 5164.4 and AIC = 5135.43.

The Figure 4 shows a normal Q-Q plot and it indicates that the residuals are somewhat close to normality except for extreme value.

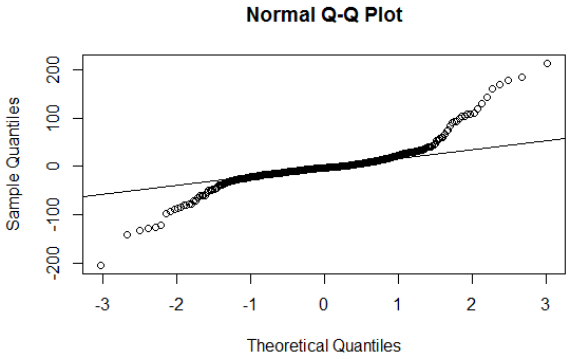

Figure 4: Normal Q-Q plot of the residuals

3 RESULTS AND CONCLUSION

Measurement of PD is made on a daily basis for 500 days and an ARIMA model is developed using 400 days data as explained in the previous section. To predict the data for another 100 days, the forecast package in R systems for statistical computing is used. The forecast package implements automatic forecasting using exponential smoothing, ARIMA models, the Theta method, cubic splines, as well as other common forecasting methods [14]. The output from the forecast function includes at least the following information: the original series, point forecasts, prediction intervals of specified coverage, the forecasting method used and information about the fitted model, residuals from the fitted model, and one-step forecasts from the fitted model for the period of the observed data. The plot of forecasted data for PD is as shown in Figure 5.

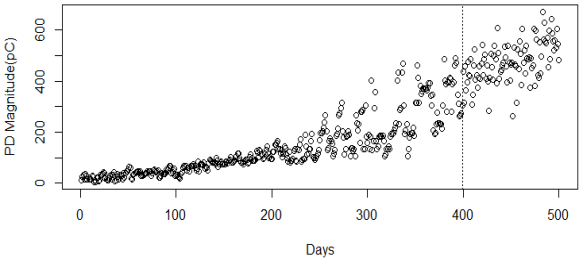

Figure 5: Plot of PD with forecasted data

The extended data set is quite useful in the life estimation study of RIP insulation using PD data or other diagnostic parameters like dissipation factor. The results of this analysis will be published later.

REFERENCES

[1] Phatchakorn Areekul, Tomonobu Senjyu, Hirofumi Toyama, and Atsushi Yona, "A Hybrid ARIMA and Neural Network Model for Short-Term Price Forecasting in Deregulated Market", IEEE Trans. on Power Systems, Vol.25, pp. 524-530, 2010

[2] Peiyuan Chen, Troels Pedersen, Birgitte Bak-Jensen and Zhe Chen, "ARIMA-Based Time Series Model of Stochastic Wind Power Generation", IEEE Trans. on Power Systems, Vol.25, pp. 667-676, 2010

[3] Eva González-Romera, Miguel Á. Jaramillo-Morán and Diego Carmona-Fernández, "Monthly Electric Energy Demand Forecasting Based on Trend Extraction", IEEE Trans. on Power Systems, Vol.21, pp. 1946-1953, 2006.

[4] Javier Contreras, Member, Rosario Espínola, Francisco J. Nogales, and Antonio J. Conejo, "ARIMA Models to Predict Next-Day lectricity Prices", IEEE Trans. on Power Systems, Vol.18, pp. 1014-1020, 2003.

[5] Nima Amjady, "Short-Term Hourly Load Forecasting Using Time-Series Modeling with Peak Load Estimation Capability", IEEE Trans. on Power Systems, Vol.16, pp. 498-505, 2001.

[6] N.S. Jyothi, T.S. Ramu and Manoj Mandlik, "Temperature Distribution in Resin Impregnated Paper Insulation for Transformer Bushings", IEEE Trans. Dielectr. Electr. Insul., Vol. 17, pp. 931-938, 2010.

[7] N.S. Jyothi, T.S. Ramu, "Statistical Methods for Accelerated Life Testing with Particular Reference to Resin Impregnated Paper Bushings", Proceedings of IEEE-PES Asia-Pacific Power and Energy Engineering Conference, March 27-29, 2012, Shanghai, China.

[8] George E.P. Box, Gwilym M. Jenkins and Gregory C. Reinsel, Time Series Analysis: Forecasting & Control, Pearson Education Inc., 2009.

[9] Peter J. Brockwell and Richard A. Davis, Time Series: Theory and Methods, Springer, 2006.

[10] Robert H. Shumway and David S. Stoffer, Time Series Analysis and Its Applications With R Examples, Springer, 2009.

[11] Jonathan D. Cryer and Kung-Sik Chan, Time Series Analysis with Applications in R, Springer, 2008.

[12] G. Gardner, A.C. Harvey, and G.D.A. Phillips, "An algorithm for exact maximum likelihood estimation of autoregressive-moving average models by means of Kalman filtering", Journal of the Royal Statistical Society, Series C (Applied Statistics), Vol. 29, pp. 311–322, 1980.

[13] Richard H. Jones, "Maximum Likelihood Fitting of ARMA Models to Time Series with Missing Observations", Technometrics, Vol. 22, No. 3, pp. 389-395, 1980.

[14] Rob J. Hyndman and Yeasmin Khandakar, "Automatic Time Series Forecasting: The forecast Package for R", Journal of Statistical Software, vol. 27, issue 3, pp. 1-22, 2008.

Dr. N. S. Jyothi was born in Thrissur district of Kerala, India. He received the B.Tech. degree from the Government Engineering College, Thrissur, University of Calicut, India, M.Tech. from the Regional Engineering College, Calicut, India and Ph.D. from Indian Institute of Science, Bangalore, India. He is a senior member of IEEE. Presently he is working as an Associate Professor in the Department of Electrical & Electronics Engineering, Malnad College of Engineering, Hassan, India.

Bio-Medical Robotics

Suveg.V.Iyer
III Sem, M.Tech. Industrial Automation and Robotics
Dept., of Mechanical Engineering
Malnad College of Engineering
Hassan

Abstract: **The medical methods and the facilities available are outdate and thus have to be revamped with the aid of technology in such a mannerthat the results can be obtained without having to undergo a heavy investment. This is a cross disciplinary method where the advantages of mechatronics and robotics technology is used to alter the medical process to achieve a better result. The expected results include how the new methods and facilities available can be made reachable for a higher number of specialists working in the field of medicine.**

***Keywords*-Surgical Robots, Mechatronics, Teleoperation**

I. INTRODUCTION

The field of Medical science is directly related to all living beings hence great care is to be taken before initiating an action, as it directly affects the biological system of the living being. Continuous study has been taking place on how the effects of medical actions affecting the biological system could be reduced. On analysing the medical operationsone can directly arrive at a result that the instruments used in medical field are the prime objects causing uneasiness to the biological system. Thus by designing highly sophisticated instruments solves the major problem. That gives the birth for mechatronics in medical field.

Some of the other problems faced in medical field are the lack of personnel, requirement of highincision, and continuous work hours for the existing personnel etc. On analysing the above issues with the technical perspective the introduction of robotics in the field has emerged.

A.BIOMEDICAL ROBOTICS

Robotics is an interdisciplinary field which has started to boom in the near future. On all Robotics designing the prime feature or condition which satisfies is its ability to produce precise result with repeatability .This feature is the major reason for which an innovation of introducing robots into medical field was made which gave an overwhelming result. But still it has to be noted that the implementation of robots in this field is still in its infant stage only. Continuous study has proved that robots can be used for complex medical operations effectively.

B. LITERARY REFERENCE

In this section references are made toscholarly papers and discussed the implementation of mechatronics in the field of medicine.

Pablo discusses about how children with motor difficulties can be treated with a hippotherapy method which is a physical method of treatment. For this purpose they have used specially designed hippotherapy simulator. The simulator used is “Core Trainer Exercise Equipment, JOBA” and is developed by Mutsuhito (Panasonic) which is equipped with the ability to work in 9 speeds and 3 predefined programmes. The four outcome variables are received which are recorded at three different timings. The variables are:-

- Sitting balance
- Measurement of hip abduction range of motion
- Electromyography activity in adductors- Global motor development

Egger uses two mechatronics aided designed system namely the AMIGO(Advanced multimodality image guided operating suite) designed by Brigham and women’s hospital in Boston .The AMIGO system is capable of 3T MRI and is an advanced version of MRI. The second system discussed is the entire process where imaging, diagnosing, modelling visualisation etc., which are entirely carried out with the help of newer systems. This strongly recommends for more use of mechatronics in medicine.

Muller& Saeed discusses on how in a magnetic environment like MRI remote control technology can be implemented. The Remote control of a catheter guidance uses catheter tip, electromagnetic microcoil, hydraulically actuated catheters. Thus it gives an idea of how mechatronics can be implemented even in a magnetic field without having it as a factor of hindrance for the usage of specialized designed systems.

C.MANIPULATION OF A MECHATRONICS SYSTEM

The process of manipulating mechatronics systems depends on the application for which the system has to be developed. In general some of the factors affecting the design of a mechatronics system include the biomechanics, kinematics of the system when motion carrying a certain load etc. Thus before a designing system, basic factors affecting the system has to be studied and neutralised by using the most optimized method for development.

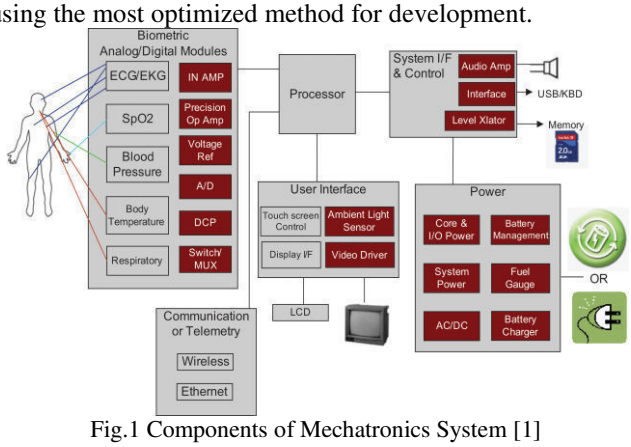

Fig.1 Components of Mechatronics System [1]

Figure 1 gives a clear representation of the components of a general bio mechatronics system. All the mechatronics system irrespective of the application, when generalized must contain the above given components. Thus the entire mechatronics system can be classified into many subsystems which include Sensing feature or detection phase, Processing, Communication, Power source, User

interface etc. Based on the application the usage of type of subsystem components may differ. The result of a mechatronics system developed for any specific purpose lies in how well the developer can interface all the subsystems with minimal amount of discrepancies and loss of data.

Particularly when the system is designed for application as a part of human body the basic principle pertaining to be solved are the three principles of biomechanics which are:

a) Body powered prostheses
b) Myoelectric prostheses
c) Air splint prostheses

The commonly designed mechatronics system for human body is in the rehabilitation of limbs. The foremost problem for designing these types of systems are the defining of type of joint and characteristics that the joint is required to contain. Thus by analysing the above said prostheses types, some of the discrepancies can be neutralised.In the medical applications the basic requirement is components which are flexible and at the same time should be lightweight as the entire system should be as mobile as possible. This feature is imparted to the system easily by developing the system by mechatronics subsystems.

II.BIOMEDICAL ROBOTICS

A. DEFINITION OF THE TERM

The term biomedical robotics is a new concept coined in last two decades. This term can bebetter defined by using robot assisted medical operations which primarily deals with surgeries. The robot assisted surgeries are becoming a great platform for research since the concept is in its infant stage. The rapid development of this new technology is basically due to high acceptance of the system by both surgeons and patients and due to the current available resources.

Fig.2The Da Vinci Robot [2]

B.HISTORY

Since it is a modern day concept the history of medical robotics is as far as 1983.It was when the first surgical robot 'HEARTTHROB' was developed and used in Vancouver. In 1984, this robo was practically used for performing an orthopaedic surgery. In 1985 'UNIMATION PUMA 200' was used for brain biopsy using CT. Later in 1992 'PROBOT' was developed to perform prostatic surgery. It was the first pure robotic surgery and in the same year 'ROBODOC' was developed. The most common surgical robot 'THE DA VINCI 'shown in Fig.2was developed at SRI international.

The major breakthrough for this technology came in May2006 when an artificial intelligence doctor performed the surgery and the result was better than any average doctor could perform. The design was such a way that it had in its database about 10000 similar surgery records.

C. LITERARY REFERENCE

Rebecca et al., have clearly discussed on how the usage of surgical robots offers potential benefits to patients and minimizes the effort and time of the on field doctor and his medical team. The paper discusses on how robotic surgery could be made as a routine practice. The case study for comparison between laparoscopic surgery and robot assisted surgery is done based on a curative treatment of rectal cancer. Thus giving guidance to healthcare organisations on how to successfully implement and integrate robotic surgery without affecting the communication and teamwork [3].

Guixiang et al., have highlighted the importance of the safety factors and also reported the comparative analysis on efficacy of robot assisted colorectal surgery (RCS) and laparoscopic colorectal surgery (LPS). Some of the advantages of RCS over LPS discussed include a three-dimensional image, convenient movements of the robotic arm, no tremor, motion scaling, a short learning curve, dexterity and ambidextrous capability. The result obtained through their analysis was that the blood loss and time to recover was less for RCS when compared with LPS.

D.APPLICATION

The application of biomedical robots can be given based on the types of surgery performed. Thus they are given as:

1. General surgery: - Robot assisted oesophageal and pancreatic surgerycan be done by using the da Vinci surgical robot. Liver resection was done using a robot assisted surgery with great success.

2. Cardiothoracic surgery: - Robot-assisted MIDCAB and Endoscopic coronary artery bypass (TECAB) operations are being performed with the da Vinci system. Mitral valve repairs and replacements can been performed.

3. Cardiology and electrophysiology: - The Stereotaxic Magnetic Navigation System (MNS) has been developed to increase precision and safety in ablation procedures for arrhythmias and atrial fibrillation while reducing radiation exposure.

These are the major surgery performed by robots. Some of the other applications of medical robots are:

i. Colon and Rectal Surgery

ii. Gastrointestinal surgery
iii. Gynaecology
iv. Neurosurgery
v. Orthopaedics
vi. Paediatrics
vii. Radiosurgery

Fig.3Assisting Robot [4]

The above given applications are all surgical robots. Other application includes theatre robots, assisting nurse robots (Fig.3) based on voice recognition technology etc.

E.CASE STUDY

In surgical robots the most common type is the robots used for laparoscopic surgeries. The case which is analysed here is [5]

1) LAPAROSCOPIC SURGICAL ROBOT
INTRODUCTION

A new type of pneumatic end-effector is developed for the gripping motion. The gripping force is adjustable by the controlling pressure using a pneumatic system consisting of a compressor, air pump, 3-way solenoid valves (SVs), speed controller. This gripping system is decoupled from the external arm and the pitching/yawing joint, unlike existing laparoscopic surgical robots. Therefore, sufficient gripping force is obtained and maintained regardless of the end-effectors' different postures.

The surgical robot system adopts a hands-on-throttle-and-stick (HOTAS) controller as shown in Fig.4for the surgeon's control interface. HOTAS is used for flight control in the aerospace field, and it can control hundreds of functions and provide feedback to the pilot about flight conditions.

Fig.4 iHotas [5]

SYSTEM ARCHITECTURE

The system consists of the HOTAS as in interface that can reflect the surgeon's decision, the control 6-axis external robot arm, and the surgical instrument with the pneumatic control system shown in Fig.11.To improve the function of the HOTAS controller; a 6-axis force/torque sensor is used. The surgical robot system could be divided into two parts: external arm and surgical instrument.

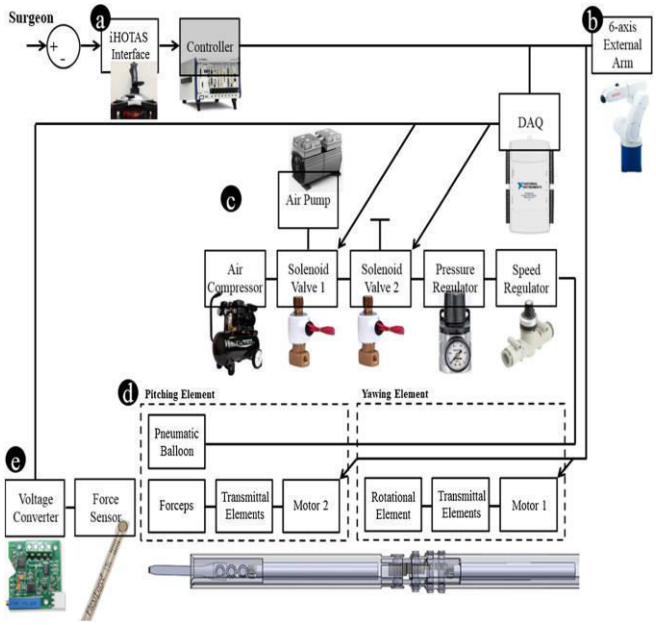

Fig.5 System Architecture [5]

EXTERNAL ARM

For translational motion, fulcrum point motion, and the surgical instrument's rolling motion, a 6-axis external arm is used. The external arm moves on the basis of the fulcrum point and translational motion according to the user's iHOTAS control.

SURGICAL INSTRUMENT

Outer shells are manufactured using a 3D printer to the nearest sub-millimetre resolution and to assemble several parts such as micro-motors, gears, and joint links. The surgical instrument is 300-mm long (Fig.6) for surgicalusability. The outer diameter is 8-mm. The driving force of gripping motion is generated by the pneumatic system's compressor. The gripping motion is achieved by inflating and deflating the catheter balloon. The air compressor and air pump are used to pump compressed air into and suck the same out of the catheter balloon, respectively. The compressed air was controlled using SVs, a speed regulator, and a pressure regulator. The pneumatic gripping system enabled complex yawing and pitching movements, provided sufficient gripping force, and is decoupled from the external arm within an 8mm outer diameter. The weight of the whole surgical instrument is 36 g.The weights of the driving part and extension part with coupler are 15 g and 21 g, respectively.

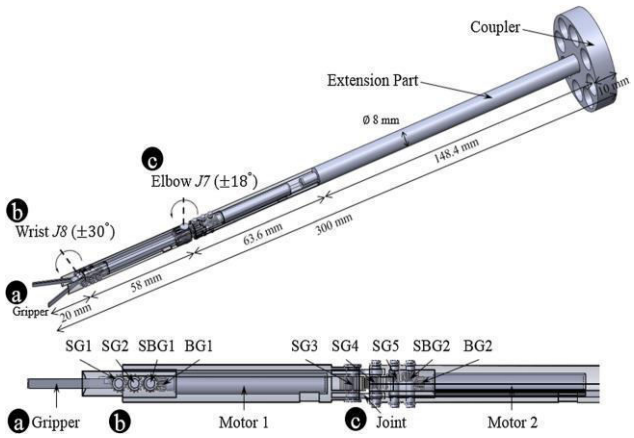

Fig.6External Arm [5]

III.TYPES OF BIOMEDICAL ROBOTS

The different types of robots based on application which are currently used in the medical field are:-

1. Neurology: -The NeuroMate shown in Fig.7wasdeveloped by 'Innovative Medical Machines International'. In addition to biopsy, the system is marketed for deep brain stimulation, stereotactic electroencephalography, transcranial magnetic stimulation, radiosurgery, and neuroendoscopy.

2. Orthopaedics: - Robodoc (Fig.7) is an orthopaedics surgical robot developed by 'Integrated Surgical Systems' which works along withOrthoDoc, a surgical planner. Other robot systems include the Stanmore Sculptor,The Navio PFS,the iBlock,the RIO robotic arm etc.

Fig.7NEUROMATE [6]&ROBODOC [6]

3. General Laparoscopy: - SOFAR developed Telelap ALF-X, is a four-armed surgical robotic system. The system uses eye tracking to control the endoscopic view and to enable activation of the various instruments. Other system includes FreeHand, da Vinci, and Zeus.

4. Radiosurgery: -The CyberKnife is a frameless radiosurgery system consisting of a robotic arm holding a linear accelerator, a six degree of freedom robotic patient table called the RoboCouch, and an X-ray imaging system that can take real-time images in two orthogonal orientations simultaneously.

5. Assistive robotic systems: -Handy 1 became the first commercial assistive robot; it interacts with different trays for tasks and is controlled by a single switch. Exact Dynamics' iARM, is a robotic arm with a two-fingered grasper that attaches to electric wheelchairs and can be controlled via keypad, joystick, or single button.

IV.FUTURE OF BIOMEDICAL ROBOTICS

As discussed earlier the application of robot systems in the field of medicine is a new concept and is in its infant stage. Thus it is one of the sought after research platforms since the scope for research and development is large in this interdisciplinary field. Some of the on-going researches on biomedical robots can be listed as:

i. RAVEN II and MiroSurge: -They are the two prominent academic robot-assisted surgical systems that are currently used for research into endoscopic telesurgery. RAVEN II is shown in Fig.8

ii.TraumaPod:-TraumaPod (Fig.8) is a semi-autonomous telerobotic surgical system designed to be rapidly deployable. The surgical cell consists of a surgical robot, Scrub Nurse Subsystem, Tool Rack System, Supply Dispensing System, Patient Imaging System.

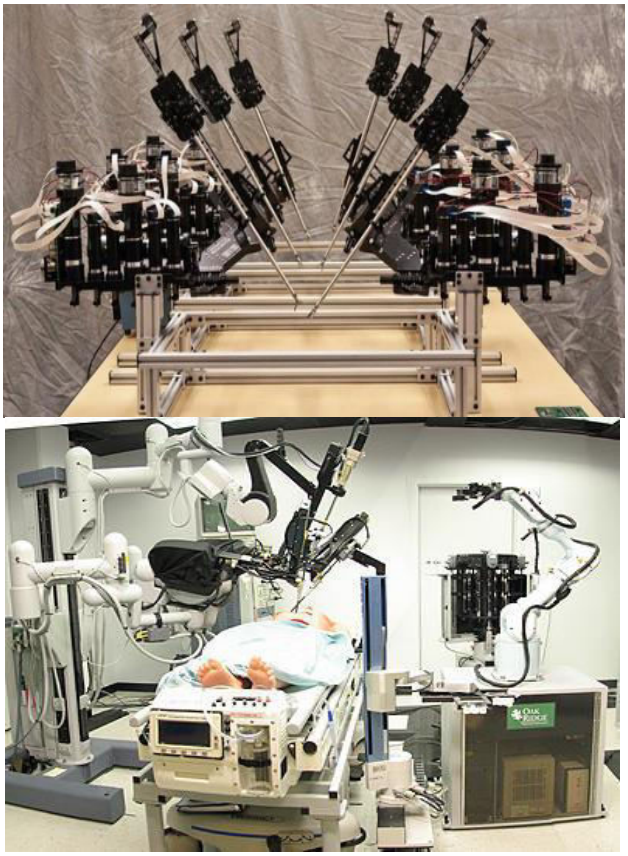

Fig.8 RAVEN II [6] & TRAUMAPOD [6]

iii.Amadeus: -Titan Medical Inc. is currently developing Amadeus, a four-armed laparoscopic surgical robot system, which uses snakelike multiarticulating arms for improved

manoeuvrability, and the system is being designed to facilitate teleoperation for long-distance surgery.

iv.NeuroArm and MrBot: -The neuroArm is a two-armed, MRI-guided neurosurgical robot actuated by piezoelectric motors. The MrBot is a parallel linkage arm designed for MRI-guided access of the prostate gland, actuated by novel pneumatic stepper motors.

v.HeartLander: -HeartLander is a minimally invasive robot that uses suction to crawl around the surface of the heart. The system is designed for intrapericardial drug delivery, cell transplantation, epicardial atrial ablation etc.

V.CONCLUSION

Thus the contribution made by mechatronics and robotics in the field of medicine is gradually increasing mainly due to the increase in number of outcomes in this field due to research and development. As stated earlier this multidisciplinary field have just started its incremental curve which gives an optimistic hope for further contributions. The success of this field is due to the fact that both the surgeons and patients have accepted the new improved method which is a satisfactory condition.

Thus the statement made by Murray Eden, Chief of Biomedical engineering and instrumentation, National institute of Health division of Research services, Bethesda that " Efforts to drive health-care costs down have not braked the development of new technology. A few individual engineers have turned to design expensive devices, but the direction taken by most developers is toward greater convenience, higher quality and finer resolution as well as novel methods of diagnosis and therapy" are literally coming to reality through the advancement of medicalmechatronics and biomedical robotics science.

VI.REFERENCE

[1]Ana-Maria Amancea,IoanDoroftei,AlexandruBarnea, Florentina Adăscăliţei 'Design And Implementation Of A Mechatronic System For Lower Limb Medical Rehabilitation' International Journal of Modern Manufacturing Technologies, Vol. IV, No. 2 / 2012,

[2] Rebecca Randell1, Joanne Greenhalgh, Jon Hindmarsh, Dawn Dowding, David Jayne, Alan Pearman,Peter Gardner, Julie Croft and Alwyn Kotze 'Integration Of Robotic Surgery Into Routine Practice And Impacts On Communication, Collaboration, And Decision Making: A Realist Process Evaluation Protocol' Implementation Science 2014 Vol 9 52.2 May 2014

[3].Pablo Herrero, Ángel Asensio, Elena García, Álvaro Marco, Barbara Oliván, Alejandro Ibarz, Eva M Gómez-Trullénand Roberto Casas 'Study Of The Therapeutic Effects Of An Advanced Hippotherapy Simulator In Children With Cerebral Palsy: A Randomised Controlled Trial'BMC Musculoskeletal Disorders2010, 11:71,16 April 2010.

[4] Jan Egger 'Image-Guided Therapy System For Interstitial Gynaecologic Brachytherapy In A Multimodality Operating Suite' SpringerPlus 2013 2:395, 21 August 2013.

[5] Leah Muller, Maythem Saeed, Mark W Wilson and Steven W Hetts 'Remote Control Catheter Navigation: Options For Guidance Under MRI'Journal of Cardiovascular Magnetic Resonance 1 June 2012.

[6] Daping Yu, Yi Han, Shijie Zhou, Xiaoyun Song, Yunsong Li, Ning Xiao and Zhidong Liu 'Video-Assisted Thoracic Bronchial Sleeve Lobectomy With Bronchoplasty For Treatment Of Lung Cancer Confined To A Single Lung Lobe: A Case Series Of Chinese Patients'Journal of Cardiothoracic Surgery 4 April 2014.

[7] Ryan A. Beasley 'Medical Robots: Current Systems And Research Directions'6 July 2012.

[8] Roberto Cirocchi, Carlo Boselli, Alberto Santoro, Salvatore Guarino, Piero Covarelli, Claudio Renzi, Chiara Listorti, Stefano Trastulli, Jacopo Desiderio, Andrea Coratti, Giuseppe Noya, Adriano Redlerand Amilcare parisi 'Current Status Of Robotic Bariatric Surgery: A Systematic Review'BMC Surgery 7 November 2013.

[9] Guixiang Liao, Zhihong Zhao, Shuhui Lin, Rong Li, Yawei Yuan, Shasha Du, Jiarong Chen and Haijun Deng 'Robotic-Assisted Versus Laparoscopic Colorectal Surgery: A Meta-Analysis Of Four Randomized Controlled Trials'World Journal of Surgical Oncology 26 April 2014.

[10]Chiwon Lee, Woo Jung Park, Myungjoon Kim, Seungwoo Noh, Chiyul Yoon, Choonghee Lee, Youdan Kim,Hyeon Hoe Kim, Hee Chan Kim and Sungwan Kim 'Pneumatic-Type Surgical Robot End-Effector For Laparoscopic Surgical-Operation-By-Wire 'Biomedical Engineering Online10 September 2014.

CHANNEL ESTIMATION ON MIMO-OFDM SYSTEM

Hussana Johar R.B.[1]
Asst.Professor, Dept of TCE,
GSSSIETW, Mysuru,
Karnataka, India

Dr. Sujatha B.R.[2]
Associate Professor, Dept of ECE,
Malnad College of Engineering, Hassan,
Karnataka, India

***Abstract*—Wireless communication systems face several problems. This includes frequency fading, multipath fading, Inter Carrier Interference (ICI), Inter Symbol Interference (ISI) etc,. Requirement of a larger transmit power at high rate, spectral efficiency and low bit rate capacity are other disadvantages. OFDM is an effective technique for high data rate wireless communication in multipath channels and fading environments. Recently, multiple input multiple output (MIMO) channels have been introduced to achieve high data speeds as required by the next-generation communication systems. This requires channel modeling and estimation. The channel characteristics can be estimated by using a preamble or pilot symbols known to both transmitter and receiver, which employ various interpolation techniques to estimate the channel response of the subcarriers between pilot tones. This method can greatly reduce interference because the multiple antennas use the same frequency to transmit data in the OFDM transmission system, which can be applied to wireless MIMO-OFDM communication system with double selective fading.**

***Keywords*— MIMO-OFDM, channel estimation, Pilot, LS, MMSE, interpolation, LS-Spline.**

I INTRODUCTION

Wireless communication system offers ubiquitous communication 'anytime, anywhere'. However, the wireless environment is hostile and communication signals are subjected to frequency fading, multipath fading, ICI, ISI etc. Diversity is one of the methods adopted to combat these problems. By far the most promising multiple antenna technology today happens to be the so called multiple input multiple-output (MIMO) system. These MIMO systems are being considered to improve the range and performance of communication systems.

OFDM is a subset of frequency division multiplexing in which a single channel utilizes multiple orthogonal sub-carriers on adjacent frequencies. In addition the sub-carriers in an OFDM system are overlapping to maximize spectral efficiency without interference.

Figure.1: MIMO Evolution

Thus, lot of research is going on for channel estimation and literature provides various techniques and their performance.
The channel gain estimation algorithm [3] for the MIMO-OFDM system under the high mobility condition has been analysed and simulated.. This method aims to achieve the robust MIMO-OFDM channel gain estimation by using only the Kalman filter from the canonical state space models. It consists of a state equation composed of channel gain and the driving source. It also includes an observation equation composed of the pilot symbols, channel gain and AWGN. The remarkable features of this method are that the channel gain estimation accuracy does not depend on the mobile speed, the number of channel paths and the number of transmitting antennas. Therefore, this method is the practical MIMO-OFDM channel gain estimation method. The proposed method estimates the channel gain with reduced computational complexity.

Channel estimation technique for an orthogonal frequency division multiplexing broadband system over a doubly selective channel is very challenging. This is mainly due to the significant Doppler shift, which results in a time-frequency doubly-selective (DS) channel. J. J. Beek, and et.al[7] have proposed a novel channel estimation system based on distributed compressive sensing (DCS) theory. The special decoupling form originating from a novel sparse pilot pattern is designed for such estimation, which results in an ICI-free structure and enables the DCS application to make joint estimation of these vectors accurately.

Rest of the paper is organized is as follows. In section II MIMO-OFDM is explained in detail followed by channel estimation procedure in section III. Simulation experiment results and analysis is given in section IV followed by conclusion in section V.

II. MIMO-OFDM

System model for MIMO OFDM system as shown in figure 2 with Nt transmit (TX) and Nr receive (RX) antennas. In addition to the spatial and temporal dimension of MIMO, OFDM adds one extra dimension to exploit, namely, the frequency dimension. In general, the incoming bit stream is first encoded by a one-dimensional encoder after which the encoded bits are mapped onto the three available dimensions by the Space-Time-Frequency (STF) mapper. After the STF mapper, each Tx branch consists of almost an entire OFDM transmitter.

On the receiver side as shown in figure 3, the CP is removed and the FFT is performed for every receiver branch. In the context of the unified view, overall STF detection and decoding must be performed to recover the binary data stream. In general, however, because the MIMO algorithms are single carrier algorithms, MIMO detection is performed per OFDM subcarrier. The received signals of subcarrier i are routed to the i-th MIMO detector to recover the Nt QAM symbols transmitted on that subcarrier. Next, the symbols per Tx stream are combined and finally, STF demapping and decoding are performed on these Nt parallel streams and the resulting data are combined to obtain the binary output data.

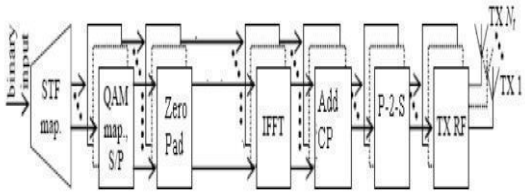

Figure.2

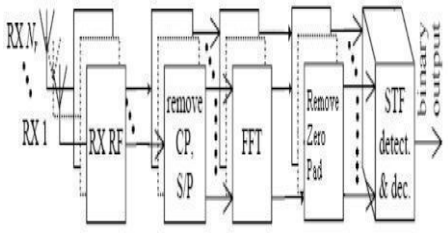

Figure.3

It is also seen that OFDM has the advantage that it introduces a certain amount of parallelism by means of its Nc subcarriers. This fact can be exploited by MIMO OFDM i.e., if MIMO detection is performed per subcarrier, then a given detector is allowed to work Nc times slower than the MIMO detector of an equivalent single carrier system with comparable data rate. However Nc such detectors are required and they can work in parallel, which might ease the implementation.

III. CHANNEL ESTIMATION

Channel Estimation is the process of characterizing the effect of the physical medium on the input sequence. Even with a limited knowledge of the wireless channel properties, a receiver can gain insight into the data sent over by the transmitter..

Two types of channel estimation techniques in practice are:

1. Pilot based channel Estimation
2. Blind Channel Estimation

In Training Based Channel Estimation, channel is estimated based on the training sequence which is known to both transmitter and receiver. The receiver can utilize the known training bits and the corresponding received samples for estimating the Channel. Least Squares (LS) and Minimum Mean Squares (MMSE) methods arrived.

A. Least Squares (LS)

The Least Squares Error (LSE) estimation method can be used to estimate the system h[m] by minimizing the squared error between estimation and detection.

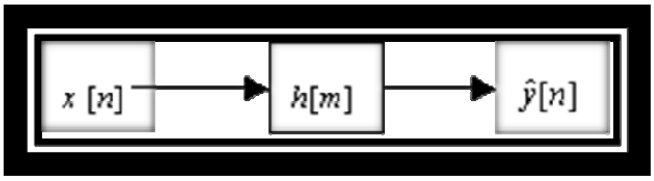

Figure.4

In matrix form, it can be written as [Y] =[X][H]. The error 'e' can be defined as e = y'-y Where y' is the expected output.

The squared error (S) can be defined as

$$S = |e|^2 \quad (1)$$

$$S = (y' - y)^2$$

$$S = (y' - y)*(y' - y)^t$$

Where superscript 't' stands for complex transpose of a matrix.

$$S = (y'' - Xh)*(y'' - Xh)^t \quad (2)$$

This equation can be minimized by taking its derivative w.r.t 'h' and equating it to zero.

$$h'' = (X^T X)^{-1} X^t y$$

which can be written as

$$h'' = X^{-1} y$$

$$hls = X^{-1} y$$

This equation can be implemented on SISO as well as MIMO systems.

B. Minimum Mean Square Error (MMSE)

The MMSE estimator minimizes the mean-square error. If 'X' is transmitted over a channel 'h' such that y = X h Error is given as e = y'' – y Where y" is expected output.

$$\text{mean}\{(y'' - y)^2\} = E\{(y'' - y)^2\} \quad (3)$$

where 'E' is operator for expected value and correlation can be used to derive the equations for finding the channel response.

R_{gg} = auto covariance matrix of 'g'

R_{YY} = auto covariance matrix of 'Y'

R_{gY} = cross covariance matrix of 'g' and 'Y'

The estimated channel H_{mmse} can be determined by the equation

$$H_{mmse} = F * (R_{gY} * R_{YY}^{-1} * Y) \quad (4)$$

Where F is a noise matrix

$$R_{gY} = R_{gg} * F' * X' \quad (5)$$

$R_{YY} = X * F * R_{gg} * F' *X' +$ variance of noise $* [I]$

The equation can be used for both SISO as well as MIMO systems.

C. Blind Channel Estimation Techniques

Although ISI can be avoided, via the use of cyclic prefix in OFDM modulation, the phase and gain of each sub channel is needed for coherent symbol detection. An estimate of these parameters can be obtained with pilot/training symbols, at the expense of bandwidth. Blind channel estimation methods avoid the use of pilot symbols, which makes them good candidates for achieving high spectral-efficiency. Existing blind channel estimation methods for OFDM systems can be classified as:

1. Statistical
2. Deterministic

The statistical methods explore the cyclo-stationarity that the cyclic prefix induces to the transmitted signal. They recover the channel using cyclic statistics of the received signal, or subspace decomposition of the correlation matrix of the pre-DFT received blocks. The deterministic methods process the post DFT received blocks, and exploit the finite alphabet property of the information bearing symbols. Maximum likelihood and iterative Bayesian methods are two examples.

D. Equalization

The technique employed is from the deterministic class of blind channel estimation that involves the use of equalizers. An equalizer removes the channel effects on a transmitted signal and reduces the Intersymbol Interference (ISI). The equalizer transfer function needed to compensate the channel distortion is the inverse of the channel transfer function, given by the following equation

$$H_e (f) = (H_{ch}(f))^{-1} \quad (6)$$

E. Adaptive Equalization

Adaptive Equalization, particularly decision-directed adaptive equalization, successfully cancels ISI when the initial probability of error doesn't exceeds one percent. If the probability of error exceeds one percent, the decision directed equalizer might not converge. A common solution to the problem is to initialize the equalizer with an alternate process, such as a preamble, to provide good channel error performance, and the switch to decision directed mode. To avoid the overhead represented by a preamble, many systems designed to operate in a continuous mode use blind equalization algorithms to form initial channel estimates. These algorithms adjust filter co-efficient in response to sample statistics rather than in response to sample decisions.

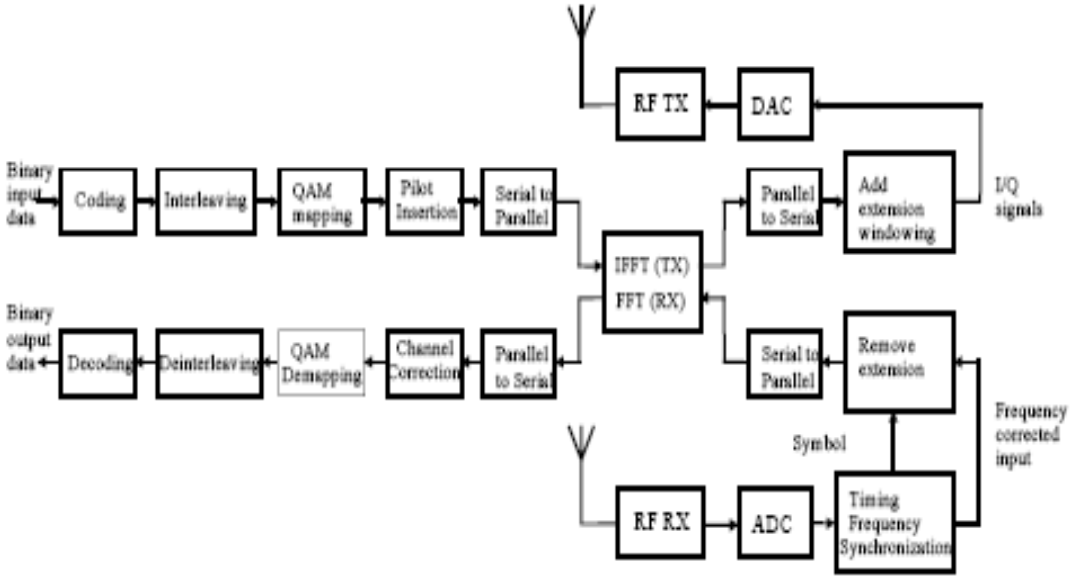

Figure.5: Channel estimation by pilot carrier technique using MIMO-OFDM system

The general block diagram of the baseband processing of an OFDM transceiver is shown in Figure: 5 following the data-stream from transmitter to receiver. In the transmitter, a convolutional encoder encodes the binary input data. After interleaving, the binary values are mapped on Quadrature Amplitude Modulation (QAM) values. In order to correct the signal in the receiver for a possible phase drift, pilot carriers can be introduced. But in this work we assume optimal timing and, thus, no pilot carriers will be used. In the Serial to Parallel block, the serial QAM input symbol-stream is converted to a parallel stream with width equal to the number of sub carriers. These parallel symbols are modulated onto the sub carriers by applying the Inverse Fast Fourier Transform. In order to get an output spectrum with a relative low out of-band radiation, the size of the IFFT can be chosen larger than the number of sub carriers that is actually used to transmit the data[10].The OFDM receiver basically performs the reverse operations of the transmitter, together with additional training tasks.

IV SIMULATION RESULTS AND ANALYSIS

PILOT BASED ESTIMATION

Least Squares (SISO): As shown in figure.6 the values of SNR w r t MSE,MMSE values for SISO is less compared to that of MIMO channel as shown in figure.9,10.

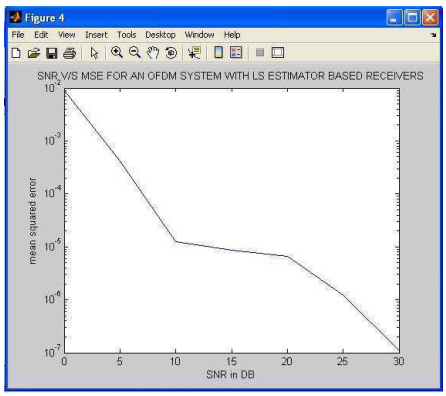

Figure 6: SNR v/s MSE LS SISO PLOT

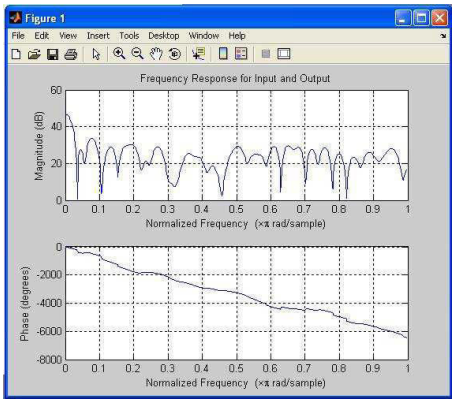

Figure 7: Frequency Response of LS SISO

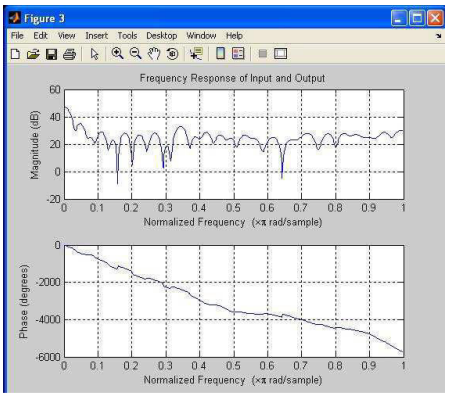

Figure 8: Frequency Response LS MIMO Minimum Mean Square Error (SISO)

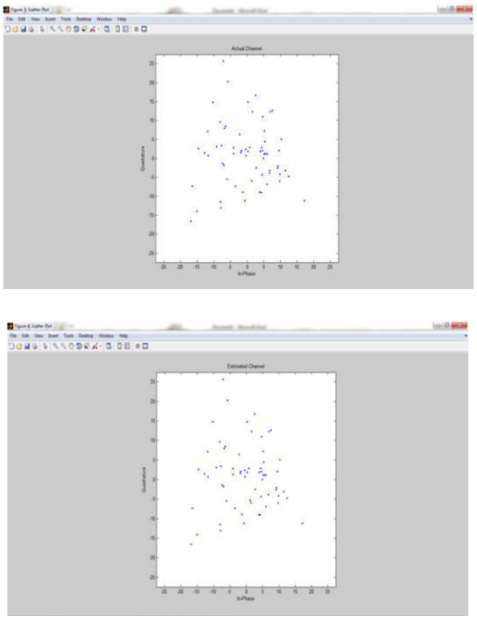

Figure 9: MMSE SISO Channel Scatter Plots

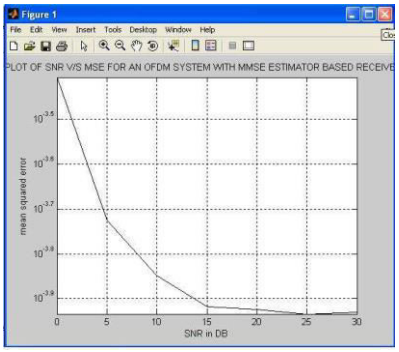

Figure 10: SNR v/s MSE MMSE MIMO Estimator Plot Minimum Mean Square Error (MIMO)

As shown in figure.11&12 the values of Bit error rate w r t MMSE values for MIMO is high compared to that of SISO channel

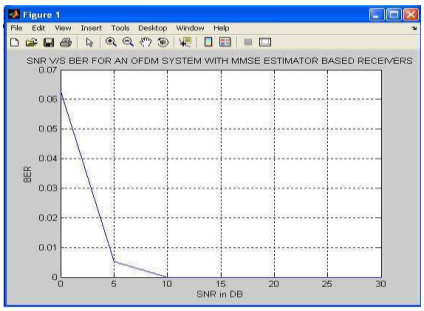

Figure 11: Bit error Rate MMSE MIMO Plot

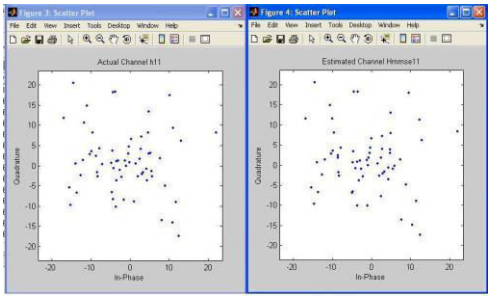

Figure 12: MMSE MIMO channel Scatter Plots

V. Conclusion

The OFDM-MIMO technique has been chosen for various current and future communication systems for many applications that need high speed data transmission. In this paper, OFDM, channel estimation is done for suppressing the interference and ensuring signal detection. Due to accurate channel estimation, OFDM is able to use the coherent detection for 3-dB signal to Noise ratio (SNR) gain over differential detection. MIMO transmission greatly improves the capacity of wireless communications. Since OFDM can convert a frequency selective channel into parallel flat fading channels, it is natural to combine MIMO with OFDM to provide high rate data transmission over frequency selective channels. However, channel estimation in MIMO-OFDM systems is challenging due to the presence of multiple transmits antennas. The implemented channel estimation algorithm is seen to greatly reduce interference because the different antennas use the same frequency to transmit data in the OFDM transmission system, which can be applied to wireless mobile MIMO-OFDM communication system with double selective fading.

References

[1] Tareq Y. Al-Naffouri, K. M. Zahidul Islam, Naofal Al-Dhahir, and Sili Lu,“ A Model Reduction Approach for OFDM Channel Estimation Under High Mobility Conditions” IEEE transactions on signal processing, vol.58, no.4, pp. 2181-2193, 2010.

[2] Jinchang Lu, Maode Ma, “Cognitive radio-based framework and self-optimizing temporalspectrum block scheduling for QoS provisioning in WiMAX,” Computer Networks, vol.55,no.6, pp. 1291–1309, 2011.

[3] Wessam M. Afifi, Hassan M. Elkamchouchi, “A New Adaptive Channel Estimation for Frequency Selective Time Varying Fading OFDM Channel,” In Proceedings of the IEEE ICCES'09 conference, pp. 573 - 578, Dec 2009.

[4] Dulal Haque, Rubaiyat Yasmin, Shaikh Enayat Ullah and M.A.F.M. Rashidual Hasan, “Performance evaluation of a concatenated interleaved FEC scheme Based OFDM system”, Asian Journal of Information Technology, pp. 277-280, 2008.

[5] Ahmed Sghaier, Shawki Areibi and Bob Dony, “A pipelined implementation of OFDM transmission on reconfigurable platforms”, IEEE Canadian conference on Electrical and Computer Engineering, pp. 801-804, May 2008.

[6] Mehmetkemalozdemir, Huseyinarslan, “Pilot-Based LMMSE Channel Estimation for OFDM Systems With Power–Delay Profile Approximation,” IEEE transactions on vehicular technology, vol.59, no.1, pp.150-159, 2010.

[7] Paula M. Castro, Jose A. Garcıa-Naya, Adriana Dapena, Daniel Iglesia, “Channel estimation techniques for linear precoded systems:Supervised, unsupervised, and hybrid approaches,” International journal of Emerging Signal Processing, vol.3 ,no.4, pp. 1578–1588, 2011.

[8] Eugene Golovins, Neco Ventura, “Optimisation of the pilot-to-data power ratio in the wireless MIMO-OFDM system with low-complexity MMSE channel estimation”, International Journal of Computer Communications , vol.32, no. 3, pp.465 -476, 2009.

[9] Chao-Cheng Tu, Benoit Champagne, “Subspace-Based Blind Channel Estimation for MIMOOFDM Systems With Reduced Time Averaging ”, IEEE Transaction of vehicular Technology, vol.59, no.3, pp.1 -5,2007.

[10] M. Morelli and U. Mengali, “A comparison of pilot-aided channel estimation methods for OFDM systems,” IEEE Trans. Signal Process, vol. 49, no. 12, pp. 3065–3073, Dec. 2001.

[11] S.Galih, R.Karlina, A.Irawan, T.Adiono, A.Kurniawan, Iskandar, “Low Complexity Partial Sampled MMSE Channel Estimation for Downlink OFDMA IEEE 802.16e System’’, Intelligent Signal Processing and Communication Systems, 2009. ISPACS 2009. International Symposium, pp. 162-166, Jan 2009.

[12] F.Delestre and Y.Sun, “Pilot Aided Channel Estimation for MIMOOFDM Systems”, Proceedings of London Communications Symposium, pp 356-360, June 2009.

An Overview of PAPR Reduction Techniques for Performance Enhancement of OFDM

Shrishail Bhat
Department of Electronics and Communication Engineering
Anjuman Institute of Technology and Management,
Bhatkal, India
shrishailbhat@gmail.com

Kiran V Shanbhag
Department of Electronics and Communication Engineering
Anjuman Institute of Technology and Management,
Bhatkal, India
shanbhagkiranv@gmail.com

Harish M
Department of Electrical Engineering
University of Wyoming
Wyoming, USA
harishmuralidhar@gmail.com

Abstract— **OFDM is an efficient modulation technique for transmitting large amounts of digital data over high speed communication channels. One major disadvantage of OFDM is that the time domain OFDM signal which is a sum of several sinusoids leads to high peak to average power ratio (PAPR). Number of techniques have been proposed in the literature for reducing the PAPR in OFDM systems. In this paper the various techniques proposed for reducing the PAPR have been discussed. The selection criteria for choosing these techniques have also been discussed. The goal is to convey the fundamental ideas and intuitive understanding of the concept introduced. This is done primarily to give an overview of the various techniques known today for PAPR reduction.**

Keywords- OFDM, fading, PAPR, BER, Signal Scrambling, Signal Distortion

I. INTRODUCTION

Multipath propagation in wireless communications leads to fading which significantly degrades the system performance. Fading can be frequency-flat or frequency-selective. Frequency-flat fading channels can be easily equalized whereas tackling a frequency-selective fading channel is still a challenge [1]. One way to mitigate the frequency-selective fading seen in a wide band channel is to use a multicarrier technique which subdivides the entire channel into smaller sub-bands or subcarriers [2].

Orthogonal Frequency Division Multiplexing (OFDM) is one such multicarrier modulation technique which uses orthogonal subcarriers to convey information. In the frequency domain, since the bandwidth of a subcarrier is designed to be smaller than the coherence bandwidth, each subchannel is seen as a flat fading channel which simplifies the channel equalization process. In the time domain, by splitting a high-rate data stream into a number of lower-rate data stream that are transmitted in parallel, OFDM resolves the problem of ISI in wide band communications. OFDM has been adopted as a modulation of choice by many wireless communication systems such as wireless LAN (IEEE 802.11a and 11g) and DVB-T (Digital Video Broadcasting-Terrestrial). However, it suffers from several drawbacks, important among which, is high Peak-to-Average Power Ratio (PAPR) which degrades the transmit power efficiency.

A number of approaches have been proposed to deal with the PAPR problem. These techniques include amplitude clipping [3], clipping and filtering [4], coding [5], tone reservation (TR) [6], tone injection (TI) [6], active constellation extension (ACE) [7], and multiple signal representation techniques such as partial transmit sequence (PTS) [8], selected mapping (SLM) [9], and interleaving [10]. These techniques achieve PAPR reduction at the expense of transmit signal power increase, bit error rate (BER) increase, data rate loss, computational complexity increase, and so on.

In this paper we describe some important PAPR reduction techniques for multicarrier transmission with a few illustrative examples. We also mention some of the criteria for selecting a PAPR reduction technique.

II. OFDM SYSTEM CONFIGURATION

The orthogonality of the carriers means that each carrier has an integer number of cycles over a symbol period. Due to this the spectrum of each carrier has a null at the centre frequency of each of the other carriers in the system. This results in no interference between the carriers, allowing them to be spaced as close as theoretically possible. To generate OFDM successfully the relationship between all the carriers must be carefully controlled to maintain the orthogonality of the carriers. For this reason, OFDM is generated by firstly choosing the spectrum required based on the input data, and modulation scheme used. Each carrier to be produced is assigned same data to transmit. The required amplitude and phase of them are calculated based on the modulation scheme. The required spectrum is then converted back to its time domain signal using an Inverse Fourier Transform (IFT). In most applications, an Inverse Fast Fourier Transform (IFFT) is used. The IFFT performs the transformation very efficiently and provides a simple way of ensuring the carrier signals produced are orthogonal.

The Fast Fourier Transform (FFT) transforms a cyclic time domain signal into its equivalent frequency spectrum. This is done by finding the equivalent waveform, generated by a sum of orthogonal sinusoidal components. The amplitude and phase of the sinusoidal components represent the frequency spectrum of the time domain signal. The IFFT performs the reverse process, transforming a spectrum (amplitude and phase of each component) into a time domain signal. An IFFT converts a number of complex data points, of length that is a power of 2, into the time domain signal of the same number of points. Each data point in frequency spectrum used for an FFT or IFFT is called a bin. The orthogonal carrier required for the OFDM signal can be easily generated by setting the amplitude and phase of each frequency bin, thus performing the IFFT.

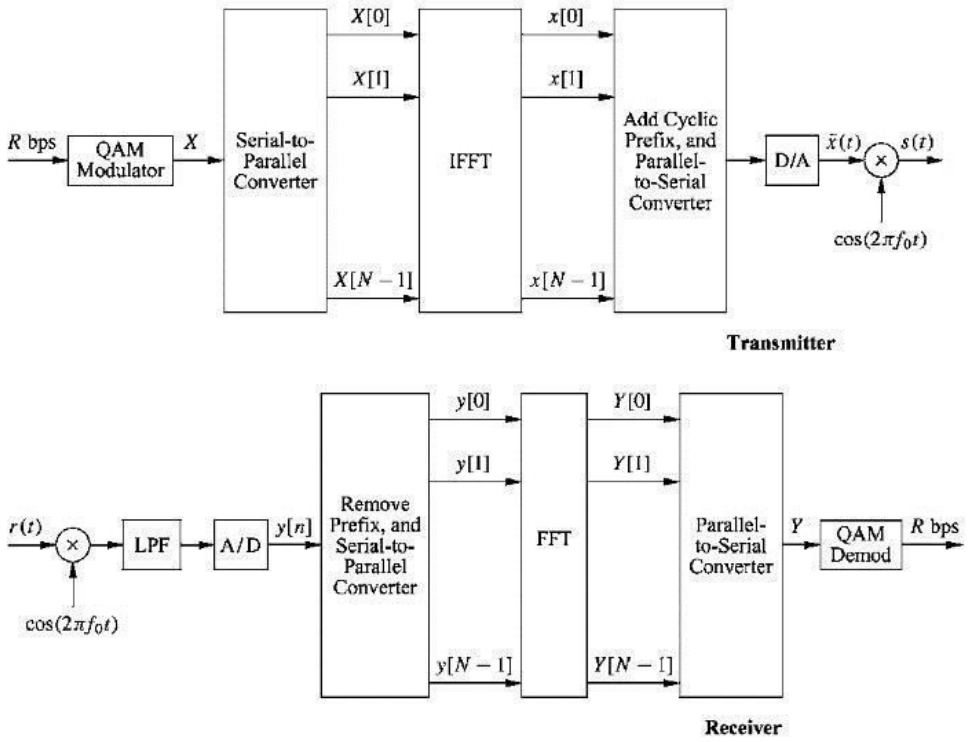

Fig. 1. OFDM with IFFT/FFT Implementation

Fig. 1 shows the configuration for a basic OFDM Transmitter and Receiver using IFFT/FFT. The signal generated is at base band and so to generate an RF signal, the signal must be filtered and mixed to the desired transmission frequency.

III. PAPR IN OFDM SYSTEM

High Peak-to-Average Power Ratio has been recognized as one of the major practical problem involving OFDM modulation. High PAPR results from the nature of the modulation itself where multiple subcarriers / sinusoids are added together to form the signal to be transmitted. When N sinusoids add, the peak magnitude would have a value of N, where the average might be quite low due to the destructive interference between the sinusoids. High PAPR signals are usually undesirable for it usually strains the analog circuitry. High PAPR signals would require a large range of dynamic linearity from the analog circuits which usually results in expensive devices and high power consumption with lower efficiency (for e.g. power amplifier has to operate with larger back-off to maintain linearity).

In OFDM system, some input sequences would result in higher PAPR than others. For example, an input sequence that requires all such carriers to transmit their maximum amplitudes would certainly result in a high output PAPR. Thus by limiting the possible input sequences to a smallest sub set, it should be possible to obtain output signals with a guaranteed low output PAPR.

The PAPR of the transmit signal x(t) is the ratio of the maximum instantaneous power and the average power.

By definition,

$$PAPR = \max_{0 \le t \le T} \frac{[x(t)]^2}{E\{|x(t)|^2\}} \quad (1)$$

where $E\{.\}$ denotes expectation operator.

If a signal is a sum of N signals each of maximum amplitude equal to 1 Volt, then it is conceivable that we could get a maximum amplitude of N Volts, that is, all N signals add at a moment at these maximum points.

For an OFDM signal, that has 126 carriers each with normalized power of 1W, then the maximum PAPR can be as large as 10 log10 126 or 21 db. This is at the instant when all 126 carriers combine at their maximum point unlikely but possible. The RMS PAPR will be around half of the number as 10-12 db.

The large amplitude variation increases in-band noise and increases the Bit Error Rate (BER) which the signal has to go through amplification nonlinearities.

The cumulative distribution function (CDF) of the PAPR is one of the most frequently used performance measures for PAPR reduction techniques [11]. In the literature, the complementary CDF (CCDF) is commonly used instead of the CDF itself. The CCDF of the PAPR denotes the probability that the PAPR of a data block exceeds a given threshold.

IV. PAPR REDUCTION TECHNIQUES

A. Signal Scrambling Techniques

1) Block Coding

The paper by Wilkinson and Jones [12] proposes a block coding scheme for the reduction of the peak to mean envelope power ratio of multicarrier transmission systems. The main idea behind this paper is that PAPR can be reduced by block coding the data such that set of permissible code words does not contain those which result in excessive peak envelope powers (PEPs). There are three stages in the development of the block coding technique. The first stage is the selection of suitable sets of code words for any number of carriers, any M-ary phase modulation scheme, and any coding rate. The second stage is the selection of the sets of code words that enable efficient implementation of the encoding /decoding. The third stage is the selection of sets of code words that also offer error deduction and correction potential.

There are a number of approaches to the selection of the sets of code words. The most trivial brute force approach is sequential searching of the PEP for all possible code words for a given length of a given number of carriers. This is simple and appropriate for short codes because it requires excessive computation. Most sophisticated searching techniques such as natural algorithms can be used for the selection of longer code words. The encoding and decoding, with sets of code words selected from searches, can be performed with a look up table or using combinatorial logic exploiting the mathematical structure of the codes.

2) Selective Mapping

The paper by Bauml et.al. [13] proposes a method for the reduction of peak to average transmit power of multicarrier modulation systems with selected mapping. In selected mapping (SLM) method a whole set of candidate signals is generated representing the same information, and then the most favourable signal as regards to PAPR is chosen and transmitted. The side information about this choice needs to be explicitly transmitted along with the chosen candidate signal.

SLM scheme is one of the initial probabilistic approaches for reducing the PAPR problem, with a goal of making occurrence of the peaks less frequent, not to eliminate the peaks. The scheme can handle any number of subcarriers and drawback associated with the scheme is the overhead of side information that needs to be transmitted to the receiver.

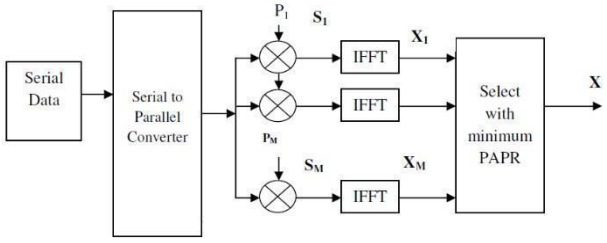

Fig. 2. A block diagram of the SLM technique

Fig. 2 shows a block diagram of the selective mapping technique with M statistically independent sequences.

3) Partial Transmit Sequence

The paper by Muller and Hubber [8] proposes an effective and flexible peak power reduction scheme for OFDM system by combining Partial Transmit Sequences (PTS). The main idea behind the scheme, is that, the data block is partitioned into non-overlapping sub blocks and each sub block is rotated with a statistically independent rotation factor. The rotation factor, which generates the time domain data with the lowest peak amplitude, is also transmitted to the receiver as side information.

PTS is also probabilistic scheme of reducing PAPR. PTS scheme can be interpreted as a structurally modified case of SLM scheme and, it is found that the PTS schemes performs better than SLM schemes. When differential modulation is used in each subblock, no side information needs to be transmitted to the receiver.

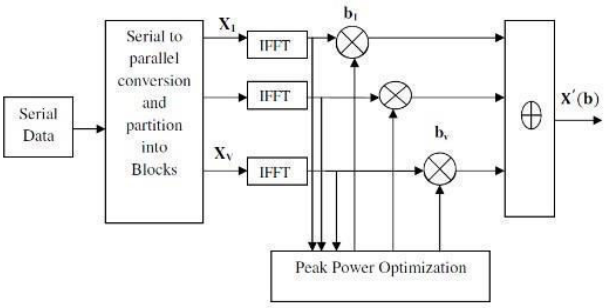

Fig. 3. A block diagram of the PTS technique

Fig. 3 shows a block diagram of the partial transmit sequence technique.The data in frequency domain X is separated into V non-overlapping sub-blocks and each subblock vectors has the same size N.

4) Interleaving

The paper by Jayalath and Tellambura [14] presents interleave based technique for improving the peak to average power ratio of an OFDM signal. Highly correlated data frames have large PAPR, which could thus be reduced, if long correlation patterns were broken down. The paper proposes a data randomization technique for the reduction of the PAPR of the OFDM system.

The paper also proposes an adaptive technique to reduce the complexity of the scheme. The key idea in adaptive interleaving is to establish an early terminating threshold i.e. the search is terminated as soon as the PAPR value reaches below the threshold, rather than searching all the interleaved sequences. The low threshold will force the adaptive interleaving (AIL) to search for all the interleaved sequences, whereas for the large threshold value, AIL will search only a fraction of the interleaved sequences.

The most important aspect of this method is that it is less complex than the PTS method but achieves comparable results. The scheme does not provide the guaranteed PAPR reduction and for the worst case PAPR value of N. Therefore, higher order error correction method should be used in addition to this scheme.

5) Tone Reservation

In this method, the basic idea is to reserve a small set of tones for PAPR reduction. The problem of computing the values for these reserved tones that minimize the PAPR can be formulated as a convex problem and can be solved exactly. The amount of PAPR reduction depends on the numbers of reserved tones, their location within the frequency vector, and the amount of complexity. This method describes an additive method for reducing PAPR in multi-carrier transmission, and shows that reserving a small fraction of tones leads to large reductions in PAPR ever with simple algorithm at the transmitter, and with no additional complexity at the receiver. When the number of tones N is small, the set of tones reserved for PAPR reduction may represent a non-negligible fraction of the available bandwidth and can result in a reduction in data rate. TR method has the advantages of being less complex, no special receiver operation, and no need for side information. Tone reservation is based on adding a data block dependent time signal to the original multicarrier signal to reduce its peaks. This time domain signal can be easily computed at the transmitter and stripped off at the receiver.

6) Tone Injection

This is an additive method, which achieves PAPR Reduction of multicarrier signals with no data rate loss. The basic idea is to increase the constellation size so that each of the points in the original basic constellation can be mapped into several equivalent points in the expanded constellation. Since each information unit can be mapped into one of several equivalent constellation points, these extra degrees of freedom can be exploited for PAPR reduction.

The method is called Tone Injection, as substituting the points in the basic constellation for the new points in the larger constellation is equivalent to injecting a tone of the appropriate phase and frequency in the multi-carrier symbol.

7) Active Constellation

The paper by Knongold and Jones [7] proposes a technique for PAPR reduction similar to Tone Injection Technique. In the active constellation extension technique, some of the outer signal constellation points in the data block are dynamically extended towards the outer side of the original constellation such that the PAPR of the data block is reduced. The main idea of this scheme is easily explained in the case of a multicarrier signal with QPSK modulation in each sub-carrier. In each sub-carrier there are four possible constellation points that lie in each quadrant in the complex plane and are equidistant from the real and imaginary axes. Assuming white Gaussian noise, the maximum likelihood decision region are the four quadrants bounded by the axes, thus, a received data symbol is absorbed. Any point that is farther from the decision boundaries than the normal constellation point (Proper quadrant) will offer increased margin which guarantees a lower BER. The Active Constellation Extension (ACE) idea can be applied to other constellation as well such as QAM and MPSK constellation, because the data points that lie on the outer boundaries of the constellation have room for increased margin without degrading the error probability for other data symbols. This scheme simultaneously decreases the BER slightly while substantially reducing the peak magnitude of the data block. Furthermore there is no loss in data rate and no side information is required. However these modification may increase the transmit signal power for the data block and usefulness of the scheme is restricted to a modulation with a large constellation side.

B. Signal Distortion Techniques

1) Clipping and Filtering

The paper by May and Rholing [15] proposes the method of PAPR reduction by manipulating the OFDM signal with a suitable additive correcting function. In this approach, the amplitude peaks are corrected (or signal is modified) in such a way that a given amplitude threshold of the signal is not exceeded after the correction.

The OFDM signal is corrected by adding it with a corrective function k(t). This correction limits the signal s(t) to A0 at positions of tn of amplitude peaks. This method produces no out-of-band interference and causes interference of the OFDM signal with minimal power. If the OFDM signal is not oversampled, then the correction scheme is identical with clipping and each correction of an amplitude peak causes interference on each sub carrier and the power of the correcting function is distributed evenly to all sub carriers. To apply this correcting scheme, the signal s(t) is oversampled by a factor of four and normalized so that the signal power is one. Then the signal is corrected with k(t).

2) Peak Windowing

The paper by van Nee and Wild [16] proposes that as large PAP ratios occur only infrequently, it is possible to remove these peaks at the cost of a slight amount of self interference. Clipping is one example of a PAPR reduction technique creating self interference. Peak Windowing technique provides better PAPR reduction with better spectral properties than clipping. Peak windowing can achieve PAPR around 4dB for an arbitrary subcarriers, at the cost of slight increase in BER and out-of-band (OOB) interference.

In windowing technique a large signal peak is multiplied with a certain window, such as Gaussian shaped window, cosine, Kaiser and Hamming window. Since the OFDM signal is multiplied with several of these windows, the resulting spectrum is a convolution of the

original OFDM spectrum with the spectrum of the applied window. Ideally the window should be as narrow band as possible, on the other hand the window should not be too long in the time domain because that implies that many signal samples are affected increasing the BER. With windowing method, PAPR can be reduced down to about 4dB, independent of the number of sub carriers. The loss of SNR caused by the signal distortion is limited to about 0.3dB.

3) Envelope Scaling

The paper by Foomooljareon and Fernando [17] proposed an algorithm to reduce PAPR by scaling the input envelope for some sub carriers before they are sent to IFFT. The main idea behind the scheme is that the envelopes of all the subcarriers input, with PSK modulation, are equal. The envelope of the input in some subcarriers can be scaled to obtain the minimum PAPR at the output of IFFT. The final input that gives the lowest PAPR will be sent to the system. The input sequences has the same phase information as the original one but the envelopes are different. So the receiver can decode the received sequence without any side information.

The main idea behind the scheme is that the envelope of the input in some subcarriers is scaled to obtain the minimum PAPR at the output of the IFFT. The scheme seems only suitable to PSK schemes, where all the envelope of all subcarriers input are equal. When the OFDM system implements the QAM modulation scheme, the carrier envelope scaling will result in the serious BER degradation. To limit the BER degradation, amount of the side information would also be excessive when the number of subcarriers is large.

4) Random Phase Updating

The paper by Nikookar and Lidsheim [18] proposes a novel random phase updating algorithm for the peak to average power ratio (PAPR) reduction of the OFDM signal. In the random phase updating algorithm, a random phases generated and assigned for each carrier. The random phase update is continued till the peak value of the OFDM signal is below the threshold. The threshold can be dynamic and the number of iterations for the random phase update is limited.

After each phase update, the PAPR is calculated and the iteration is continued till the minimum threshold level is achieved or the maximum number of iterations has been reached. The random phase increments distribution can be considered uniform or Gaussian. The phase shifts have to be known at the transmitter and the receiver. In this scheme, the BER performance won't degrade only if the receiver knows all the phase changes. This implies a large amount of side information. The efficiency of the algorithm is mainly related to the selected threshold level and consequently number of iterations and not the number of carriers. The algorithm can be improved using the quantization and grouping of phases, and with dynamic threshold.

5) Peak Reduction Carrier

The paper by Tan and Wassell [21] proposes the use of the data bearing peak reduction carriers (PRCs) to reduce the effective PAPR in the OFDM system. The technique involves the use of a higher order modulation scheme to represent a lower order modulation symbol. This allows the amplitude and phase of the PRCs to lie within the constellation region representing the data symbol to be transmitted. For example, to use a PRC that employs a 16 PSK constellation to carry QPSK data symbol, the 16 phases of the 16 PSK constellations are divided into four regions to represent the four different values of the QPSK symbol.

This technique uses the higher order modulation schemes for representing lower order modulation scheme data. This will incur the penalty of an increased probability of error, thus worsening the overall BER performance. So there exists a tradeoff between PAPR reduction and BER performance when selecting the constellation of the PRCs.

6) Companding

The paper by Wang et.al [22] proposes a simple and effective companding technique to reduce the PAPR of OFDM signal. The OFDM signal can be assumed Gaussian distributed, and the large OFDM signal occurs infrequently. So the companding technique can be used to improve OFDM transmission performance. -law companding technique is used to compand the OFDM signal before it is converted into analog waveform. The OFDM signal, after taking IFFT, is companded and quantized. After D/A conversion, the signal is transmitted through the channel. At the receiver end then the received signal is first converted into digital form and expanded. Companding is highly used in speech processing where high peaks occur infrequently. OFDM signal also exhibit similar characteristic where high peaks occur infrequently.

Companding technique improves the quantization resolution of small signals at the price of the reduction of the resolution of large signals, since small signals occur more frequently than large ones. Due to companding, the quantization error for large signals is significantly large which degrades the BER performance of the system. So the companding technique improves the PAPR in expense of BER performance of the system.

V. CRITERIA FOR SELECTION OF PAPR REDUCTION TECHNIQUE

There are many factors that should be considered before a specific, PAPR reduction technique is chosen. These factors include PAPR reduction capability, power increase in the transmit signal, BER increase at the receiver, loss in data rate, computation complexity increase and so on. Let us briefly discuss each of them.

A. PAPR Reduction Capability

Clearly this is the most important factor in choosing a PAPR reduction technique. Careful attention must be paid to the fact that some techniques result in other harmful effects. For example the amplitude clipping technique

clearly removes the time domain signal peaks but results in in-band distortion and out-of-band radiation.

B. Power Increase in the Transmit Signal

Some techniques require a power increase in the transmitted signal after using PAPR reduction techniques. For example Tone reservation (TR) requires more signal power because some of its power must be used for the peak reduction carriers (PRC). Tone injection (TI) uses a set of equivalent constellation point for an original constellation point to reduce PAPR. Since all the equivalent constellation points require more power than the original constellation points, the transmit signal will have more power after applying Tone injection (TI). When the transmit signal power should be equal to or less than that before using a PAPR reduction technique, the transmit signal should be normalized back to the original signal power level resulting in BER performance degradation for these techniques.

C. BER Increase at the Receiver

This is also an important factor and closely related to the power increase in the transmit signal. Some technique may have an increase in BER at the receiver if the transmit signal power is fixed or equivalently may require large transmit power to maintain the BER after applying the PAPR reduction techniques. For example the BER after applying Active constellation Extension (ACE) will be degraded if the transmit signal power is fixed. In some techniques such as SLM, PTS and Interleaving, the entire data block may be lost if the side information is received in error. This also may increase BER at the receiver.

D. Loss in Data Rate

Some techniques require the data rate to be reduced. In block coding technique one out of four information symbol is to be dedicated to controlling PAPR. In SLM and PTS and Interleaving, the data rate is reduced due to the side information used to inform the receiver of what has been done in the transmitter. In these techniques the side information may be received in error, unless some form of protection such as channel coding is employed. When channel coding is used the loss in data rate due to side information is increased further.

E. Computational Complexity

Computational complexity is yet another important consideration in choosing a PAPR reduction technique. Technique such as PTS find a solution for the PAPR reduced signal by using many iteration. The PAPR reduction capability of interleaving technique is better for large number of interleavers. Generally more complex techniques have better PAPR reduction capabilities.

F. Other Considerations

Many of the PAPR reduction techniques don't consider the effect of the components in the transmitter such as the transmitter filter, digital to analog converters (D/A) and transmit power amplifier. In practice PAPR reduction techniques can be used only after careful performance and cost analysis for realistic environment.

Table 1 gives a comparison of different PAPR reduction techniques with respect to different parameters.

Table 1. Comparison of PAPR reduction techniques

Techniques	Parameters		
	Distortion less	Power Enhancement	Data Rate Loss
Clipping and Filtering	No	No	No
Coding	Yes	No	Yes
Partial Transmit Sequence (PTS)	Yes	No	Yes
Selective Mapping	Yes	No	Yes
Interleaving	Yes	No	Yes
Tone Reservation	Yes	Yes	Yes
Tone Injection	Yes	Yes	No
Active Constellation Extension	Yes	Yes	No

VI. SIMULATION RESULTS

Simulation was carried out to examine the PAPR of an OFDM system using two signal scrambling techniques, namely, Selective Mapping (SLM) and Partial Transmit Sequence (PTS).

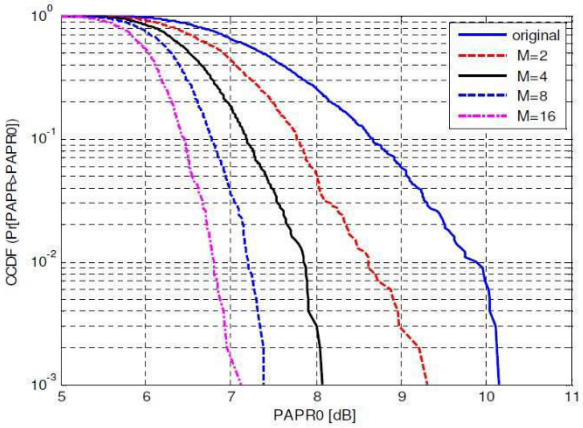

Fig. 4 (a) CCDF using SLM method with N=64

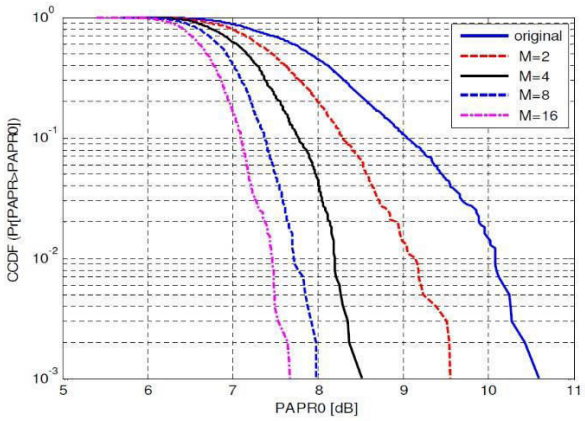

Fig. 4 (b) CCDF using SLM method with N=128

Fig. 4 (a) and 4 (b) show the CCDF as a function of PAPR distribution when SLM method is used with 64 number of subcarriers and 128 number of subcarriers (N=64 and N=128) respectively. As the number of branches (M) increases, the PAPR gets smaller. It can be observed that for N=128, the original unmodified OFDM has a PAPR that exceeds 10.5 dB. By using SLM method, the PAPR is reduced to as low as 7.8 dB (with M=16).

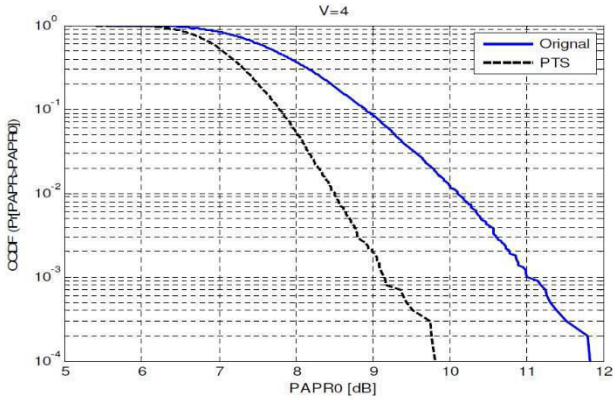

Fig. 5 CCDF using PTS method for N=256

Fig. 5 shows the CCDF as a function of PAPR distribution when PTS method is used with 256 number of subcarriers. The unmodified OFDM has a PAPR that exceeds 11.9 dB. By using PTS method, the PAPR is reduced by 2 dB to as low as 9.9 dB.

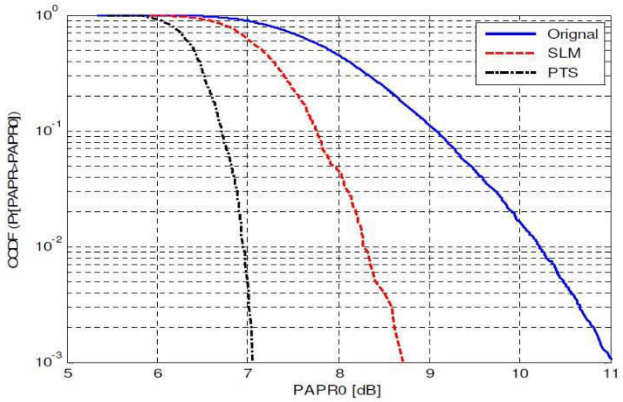

Fig. 6 (a) CCDF using SLM and PTS method with N=64

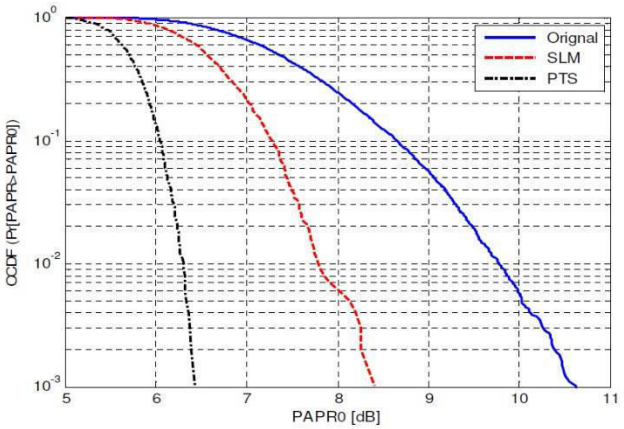

Fig. 6 (b) CCDF using SLM and PTS method with N=128

Fig. 6 (a) and 6 (b) show the CCDF as a function of PAPR distribution when SLM and PTS method is used with 64 and 128 number of subcarriers respectively. It can be observed that for N=128, the original OFDM has a PAPR of 10.5 dB. SLM technique reduces the PAPR to 8.5 dB and PTS technique further reduces the PAPR to 6.4 dB.

VII. CONCLUSION

Orthogonal frequency division multiplexing is a form of multicarrier modulation technique with high spectral efficiency, robustness to channel fading, immunity to impulse interference, uniform average spectral density capacity of handling very strong echoes and less nonlinear distortion. It is recently being used for both wireless and wired high rate digital data communications. Despite its many advantages, OFDM has a drawback which cannot be ignored, that is, high peak to average power ratio (PAPR). High PAPR causes saturation in power amplifiers, leading to inter modulation products among the sub carriers and disturbing out of band energy. Therefore, it is necessary to reduce the PAPR. Several techniques have been proposed such as clipping, windowing, coding, pulse shaping, tone reservation, tone injection, companding etc. But most of these techniques are unable to achieve simultaneously a large reduction in PAPR with low complexity, with low coding overhead, without performance degradation and without transmitter and receiver symbol handshake.

Basic requirement of practical PAPR reduction techniques include the compatibility with the family of existing modulation schemes, high spectral efficiency and low complexity. There are many factors to be considered before a specific PAPR reduction technique is chosen. These factors include PAPR reduction capacity, Power increase in transmit signal, BER increase at the receiver, loss in data rate, computational complexity increase and so on. No specific PAPR reduction technique is the best solution for all multi carrier transmission. Rather the PAPR reduction technique should be carefully chosen according to various system requirements.

REFERENCES

[1] Theodore S. Rappaport, Wireless Communications: Principles and Practice, *Pearson Education India*, 2009

[2] Andrea Goldsmith, Wireless Communications, *Cambridge University Press,* 2005

[3] R. O'Neill and L. B. Lopes, "Envelope Variations and Spectral Splatter in Clipped Multicarrier Signals," *Proc. IEEE PIMRC '95*, Toronto, Canada, Sept. 1995, pp. 71–75.

[4] X. Li and L. J. Cimini, Jr., "Effect of Clipping and Filtering on the Performance of OFDM," *IEEE Commun. Lett*., vol. 2, no. 5, May 1998, pp. 131–33.

[5] A. E. Jones, T. A. Wilkinson, and S. K. Barton, "Block Coding Scheme for Reduction of Peak to Mean Envelope Power Ratio of Multicarrier Transmission Scheme," *Elect. Lett.,* vol. 30, no. 22, Dec. 1994, pp. 2098–99.

[6] J. Tellado, Peak to Average Power Reduction for Multicarrier Modulation, Ph.D. dissertation, Stanford Univ., 2000.

[7] B. S. Krongold and D. L. Jones, "PAR Reduction in OFDM via Active Constellation Extension," *IEEE Trans. Broadcast.,* vol. 49, no. 3, Sept. 2003, pp. 258–268.

[8] S. H. Müller and J. B. Huber, "OFDM with Reduced Peak–to–Average Power Ratio by Optimum Combination of Partial Transmit Sequences," *Elect. Lett.,* vol. 33, no. 5, Feb. 1997, pp. 368–69.

[9] H. Breiling, S. H. Müller–Weinfurtner, and J. B. Huber, "SLM Peak-Power Reduction without Explicit Side Information," IEEE Commun. Lett., vol. 5, no. 6, June 2001, pp. 239–41.

[10] G. R. Hill, M. Faulkner, and J. Singh, "Reducing the Peak-to-Average Power Ratio in OFDM by Cyclically Shifting Partial Transmit Sequences," *Elect. Lett.,* vol. 36, no. 6, Mar. 2000, pp. 560–61.

[11] Seung Hee Han and Jae Hong Lee, "An Overview of Peak-To-Average Power Ratio Reduction Techniques for Multicarrier Transmission", *IEEE Wireless Communications,* April 2005. pp. 56-65.

[12] Wilkison, T.A. and Jones, A.E., "Minimization of the peak to mean envelope power ratio of multicarrier transmission schemes by block coding", *IEEE Vehicular Technology Conference,* Vol.2., Jul 1995.

[13] Bauml, R.W., Fischer, R.F.H., and Huber, J.B. Reducing the peak to average power ratio of multi carrier modulation by selective mapping", *IEEE Electronics Letters,* Vol.32, Oct 1996.

[14] Jayalath, A.D.S., and Tellambura, C., "The use of interleaving to reduce the peak to average power ratio of an OFDM signals", *IEEE Global telecommunications conference,* Vol.1, Nov 2000.

[15] May, T., and Rohling , H., "Reducing the peak to average power ratio of OFDM", radio transmission system", *IEEE Vehicular Technology Conference,* Vol. 3, May 1998.

[16] Van Nee, R., and Wild, A., "Reducing the peak to average power ratio of OFDM", *IEEE Vehicular Technology Conference,* Vol.3, May 1998.

[17] Foomooljareon, P. and Fernando, W.A.C., "Input sequence envelope scaling in PAPR reduction of OFDM", *IEEE 5th International Symposium on Wireless Personal Multimedia Communications,* Vol.1, Oct 2002.

[18] Nikookar, H., and Lidsheim, K.S., "Random phase updating algorithm for OFDM transmission with low PAPR", *IEEE Transaction on Broadcasting,* Vol.48, Jun 2002.

[19] Shrishail Bhat, Sujatha B R, Kiran V Shanbhag, "A Rate ½ Convolutional Coded Single Carrier Frequency Division Multiple Access Scheme for Rayleigh Fading Channel", *International Journal of Research in Information Technology (IJRIT), ISSN 2001-5569,* Volume 1, Issue 6, June 2013, pp. 266-272.

[20] V. Vijayarangan, R. Sukanesh, An Overview of Techniques for Reducing Peak to Average Power Ratio and its Selection Criteria for Orthogonal Frequency Division Multiplexing Radio Systems, *Journal of Theoretical and Applied Information Technology,* 2009, pp. 25-36.

[21] Tan, C.E. Wassell, I.J., "Data bearing peak reduction carriers for OFDM systems", *IEEE Proceedings of the 2003 Joint Conference of the Fourth International Conference of Information, Communications and Signal Processing, 2003 and the Fourth Pacific Rim Conference on Multimedia,* Vol.2, Dec 2003.

[22] Wang, X., Tjhung, T.T., Ng, C.S., "Reduction of peak to average power ratio of OFDM system using a companding technique", *IEEE Transactions on Broadcasting,* Vol.25, Sep 1999.

Steady State Operation of Induction Generator With Improvements in THD

Raghvendraprasad Deshpande[1]
Research Scholar
Department of E&E Engineering
Malnad College of Engineering
Hassan - 573 202, India.
raagu.deshpande@gmail.com

M. S. Raviprakasha[2]
Professor
Department of E&E Engineering
Malnad College of Engineering
Hassan - 573 202, India.
ravidmagge@rediffmail.com

Abstract - Self Excited Induction Generator (SEIG) is an isolated power source whose frequency and terminal voltage can be controlled using excitation capacitance. For improving power quality of SEIG and for controlling current, APF strategy is employed. SAPF is connected at Point of Common Coupling (PCC) along with three phase PWM current controlled Voltage Source Inverter. Proposed controller strategy for SAPF performs well under steady state condition. SAPF gives very good robust behavior and dynamic response upon changes in load parameters. The simulation results with the use of unbalanced and nonlinear loads have showed the effectiveness in terms of improvements in harmonics reduction in wind based isolated power system.

Index terms – Power Quality, THD

I. INTRODUCTION

Recently, SEIGs are utilized as better electro-mechanical converter driven by Renewable Energy Resources. More importance is given to wind energy since it is clean resource which produces electricity with no outflow of pollutant gas. Induction generators are mostly used in remote and isolated areas because of benefits such as less maintenance and simple operation. The PQ issues at isolated power source are of major concern. These are mainly production of harmonics at PCC due to non-linear loads. The harmonics create difficulties in power system and also in consumer products, like, vibration of motor, apparatus overheating, blowing of capacitor, low power factor etc. Shunt Active Power Filter (SAPF) are usually used to improve energy quality taken from the grid where low current harmonics are desirable and also with active power filter it is possible to prevent/ mitigate any kind of harmonic generation.

Artificial Intelligence has been recently introduced in the harmonic extraction and the control of Active Power Filter. The interest in the involvement of using ANN for harmonic content extraction was proposed and discussed in [1]. SAPF injects a suitable non-sinusoidal current (compensating current) into the system at the PCC and makes source current sinusoidal. The performance comparison of different techniques for assessing reference-compensating current for a three-phase SAPF were presented in [3]. The techniques compared were instantaneous Power Balance, Fourier series method and DC-link voltage regulation method. Their performance is studied under ideal (balanced and sinusoidal), non-ideal (un-balanced and distorted) supply voltage conditions and at different load conditions. The command current streams of the active filter are derived utilizing load and source reference currents [3].

SEIG is by all accounts most suitable for wind vitality. The SEIG was represented in d-q axes by [4-6], that has produced voltage fluctuations. As a part of finding the capacitance necessary for SEIG is represented in [7]. The smooth control of SEIG may be accomplished by the use of Static Var compensators (SVC) but large size capacitors and inductors are needed [8]. In this work, a methodology is presented to mitigate harmonics in isolated power source based on SEIG. A MATLAB based model is developed, which yield a THD of less than 5 %, well within the compliance of IEEE 519 standards.

II. METHODOLOGY

A schematic of the proposed control scheme is indicated in figure 1, which comprises of three phase star connected Induction Generator driven by small scale hydro-electric turbine. By associating altered terminal capacitor the generator can be operated as SEIG as to result in generation of terminal voltage. To compensate the current harmonics produced by nonlinear loads, SAPF are most commonly used. Block diagram of SAPF control strategy is revealed in figure 2. Hysteresis controller is used for controlling of SAPF switches in order to generate switching signals. The instantaneous reference current of the APF (i^*_{ca}, i^*_{cb},i^*_{cc}) are obtained by subtracting the load currents (i_{la},i_{lb},i_{lc}) from reference current template (i^*_{sa},i^*_{sb}, i^*_{sc}). Switching pulses for VSI are obtained by subtracting (i^*_{fa}, i^*_{fb}, i^*_{fc}) from the symphonious current produced by SAPF. From instantaneous power and voltage of AC source, reference currents are obtained.

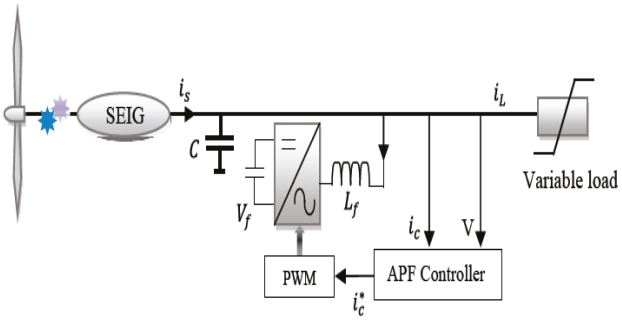

Figure 1. System description along with SAPF and SEIG

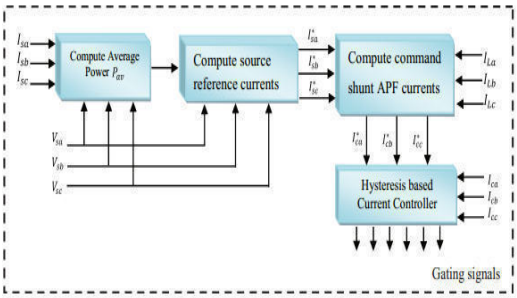

Figure 2. Block Diagram of SAPF

The instantaneous source voltages is are :

$$v_{sa}(t) = v_{sm}\sin(\omega t)$$
$$v_{sb}(t) = v_{sm}\sin(\omega t - \frac{2\pi}{3}) \quad (1)$$
$$v_{sc}(t) = v_{sm}\sin(\omega t - \frac{4\pi}{3})$$

Power p_{avg} can be written as

$$P_{avg}(t) = V_{sa}(t)i_{La}(t) + V_{sb}(t)\,i_{Lb}(t) + V_{sc}(t)i_{Lc}(t) \quad (2)$$

Instantaneous three phase responsive force in every phase gets to be:

$$q_{La} = V_b I_{Lc} - V_c I_{Lb}$$
$$q_{Lb} = V_c I_{La} - V_a I_{Lc} \quad (3)$$
$$q_{Lc} = V_a i_{Lb} - V_b I_{La}$$

Nonlinear load delivering active and reactive power must satisfy (3) and (4).

$$p_L = p_s + p_c = p_{L1} + p_{Lh} \quad (4)$$
$$q_f = q_L \quad (5)$$

Harmonic and reactive power Compensation, P_f can be derived as:

$$P_f(t) = V_{sa}(t)i_{ca}(t) + V_{sb}i_{cb}(t) + V_{sc}(t)\,i_{cc}(t) \quad (6)$$

The reference compensating currents can be expressed as:

$$i_{sa}^* = I_{La} - \frac{p_{L1}}{v_{sa}^2+v_{sb}^2+v_{sc}^2}V_a \quad (7)$$
$$i_{sb}^* = I_{Lb} - \frac{p_{L1}}{v_{sa}^2+v_{sb}^2+v_{sc}^2}V_b \quad (8)$$
$$i_{sc}^* = I_{La} - \frac{p_{L1}}{v_{sa}^2+v_{sb}^2+v_{sc}^2}V_c \quad (9)$$

APF currents are computed as:

$$i_{ca}^* = i_{sa}^* - i_{La}$$
$$i_{cb}^* = i_{sb}^* - i_{Lb} \quad (10)$$
$$i_{cc}^* = i_{sc}^* - i_{Lc}$$

III. Control Scheme

Hysteresis Current Controller (HCC) is utilized to produce the switching pulses to control VSI switches as shown in figure 3. Precise instantaneous control exchanging of IGBT gadgets ought to be such that the lapse sign becomes zero, hence for this purpose HCC with altered band utilized to determine the exchanging signs of the three stage IGBT based VSI span. The upper gadget and the lower device in one stage leg of VSI ought to be exchanged in complimentary way. The APF reference streams contrasted and detected with source currents are used to create the firing pulses which makes the inverter switches active for reducing current error.

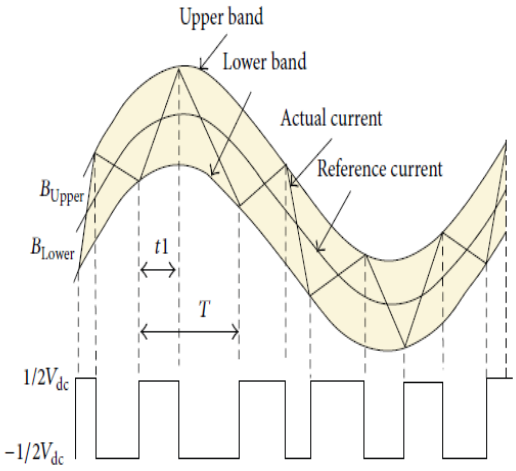

Figure 3. Hysteris Control scheme

By modifying the little power streaming in to dc capacitor, voltage control of the dc bus is performed hence compensating the conduction and switching losses. In request to dispense with the enduring state mistake and lessen the swell voltage. Proportional Integral is used and expressed as:

$$H(S) = KP + K_I/S \quad (11)$$

IV. Results and Discussions

The simulation outcomes are obtained to confirm the effectiveness of proposed control strategy. The non-linear load is an uncontrolled unbalanced three phase RL load. Nonlinear load current obtained through simulation without harmonics compensation is shown in figure 4. It is observed

that the current waveform is distorted and contains harmonics of the order of 28.38%.

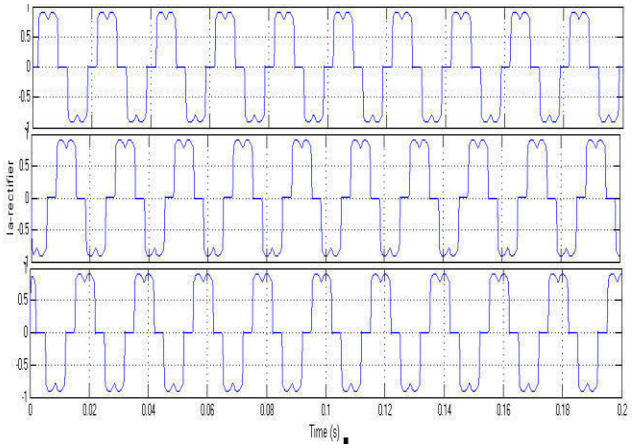

Figure 4. Non-linear load current without capacitor filter & SAPF.

The unbalanced load RL current before compensation without capacitor filter and APF is shown in figure 5. From the waveforms obtained, it can be inferred that the harmonic content in the load side is more and it is non-sinusoidal.

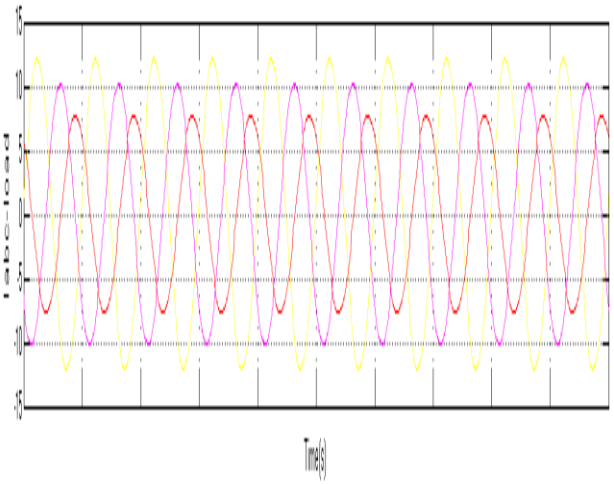

Figure 5. Unbalanced load currents without Capacitor filter & SAPF.

The simulation results obtained verifies the viability of proposed control plan. The waveform of nonlinear load current with the use of capacitor filter is shown in figure 6. It can be inferred that the nonlinear load contains less harmonics (3.28%) when compared to current waveform without any compensation. The source current after compensation using capacitor filter is shown in figure 7. The source current is sinusoidal with reduced harmonic distortion(3.28%). The simulation results obtained verifies the effectiveness of proposed SAPF control scheme. The uneven current waveform after deploying SAPF is depicted in Figure 8. It is observed that with the use of APF the unbalanced load current is sinusoidal.

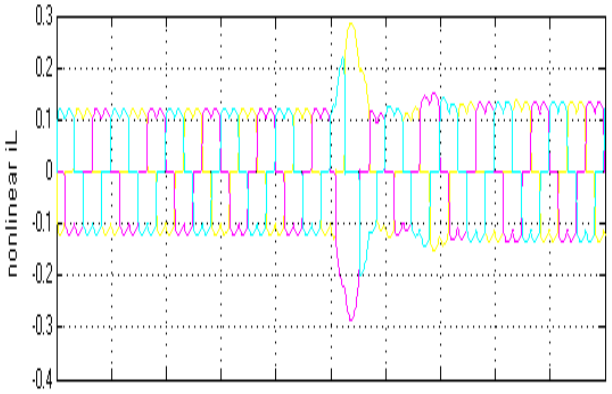

Figure 6.Nonlinear load current with capacitor filter.

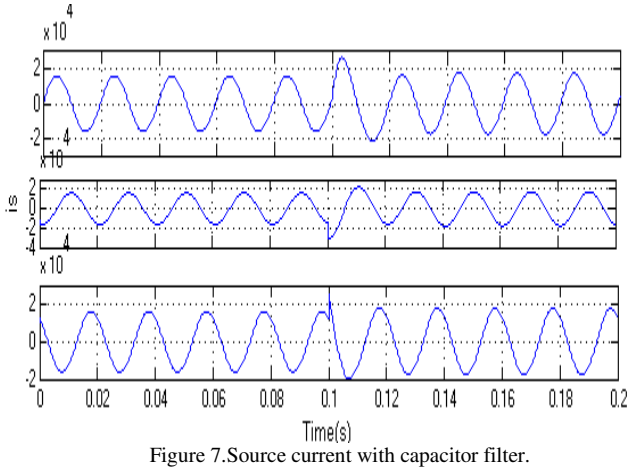

Figure 7.Source current with capacitor filter.

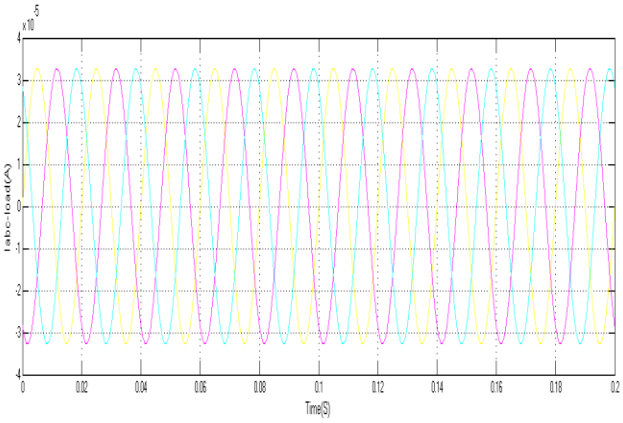

Figure 8. Unbalanced load current with APF.

The non-linear load current after compensation is shown in figure 9. It is clear that the load current is non-sinusoidal. It is mainly because of the characteristics of load. From the results obtained , it is clearly observed that the SAPF is able to reshape the current waveform, and attempt has been made to reduce %THD. SAPF supplies the reference current as indicated in figure 10.

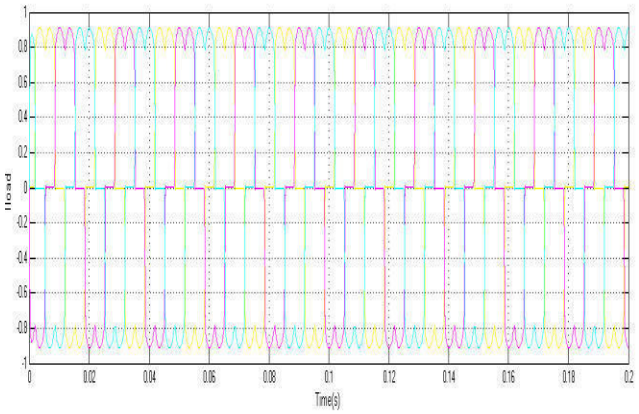

Figure 9. Non-linear load current with APF.

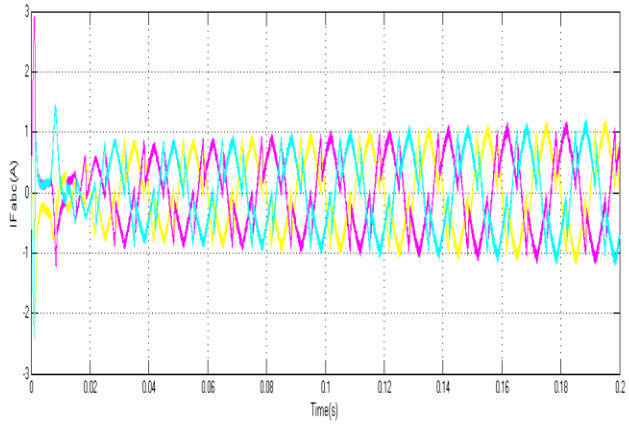

Figure 11. Reference currents by SAPF.

Figure 12 reveals the source current waveform after compensation, which shows significant improvements, hence, current waveform is sinusoidal. Figure 13 and figure 14 shows the simulation result of stator voltage and current of the SEIG with immersion. It is observed that the phase voltage gradually begins to develop and achieves steady state as and when the self excitation phenomenon is completed.

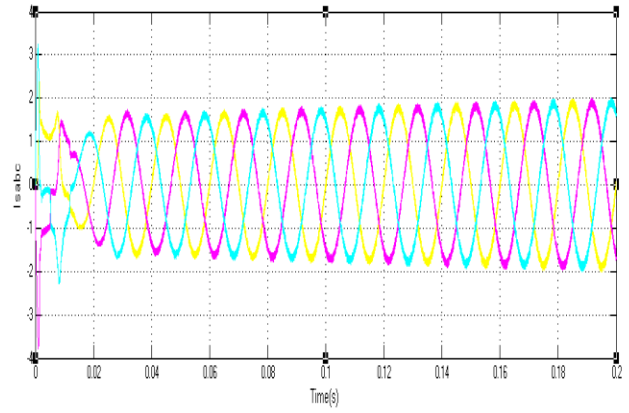

Figure 12.Source Current after compensation with SAPF.

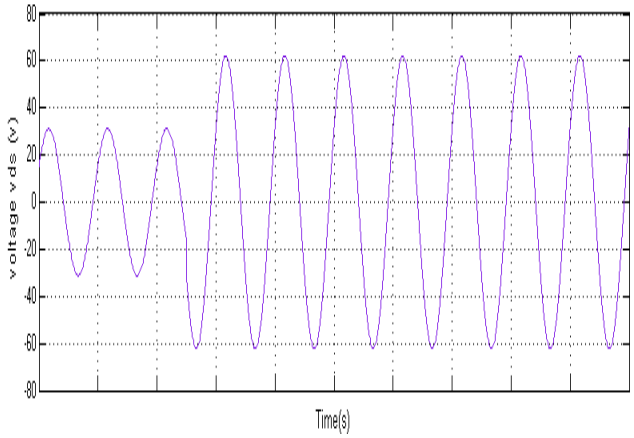

Figure 13. Stator voltage of SEIG with saturation.

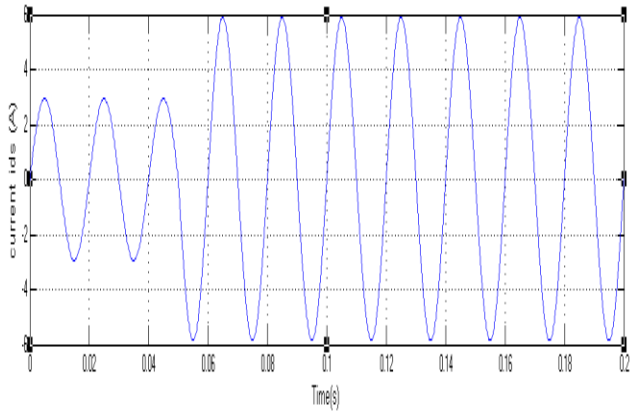

Figure 14. Stator current of the SEIG with saturation.

In order to evaluate the performance of the proposed system, FFT analysis is carried out. Figure 15 shows the FFT analysis without harmonic compensation. Before compensation the source current has the value of THD of 28.38%. The source contains more harmonics without using capacitor filter and SAPF.

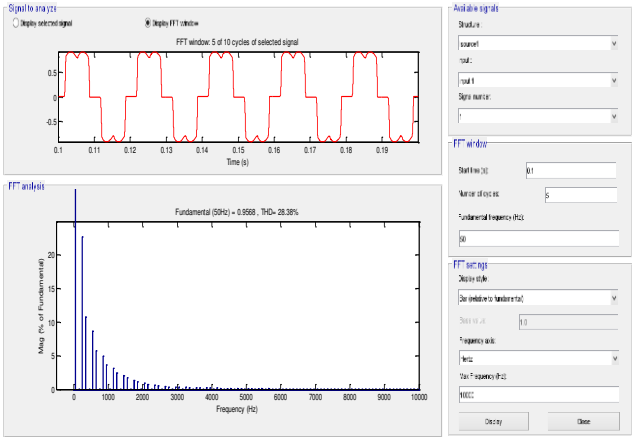

Figure 15. Spectrum analysis without the use of Capacitor filter & SAPF.

Figure 16 shows FFT analysis of source current with capacitor filter. After compensation, harmonic content in the waveform has the THD of 3.28%. The source current contains less amount of harmonics. By using capacitor filter technique, THD value is reduced from 28.38% to 3.28%.

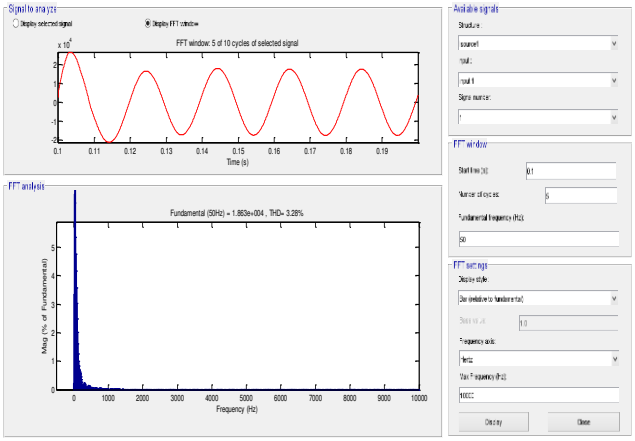

Figure. 16 Spectrum analysis with the use of Capacitor Filter.

Figure 17 shows FFT analysis of source current with the use of SAPF. After compensation the source current has the value of THD of 1.72%. The source current contains less amount of harmonics than the capacitor filter. By using SAPF the THD value is reduced to 1.72% from 28.38%. The comparison of harmonic contents, with and without compensation scheme is tabulated in Table I.

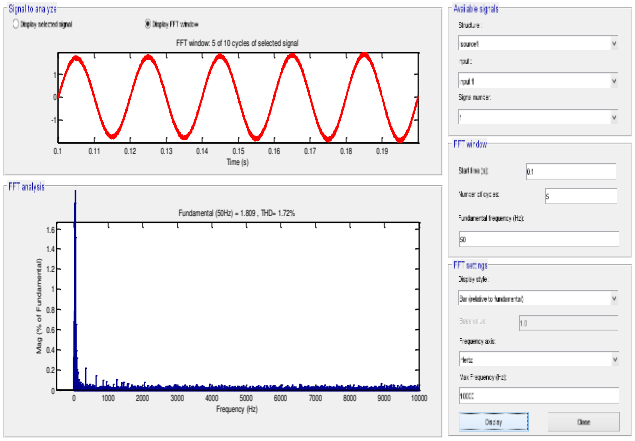

Figure 17. Spectrum analysis with the use of SAPF.

TABLE I. : COMPARISON OF HARMONICS CONTENTS.

% THD		
Wihout compensation	With Capacitor	With SAPF
28.38%	3.28%	1.72%

V. CONCLUSIONS

The method using SAPF for THD reduction is discussed. Results obtained with the capacitor filter and with APF are analysed. The simulation results shows that the proposed control technique which utilizes PQ theory and hysteresis control technique, yields in improvements in the current waveform. There are many possibilities that can be attempted for future work, such as : The voltage flicker is essentially created by the variations in the load reactive current. The proposed APF system is potentially able to perform this task, since it has fast reactive current compensation capability. Studying the application of APF system for voltage flicker reduction is recommended as a topic for future work.

ACKNOWLEDGMENTS

This work is carried out at the Research Centre, Dept. of Electrical & Electronics Engineering, affiliated to Visvesvaraya Technological University, Belagavi, Karnataka, India and financially supported by the World bank assisted, MHRD-initiated, TEQIP II -1.2 project, Malnad college of Engineering, Hassan, Karnataka State, India.

REFERENCES

[1] D.Joshi, K. S. Sandhu, and M. K. Soni, "Performance Analysis of Self-Excited Induction Generator Using Artificial Neural Network", Iranian Journal Of Electrical And Computer Engineering, Vol. 5, No. 1,pp 57-62, WINTERSPRING 2006.

[2] ShanmughaSundaram, K.J.PoornaselvanN.Devarajan, "Comparison of Reference Compensating Current Estimation Techniques for Shunt Active Filter", Conferences-2005 prague papers pp 493-149.

[3] Bhim Singh, Kamal Al-Haddad, and Ambrish Chandra: "A New Control Approach to Three-phase Active Filter for Harmonics and Reactive Power Compensation",IEEE Transactions on Power Systems, Vol. 13, No. 1, pp. 133-138, Feb. 1998.

[4] Vargil Kumar E, Narasimham PVRL, Sarma AVRS, "Steady State Investigation of Self Excited 3 Phase Induction Generator with Novel Leading VAR Controller and Mitigation of Harmonics Using Active Power Filter", IEEE International Conference on Power and Energy (PECon2010), pp 495-500,Nov 29 - Dec 1, 2010.

[5] Avinash Kishore, G. Satish Kumar, "Dynamic Modeling and Analysis Of Three Phase Self Excited Induction Generator using Generalized State-Space Approach", IEEE International Symposium on Power Electronics, Electrical Drives, Automation and Motion, SPEEDAM, pp 52-59, 2006.

[6] T. Chan, "Capacitance Requirements of Self-Excited Induction Generators." IEEE Transactions on Energy Conversion, Vol. 8, No. 2, June 1993, pp. 304-311.

[7] Grantham C., Sutanto D. and Mismail B.,"Steady-state and Transient Analysis of Self-Excited Induction Generators," Proceedings, IEE, pt. B, vol. 136, no. 2, pp. 61-68.

[8] Chang, G.W., "A New Method For Determining Reference Compensating Currents of The Three Phase Shunt Active Power Filter", IEEE Power Eng., review, March 2001, pp 63 –65.

ISBN: 978-93-84659-38-7